Clickable Lipid Reporters as Chemical Tools for Imaging and Tracking Lipids

A Dissertation Presented for the

Doctor of Philosophy

Degree

The University of Tennessee, Knoxville

Christelle Anne Fernandez Ancajas

August 2023

Acknowledgements

I would like to take a moment to express my heartfelt gratitude and appreciation to the wonderful individuals who have played significant roles in shaping my academic and personal journey. Their unwavering support, love, and guidance have been instrumental in my achievements, and for that, I am truly grateful. First and foremost, I want to thank my parents, whose unwavering support and boundless love have been the foundation of my success. Your belief in me, even during my most challenging moments, has given me the strength to persevere and reach for my dreams. I am forever grateful for the sacrifices you have made and the countless ways you have shaped my life. Thank you to my aunt, Victoria, your presence in my life has been a constant reminder of the importance of family and the power of unconditional support. To my dear sister, Christine, thank you for always looking up to me and being my biggest cheerleader. Your unwavering love, admiration, and constant belief in my abilities have been a tremendous source of motivation throughout my journey.

I am also immensely grateful to my undergraduate advisors, both past and present. I thank Dr. Foster for for sparking my interest in cell biology and for warmly welcoming an inexperienced undergraduate into his lab. To Dr. Thoburn, thank you for your guidance during my formative years in research. Your wisdom and mentorship helped shape my academic interests and laid the groundwork for my future endeavors, especially in our shared passion for organic chemistry. And to Dr. Schreiner, thank you for always instilling in me the belief that I can go big in research. Your unwavering confidence in my abilities has been a driving force behind my aspirations. I am indefinitely grateful to my graduate committee, Dr. Campagna, Dr. Calhoun, and Dr. Reynolds for your support and intellectual guidance as well. They are individuals whom I

greatly admire. I thank them for the valuable discussions in and out of defenses and for supporting my curiosity. Finally, I am indebted to Dr. Best for your invaluable guidance and mentorship. Your expertise, patience, and belief in my potential have been pivotal in my growth as a researcher. I am grateful for the opportunities you have provided me to learn under your mentorship and for the trust you have placed in my abilities.

A heartfelt appreciation goes out to my lab coworkers, especially Ruhani and Megan, two remarkable scientists who joined me on this journey. Through our shared struggles and triumphs, we have formed a bond that goes beyond research. Your unwavering support, words of encouragement, and understanding during challenging times have been invaluable. I must thank the members of the Best Lab, both past and present, Lucia, Sarah, Alexa, Matt, Kazi, Mayesha, Brooke, Justin, and Michael. I am incredibly fortunate to have had all of you as irreplaceable collaborators and dear friends throughout my academic and research journey. I am grateful for the camaraderie we have developed. I also owe much to Aeric (Yue Zhou)- thank you for sharing your biological and experimental knowledge with me. I would also like to express my gratitude to Dr. Adam Carr, who guided me during my initial months of graduate school. Your mentorship and willingness to show me the ropes in research when I was still learning have been transformative. Furthermore, I would like to extend my thanks to Dr. Jinchao Lou for demonstrating that passion and attitude towards science can transcend barriers. Your commitment to advancing knowledge and your contagious enthusiasm have inspired me to push boundaries and pursue excellence.

I am also thankful for my friends in and out of Knoxville. You all have been great positive sources of light in this journey. Virginia, Zarin, and Isabel, thank you. It’s nice to have people to

talk to who are going through similar experiences. I would also like to express my heartfelt gratitude to SalsaKnox for providing a warm and welcoming community. Being part of the team for a few years has been a profound learning experience, imparting in me the virtues of discipline and leadership. It has been enjoyable and fulfilling.

To all those mentioned above, and to the countless others who have supported me on my journey, I want to express my heartfelt appreciation. Your contributions, no matter how big or small, have profoundly impacted my academic and personal growth. The pandemic might have taken a slight toll on us, but together, we've weathered the storms and come out stronger. I'm truly grateful for having you in my life and the invaluable role you've played in shaping the person I am today. Thank you from the bottom of my heart.

Abstract

The regulation of lipid metabolism is crucial for maintaining the human body, as disruptions in lipid homeostasis have drastic implications. While lipids are known for their roles as energy stores as well as for cellular compartmentalization, certain lipid classes can serve as signaling agents that govern cellular behavior and physiology or as biomarkers whose concentration and spatial organization impacts cell fate. Thus, dysregulation in these processes coincide with a variety of diseases and cancers. However, the ability to track lipids has been a long-standing challenge in the area of chemical biology since lipids are chemically diverse and undergo continuous interconversion within their complex biosynthetic pathways. A popular method to address this challenge is the lipid metabolic labeling platform whereby click-tagged substrates are introduced to cells and metabolized to generate click-tagged lipids. These lipids can be modified through click chemistry to enable selective labeling, detection, and imaging. In Chapter 1, we review scientific endeavors that took advantage of this platform. In Chapters 2 and 3, we describe the development and application of new precursors to 1) label a particular phospholipid, phosphatidylserine (PS), by headgroup labeling and 2) to label several lipid classes by glycerol-tagging. We confirmed the successful infiltration of these precursors into the lipid pathways of *S. cerevisiae* via mass spectrometry (MS), fluorescence imaging after click reaction with fluorescent dye, and lipid class separation by fluorescence-based thin-layer chromatography (TLC). In Chapter 2, we have synthesized novel azido-serine precursors and confirmed its conversion to PS lipid products. In Chapter 3, the same techniques were applied to assess a panel of azido-monoacylglycerol (MAG) precursors in their ability to label neutral lipids and phospholipids. Chapter 4 describes an extension to the goal of “bulk” glycerophospholipid

labeling with the synthesis of an azide-tagged phosphatidic acid precursor. Finally, Chapter 5 describes cysteine and serine analogs equipped with electrophilic and clickable tags as substrate mimics to probe the PS synthase enzyme active site. All in all, this novel set of clickable reporters add to the rapidly expanding toolbox of lipid probes for chemical biology applications.

Table of Contents

List of Tables

List of Figures

List of Schemes

List of Abbreviations

AcOH	Acetic acid
Acyl-CoA	Acyl coenzyme A
Ag_2O	Silver(I) oxide
Ar	Argon
Boc	*tert*-Butyl carbamate
C. albicans	*Candida albicans*
CD_3OD	Deutarated methanol
$CDCl_3$	Deutarated chloroform
CDP-DAG	Cytidine diphosphate diacylglycerol
Cds1	CDP-DAG synthase
CH_2Cl_2	Methylene chloride
$CHCl_3$	Chloroform
Cho-P	Choline phosphate
CL	Cardiolipin
CTCF	Corrected total cell fluorescence
CuAAC	Copper(I)-catalyzed azide-alkyne cycloaddition
Cy3	Cyanine dye 3
Cy5	Cyanine dye 5
DAG	Diacylglycerol
DART	Direct analysis in real time
DBCO	Dibenzocyclooctyne
DBU	1,8-diazabicyclo[5.4.0]undec-7-ene
DCM	Methylene chloride
Dga1	Acyl-CoA diacylglycerol acyltransferase
DIC	Differential interference contrast
DMAP	*N,N*'-dimethylaminopyridine
DMF	*N*,*N*-dimethylformamide
DMSO	Dimethylsulfoxide
DOPE	1,2-Dioleoyl-*sn*-glycero-3-phosphoethanolamine
EDC	1-Ethyl-3-(3-dimethylaminopropyl) carbodiimide
ER	Endoplasmic reticulum
ESI	Electrospray ionization
Et_3N	Triethylamine
Etn-P	Ethanolamine phosphate

EtOAc	Ethyl acetate
EtOH	Ethanol
FA	Fatty acid
FFA	Free fatty acid
G-3-P	Glycerol-3-phosphate
Gal	Galactose
GFP	Green fluorescent protein
GL	Glycerolipid
Gly	Glycerol
GPI	Glycophosphatidylinositol
GPL	Glycerophospholipid
HBr	Hydrobromic acid
HBTU	O-(benzotriazol-1-yl)-*N*,*N*,*N*',*N*'-tetramethyluronium hexa-fluorophosphate
HCl	Hydrochloric acid
Hex	Hexanes
HOBt	Hydroxybenzotriazole
HPLC	High-performance liquid chromatography
HRMS	High resolution mass spectrometry
IEDDA	Inverse electron-demand Diels-Alder
KI	Potassium iodide
KM_nO_4	Potassium permanganate
LD	Lipid droplet
$LiAlH_4$	Lithium aluminum hydride
m-CPBA	*meta*-Chloroperozybenzoic acid
MAG	Monoacylglycerol
MeCN	Acetonitrile
MeOH	Methanol
MFI	Mean fluorescent intensity
MQ	Milli-Q purified water
MS	Mass spectrometry
N_2	Nitrogen
Na_2SO_4	Sodium sulfate
NaN_3	Sodium azide
NaOH	Sodium hydroxide

NH_4OH	Ammonium hydroxide
NMR	Nuclear magnetic resonance
NR	Nile red
p-TsCl	*p*-Toluene sulfonyl chloride
p-TsOH	*p*-Toluenesulfonic acid
PA	Phosphatidic acid
PAP-1	Phosphatidic acid phosphatase-1
PBS	Phosphate buffered saline
PC	Phosphatidylcholine
PCC	Pearson's correlation coefficient
PDME	Phosphatidyl-dimethylethanolamine
PE	Phosphatidylethanolamine
PEMT	Phosphatidylethanolamine methyltransferase
PFA	Paraformaldehyde
PG	Phosphatidylglycerol
PGP-Pase	Phosphatidylglycerol phosphate phosphatase
PI	Phosphatidylinositol
PIP2	Phosphatidylinositol-4,5-biphosphate
PIS	Phosphatidylinositol synthase
PKC	Protein kinase C
PLC	Phospholipase C
PLD	Phospholipase D
PM	Plasma membrane
PMME	Phosphatidyl-monomethylethanolamine
PS	Phosphatidylserine
Psd	Phosphatidylserine decarboxylase
PSS1	Phosphatidylserine synthase-1
PSS2	Phosphatidylserine synthase-2
RBF	Round-bottom flask
R_f	Retention factor
RP	Reverse phase
S. cerevisae	*Saccharomyces cerevisae*
SATE	*S*-acetyl-thioethyl
SDS-PAGE	Sodium dodecylsulfate polyacrylamide gel electrophoresis

SM	Sphingomyelin
sn	Stereospecific numbering
SPAAC	Strain-promoted azide-alkyne cycloaddition
TAG	Triacylglycerol
TCA	Trichloroacetic acid
THF	Tetrahydrofuran
TLC	Thin layer chromatography
TOF	Time-of-flight

Chapter 1. Introduction

A portion of this Chapter has been published as a review article: Ancajas, C. F.; Ricks, T. J.; Best, M. D., Metabolic labeling of glycerophospholipids via clickable analogs derivatized at the lipid headgroup. *Chem. Phys. Lipids* **2020,** *232*, 104971.

1.1 Understanding the complexity of lipids

1.1.1 Structure and properties of lipids

Understanding the complexity of lipids and their roles in biological processes has been an area of increasing interest, particularly since this has led to continual expansion in the knowledge that lipids are involved in critical signaling events. While lipids are well-known for their role in energy storage and cellular compartmentalization, they are also key actors in signaling pathways,[1] and participate in intracellular trafficking[2, 3] and posttranslational lipidation of proteins.[4] Moreover, only particular and specific lipid families participate in these diverse and complex cellular processes.[5] In a cell, enzymes are constantly working to produce structurally diverse lipids that can be categorized into different lipid classes: Fatty acids, glyceride lipids, and non-glyceride lipids. Glycerolipids (GLs) and glycerophospholipids (GPLs), the two main foci of the work described in this dissertation, are defined by their structures and roles in cellular processes. Glycerolipids contain a glycerol backbone that can be mono-, di-, or tri-esterified with lipophilic chains to produce monoacylglycerols (MAGs), diacylglycerols (DAGs), and triacylglycerols (TAGs), respectively (**Figure 1.1B**). Meanwhile, glycerophospholipids are derivatives of L-Glycerol 3-phosphate or *sn*-glycerol-3-phosphate (G-3-P) where the third carbon of glycerol (*sn*-3 position) bears a phosphate or phosphodiester moiety with the type of phosphodiester-linked headgroup

that defines the phospholipid class that they belong to (**Figure 1.1A**).[6] Variation can also arise within these lipid families where the two hydroxyl groups at the *sn*-1 and *sn*-2 positions of G-3-P form ester linkages with two fatty acids (FAs) of varying lengths and degrees of unsaturation (**Figure 1.1C**).[7] Records of the different lipid classifications, structures and their nomenclatures are well-curated.[6, 8]

1.1.2 Roles of glycerolipids and glycerophospholipids in cells

Glycerolipids have diverse roles in energy storage and signaling pathways. Firstly, TAGs comprise one of the major types of GLs and are the primary form of energy storage for fatty acids. Moreover, TAG hydrolysis is critical for the mobilization of FAs, which are key biosynthetic substrates for the production of lipids. TAGs along with other neutral lipids are also the most sbundant constituents of lipid droplet (LD) organelles, which typically play a role in cell energy homeostasis and lipid metabolism.[9, 10]

Apart from their function as energy reservoirs, GLs, particularly DAGs, act as second messengers in intracellular signaling pathways.[11] In one example, DAG that is produced from hydrolysis of phosphatidylinositol-4,5-biphosphate (PIP_2), activates the calcium-dependent protein kinase C (PKC), which once activated, phosphorylates target proteins and causes cellular responses.[11] **Figure 1.1B** shows the two forms of DAG: 1,2-diacylglycerol and 2,3-diacylglycerol. TAGs and DAGs represent two classes of lipids that can be potential metabolites derived from the MAG probes discussed in Chapter 3.

MAGs generally serve as intermediates in the catabolism and anabolism of neutral lipids. DAG is broken down by lipases into MAG, glycerol, and FAs. These lipolysis products can be

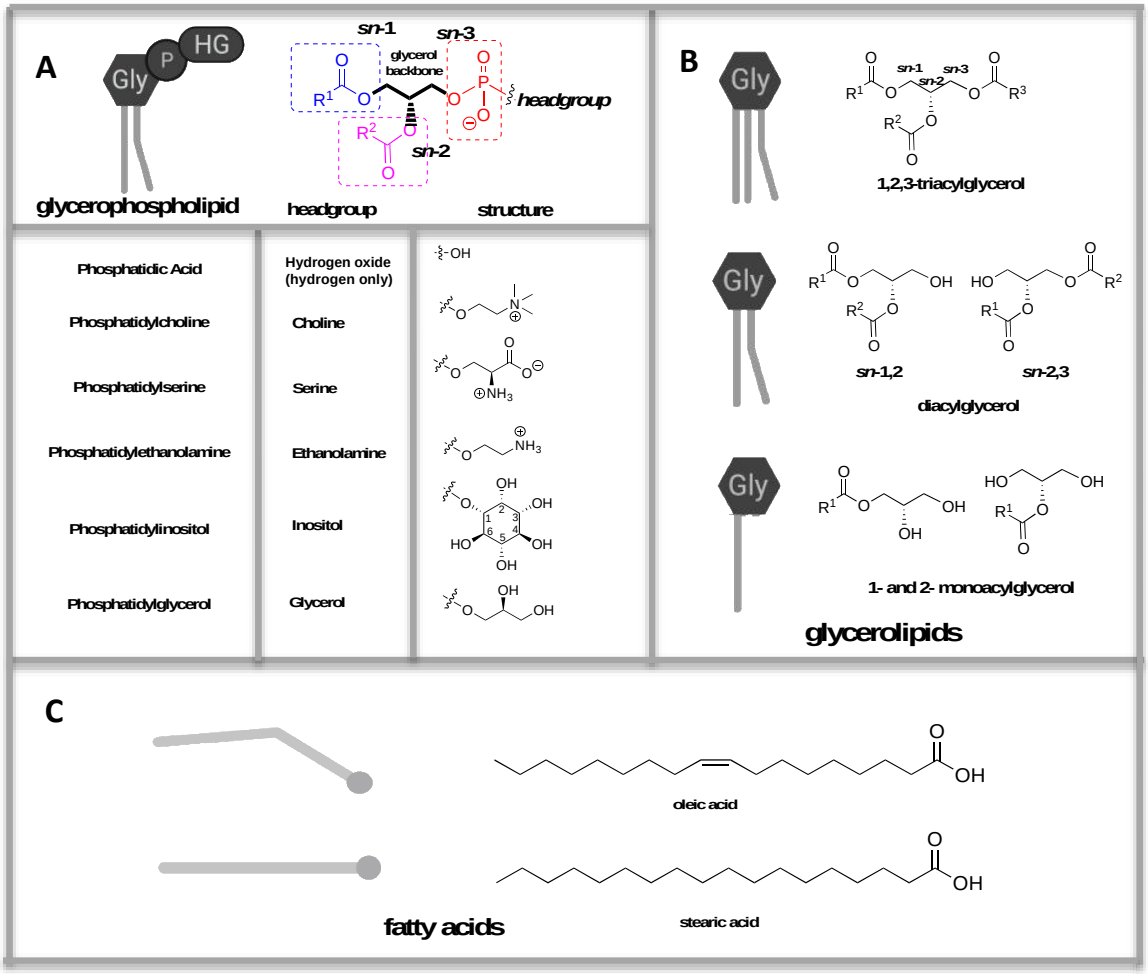

Figure 1.1. Representive structures of two lipid categories: Glycerolipids and glycerophospholipids. A. General structures of glycerophoslipids are shown and are categorized by the headgroup attached at the sn-3 position of the glycerol backbone. R1 and R2 groups at the sn-1 and sn-2 position denote fatty acyl tails. A cartoon depiction of a typical glycerophospholipid is shown on the left. Abbreviations are: Gly, glycerol; P, phosphate; HG, headgroup. **B.** On the right are structures of glycerolipids: triacylglyceorols (TAGs), diacylglycerols (DAGs), and monoacylglycerols (MAGs). **C.** Fatty acid tails are the lipid building blocks and determine lipid species depending on the number of carbons and degrees of unsaturation. Shown is an example of a FA with 18 carbons which can be saturated (stearic acid), unsaturated (oleic acid), or polyunsaturated (not shown).

further converted back into TAG for energy storage or for metabolism consumption.[10, 12] Once generated, MAGs can also serve as precursors for the synthesis of lipid mediators, such as endocannabinoids and prostaglandins, which regulate various physiological processes including inflammation, pain perception, and appetite.[12, 13]

On the other hand, glycerophospholipids or phospholipids play key structural roles in cells as they are the primary constituents of the biological membranes of eukaryotic cells along with sphingolipids, sterols, and embedded membrane proteins. Moreover, biological membranes from different tissues, cell type, and organelle carry different proportions of each of these phospholipid classes.[14] Phosphatidylcholine (PC), which contains a trimethylammonium group, is the most abundant glycerophospholipid in eukaryotes, comprising 40-50% of total phospholipids content. This is followed by phosphatidylethanolamine (PE), containing of a simple ammonium group. Certain phospholipids are found in lesser percentages in the cell. Phosphatidylserine (PS) bears a net negative charge and constitutes only 2-15% of total phospholipids in mammalian cell membranes[15] and ~20% in yeast.[16, 17] PS is mostly found in the cytosolic side (inner leaflet) of the plasma membrane and its extracellular exposure serves as an “eat me” signal for phagocytes.[18] Phosphatidic acid (PA), perhaps the simplest phospholipid, is a signaling lipid that is tightly maintained at even lower concentrations because of its regulatory roles in processes such as cell migration and proliferation.[19] Phosphatidylinositol (PI), which contains an inositol carbohydrate moiety at the polar head, is another low abundance phospholipid that plays critical roles in cell signaling.[20] In addition to the varying abundance and localization within different membranes, these lipids are also asymmetrically distributed between the inner and outer leaflet of different cellular bilayers, reflecting the different functions of the two faces of cell membranes. Neutral

phospholipids including PC, sphingomyelin (SM), and glycerolipids are more commonly found in the outer leaflets of membranes while negatively charged phospholipids such as PS and PA are more concentrated in the cytosolic side of the plasma membrane.[21]

1.1.3 Lipids in disease and disorders

As enumerated in the previous section, lipids can be utilized for fat and energy storage or for membrane components. With such complex roles and diverse structures associated with lipids, it is no wonder that dysregulation of lipid production and metabolism are often associated with human diseases.[22-24] For example, an excessive or insufficient amount of lipidic fat can have negative implications, as exemplified in nonalcoholic fatty liver disease, Type 2 diabetes, cancer, etc.[13, 25, 26] Moreover, the diverse characteristics of various lipids have shed light on their roles in cell survival and proliferation. For example, the disruption of the well-conserved membrane asymmetry and the exposure of PS at the outer cell surface has physiological consequences since these events are known to cause a bleeding disorder- Scott syndrome.[27] Moreover, the extrafacial exposure of PS is a signal for apoptosis and cell death[28] or as a beacon for macrophages to engulf and clear cells for phagocytosis.[18] Even significantly, PS is a critical biomarker since its extracellular presentation is more prominent on metastatic cancer cells than normal cells.[29] All in all, dysregulation of lipid pathways or the unnatural aggregation of a phospholipid class can alter natural biological processes and is the cause of several diseases and are diagnostics for cancer.

1.2 Approaches to lipid metabolic labeling and tracing

The ability to selectively label and analyze target biomolecules within their native environments of living cells and organisms has long been a prominent goal of biological research.[30] This endeavor has faced profound challenges due to the vast complexity of metabolic networks, in which a plethora of variations of each biomolecule are constantly undergoing nuanced transformations that alter structure and thereby dictate function, which are often dysregulated in disease.[24, 31] Therefore, it is exceedingly difficult to focus in on one particular biomolecule or family of compounds for study. Despite these challenges, the potential payoff for this pursuit is very high, as these techniques enable the tracking of features corresponding to biosynthesis, subcellular localization, and trafficking that are at the core of many fundamental biological questions.[32-35] Within this realm, lipid metabolic labeling strategies, which employ synthetic substrate analogs bearing diminutive click chemistry tags that are capable of hijacking metabolic pathways and producing tagged products in cells, have emerged as invaluable chemical tools. In this arena, strategies for the effective labeling of important lipid targets have begun to be reported, which have paved the way for initial applications of this strategy to address biological questions.[36-38]

1.2.1 Early approaches to metabolic tracing

A key challenge that needs to be overcome to achieve the production of labeled versions of products in cells pertains to problems associated with modifying natural substrates, and particularly that these modifications may suppress entry into metabolic networks. For this reason, many early labeling strategies were fairly conservative, primarily focusing on isotopically

labeled versions of native substrates, which have the benefit of most closely resembling native substrates due to subtle introduction of heavy atoms. As a result, experiments exploiting the production of isotopically labeled lipid products have been invaluable for understanding a variety of aspects of lipid biosynthesis.[39, 40]

The use of radioisotopes was a fundamental discovery, especially for elucidating various pathways of lipid metabolism. For instance, tritiated water (^3H_2O) and tritiated glucose (1-^{3}H-glucose) have been used to trace the incorporation of hydrogen atoms into fatty acids during fatty acid synthesis or degradation.[41, 42] Other examples include precursors such as glucose or acetate that have been labeled with ^{14}C, which has allowed researchers to track the fate of carbon atoms within lipids. However, coupling the metabolic incorporation of these labels with mass spectrometry and nuclear magnetic resonance techniques were found to be generally laborious and impractical.[43] Moreover, isotope labeling was routinely utilized for internal standard purposes and not as tracers for studying metabolism dynamics. Later on, it was also becoming clear that the widespread use of radioisotopes is inconvenient and unsafe. In the meantime, stable isotopes have simultaneously emerged as a more comprehensive platform in the study of metabolism.[44] Quantitative assessment of high amounts of lipid content using ^{13}C glucose was possible with the lipidome isotope labeling of yeast workflow (LILY). For the first time, the production of ^{13}C labeled yeast lipids was analyzed by high resolution mass spectrometry [45] instead of by direct infusion techniques. This technique also circumvented the laborious prerequisite of chemically synthesizing isotope-labeled lipid standards.[46] However, the disadvantage with performing these traditional techniques is that the spatial information about the lipids are lost since these methods involve bulk biochemical assays. This approach has been

limited in terms of the ability to image the localization of lipid products at the site of synthesis, although that has now changed due to advancements in mass spectrometry-based imaging methods.[47-49]

1.2.2 Methods for fluorescence imaging of lipids

Cellular fluorescence microscopy is a stalwart technique in interrogating biological systems due to the ability to analyze changes in molecular subcellular localization. The conventional imaging probes for lipids are usually fluorescent analogs of of these molecules. These can either be a simple fluorophore-conjugated lipid[50-52] or a caged photoresponsive lipid,[53] with the caveat that it must be photostable to withstand long-term studies. However, this requires the introduction of bulky fluorescent reporters onto labeled products, which often disrupts the natural lipid behavior and environment.[54] Moreover, the synthesis of fluorescent probes is typically challenging and low-yielding and the application is limited to a narrow area of research.[55]

Genetically encoded biosensors have also been utilized to track lipids *in vivo* but can be unreliable depending on the application.[56] One example of such probe is a genetically encoded green fluorescent protein (GFP) which is usually fused with domains that bind to a lipid.[57] However, these genetically encoded proteins can bind to a cluster of that lipid and may interfere with its normal cellular function. These probes could exhibit varying ligand affinity or specificity,[58] are often pH-sensitive, may have short-term photostability, and might lead to altered metabolic states.[57, 59] Thus, with such probes, great caution must be paid for misleading results in the study of native lipid metabolism and transport.

1.3 Bioorthogonal reporter strategy for lipid metabolic labeling

A key advancement in metabolic labeling came with the discovery of biorthogonal strategies for bioconjugation, involving reactions that utilize functional groups that are orthogonal to those that exist in biological systems.[60-63] Phrased another way, these reactions exploit probes bearing pairs of reactive tags that do not exist in biological systems (or minimally exist), do not react with other functional groups present in biology (or react as little as possible), but reliably react with one another under ambient conditions to produce stable labeled products. This was a longstanding challenge since, due to the vast complexity of functional groups present in nature, it is quite challenging to discover bioorthogonal reactions. A breakthrough came through the advancement of the 'click chemistry' philosophy, which focused on the development of high-yielding reactions that occur under ambient conditions utilizing 'spring-loaded' reactants.[64] These attributes translated into strong biorthogonal features for prototypical bioconjugation reactions including the copper catalyzed azide-alkyne cycloaddition (CuAAC)[65-68], and the Staudinger ligation between azide and phosphine reagents[69-72] (**Figure 1.2**).

An additional benefit of these biorthogonal conjugation reactions is that many of them employ reactive tags that are very small, such as azide and alkyne, consisting of only three and two atoms, respectively, for the tags themselves. This attribute has been key for overcoming the challenge of developing effective modified substrate analogs. Therefore, minimally modified substrate analogs strategically altered by the addition of reactive tags such as azide and alkyne could act as effective precursors for biosynthetic machinery when fed to cells so as to produce labeled downstream products via native metabolic pathways. These products bearing clickable tags can then be post-modified with bulky reporter groups such as fluorescent dyes and biotin to

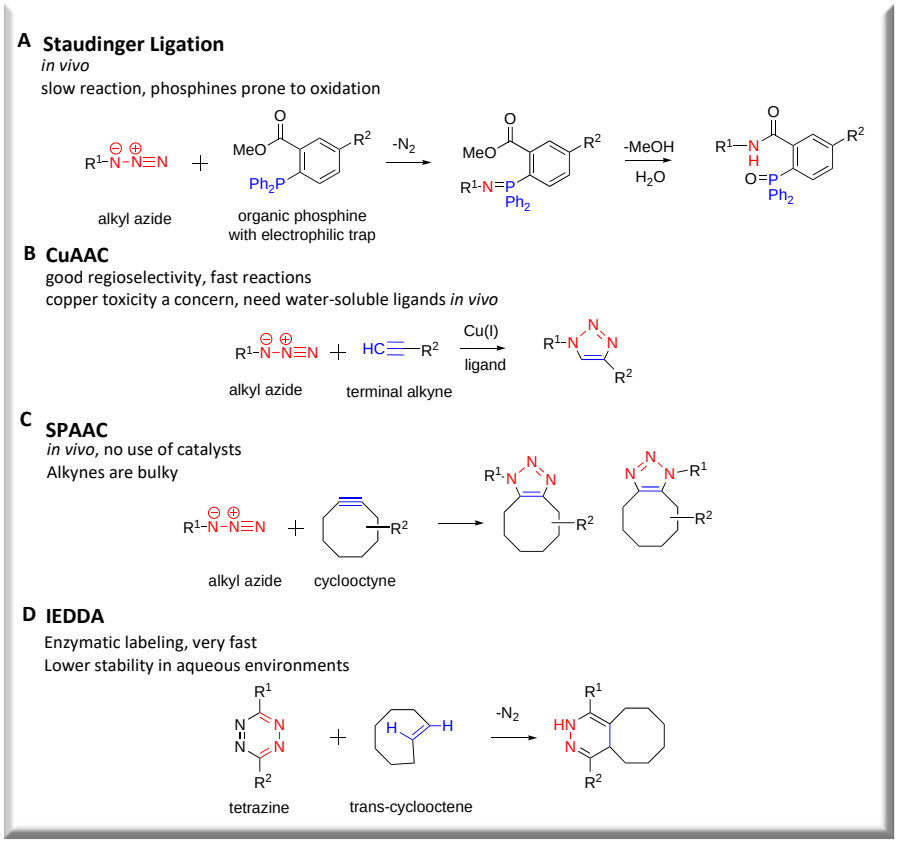

Figure 1.2. Bioorthogonal reactions. Reaction of azides with phosphines for Staudinger ligation (**A**) and terminal alkynes for the quintessential "click" reaction (**B**) were discovered as the first organic chemical reactions to be used within a biological context. Finally, Strain-promoted azide-alkyne cycloaddition (SPAAC) enabled copper-free reactions (**C**) along with the efficient Tetrazine ligation or inverse electrondemand Diels-Alder reaction (**D**).

enable selective interrogation of the progeny of the target probe. This transformative metabolic labeling procedure was first demonstrated for the labeling of cell surface glycoproteins using azide-modified mannose analogs as precursors for sialic acid-containing glycans.[73] Since that time, metabolic labeling strategies have been extended to all families of biomolecules, including carbohydrates,[74-76] nucleotides,[77-80] proteins,[81-85] and lipids,[86-88] and have led to dramatic advancements in the ability to scrutinize biological systems (**Figure 1.3**).

Concomitantly, numerous improvements have been made to bio-orthogonal reactions to balance reactant stability with reaction kinetics. A key advancement involved the development of the strain-promoted azide-alkyne cycloaddition (SPAAC),[89-91] which circumvents the need for problematic copper catalyst in click chemistry reactions. The use of copper(I) ions remains a concern despite the many efforts of implementing ligands[92] that reduce its apparent toxicity since high Cu(I) concentrations of up to 500uM have been routinely effective[93] for complete click reactions- an amount that may not be tolerated by every organism. In addition, new tags and reactions such as the inverse electron-demand Diels-Alder (IEDDA) cycloaddition reaction between tetrazine and *trans*-cyclooctene tags[94-96] have expanded the toolbox for bioconjugation (**Scheme 1.1**). The azide is the chemical reporter of choice in this work because of its small size, bioorthogonality, reaction versatility, and because it allows for conjugation via SPAAC using cyclooctyne reagents, which is particularly useful for studies performed inside live cells. Please note that while numerous conditions and reagents have been developed for these reactions, only generalized reactions are shown in **Scheme 1.1**. In addition, while we show specific combinations of probe tags and reagents in these figures, these can often be swapped (i.e. utilizing alkyne-tagged probes and azide-functionalized reagents).

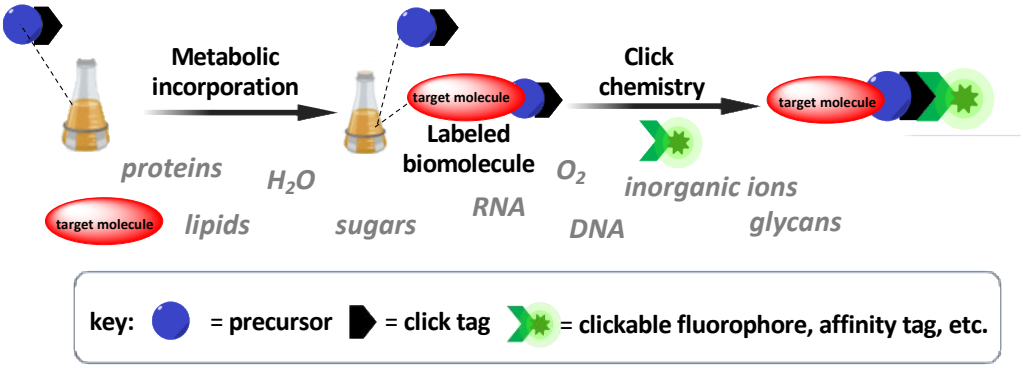

Figure 1.3. Bioorthogonal chemical reporter strategy. Example of an experimental plaform for metabolic labelling using bioorthogonal chemistry within cells. A precursor that mimics a biomolecule containing an unnatural chemical reporter or "click" tag proceeds to label the target biomolecule of interest after its metabolic incorporatioin. These labeled biomolecule products can be selectively derivatized via bioorthogonal click reactions to introduce reporter groups such as fluorescent dyes or affinity tags, thereby enabling detection of products by a range of techniques.

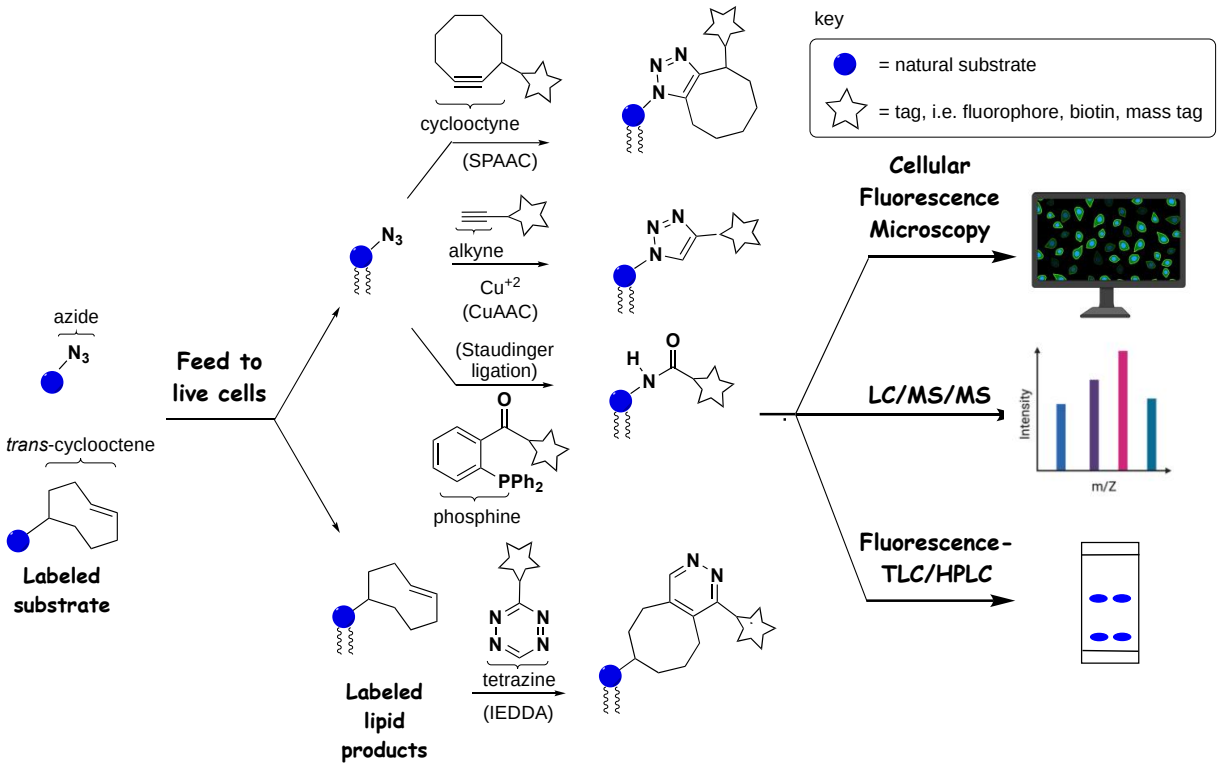

Scheme 1.1. Workflow for lipid metabolic labeling.Derivatized substrate analogs containing clickable groups such as azide, alkyne (not shown) or trans-cyclooctene can be fed to cells to enter biosynthetic pathways and produce tagged products. These products can be derivatized via click reactions including CuAAC, SPAAC, the Staudinger Ligation, and IEDDA to introduce reporter groups such as fluorescent dyes, thereby enabling detection of products by a range of techniques exemplified by fluorescence microscopy, thin layer chromatography (TLC) or high-performance liquid chromatography (HPLC), and mass spectrometry (MS).

Finally, this series of bioorthogonal reactions provides us with a toolbox from which we can select tags to attach to our precursor to label the biomolecule of interest. The location of the label, however, must also be considered since the labeling of the target lipid primarily depends on the ability of the probe to infiltrate natural biosynthetic pathways. Thus, before discussing recent labeling advances, we should take a quick peak at lipid metabolic networks which we will be the focus of the next section.

1.3.1 Overview of lipid metabolism

A simplified picture of transformations in both mammalian and yeast systems is shown in **Figure 1.4** and **1.5**, respectively. As is typical of metabolic networks, here we find a complex series of interconversions highlighted by two major pathways that are linked by feedback loops (**Figure 1.4**). G-3-P is esterified by a fatty acid coenzyme A ester (Acyl-CoA) to generate lyso-PA (*sn*-1) which is then further acylated with a FA at the *sn*-2 position to generate PA. The Kennedy Pathway commences with choline and culminates with PC, while the cytidine diphosphate diacylglycerol (CDP-DAG) pathway converts G-3-P through the intermediate PA to CDP-DAG. However, these pathways are linked via the hub of PC, PA, and diacylglycerol (DAG), which are interconverted by phospholipase, phosphatase, and kinase enzymes, and have been targets of metabolic labeling. These core pathways feed into the biosynthesis of downstream lipids including PI, PG, and PS. PI acts as the precursor for the phosphatidylinositol polyphosphate (PIP_n) family[97] as well as glycophosphatidylinositol (GPI) anchors, the latter of which are attached onto proteins to anchor them onto the surfaces of cellular membranes.[98]

Since lipid metabolic networks are often significantly different in varying organisms, we also place focus on the lipid biosynthesis and metabolism in yeast (**Figure 1.5**). In yeast, the major glycerophospholipids can be produced via *de novo* synthesis (CDP-DAG pathway) or through an exogenous pathway (Kennedy pathway).[99] PA, which is synthesized following conversion of glycerol-3-phosphate to lyso-PA, is a central metabolic intermediate that feeds into both pathways. PA can be converted to CDP-DAG, which acts as the precursor for PS, PG, or PI. PS biosynthesis occurs by reaction between CDP-DAG and serine, with the latter acting as the phosphate group acceptor via the side chain hydroxyl group. Then from PS, PE is synthesized by

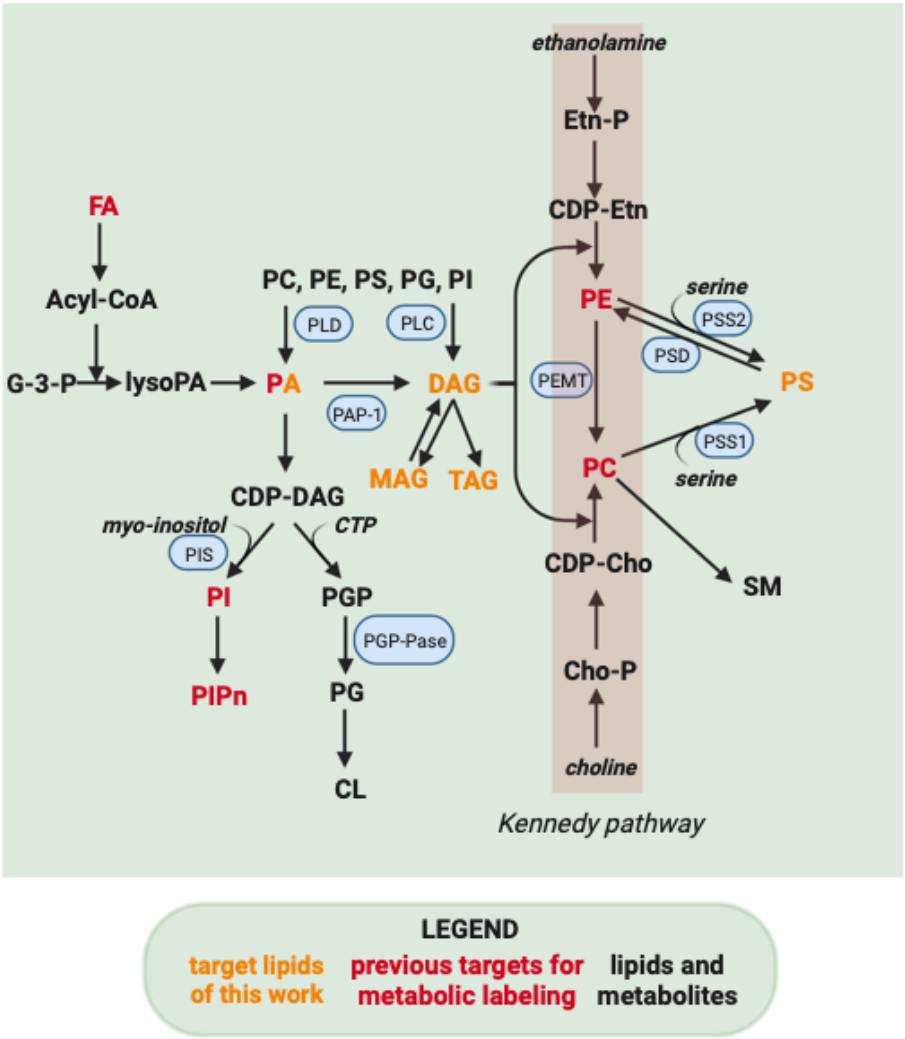

Figure 1.4. Pathway for synthesis of glycerolipids in mammals. Lipids that have been explored for bioorthogonal tagging are in red while those in orange are lipid targets relevant in this dissertation. Other lipids are in black text and their soluble precursors are italicized with the enzymes enclosed in blue. Soluble precursors: glycerol, ethanolamine, choline, serine, inositol, CTP. The abbreviations used are: G-3-P, glycerol-3-phosphate; lysoPA, lysophosphatidic acid; PA, phosphatidic acid; CDP-DAG, cytidine diphosphate -diacylglycerol; PI, phosphatidylinositol; PGP, phosphatidylglycerol phosphate; PG, phosphatidylglycerol; CL, mature cardiolipin; PS, phosphatidylserine; PE, phosphatidylethanolamine; SM, sphingomyelin; PMME, phosphatidylmonomethylethanolamine; PDME, phosphatidyl-dimethylethanolamine; CDP-Etn, CDP-ethanolamine; Etn-P, ethanolamine phosphate; PC, phosphatidylcholine; CDP-Cho, CDP-choline; Cho-P, choline phosphate; DAG, diacylglycerol; TAG, triacylglycerol; MAG, monoacylglycerol; FFA, free fatty acids. Genes and their enzymes: PSS1, PS synthase-1; PSS2, PS synthase-2; PSD, PS decarboxylase; PEMT, PE methyltransferase; PGP-Pase, Phosphatidylglycerol phosphate phosphatase; PIS, PI synthase; PAP-1, Phosphatidic acid phosphatase-1; PLD, Phospholipase D; PLC, Phospholipase C.

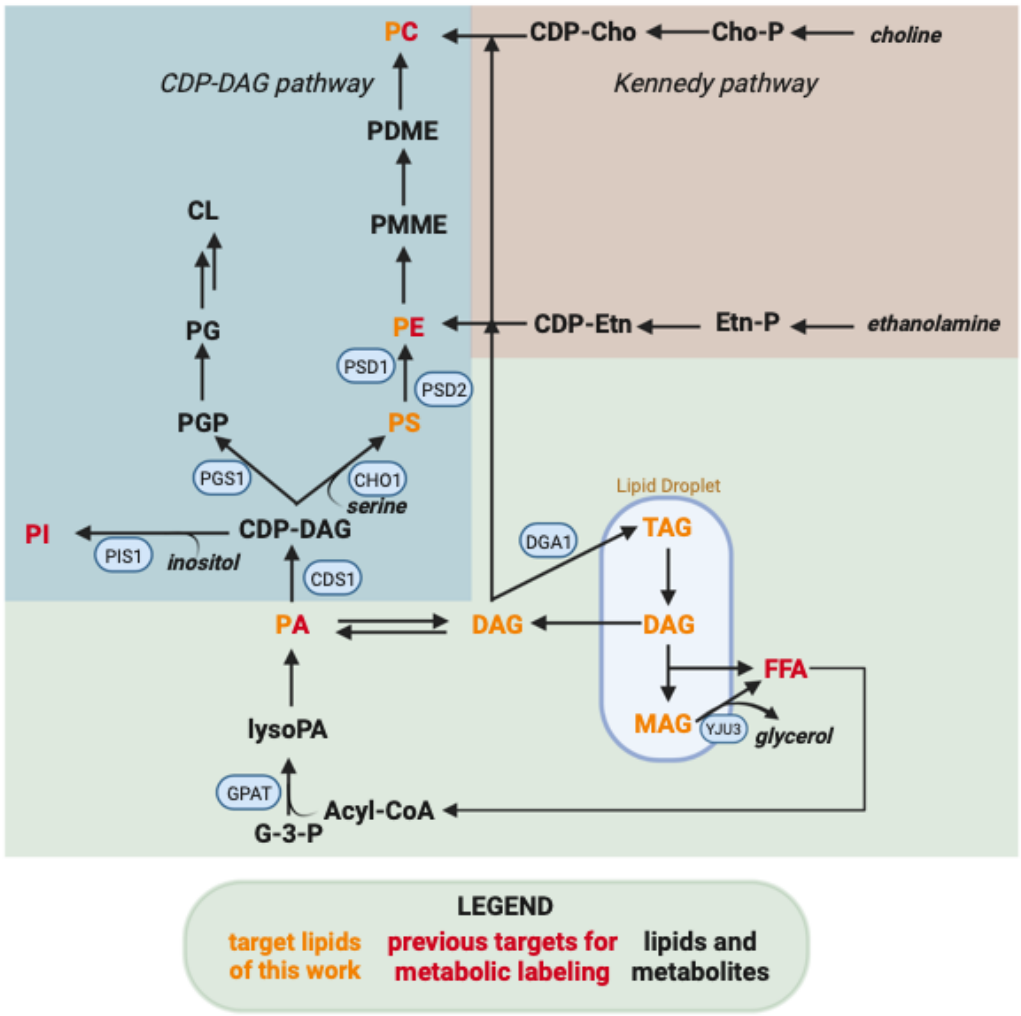

Figure 1.5. Glycerolipid biosynthetic pathways in yeast. The pathways shown are color-coded for the biosynthesis of phospholipids and relevant pathways under investigation. Lipids that have been explored for bioorthogonal tagging are in red while those in orange are lipid targets relevant in this dissertation. Other lipids are in black text and their soluble precursors are italicized with the enzymes enclosed in blue. Soluble precursors: glycerol, ethanolamine, choline, serine, inositol, CTP. Genes and their enzymes: Yju3, Monoacylglycerol lipase; Dga1, Acyl-CoA diacylglycerol acyltransferase; Cds1, CDP-DAG synthase; Pis1, PI synthase; Pgs1, PGP synthase; Cho1, PS synthase; Psd1, PS decarboxylase (Mitochondria); Psd2, PS decarboxylase (Vacuole, Endomembranes). This figure was modified from prior literature.[99]

decarboxylation via two PS decarboxylase enzymes (Psd1 and Psd2), followed by several methylation steps to generate PC. PE and PC can also be produced via the Kennedy pathway from ethanolamine and choline, respectively, along with DAG as a common precursor. Through this pathway, mutants lacking PS[100] and PE[101] synthesis when supplemented with ethanolamine can produce PC. Phospholipid catabolism or turnover can also occur through catalysis by phospholipases or lipid phosphatases (dephosphorylation of phospholipids). For example, PA can be dephosphorylated to DAG. From there, neutral lipids including DAG and TAG are also synthesized. Acyltransferase enzymes convert DAG to TAG, which is essential for formation of lipid droplets. As important is the degradation of TAG by lipases, producing DAG or MAG and essential free fatty acids (FFAs). Glycerol is also produced upon DAG conversion to MAG by Yju3 lipase.[99] All in all, these complex metabolic networks are important to keep in mind when designing substrate analogs to target particular lipid species by taking into account the different pathways by which that molecule is formed and altered.

1.3.2 Location of the click tag is critical

Metabolic labeling strategies have built upon prior work in imaging lipids in cells; for example, Schultz and co-workers demonstrated that they could deliver and image clickable PA compounds in cells.[53, 102] From there, early success was found in lipid metabolic labeling by utilizing FA analogs bearing clickable tags including azide and alkyne at the terminus of the hydrophobic acyl chain. This approach circumvents the issue of obstructing biosynthetic transformations since these tags can be conveniently hidden at the end of these long hydrocarbon chains. As a result, clickable FAs have provided tremendously important probes for

tracking fatty acid metabolism[103, 104] and characterizing proteins that undergo posttranslational lipidation processes by using strategies including post-derivatization via click chemistry, affinity chromatography purification, and mass spectrometry (MS)-based proteomics to identify labeled proteins.[105, 106] For example, Thiele and co-workers reported a sophisticated multiplexed MS platform for tracking lipid metabolism. This approach enabled single-cell analysis, high sample throughput, and enhancement of product ionization by derivatizing labeled lipids with a clickable reporter.[107] However, many applications of lipid labeling hinge upon the selective labeling of lipid molecules containing a particular headgroup which is challenging to accomplish using FA tracers since tagging the fatty acyl chain is nonspecific (**Figure 1.6A**). Alternatively, modified substrate analogs have been developed that alter the lipid headgroup in order to differentiate between lipid molecules (**Figure 1.6B**). In this endeavor, it is challenging to develop clickable precursors that can successfully mimic the native substrate for incorporation into specific lipid products. The next section highlights recent efforts utilizing headgroup labeling of precursors to generate glycerophospholipid reporters.

1.4 Strategies for metabolic labeling of glycerophospholipids

Of the biomolecule families that have been studied, the development of metabolic labeling strategies targeting GPLs has progressed at a rather sluggish pace. However, these lipids represent a key target group for studies since they act as signaling molecules that regulate critical biological processes, their subcellular localization is a key aspect for controlling their function, and due to the vast complexity of lipid metabolic networks consisting of numerous combinations of lipid headgroups and acyl chain compositions that are constantly undergoing enzymatically driven interconversions.

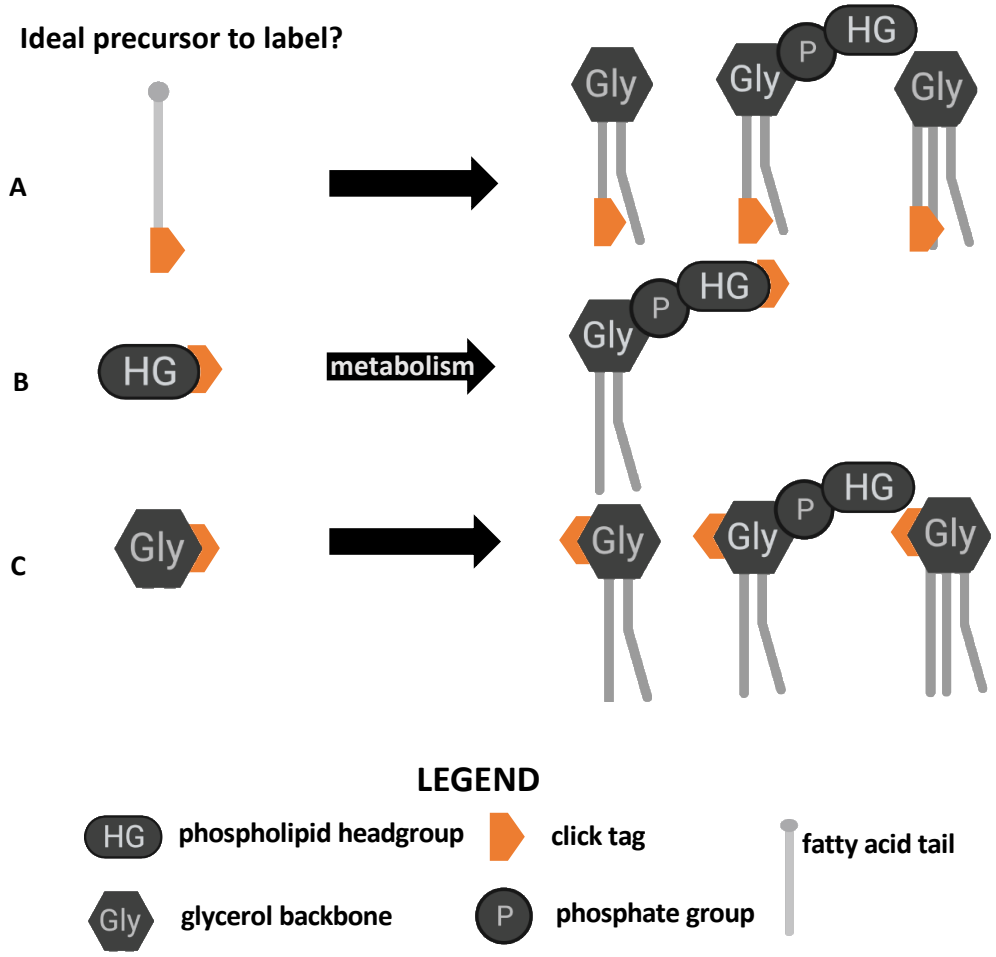

Figure 1.6. Strategies for lipid metabolic labeling using bioorthogonal click tagging of lipid building blocks. Clickable groups can be attached as a component of the fatty acid tail (**A**), the head group (**B**), or the glycerol backbone (**C**). After metabolic inporporation, the location of the cick tag will determine the classes of lipid reporters generated.

1.4.1 Labeling of PC and PA products

A pioneering effort in the field of metabolic labeling of phospholipids was the report of the labeling of PC by Salic and co-workers in 2009.[88] To achieve this, the native substrate choline was modified into propargylcholine (**PCho**) to incorporate a clickable tag into PC products (**Figure 1.7**). This modification entails the conversion of one native methyl group into the new propargyl moiety, in essence adding two additional carbons by changing one hydrogen into a CCH unit, culminating in a minor manipulation to minimize potential steric clash in the active sites of biosynthetic enzymes. Previous studies had indicated that a methyl of the choline group could be replaced with an alkyl group of up to 5 carbons to produce metabolically active substrate analogs.[108] Metabolic PC labeling via click chemistry was confirmed to be successful through dose-dependent intensity increases in fluorescence microscopy images of NIH 3T3 cells after treatment with a clickable partner azide-tagged fluorophore. This fluorescence was abrogated by treatment with phospholipase C (PLC) that decomposes PC, but restored upon treatment with PLC and EDTA, the latter of which occupies calcium that is needed for PLC activity. Fluorescence and immune-microscopy imaging experiments also showed that labeled PC molecules matched the subcellular localization of native PC, with products primarily localized at the Golgi and ER (site of biosynthesis) as well as the plasma membrane (PM) and mitochondria (to which PC is trafficked). Additionally, tandem MS experiments were performed to investigate incorporation, and observed mass peaks correlated with labeled PC products resulting from **PCho**, for which acyl chain compositions closely mirrored those of native PC. Kinetic studies indicated that staining was readily observable within 30 min and intensity increased up to 24 h, with pulse chase studies indicating that the labeled PC population remained stable. Finally, imaging studies were

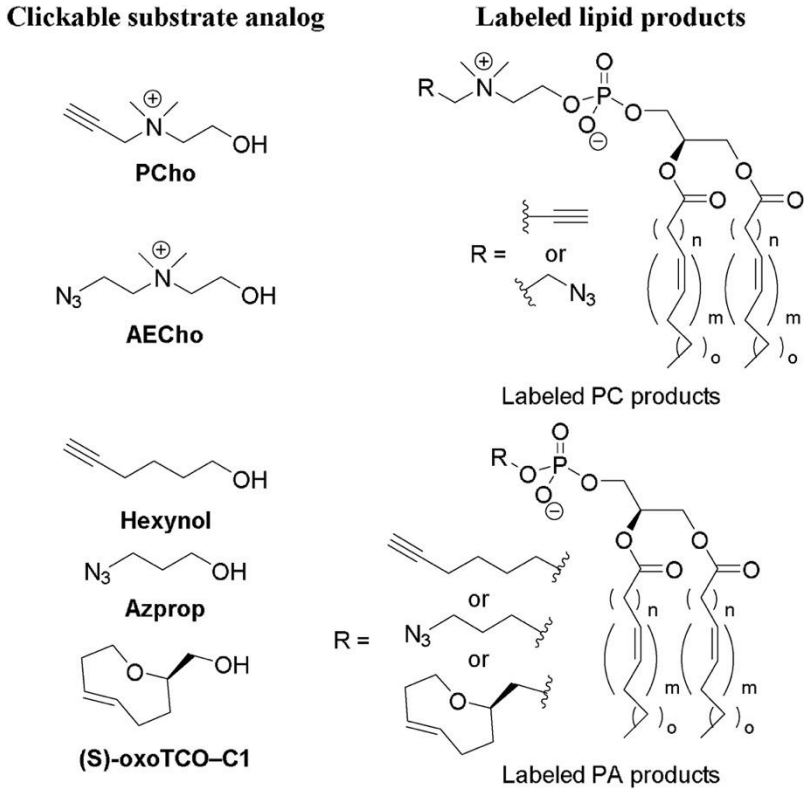

Figure 1.7. Metabolic labeling strategies for labeling PC and PA using clickable substrate analogs.

successful in mice. This result provided an exciting initial effort in lipid metabolic labeling.

In subsequent work, a two-color labeling protocol was developed for imaging different pools of PC products in cells.[109] To do so, azido-choline substrate analogs were analyzed, and while both azidoethyl- and azidopropyl-choline were found to be effective, the former (**AECho**) was determined to be incorporated more efficiently. Impressively, almost 20% of PC lipids were found to contain an azidoethyl tag at the highest concentration and after 24 hours, even in the presence of 30 μM of natural choline. For 2-color labeling, cells treated with either **PCho**, **AECho** or both were first labeled via SPAAC to selectively derivatize and image products labeled by **AECho**, which contain an appended azide moiety. Subsequently, products resulting from **PCho** were labeled by CuAAC or the Staudinger Ligation. While these two probes showed similar localization in proof-of-concept studies, this approach opens the door to differentiating pools of PC products generated under different conditions. Duan and co-workers also utilized **PCho** to develop a ratiometric labeling strategy for MCF-7 cells employing an azido-cresyl violet reagent that is blue-shifted upon CuAAC.[110]

While the prior effort achieved infiltration of the Kennedy pathway, Baskin and co-workers have explored the labeling of lipid products of PC hydrolysis by phospholipase D (PLD) enzymes, which are important due to their regulation of processes such as cell growth, division, and migration, with aberrant behavior leading to disease. Their initial reports took advantage of the discovery that hydrolysis of PC by PLD, which normally produces PA, can be intercepted using short chain alcohols to produce phosphodiester analogs of PA. Initially, alkynols including 6-hexynol (**Hexynol**) were identified as substrates for PLD, but this required post-derivatization via CuAAC, which can be problematic due to copper toxicity.[111] Therefore, in follow-up work, 3-

azidobutanol (**Azprop**) was explored as a precursor that is amenable to SPAAC derivatization (**Figure 1.7**). This approach was coined IMPACT (Imaging Phospholipase D Activity with Clickable Alcohols via Transphosphatidylation).[112] Systematic studies including fluorophore labeling and analysis via fluorescence-coupled HPLC, MS analysis of labeled products after clicking on an ammonium group to enhance ionization, and cellular fluorescence microscopy imaging revealed robust labeling of PLD products in HeLa cells. These studies took advantage of the ability to stimulate PLD activity using the small molecule phorbol 12-myristate 13-acetate (PMA) and suppress activity using the PLD inhibitor 5-fluo-ro-2-indolyl deschlorohalopemide (FIPI) as well as isoform-selective inhibitors. Fluorescence imaging studies in conjunction with colocalization markers also confirmed that labeled products primarily appeared in the ER (attributed to isoform-selective inhibitors to PLD1) and Golgi apparatus (arising from a mixture of PLD1 and 2). The former result was somewhat surprising, as PA synthesis in the ER has primarily been thought to result from acylation of glycerol-3-phosphate. Fluorescence recovery after photobleaching (FRAP) studies indicated rapid diffusion of labeled lipids in the ER but slower diffusion in the Golgi. Finally, enhanced IMPACT labeling in a subset of puncta led to the discovery that an mCHERRY-tagged PLD1 exhibited similar localization. Overall, these initial reports proved IMPACT to be a powerful tool for characterizing PLD activity.

Baskin and co-workers have recently advanced this work in different directions. First, IMPACT has been modified to develop a real-time imaging protocol for imaging PLD activity.[113] To do so, it was required to circumvent wash protocols that are typically necessary to remove unreacted fluorophores after click chemistry post-derivatization protocols. This was achieved by discovering that probe **(S)-oxoTCO–C1** bearing a bulky *trans*-5-oxocene (oxoTCO) unit was a

suitable substrate for PLD enzymes that could be modified by an IEDDA reactions using a fluorogenic tetrazine reagent. Therefore, the fluorescence signal is dramatically enhanced (1,600-fold) following post-labeling, enabling real-time imaging by circumventing the need to remove unreacted dyes. This approach extended imaging of PA production beyond the ER and Golgi apparatus to enable visualization of labeled products at the PM, which was attributed to the rapid time-scale of labeling. Furthermore, time-lapse movies captured trafficking of products out of the PM and into the ER and then the Golgi apparatus. Additional studies led to the conclusion that activation of PLD through the platelet-derived growth factor receptor (PDGFR) primarily impacted intracellular pools of PLD1, in contrast to activation by PMA or M1 muscarinic receptor (M1R), which acts primarily at the PM.

Additionally, the lab asked the question of whether propargylcholine probe **PCho** could also serve as a substrate for PLD enzymes.[114] This effort was inspired by the potential of interrogating both PC and PA biosynthesis using a single probe. When HeLa cells were activated with PMA and treated with **PCho**, labeled PA products were again detected, primarily as a result of PLD1 activity based on isoform-selective inhibitor studies. This was achieved by identifying varying conditions for targeting each pathway; short (20 min) treatment and PMA stimulation to target PA labeling via PLD as opposed to long (24 h) incubation periods in the absence of PMA to produce tagged PC products.

1.4.2 Labeling of inositol-containing lipid products

Beyond these core lipids, efforts have also recently emerged to label downstream lipid products. Much of this work has focused on *myo*- inositol-containing lipids due to the important signaling

roles of these molecules (**Figure 1.8**). In pioneering work, Guo and co-workers pursued the labeling of glyophosphatidylinositol (GPI) anchors, which cause the membrane-attachment of post-translationally appended proteins.[115] Doing so required the design, synthesis and study of clickable *myo*-inositol substrates, during which a variety of probes containing azidoethyl tags attached at the 3-, 4-, and 5-positions were pursued to avoid the 1-, 2-, and 6-positions at where *myo*-inositol is derivatized in GPI anchors. It should be noted that the synthesis of these particular probes is quite challenging since this requires enantioselective synthesis via the desymmetrization of *myo*-inositol. While initial studies indicated that these probes were not successful, probes with esterified hydroxyl groups were explored in an effort to increase hydrophobicity in order to cross membranes, after which ester moieties can be removed by intra-cellular esterase enzymes. Partially acylated probes exemplified by **4AEI** were found to be particularly effective for GPI labeling, as judged by fluorescence imaging and flow cytometry after CuAAC labeling as well as competitive inhibition through treatment with per-acetylated *myo*-inositol or phosphatidylinositol-specific phospholipase C (PI-PLC) to detach labeled proteins. In subsequent work, the Guo group sought a modified strategy by which they could enhance selectivity for labeling of GPI anchored proteins in cancer cells.[116] To do so, alternate probes were studied, exemplified by **Ac_2Lys4AIE**, in which an N^{ϵ},N^{ϵ}-diacetyl-L-Lysine (Ac_2Lys) moiety was linked via a self-immolating *p*-aminobenzyl alcohol (PABA) tether as a caging group at the 1-position of *myo*-inositol. This was designed such that the caging group would be removed by two enzymes, histone deacetylase (HDAC) and cathepsin L (CTSL), that are overexpressed in cancer, thereby selectively unmasking the substrate analog in diseased cells. This result was supported by flow cytometry and fluorescence indicating results showing that probes of type **Ac_2Lys4AIE**

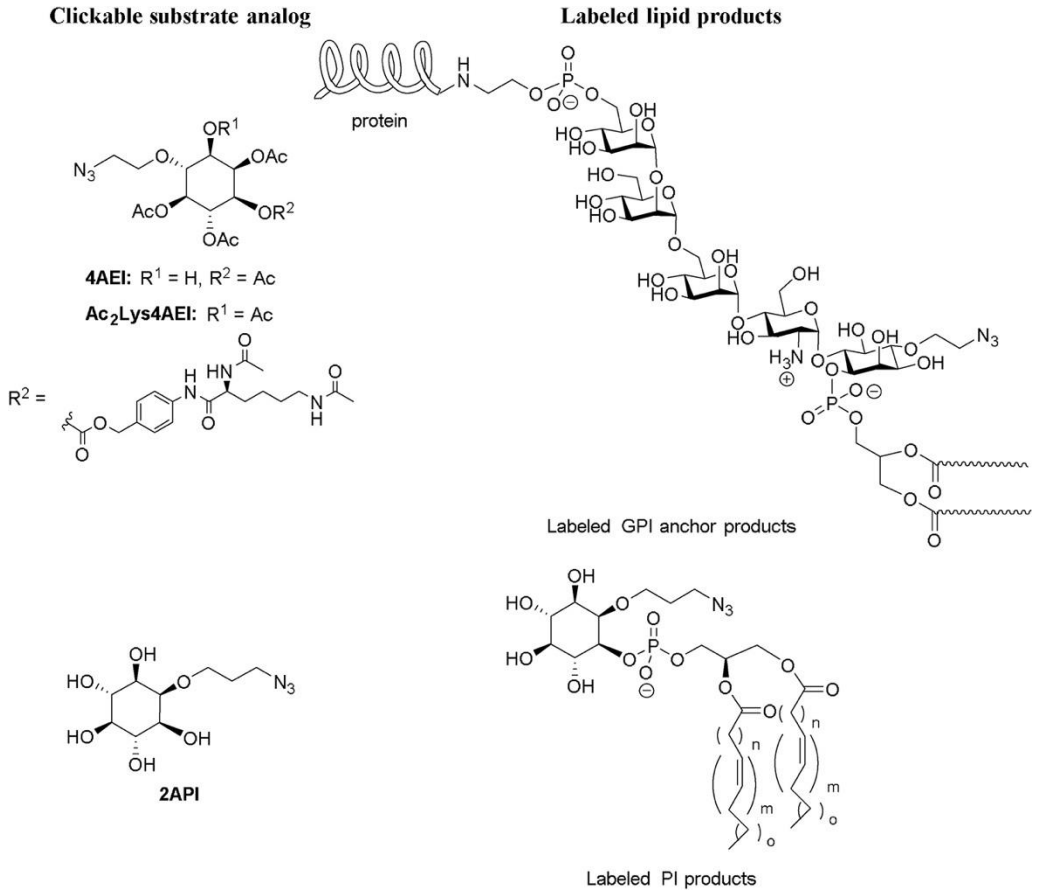

Figure 1.8. Strategies for metabolic labeling of myo-inositol-containing phospholipids.

exhibited enhanced labeling of MCF-7 breast cancer cells compared to normal human fibroblast cells (IMR-90), whereas probes of type **4AEI** resulted in similar labeling in both cell lines.

Our group has been interested in labeling *myo*-inositol-containing phospholipids including phosphatidylinositol (PI) and its downstream phosphatidylinositol polyphosphate (PIP_n) products, which are critical regulators of several key biological processes.[117] During probe development, modification of *myo*-inositol at the 3, 4, and 5 positions was avoided since these compounds are phosphorylated at those locations in nature to produce the seven core PIP_n isomers, along with the 1-position as the site of phospholipid attachment. Of the remaining 2- and 6-positions, the former was selected since inositol-1,4,5-trisphosphate (IP_3) probes modified at the 2-position have been found to effectively bind IP_3 receptors.[118-121] Therefore, probe **2API** was synthesized and studied, and found to diminish conversion of radiolabeled *myo*-inositol to PI in a cell extract PI synthase assay (**Figure 1.8**). This approach also enabled fluorescence imaging of labeled PI products in cells, which was supported by MS studies in which tagged PI products were detected as well as fluorescence-based thin-layer chromatography (TLC) experiments that yielded dose-dependent appearance of new spots that correlated with commercial PI and PIP_n standards. In this case, probe **2API** was found to be superior to peracetylated analogs. Interestingly, cell growth results were observed in which increasing concentrations of probe **2API** enhanced cell growth, in contrast to decreased growth observed when raising *myo*-inositol concentrations. This could be attributed to the potential ability of **2API** to produce important PI lipids while perhaps not repressing phospholipid biosynthesis, which natural *myo*-inositol is known to do. In addition to these articles, other clickable inositol probes have been reported as putative substrates for metabolic labeling of inositol-containing lipids.[122, 123]

While beyond the scope of glycerophospholipid labeling, we will note that success has also been achieved with sphingolipid probe development. For example, Cairo and co-workers developed clickable sphingomyelin probes and showed that sphingomyelinase enzymes still accept subsequent these compounds and products of click chemistry derivatization as substrates for hydrolysis[124]. Penno, Thiele and co-workers developed alkynyl-1-deoxysphingolipid analogs to detect restrictions in metabolism and links to mitochondrial dysfunction[125]. Wittman and co-workers have reported clickable analogs of glycosphingolipids containing mono- and disaccharides at the headgroup[126]. Finally, incorporation of azido-sugars into liposomes, either through lipidation or encapsulation, has been shown to enhance metabolic labeling of carbohydrates. [127]

All in all, a primary benefit of the lipid metabolic labeling movement is its versatility, as this technique enables a plethora of studies in which wide-ranging tags can be introduced onto labeled lipid products for detection and manipulation by a variety of techniques. Demonstrations of the applicability of this approach have rapidly progressed and have been reviewed.[38, 128, 129]

These initial reports of lipid metabolic labeling showcase wide-ranging strategies that can be invoked to successfully label important and widely variable lipid products in order to detect and study metabolism in cells. The common theme is that careful manipulation of substrate architecture, benefitting from diminutive click tags, can enable infiltration of biosynthetic machinery to produce labeled products in cells. In certain cases, enzymes can be surprisingly tolerant to substrate modifications. While these initial reports of labeling strategies have provided insights into lipid biosynthesis and trafficking, as was discussed in the prior summaries, they have also inspired numerous subsequent studies in which these techniques have been

applied for a wide range of investigations aimed at understanding lipid production and activity. This strategy has expanded applications for viral studies,[130-132] cancer imaging,[133-136] nanoparticle drug delivery platforms,[137-139] and for being utilized in conjunction with Raman spectroscopy techniques[140, 141] and electron microscopy.[142, 143]

1.5 Other advancements involving the detection and imaging of lipids

The utility of lipid metabolic labeling techniques for tracking metabolism and answering biological questions was already demonstrated in the first reports in this field. Since those initial studies, demonstrations of the applicability of this approach have rapidly progressed, and the examples that will be subsequently discussed showcase the power of metabolic labeling for studying biological processes at the molecular, cellular, and organismal levels. A primary benefit of the lipid metabolic labeling movement is its versatility, as this technique enables a plethora of studies in which wide-ranging tags can be introduced onto labeled lipid products for detection and manipulation by a variety of techniques. Labeling of PC lipids using choline probes **PCho** and **AECho**, the first of this type to be reported, has been particularly mined for applications.

1.5.1 Investigations of lipid metabolism, trafficking, localization, and protein binding

An intrinsic benefit of lipid metabolic labeling is that it enables direct imaging of the synthesis and localization of lipid products, which is invaluable for probing the complex processes of lipid metabolism and trafficking. Cairo and co-workers followed up on lipid metabolic labeling using **PCho**, **AECho** and a ketone-containing choline.[144] In doing so, they explored various live cell

imaging protocols and showed that lipid dynamics could be studied via fluorescence recovery by photobleaching, and that cells could be attached onto functionalized surfaces by click chemistry. Thiele, and co-workers used PC imaging by **PCho** to rule out exchange of lipid content at contact sites between the ER and PM.[145] In work that showed that lipid droplets (LDs) in nuclei of hepatocytes are derived from apolipoprotein B-free luminal LDs, Fujimoto and co-workers used fluorescence imaging of **PCho** labeling to demonstrate that perilipin-3-V5 decreased PC synthesis, which was reversed by a modified protein (perilipin-3-NES-V5) containing an appended nu-clear exclusion signal driving localization to the cytoplasm.[146] Liu and co-workers exploited PC lipid metabolic labeling as a tool for imaging the production and cell entry of exosomes, which are important mediators of communication and transport between cells. This was performed through both **PCho** derivatization of PC[147] as well as PLD-mediated Hexynol[148] labeling of PA. To do so, exosomes of larger sizes derived from breast cancer cell lines were enriched by centrifugation followed by fluorescence labeling. In the former study, exosomes produced by different cell lines were found to exhibit distinct variations in uptake in different organs.

1.5.2 Bifunctional lipid probes for metabolic labeling and protein crosslinking

The lipid detection toolbox continues to expand to this day and researchers are constantly developing chemical tools that allow for the simultaneous detection and imaging lipids for the investigations of lipid metabolism, trafficking, localization, and protein binding. For example, bifunctional probes have been developed as a set of tools to systematically study protein-lipid interactions and to enable visualization of lipid localization.[149-151] In these cases, bifunctional probes contain both a cross-linking group by which the probe becomes attached to bound

proteins, as well as a secondary tag that enables their enrichment and identification.[53, 152, 153] The photoactivatable cross-linking group (i.e., diazirine) attached to the lipid allows cross-linking to neighboring proteins after UV light exposure, whereas the clickable handle enables protein enrichment via biotinylation or visualization with a clickable fluorescent dye.[150, 151] A common concern with this approach is that the probe itself could enter metabolism to generate modified probes that correspond to different downstream lipids. These modified probes could then label proteins that are not bound by the original probe target, leading to false positives. Yao, Wenk, and co-workers reported an ingenious solution to this issue by exploiting metabolic labeling using **PCho** to introduce the clickable alkyne tag for post-derivatization (**Figure 1.9**).[154] Therefore, while downstream probe analogs could still be produced and label proteins, the clickable tag used for postderivatization would only be present for PC probe products resulting from metabolic labeling. Using this approach, FAs containing diazirine crosslinking groups were treated alongside **PCho** to label and identify a number of PC-binding proteins.

1.6 Conclusions and outlook

While many detection methods are known for studying DNA, RNA, and proteins, much less is known about lipids. Tracking lipids at the cellular level is a particular challenge due to the constant interconversion between lipid species that are not directly encoded in the genome. The near-impossible challenge of attempting to study lipid cell biology using traditional techniques including genetic manipulation and biochemical assays has encouraged researchers to cultivate strategies and curate efficient solutions to solve complex problems related to lipids and their roles and functions.

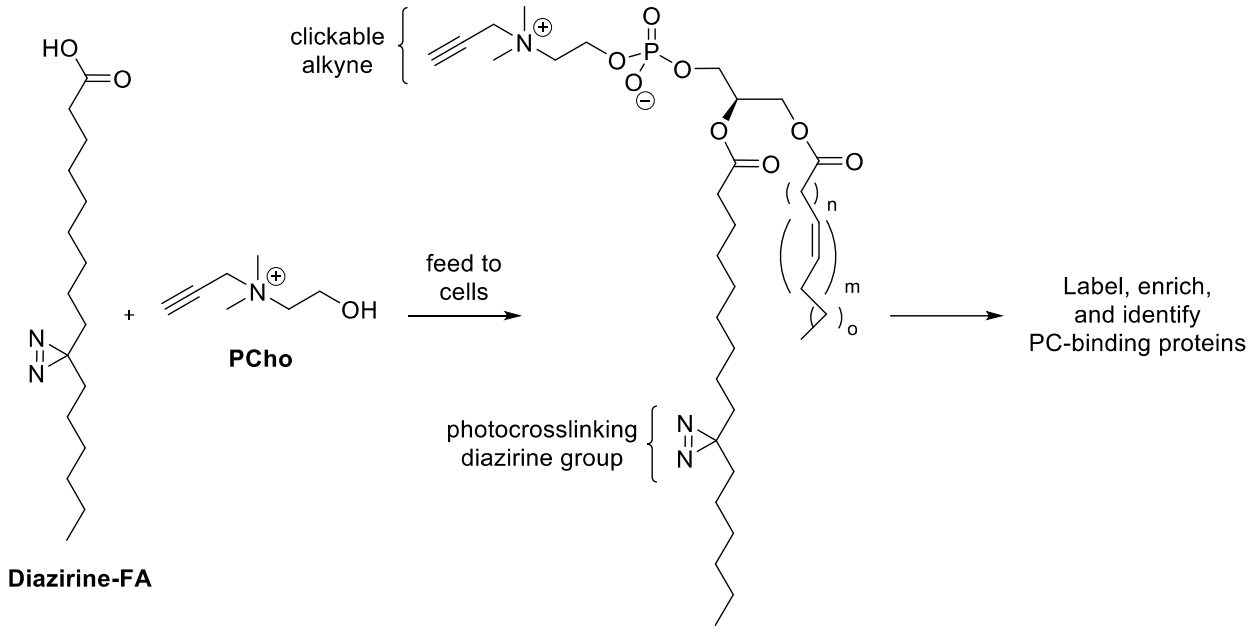

Figure 1.9. Approach using metabolic labeling to produce specific bifunctional PC probes for the global identification of PC-binding proteins. Note: the diazirine-containing acyl chain could be incorporated at different positions in labeled products.

As such, chemical biologists are constantly developing suitable tools to study lipids in their native environment to be able to 1) determine the consequences of producing a particular lipid at a particular place in a cell, 2) identify the key actors that regulate the production of specific lipids, and 3) visualize these lipids in relevant cellular compartments. Within this realm, we are particularly interested in the detection and imaging of glycerophospholipids, the most abundant lipid family, to aid in investigations of lipid metabolism and localization.

The choice of a metabolic tracer or precursor and the structural location with which to add the label has always been a huge consideration for labeling techniques. As enumerated in this first chapter, pathway-specific tracers have enabled the elucidation of the biology for a phospholipid class. Of the pathways shown in **Scheme 1.1**, successful labeling strategies have only been reported for a handful of these lipid molecules, and the work presented in this dissertation aims to fill such gaps. From (**Figure 1.6B, C**), For example, one particularly important phospholipid class has not yet been successfully labeled- the lipid phosphatidylserine. In Chapter 2, we describe how we exploited the metabolic labeling strategy to target the labeling of PS and its end-products (PE and PC). On the other hand, "unspecific" tracers, wherein the tag can be propagated throughout as many lipid classes as possible or within specific families of lipids, are equally as important. In this dissertation, we utilize lipid precursors where an azide label is attached to the glycerol backbone to more broadly label glycerophospholipids (Chapter 3 and Chapter 4) since this moiety is conserved throughout these lipid classes. Moreover, tagging of the glycerol moiety has rarely been pursued in bioorthogonal tagging so this new location could provide insight to the interactions between lipid substrate and enzyme at the molecular level.

Chapter 2. Cellular labeling of phosphatidylserine using clickable serine probes

The scientific data used in this Chapter has been published. Reprinted (adapted) with permission from Ancajas, C. F.; Alam, S.; Alves, D. S.; Zhou, Y.; Wadsworth, N. M.; Cassilly, C. D.; Ricks, T. J.; Carr, A. J.; Reynolds, T. B.; Barrera, F. N.; Best, M. D., Cellular Labeling of Phosphatidylserine Using Clickable Serine Probes. *ACS Chemical Biology* **2023**, 18, 2, 377–384. Former Best Group member S. Alam initiated studies aimed at labeling PS using a serine analog, while T.J. Ricks and A.J. Carr helped to develop lipid metabolic labeling conditions. Y. Zhou and C.D. Cassilly assisted with the growth of yeast cells and conducting PS synthase assays. D.S. Alves and N.M. Wadsworth conducted mammalian cell labeling and delivery studies that are not included in this dissertation. Otherwise, experiments were performed by C.F. Ancajas. M.D. Best, T. Reynolds, and F.N. Barrera contributed to the oversight of the project.

2.1 Abstract

Phosphatidylserine (PS) is a key lipid that plays important roles in disease-related biological processes, and therefore means to track PS biosynthesis and localization in live cells are invaluable. While lipids including PC,[88, 109, 142, 154] phosphatidic acid (PA),[112, 155, 156] glycophosphatidylinositol (GPI) anchors,[157-159] and phosphatidylinositol (PI)[117] have been successfully labeled via precursor labeling strategy, PS has not, to our knowledge, been thus far amenable for the development of bioorthogonal labeling strategies. Herein, we describe the

metabolic labeling of PS in *S. cerevisiae* cells using analogs of serine, a PS precursor, derivatized with azide moieties at either the amino (**N-L-SerN$_3$**) or carbonyl (**C-L-SerN$_3$**) groups. The conservative click tag modification enabled these compounds to infiltrate normal lipid biosynthetic pathways, producing tagged PS molecules, as supported by mass spectrometry studies, thin-layer chromatography (TLC) analysis, and further derivatization with fluorescent reporters via click chemistry to enable imaging in yeast cells. This approach shows strong prospects for elucidating the complex biosynthetic and trafficking pathways involving PS.

2.2 Significance of phosphatidylserine and its importance as a lipid metabolic target

2.2.1 PS in mammalian cells and cancer detection

Phosphatidylserine (PS) is an important biomarker that participates in diverse biological processes. PS acts as a ligand for a number of proteins, thereby driving their membrane association through non-covalent protein–lipid binding interactions.[160] A well-studied example involves Annexin A5,[161] a protein that responds to PS membrane translocation and is involved in key anti-coagulation events,[162, 163] antiphospholipid antibody syndrome,[164, 165] and has been used for imaging apoptotic cells.[166] The latter application arises since, under normal conditions, PS is primarily localized within the inner leaflet of the plasma membrane, but it is translocated to the outer leaflet during apoptosis.[167-169] In fact, a flow cytometric technique exists to detect dead cells via fluorescent labeled PS-binding protein Annexin V.[170]

Apoptosis is a natural physiological process,[171] but when regulation of apoptosis is lost, cancer cells can proliferate. Just like in apoptotic cells, the extracellular exposure of PS is also

observed in certain cancers.[169, 172] As such, PS can serve as an effective biomarker for tumors. However, it is important to note that specific biomarkers exist for the variety or types of cancer cells; thus, PS has largely been utilized for the diagnosis of broad ranges of cancer.[29] Consequently, PS is a promising target for cancer therapy. Typically, this is done by blocking PS either using monoclonal antibodies[173] or liposomal carriers.[174, 175] Our lab has in fact explored the potential of labeled PS as a way to specifically deliver liposome carriers.[176] However, utilizing PS for cancer therapy under such techniques still requires extensive review before they can be considered for clinical applications.[177]

2.2.2 PS in yeast

The biosynthesis of PS and PE plays a vital role in the pathogenesis of yeast *Candida albicans.*[178] In a 2018 study by Cassilly and Reynolds, loss of PS synthesis, and effectively, loss of cell wall integrity was partially attributed to avirulence of *C. albicans.*[179] In *S. cerevisiae*, PS concentration increases during bud emergence compared to the lipids PC and PE. PS was found in higher concentrations during budding (for cell growth and proliferation) and was determined to polarize at budding neck membranes compared to the membrane mother cell.[180]

2.2.3 Biosynthesis of PS in yeast

Despite the significance of lipids such as PS, the ability to track the biosynthesis and transport of lipid molecules *in vivo* remains a substantial challenge due to the complexity of lipid biosynthetic pathways. The abundance and subcellular localization of lipids are tightly controlled

through complex biosynthetic and trafficking networks, including vesicle- and protein-mediated transfer, and defects in any of these processes typically result in disease.[98, 181-185] While PS biosynthesis can occur through a variety of pathways depending on the organism, these processes generally exploit serine as a substrate for an exchange reaction with a lipid. For example, yeast convert cytidine diphosphate-diacylglycerol (CDP-DAG) and serine into PS and cytidine monophosphate (CMP) (**Figure 2.1**), while mammalian cells instead utilize serine for transphosphatidylation of phosphatidylcholine (PC) or phosphatidylethanolamine (PE). Another pathway for PS production involves the acylation of lyso-phosphatidylserine (LPS), a lyso-lipid that has also garnered interest for involvement in biological events including inflammatory processes.[186] PS can be converted back to these precursors through deacylation to LPS or through decarboxylation to PE followed by methylation to PC.

2.3 Design and synthesis of azido-serine probes

The choice of precursor and location for adding the click tag are important considerations for lipid metabolic labeling. We began by designing tagged analogs of serine since this is the common and direct precursor of PS production. Since the serine side chain hydroxyl group is required for linkage of the headgroup to the glycerolipid scaffold of PS, the remaining carboxyl and amine groups were both pursued as attachment points for the introduction of clickable tags, giving probes **N-L-SerN$_3$** and **C-L-SerN$_3$** (**Scheme 2.1**). We focused on azide-labeled probes to enable live-cell imaging applications through derivatization via SPAAC (copper-free click chemistry) using cyclooctyne-containing reagents, which could be complimented with labeling in cell extracts through CuAAC. We also envision that chromatographic separation by LC followed

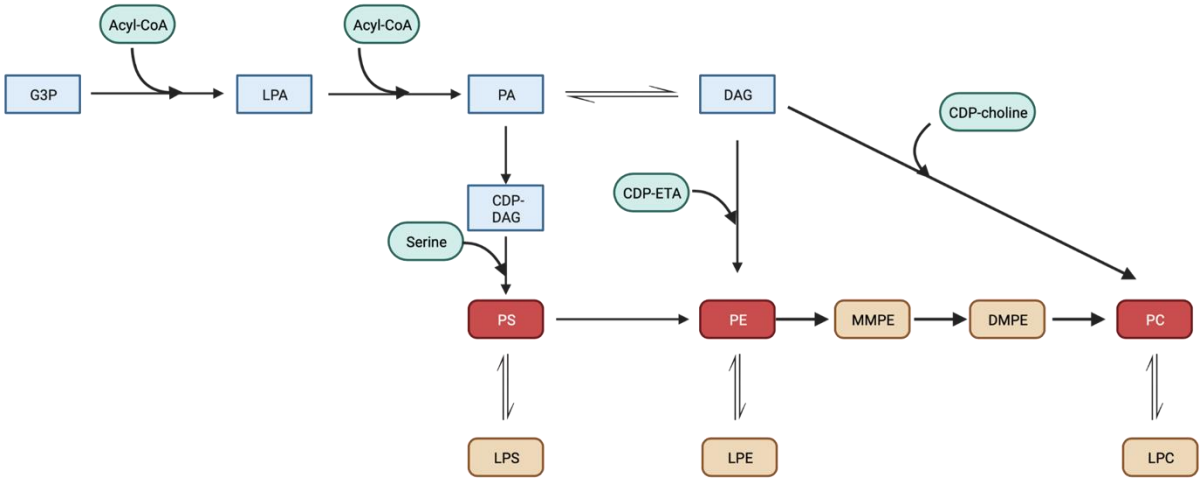

Figure 2.1. Partial yeast phospholipid biosynthetic routes showing pathways involving phosphatidylserine (PS). Click-tagged products that were detected by mass spectrometry in this study are shown in red. This figure was modified from prior literature.[187]

by MS will enhance our ability to confirm metabolic labeling by this approach to label PS and PS lipid products (**Scheme 2.1**).

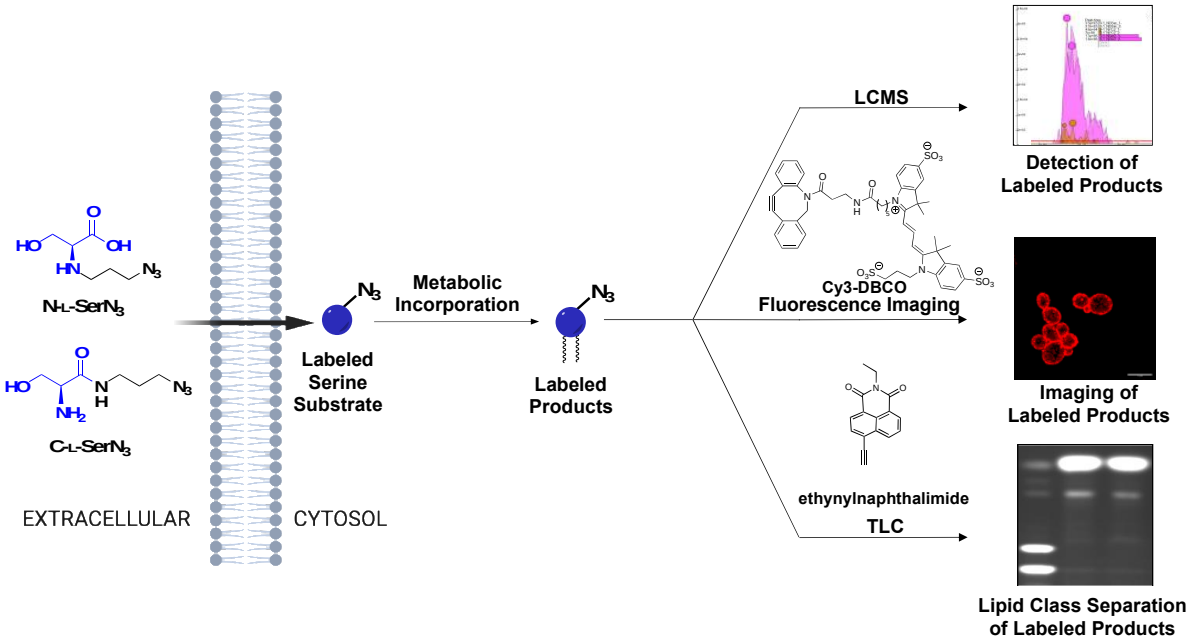

Scheme 2.1. Chemical tagging of serine for the labeling of PS lipid products. Metabolic labeling of PS by azdio-serine precursors and detection by mass spectrometry, fluorescence microscopy imaging using clickable **Cy3-DBCO** and TLC imaging via copper-catalyzed azide-alkyne cycloaddition (CuAAC). Scale bar indicates 5 µm.

Compound **N-L-SerN$_3$** contains a clickable azide tag attached via an azidopropyl moiety appended to the amino group of serine. We envisaged this compound to be a favorable serine mimic since it can retain a positive charge on nitrogen when protonated at neutral pH. This probe was synthesized from *O*-tert-butyl-L-serine *tert*-butyl ester **2.1** (**Scheme 2.2**) through alkylation with 1,3-dibromopropane to bromide **2.2**, substitution with azide to **2.3,** and deprotection to **N-L-SerN$_3$**. This compound was synthesized from a modified route which utilized bromopropylazide for alkylation from **2.1**.[188] Moreover, our new route avoids previously encountered over-alkylation or cyclization byproducts with the addition of N-methyl morpholinium chloride to **2.2**.

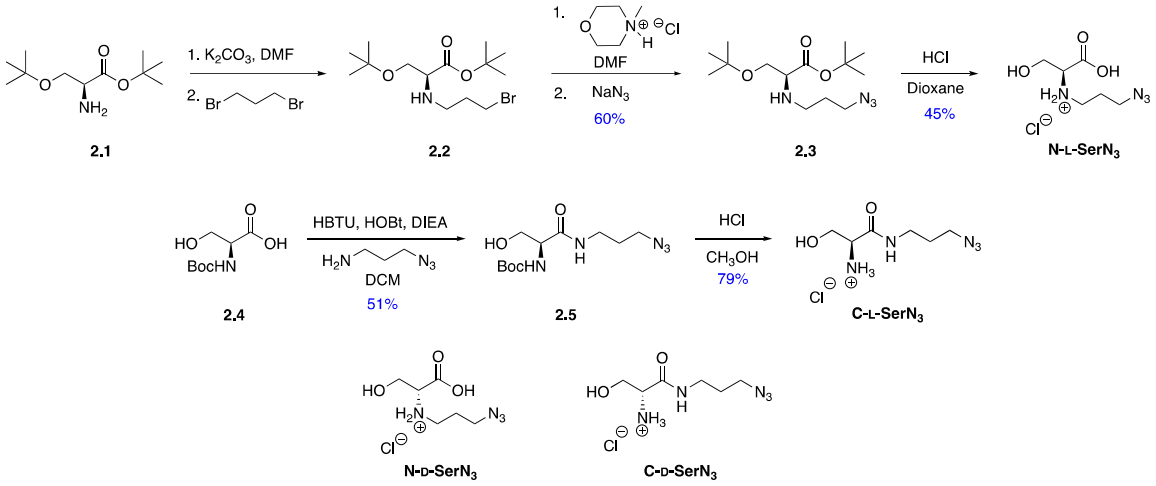

Scheme 2.2. Synthesis of clickable serine probes N-L-SerN$_3$ and C-L-SerN$_3$ and structures of control probes N-D-SerN$_3$ and C-D-SerN$_3$.

Additionally, we developed probe **C-L-SerN$_3$** by instead appending an azidopropyl chain to the C-terminus of serine by forming an amide bond. This probe modifies the charge of serine by removing the carboxylate moiety that prefers the negatively charged state at physiological pH. However, as will be discussed further in subsequent labeling experiments, we hypothesized that probe **C-L-SerN$_3$**, when incorporated into labeled PS molecules, may deter further metabolism resulting from decarboxylation into PE. This probe was synthesized from *N*-Boc-serine **2.4** through amide bond coupling to azidopropanamine to **2.5** and then Boc deprotection to produce **C-L-SerN$_3$**.

For both of these probes, enantiomeric versions **N-D-SerN$_3$** and **C-D-SerN$_3$** were synthesized by the same routes using starting materials with the opposite stereochemistry. Following synthesis, we confirmed that the optical rotations of these compounds were of equal value and opposite-in-sign of rotation for compared to the original enantiomer probes **N-L-SerN$_3$** and **C-L-SerN$_3$** (see characterization data, Section 2.6.2). It has previously been shown by an *in vitro* assay that D-serine does not compete with L-serine as a substrate for the yeast PS synthase

enzyme Cho1p until a supracellular concentration of 200 mM D-serine is supplemented, indicating the stringent stereochemical requirements of this enzyme for the natural substrate.[189] Thus, D-serine probes provide valuable negative controls for these studies that are structurally similar to the designed serine substrate analogs.

2.4 Results and Discussion

2.4.1 Cytotoxicity of azido-serine probes

With these serine probes prepared, we first sought to determine whether these compounds exhibit a deleterious effect on cell growth. Experiments were performed using *S. cerevisiae* cells, which contain significant similarities to mammalian cells in terms of the genes, enzymes, and pathways associated with lipid metabolism,[99] and for convenient access to abundant cell samples. Cells were grown in the presence or absence of each probe (1.5 mM) and measurements of optical density at 600nm (OD_{600}) were used to track optical density over time during cell culture. Following preliminary experiments at different probe concentrations, we selected 1.5 mM as a value similar to intracellular serine concentrations of ~2mM[190] and was determined from fluorescence microscopy experiments (Section 2.4.4.1). As can be seen in **Figure 2.2**, the resulting growth curves and doubling times for cells that were incubated with **N-L-SerN$_3$** or **C-L-SerN$_3$** or untreated were very similar, indicating that these probes do not cause cell toxicity at the concentrations tested. This was quite different from our previous work on PI labeling in which an azido-tagged *myo*-inositol probe yielded deleterious effects on growth.[117] In the case for probes **N-L-SerN$_3$**, **C-L-SerN$_3$** and **N-D-SerN$_3$**, the doubling times were not significantly

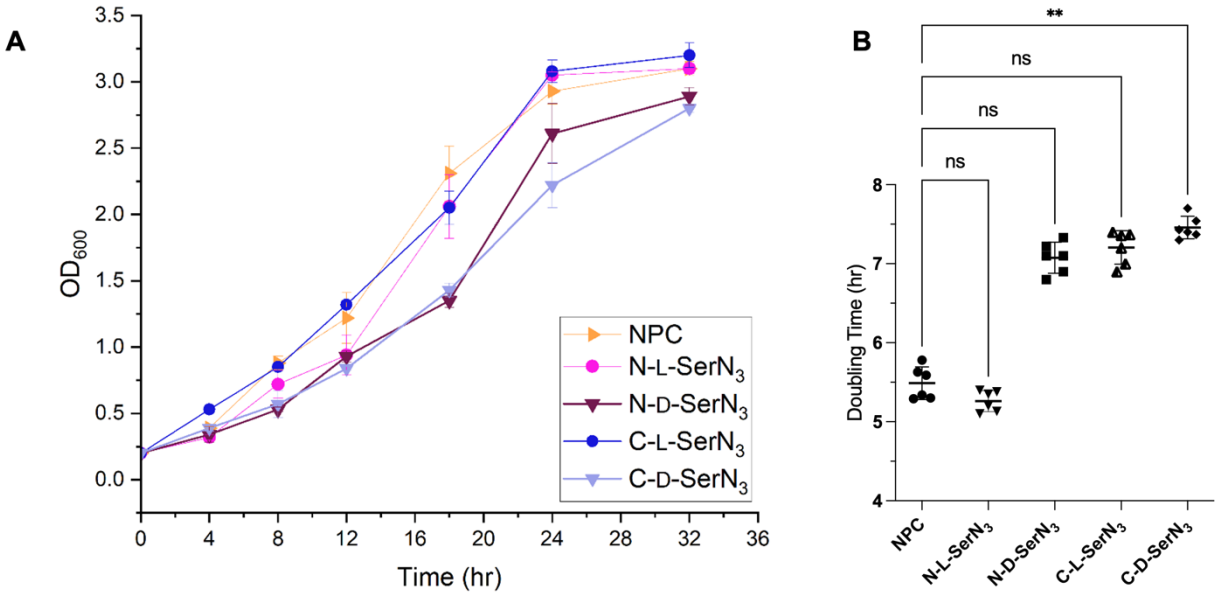

Figure 2.2. Growth of Saccharomyces cerevisiae in the presence of 1.5mM $SerN_3$ probes. A. Growth curves of S. cerevisiae cells grown in 2% galactose media in the presence of study probes (**N-L-$SerN_3$** or **C-L-$SerN_3$**) or D-serine control analogs (**N-D-$SerN_3$** or **C-D-$SerN_3$**) and in Milli-Q water (no probe control, NPC). A culture sample was taken and read for optical density through exponential phase and stationary phase at the indicated time points. Error bars indicate standard errors from six biological replicates. **B.** Doubling time calculated from growth curves in the exponential phase (from 4-18 hr). Statistical analysis was performed using Brown-Forsythe and Welch ANOVA tests, and the post-hoc analysis compares each L-serine or D-serine analog to control (**: $0.001 < p < 0.01$; ns: not significant). Note that the doubling times for **N-L-$SerN_3$**, **C-L-$SerN_3$**, and **N-D-$SerN_3$** were not significantly different from control (**NPC**).

different from that of cells not supplemented with probe, however the doubling time for **C-D-SerN$_3$** was significantly different from control (**Figure 2.2B**). Interestingly, the enantiomeric probes **N-D-SerN$_3$** and **C-D-SerN$_3$** both resulted in a slight decrease in final cell growth.

2.4.2 Confirming Fluorescence Labeling of Lipids in *S. cerevisiae* via SPAAC

We next pursued cellular fluorescence microscopy experiments as an initial step to determine whether these probes enable cellular labeling of PS or lipids in *S. cerevisiae* cells (**Scheme 2.3**). In these studies, we imaged products labeled by these probes via SPAAC using dibenzocyclooctyne-Cy3 (**DBCO-Cy3**). Cells were grown in either the presence or absence of probes **N-L-SerN$_3$**, **C-L-SerN$_3$**, **N-D-SerN$_3$**, or **C-D-SerN$_3$**, and then incubated with the fluorophore **Cy3-DBCO**, washed to remove unbound dye, fixed, and subjected to confocal fluorescence microscopy. As can be observed in **Figure 2.3**, both probes **N-L-SerN$_3$** and **C-L-SerN$_3$** yielded robust fluorescence labeling of cells, while the enantiomeric control probes **N-D-SerN$_3$** and **C-D-SerN$_3$** resulted in virtually no signal (**Figure 2.3A-E**). Furthermore, signal resulting from **N-L-SerN$_3$** and **C-L-SerN$_3$** treatment was observed to be localized at the plasma membranes of these cells.[14, 191]

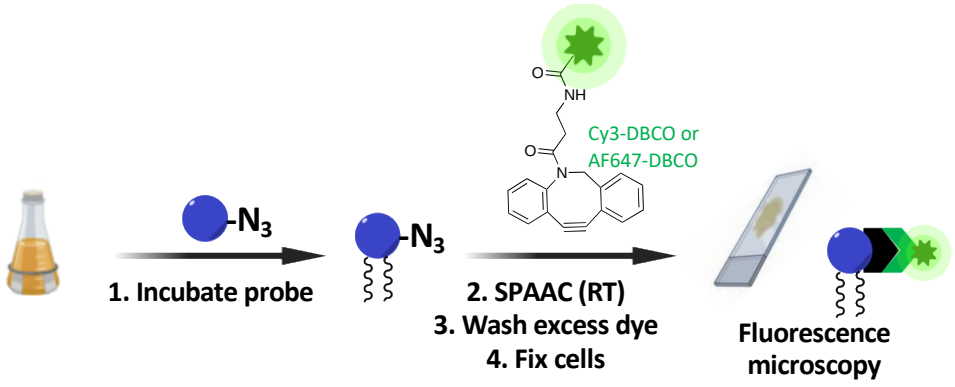

Scheme 2.3. General experimental outline for fluorescence microscopy and flow cytometry. Cells were washed to removed media and subjected to SPAAC with clickable Cy3-DBCO or AF647-DBCO. After washing excess dye, cells were fixed prior to imaging via confocal microscopy.

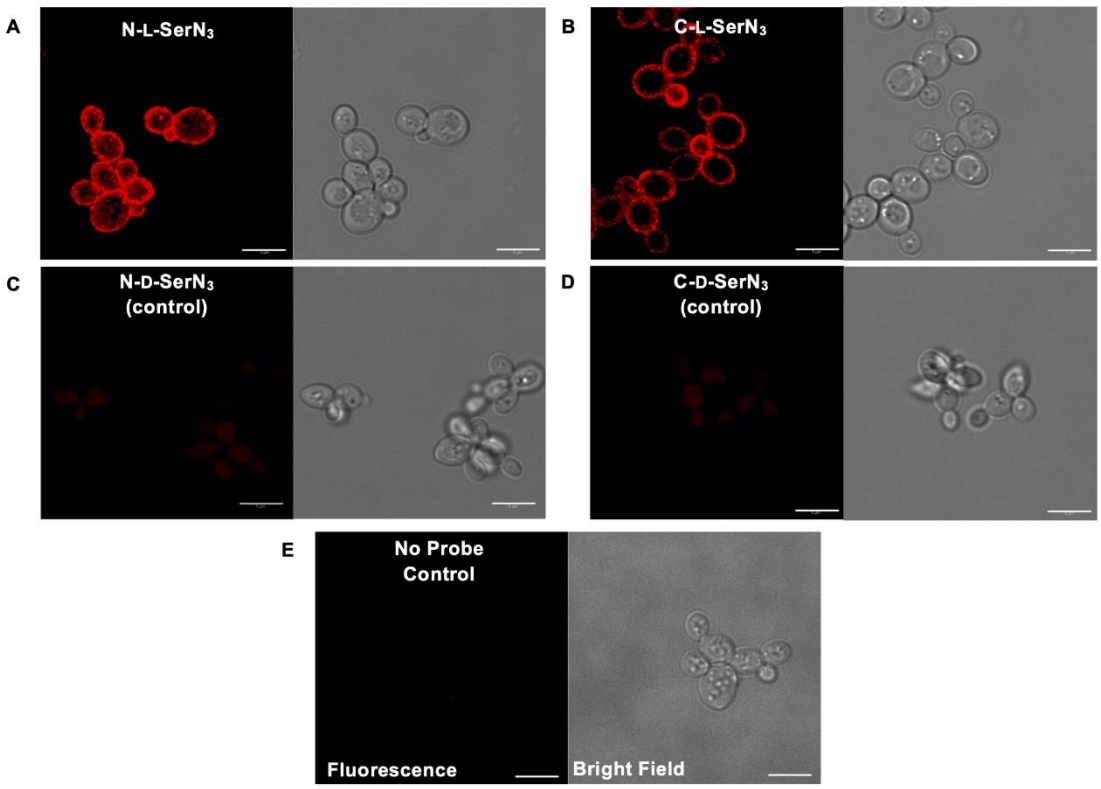

Figure 2.3. Fluorescence and brightfield micrographs of S. cerevisiae cells grown with serine probes. Yeast cells incubated with **N-L-SerN$_3$** (A), **C-L-SerN$_3$** (B), **N-D-SerN$_3$** (C), **C-D-SerN$_3$** (D) (1.5 mM), or negative controls lacking probes (E) were harvested at log phase and incubated with Cy3-DBCO (1 µM) for fluorescence labeling by SPAAC, and then fixed. Only cells treated with probes **N-L-SerN$_3$** (A) and **C-L-SerN$_3$** (B) showed fluorescence (red), which is localized to the cell plasma membrane, with all control cells exhibiting minimal signal. Bright field images are included to show the locations of cells. Scale bars denote 5 µm.

To further analyze localization of fluorescence, we performed colocalization experiments utilizing CellBright® DiD, a known plasma membrane tracer. We observed that fluorescence from both **N-L-SerN$_3$** and **C-L-SerN$_3$** coincided with DiD signal (**Figure 2.4**). To aid in interpreting colocalization of the two tracers, we calculated Pearson's Correlation Coefficients (*R*) between Cy3 and DiD fluorescence. The *R* values corroborated the confocal images wherein the SerN$_3$ probes resulted in a high degree of plasma membrane localization (**N-L-SerN$_3$**, *R* = 0.85; **C-L-SerN$_3$,** *R* = 0.76) while control samples resulted in lower *R* value (*R* = 0.31) that likely results in some residual dye being retained in the plasma membrane. The observed signal is in accordance with the known localization of PS yeast: In yeast, PS is more concentrated in the PM than the ER.[192] While we expected some fluorescence from the ER since PS also resides within the ER (site of phospholipid synthesis) and only minimally abundant in other organelles.[14,193] It is possible that particularly prominent localization at the plasma membrane compared to the ER may result from the former being more accessible to the **Cy3-DBCO** dye based on permeability, timing of the experiment, and other conditions. For example, like **Cy3-DBCO**, some disulfonated dyes can be cell permeable but their hydrophilic nature could prevent them from accumulating at specific organelles in the cell.[194] While the ER is the known biosynthetic site for PS, our labeling and click timescale as well as the fixation method does not allow us to track the point from which labeled PS is produced and trafficked to the PM. Nevertheless, these localization patterns from **N-L-SerN$_3$** match that of the expected PS abundance at the PM for yeast. Finally, these results demonstrate that **N-L-SerN$_3$** and **C-L-SerN$_3$** are effective for cellular labeling and that inversion of the lone stereocenter in each of these compounds abrogates labeling properties. Moreover, these data indicate that our probes allow for stereospecific labeling of cellular membranes.

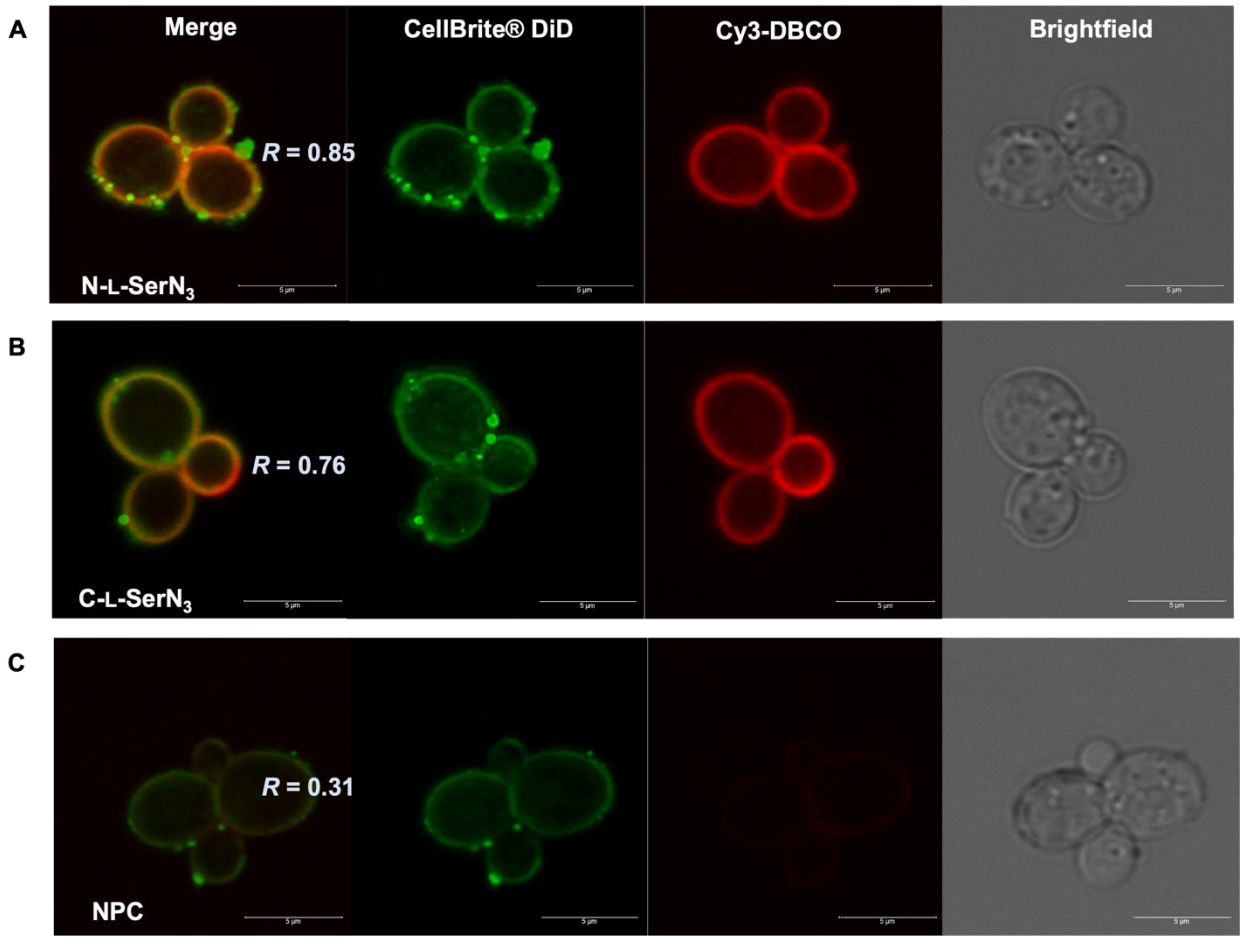

Figure 2.4. Colocalization analysis of click-based fluorescence from N-L-SerN$_3$ and C-L-SerN$_3$ with plasma membrane dye CellBright® DiD. *S. cerevisiae* cells were grown with **N-L-SerN$_3$** (**A**), **C-L-SerN$_3$** (**B**), or negative controls lacking probe (**C**), followed by click with DBCO-Cy3 (1 µM) and incubation with CellBright® DiD (1 µM), which localizes to the plasma membrane. After sequential scanning, the two channels for Cy3 and DiD fluorescence were merged and shown in the left column. Pearson's correlation coefficients (PCCs) were determined to aid in colocalization analysis of the two fluorescence signals using FIJI's Coloc2 plugin. PCCs were calculated from 30 cells per sample from 6 biological replicates (180 cells total). Note that clumping of DiD, a phenomenon that is common for this dye, was consistent for all samples from independent trials including controls. Scale bars indicate 5µm.

We also observed during **C-L-SerN$_3$** labeling experiments that fluorescence signal appeared to be enhanced in budding cells (**Figure 2.5**). This is in line with prior work by Grinstein and co-workers, in which detection of PS in *S. cerevisiae* using fluorescently labeled protein (GFP-Lact-C2) exhibited polarized fluorescence at the bud cortex and bud necks of live cells.[180] These results provided additional evidence that labeled molecules resulting from serine probes correlated with known PS localization in support of our belief that this strategy can be used in conjunction with microscopy to track PS in live cells. On the other hand, we did not observe enhanced fluorescence labeling in budding cells treated with probe **N-L-SerN$_3$** (see for example **Figure 2.3A**). We speculate that this disparity may result from PS labeled by this probe being diverted to a greater extent into downstream lipid products through decarboxylation into labeled PE, methylation into tagged PC, and further lipid metabolism. This hypothesis was analyzed through additional experiments that will be discussed in the next sections.

2.4.3 Flow cytometry analysis of cellular labeling from azido-serine probes

Having observed variations in fluorescence profiles between both sets of L-serine and D-serine probes, we next conducted flow cytometry experiments to quantify differences in fluorescence intensity among these samples. For these experiments, the flow cytometry wavelength options required us to switch to a different clickable dye for labeling. Therefore, we instead employed an AF647-DBCO dye that is active for SPAAC. Flow cytometry analysis of these cell samples (**Figure 2.6A**) was effective for confirming enhancements in fluorescence for cells labeled by **N-L-SerN$_3$** and **C-L-SerN$_3$** compared to the enantiomeric probes **N-D-SerN$_3$** and **C-D-SerN$_3$**. Fluorescence signal from click reaction with AF647-DBCO was also consistent with localization patterns observed from DBCO-Cy3 incubated cells (**Figure 2.6B**).

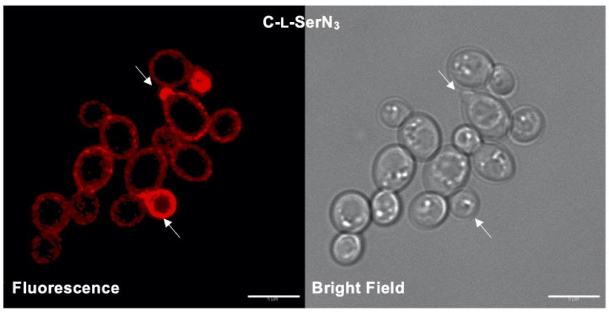

Figure 2.5. Enhanced labeling of budding cells was observed for *S. cerevisiae* cells treated with C-L-SerN$_3$. Persistence of enhanced fluorescence signal at budding sites (labeled with arrows) was observed in 15 ± 4 sets out of 50 randomly selected budding cells. Quantification was performed for 6 biological replicates. Scale bars denote 5 µm.

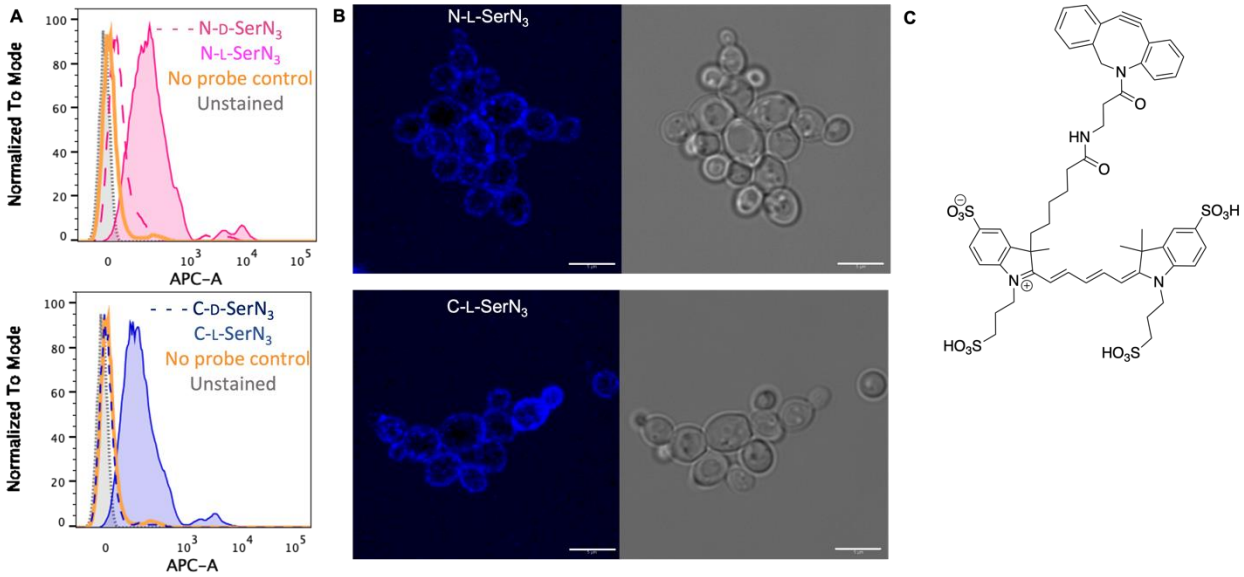

Figure 2.6. Flow cytometry analysis of S. cerevisiae cells incubated with SerN$_3$ probes. A. Representative flow cytometry histograms of S. cerevisiae cells that have been incubated with (**top row**) **N-L-SerN$_3$** probe or (**bottom row**) **C-L-SerN$_3$** probe, fixed with PFA, then treated with AFDye™ 647 DBCO. The x-axis represents AF647-DBCO fluorescence detected in the APC channel and the y-axis represents relative number of cells for six biological replicates. **B.** Representative fluorescence microscopy images for cells clicked with AF647-DBCO to ascertain similar fluorescence and localization patterns (cell membrane) as cells treated with **Cy3-DBCO** fluorophore. Scale bars indicate 5µm. **C.** Structure of AFDye™ 647 DBCO dye (AF647-DBCO or Cy5-DBCO).

2.4.4 Optimization of metabolic labeling and SPAAC

2.4.4.1 Fluorescence microscopy sample preparation and dye concentration

When planning fluorescence microscopy experiments, there are many critical considerations regarding dye compatibility, concentration of dye, fixative and permeabilization reagents, washing steps, control and negative samples, etc. During the course of this project, we established a few workflows that are suitable and time-efficient for completing lipid metabolic labeling experiments. Methanol permeabilization resulted in oversaturated fluorescent images from both control and $SerN_3$-treated cells. To overcome the issue of high cytoplasmic fluorescence and to avoid extraction of lipids, methanol permeabilization was replaced with paraformaldehyde fixation. Next, the determined optimal DBCO-Cy3 concentration was 1 µM after comparing images from cells incubated with the following concentrations: 0.2, 1, 5, and 10 µM, wherein 5 or 10 µM dye displayed oversaturated cells when observed on the Cy3 channel. The initial dye washing procedure of washing cells with cold 20% DMSO-MilliQ solution was also replaced with simple MilliQ washes to avoid solubilization and removal of lipids of interest. After optimization steps, two general protocols were followed with the difference being the order of fixation and SPAAC. The first protocol involves performing SPAAC labeling followed by fixation. The other protocol requires the fixation step to be performed before SPAAC for experiments with the multi-sulfonated dye, AF647-DBCO for semi-permeabilization.

Optimal serine probe concentration was tested by performing fluorescence microscopy. Cells were incubated with various concentrations of **N-L-SerN$_3$** and **C-L-SerN$_3$** probe (1, 1.5, 2 mM) and were subjected to SPAAC with 1.0 uM DBCO-Cy3 to compare fluorescence images. The concentration of 1.5 mM of **N/C-L-SerN$_3$** was shown to have higher fluorescence compared to no

probe control fluorescence and was thus deemed sufficient concentration for our studies (data not shown), in conjunction with growth curve experiments. Preliminary quantitative analysis of fluorescence was performed on Fiji (ImageJ2) software from replicate fluorescence micrographs. The mean cellular fluorescence intensity was calculated as corrected total cell fluorescence or CTCF by manual selection of fluorescing cells as regions of interest (ROI) per image (180 cells across images). However, over time, this method proved to be inefficient when analyzing several trials and replicates and so quantifying fluorescence via flow cytometry was instead employed.

2.4.4.2 S. cerevisiae growth and serine probe incubation time

Labeling experiments need to be carefully performed to avoid non-specific signal. For example, we considered that unmetabolized serine probes derivatized by DBCO-Cy3 dye might contribute to background fluorescence, owing to an intrinsic challenge with metabolic labeling regarding the incomplete conversion of tagged probes into labeled products. This can be minimized through vigorous washes to remove unreacted probe. To address this possibility, following labeling studies until mid-log phase (OD~0.6, 8 hr incubation) the initial media containing serine probe was rinsed out and replaced with fresh growth media for 4 more hours until late exponential growth (OD~1.0). By doing this, any residual cytosolic serine probes are expected to be further metabolized while ensuring that no more exogenous serine probe is entering cells at the same time. As can be seen in **Figure 2.7**, there was no observed difference in fluorescence for cells re-incubated in fresh media without probe when compared to those grown through the original growth procedure (**Figure 2.3**). This supports that fluorescence signal is not resulting from unmetabolized serine probes.

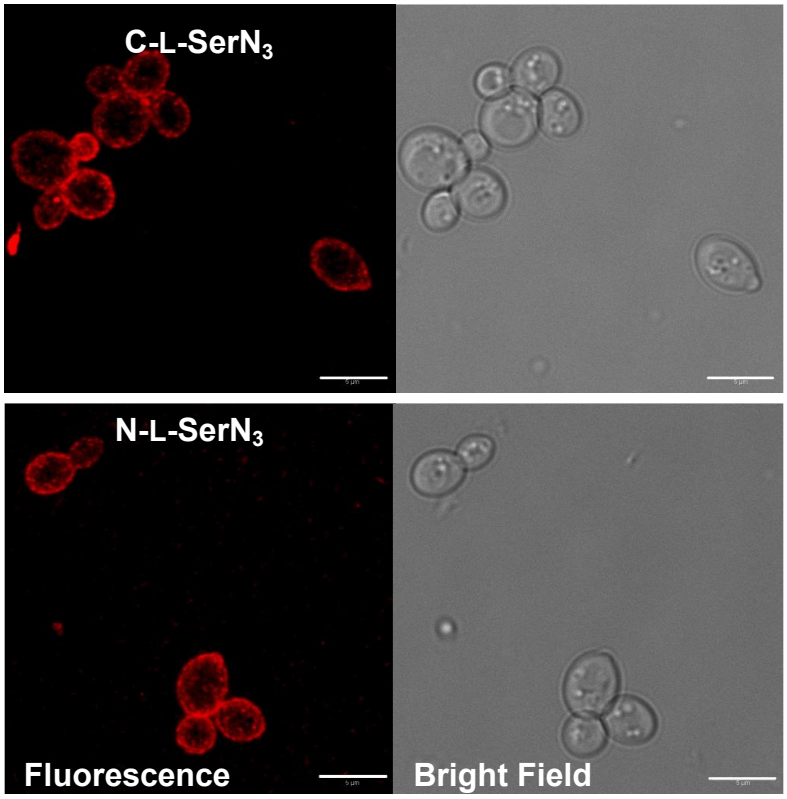

Figure 2.7. Images of cells after re-incubation to medium without $SerN_3$ probe still show fluorescence localization at the plasma membrane. S. cerevisiae cells were subjected to standard labeling procedures (1.5mM **N-L-$SerN_3$** or **C-L-$SerN_3$**) except that by mid-log phase of OD~ 0.6, initial media was removed, and cells were washed resuspended in fresh growth media without serine probes for 4 more hours. Cells were fixed, clicked with Cy3-DBCO, washed to removed excess dye, and imaged. Scale bar indicates 5µm.

2.4.5 PS probes are recognized by the ps synthase cho1p

As an initial step to directly evaluate whether these serine probes interact with PS biosynthetic machinery, we assessed their ability to inhibit the activity of PS synthase (Cho1p) from *C. albicans* for the conversion of natural serine to PS. The group of Todd Reynolds in UTK Microbiology has previously developed a robust assay utilizing cell membrane extracts containing Cho1p to convert tritium-labeled serine (^{3}H-serine) and CDP-DAG into isotopically labeled PS (^{3}H-PS).[178, 189, 195] Moreover, these experiments were performed using *C. albicans* cells since this organism is similar to *S. cerevisiae* in terms of PS biosynthetic pathway and the structure of its PS synthase enzyme (alignment of *Ca*Cho1 and *Sc*Cho1 amino acid sequences in Clustal Omega revealed 60.52% sequence identity).

These experiments showed that ^{3}H-PS production was diminished by probes **N-L-SerN$_3$** and **C-L-SerN$_3$** in a dose-dependent manner (**Figure 2.8**). Statistical analysis showed that **N-L-SerN$_3$** and **C-L-SerN$_3$** concentrations of 1, 5, 10, and 25 mM displayed significantly decreased enzyme activity. It should also be noted that significant inhibition was observed at a probe concentration (1 mM) that is lower than intracellular serine levels (~2 mM).[190] A plausible explanation for this inhibition is that these probes interact with Cho1p in a manner that competes with or blocks conversion of ^{3}H-serine to ^{3}H-PS, thereby providing evidence that these compounds effectively interact with target PS synthase enzyme of *C. albicans*. All PS Synthase Assays were performed by Yue Zhou in collaboration with Dr. Todd Reynolds' lab in the Microbiology Department.

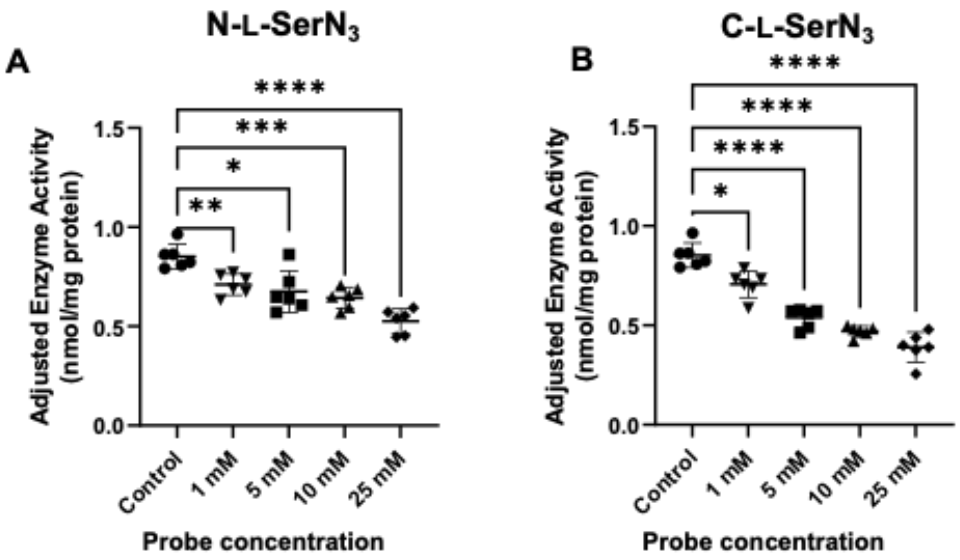

Figure 2.8. PS synthase activity assays from N-L-SerN$_3$ or C-L-SerN$_3$. Assays were performed using various concentrations (1, 5, 10, and 25 mM) of **N-L-SerN$_3$** (A) or **C-L-SerN$_3$** (B) showed that both of these probes interfere with ^{3}H-serine conversion into PS. All concentrations were compared to control (*: 0.01 <p < 0.05; **: 0.001 <p < 0.01, ***: 0.0001<p < 0.001; ****p < 0.0001). Statistical analysis was performed using Brown-Forsythe and Welch ANOVA tests. Error bars indicate standard errors for 6 biological replicates.

2.4.6 PS probes hijack lipid metabolic pathways

2.4.6.1 TLC and LCMS analysis of lipid extracts from n-tagged azido-serine probes

We next employed different techniques to determine whether these probes are in fact labeling PS. One avenue entailed mass spectrometry-based lipidomics analysis to detect lipid products bearing the added clickable handle. To do so, we generated lipid lysates (Bligh and Dyer method)[196] from *S. cerevisiae* cells grown in the presence or absence of each tagged serine analog and subjected them to LC/MS. Probe **N-L-SerN$_3$** resulted in the detection of azide-tagged products corresponding to PS, but also downstream lipids including PE and PC (representative spectra shown in **Figure 2.9**), containing the major fatty acids known to be present in *S. cerevisiae*.[192] Peaks matching expected labeled products were observed in negative mode, with retention times that were comparable to natural lipid standards (**Table 2.1**). Each of the lipid products that was observed would be expected based on phospholipid biosynthetic transformations (see the pathway substrates in **Figure 2.1**). Our results support that serine probe **N-L-SerN$_3$** is effective as a substrate for conversion to PS, after which it can then undergo decarboxylation to PE derivatives and then methylation to PC analogs. These peaks corresponding to labeled lipids were not observed for negative control probe **N-D-SerN$_3$**, further underscoring that inversion of stereochemistry rendered this molecule ineffective for labeling lipids, as suggested by our microscopy studies. Importantly, these data validate that incorporation of the clickable tag at nitrogen does not compromise the normal entry into multiple lipid biosynthetic pathways. After lipid extract sample preparation, LC/MS experiments were handed to Nick Trybala and were run at the Biological and Small Molecule Mass Spectrometry Core (BSMMSC).

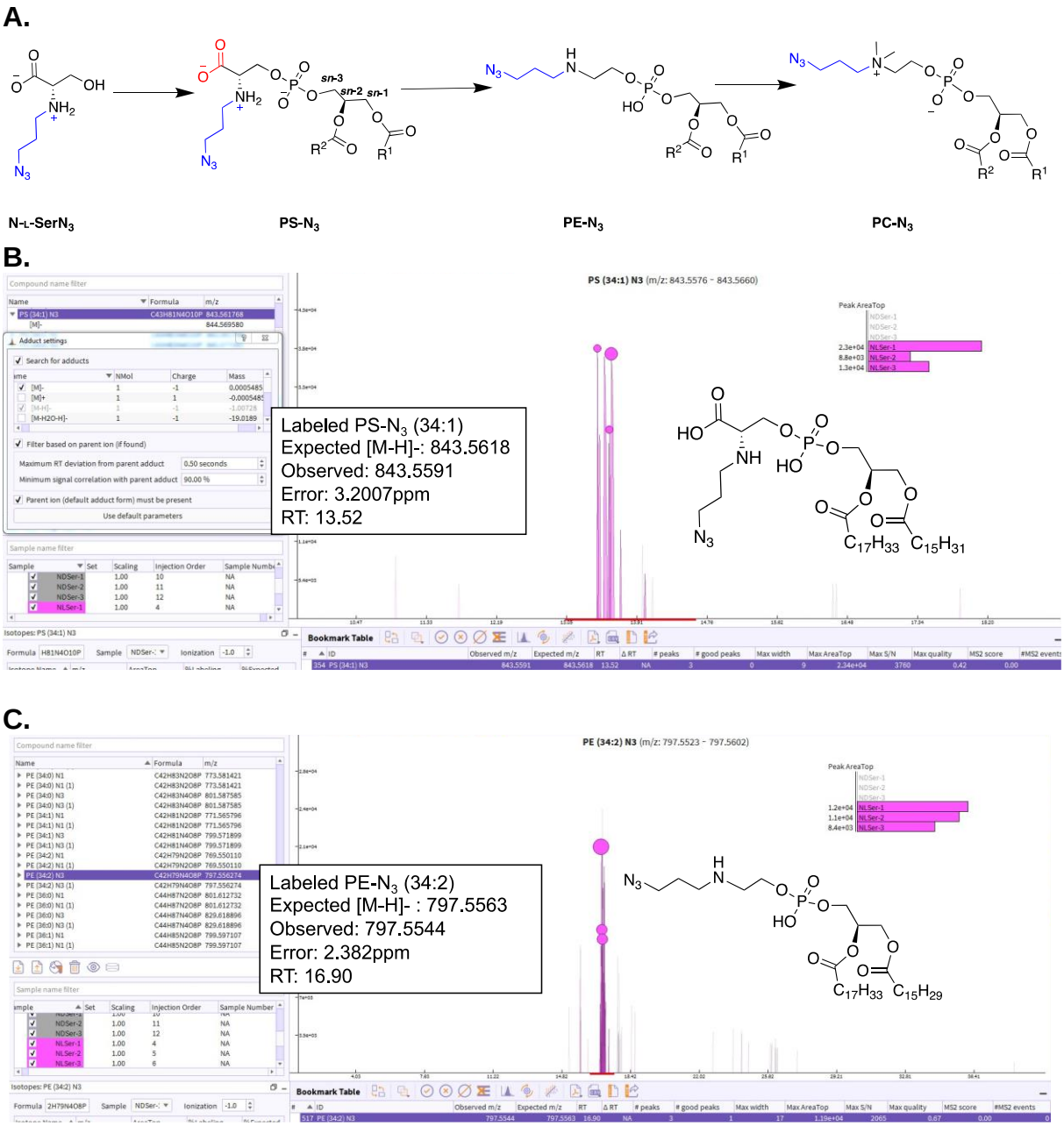

Figure 2.9. Representative mass spectra for click-tagged products of probe N-L-SerN$_3$. Products were detected by liquid chromatography mass spectrometry (LCMS) (compared to control **N-D-SerN$_3$**). **A.** General structures for N-L-SerN$_3$-labeled lipids including PS-N$_3$ decarboxylation to PE-N$_3$ and methylations to PC-N$_3$. On the mass spectra screenshots, structures are shown that match detected mass peaks for labeled PS (**B**) and PE (**C**). The x-axis shows the retention time from LC separation while the y-axis indicates the areas of peaks containing the relevant mass ion based on ion counts. The colored inset shows plots of peak areas and depicts three replicate samples treated with **N-L-SerN$_3$** (pink NL_Ser), and control, **N-D-SerN$_3$** (gray ND_Ser). Each spectrum is labeled with the expected and observed masses from detection in negative mode. Labeled lipids were identified (C12 isotope as parent peak) comparing the exact mass (±5 ppm) to a generated compound list

Table 2.1. Detected labeled PS, PE, and PC products in negative ion mode from cells incubated with N-L-SerN_3 probe. Retention times are shown and correlated to that of the observed RT for detected native lipid of the same lipid species. PC is detected as the formate adduct (FA = formic acid).

lipid	Calculated mass	Detected mass	Error (ppm)	RT	native lipid observed RT	native lipid
PS-N3 (32:2) (M-H)	813.5148	813.5112	4.425	14.67	11.97	PS (32:2) (M-H)
PS-N3 (34:1) (M-H)	843.5618	843.5591	3.201	13.52	12.70	PS (34:1) (M-H)
PE-N3 (34:2) (M-H)	797.5563	797.5544	2.382	16.90	17.59	PE (34:2) (M-H)
PC-N3 (36:1) (M+FA-H)	901.6400	901.6369	3.438	19.00	19.80	PC (36:1) (M+FA-H)
PC-N3 (34:1) (M+FA-H)	873.6087	873.6074	1.488	17.48	18.05	PC (34:1) (M+FA-H)

We also analyzed **N-L-SerN$_3$**-labeled lipid extracts via TLC separation following CuAAC with a fluorogenic ethynylnaphthalimide dye. Figure **2.10B** depicts an image of a representative TLC plate after click derivatization, while **Figure 2.10A** displays spots after primulin staining to indicate native lipids, with R_f values of lipid standards included on the left side of the figure. Note that click-derived fluorescence spots after CuAAC were visualized by fluorescence imaging before the same TLC plate was subjected to primulin staining for vieiwing natural lipids and the lipid standards. Lipid standards were included for each TLC run to identify classes of lipids and to distinguish click-labeled spots. Labeled cells that were harvested during exponential growth (lane 4*) yielded new fluorescence bands, while those obtained from stationary phase (lane 5*) did not (**Figure 2.10B**). These click-labeled spots appearing only during exponential growth and not in the stationary phase (lane 5*) could be due to the timescale of lipid metabolism or alterations in the ratio of PS to other glycerophospholipids, since it is known that the total phospholipid composition of yeast cells changes between log and stationary phases.[197]

Additionally, the lower click-labeled spot in lane 4* appeared to have a similar R_f value as the click-derived unmetabolized serine probe, owing to the migration of the PS lipid being heavily influenced by the serine headgroup. The most intense fluorescent band from this analysis appears with a retention factor (R_f = 0.44, lane 4*) that overlaps with a commercial standard for PE. There is also a faint band (R_f = 0.22) that overlaps with a commercial standard for PS, although unfortunately this is also close to the location of the unmetabolized probe (lane 3*) and to the standard for PC (R_f = 0.25). Nevertheless, these results are in line with the labeled phospholipid peaks that were detected in MS experiments.

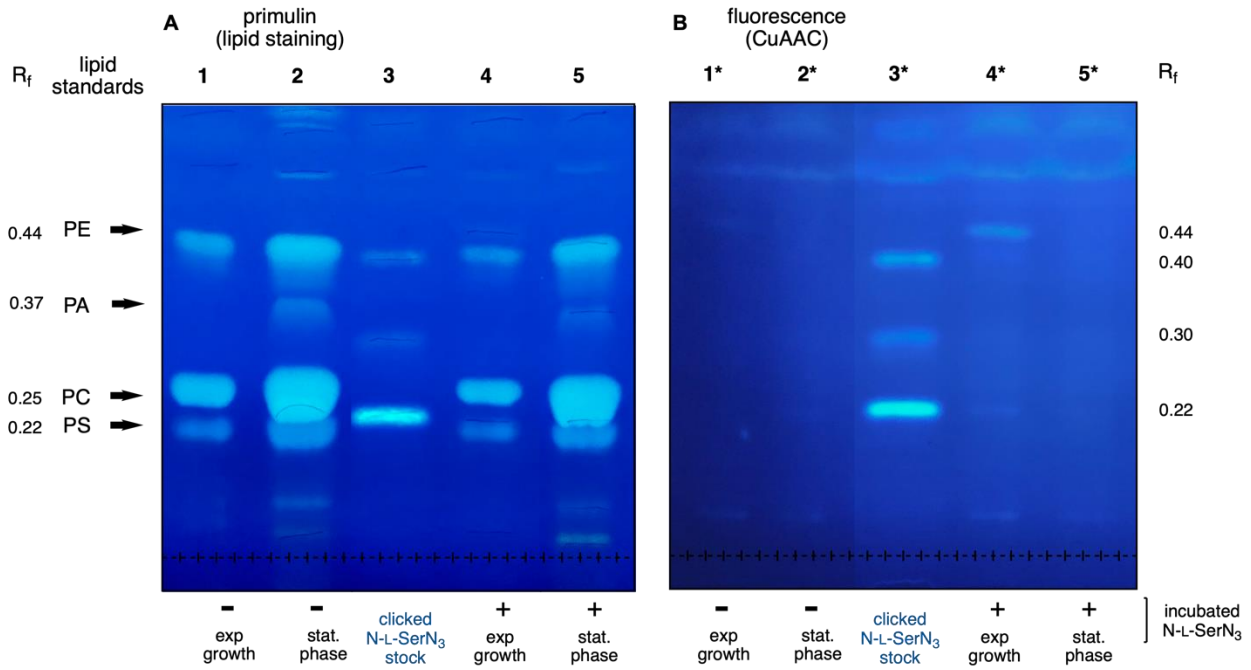

Figure 2.10. TLC separation of lipids after click-derivatization via CuAAC with fluorogenic ethynylnaphthalimide dye. **A.** TLC plate dipped in primulin stain solution to visualize phospholipids (imaged after CuAAC & primulin staining) **B**. The same TLC plate as **A** but displays click-derived fluorescence spots after CuAAC (visualized by fluorescence imaging before primulin staining) and with lanes differentiated by an asterisk. Lanes were loaded with either the unmetabolized **N-L-SerN$_3$** probe (lane 3), or lipid extracts from exponential or stationary growth cells in the absence (lanes 1 and 2, respectively) or presence (lanes 4 and 5, respectively) of **N-L-SerN$_3$**. The positions of phospholipid standards PS, PC, PA, and PE are indicated using arrows on the left side of the figure. In lane 4*, two fluorescent click-labeled bands appear close to the commercial standards for PE and PS, while the latter is also close to PC. Note that lanes 1-2 and 3-5 were stitched together from two different regions of the same TLC plate images (interior lanes were excised).

2.4.6.2 TLC and LCMS analysis of lipid extracts from C-tagged azido-serine probes

We also conducted MS studies using **C-L-SerN$_3$**, which again afforded the production of labeled versions of PS with retention times close to the PS standards that were not observed from enantiomeric control probe **C-D-SerN$_3$** (**Table 2.2**, **Figure 2.11B**). However, as opposed to our prior results with **N-L-SerN$_3$**, cells treated with **C-L-SerN$_3$** did not generate mass peaks corresponding to labeled downstream lipids PE and PC with reasonable retention times based on phospholipid standards. Once again, we analyzed labeled lipid masses that correlated with the existing fatty acid species in the yeast *S. cerevisiae*. These results are in line with our hypothesis that decarboxylation of labeled PS to PE by Psd1 or Psd2 would be deterred for lipids labeled by **C-L-SerN$_3$** since the carboxyl moiety of this compound has been modified to an amide (**Figure 2.11A**). After lipid extract sample preparation, LC/MS experiments were handed to Nick Trybala and were run at the the BSMMSC. We also performed click-tagged TLC experiments using **C-L-SerN$_3$**, (**Figure 2.12**). From this experiment, we observed a very faint new fluorescence spot that moved closely with PS standard (R_f = 0.22, lane 4*), although the faintness of this band makes it difficult to draw definitive conclusions. On the other hand, we did not observe a higher fluorescent spot in proximity of PE standard, which was opposite to what we observed for TLC analysis using **N-L-SerN$_3$** (**Figure 2.10**), providing further evidence that labeling of PE is blocked using **C-L-SerN$_3$**. All in all, these results provide evidence that labeling resulting from treatment with **C-L-SerN$_3$** could enable enhanced targeting of PS.

Table 2.2. Detected labeled PS lipid products from cells incubated with C-L-SerN$_3$ probe. Retention times are shown and correlated to that of the observed RT for detected native lipid of the same lipid species. PC is detected as the formate adduct (FA = formic acid).

lipid	Calculated mass	Detected mass	Error (ppm)	RT	native lipid observed RT	native lipid
PS-N3 (34:2) (M-H)	840.5621	840.5610	1.308	14.72	12.98	PS (34:2) (M-H)
PS-N3 (32:2) (M-H)	812.5308	812.5298	1.231	13.36	11.97	PS (32:2) (M-H)
PS-N3 (36:2) (M-H)	868.5934	868.5918	1.842	16.30	16.96	PS (36:2) (M-H)

A.

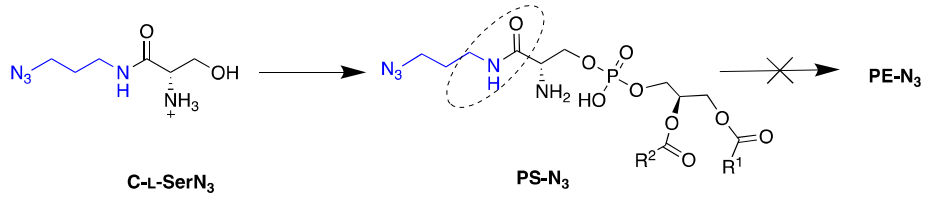

B.

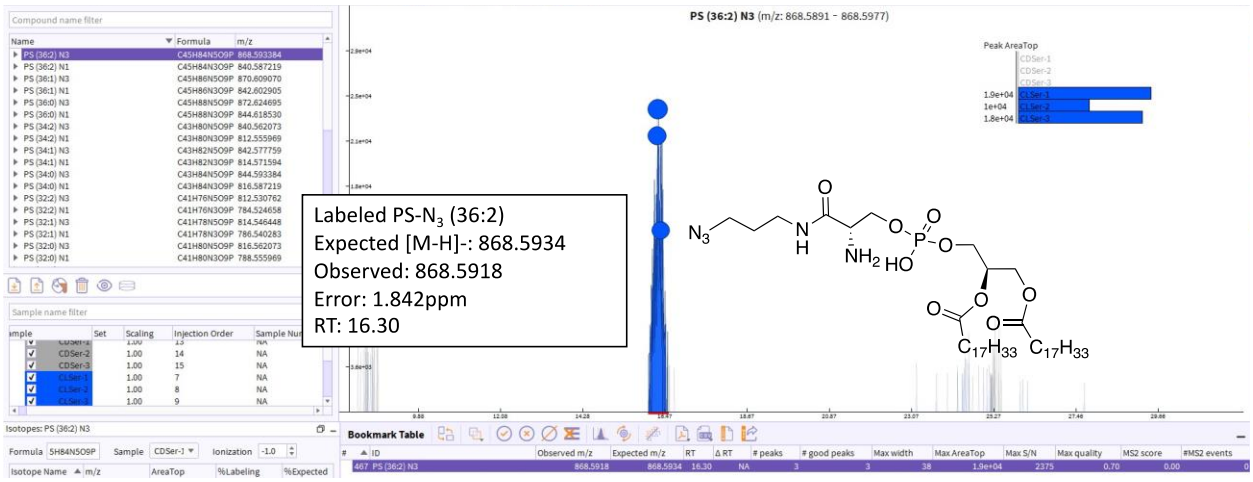

Figure 2.11. Representative mass spectra for click-tagged products of probe C-L-SerN$_3$. A. General structure for C-L-SerN$_3$-labeled PS-N$_3$ lipids showing no-go arrow for decarboxylation to PE-N$_3$ (carboxylate is replaced with amide bond in the structure). B. Products were detected by liquid chromatography mass spectrometry (LCMS) (compared to control **C-D-SerN$_3$**). On the mass spectra screenshots, the structure is shown that matches that of the detected mass peak for the labeled PS. The colored inset shows plots of peak areas and depicts two replicate samples treated with probe **C-L-SerN$_3$** (blue CLSer) and control probe **C-D-SerN$_3$** (gray CDSer).

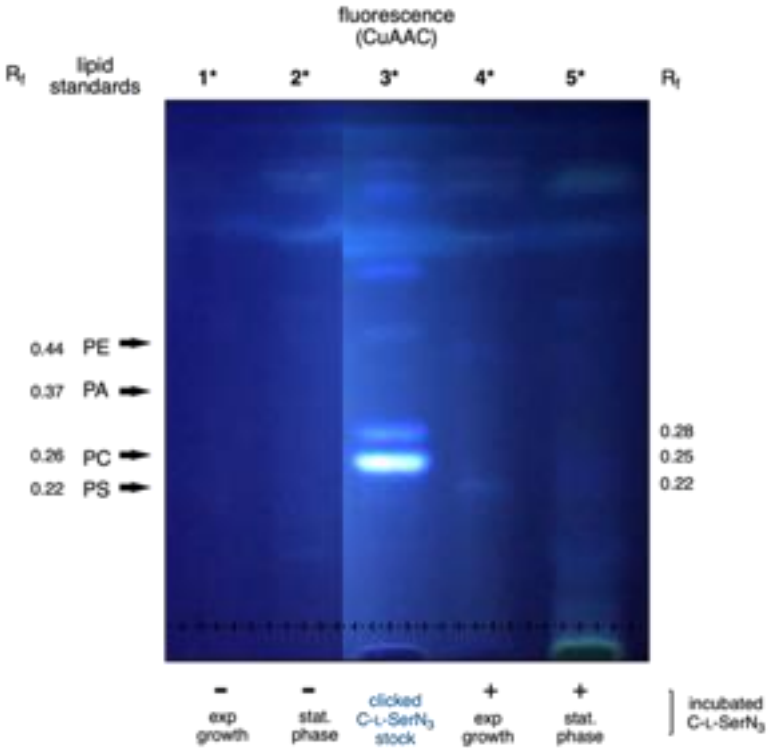

Figure 2.12. TLC separation after CuAAC with ethynylnaphthalimide for lipid extracts in the presence of C-L-serN$_3$. TLC image showing click-derived fluorescence after CuAAC. Lanes were loaded with either the unmetabolized **C-L-SerN$_3$** probe (lane 3*), or lipid extracts from exponential (lanes 1* and 4*) or stationary growth (lanes 2* and 5*) cells in the absence (lanes 1*-2*) or presence (lanes 4*-5*) of **C-L-SerN$_3$**. R_f values for phospholipid standards PS, PC, PA, and PE are indicated on the left side of the figure. In contrast to the results obtained from probe **N-L-SerN$_3$**, only one spot (lane 4*) was observed from labeling with probe **C-L-SerN$_3$** with a migration pattern close to the PS standard. This click-labeled lipid spot (lane 1*) was easily distinguishable from the clicked unmetabolized **C-L-SerN$_3$** (lane 3*), which was observed to elute at a higher R_f (0.25) than the PS standard (R_f = 0.22). Note that lanes 1*-2* and 4*-5* were stitched together from two different regions of the same TLC plate images (interior lanes were excised).

2.5 Conclusions and future outlook

These studies support that serine probes **N-L-SerN$_3$** and **C-L-SerN$_3$** act as mimics of this substrate to produce click-tagged PS in yeast cells, as judged by cellular fluorescence labeling, blockage of PS synthase activity, and the detection of labeled products via mass spectrometry and TLC. For example, we observed substantial cell-membrane labeling from cells with **N-L-SerN$_3$** and budding-localized fluorescence from **C-L-SerN$_3$**. The probe activities were abrogated simply by inverting the stereochemistry of these compounds using negative controls **N-D-SerN$_3$** or **C-D-SerN$_3$**. PS Synthase assay experiments also reveal that both **N-L-SerN$_3$** and **C-L-SerN$_3$** probes can serve as substrates for yeast Cho1p at physiologically relevant concentrations. As a complement to our results, it would be beneficial to carry out experiments with a *S. cerevisiae* cho1 knockout strain. Abrogated PS labeling when this strain is grown in the presence of serine probe would further support our results. Our MS experiments further indicate that PS products resulting from **N-L-SerN$_3$** underwent further modification to produce downstream lipids such as PE and PC, whereas **C-L-SerN$_3$** appears to show primarily PS labeling among these lipids. TLC and LCMS results are in line with our hypothesis that **C-L-SerN$_3$** exhibits less siphoning from labeled PS products via decarboxylation, which may explain the enhanced signal in budding cells observed in microscopy experiments, in accordance with properties of PS localization in *S. cerevisiae*. The **C-L-SerN$_3$** probe and its selective labeling of PS may therefore be leveraged for the intervention of phosphatidylserine trafficking, localization, and flux, while **N-L-SerN$_3$** could provide a new bioorthogonal chemical reporter of the PS → PE → PC pathway in yeast.

The current timescale of labeling for this labeling project entails an overnight incubation of 10-12 hrs in the presence of the serine probe but may also be done for shorter periods of time

and should be explored for future studies. Moreover, the production of labeled PS can likely be expedited by regulating PS synthase enzyme activity using small molecules. This method has been taken advantage of by the Baskin group wherein PLD activity was stimulated with PMA small molecule for facile observation of **Azprop** conversion to labeled PA products.[112, 198] Regulation of PS biosynthesis could be achieved with *myo*-inositol and regulatioin of DAG pyrophosphate (DGPP) phosphatase. We would expect that introduction of inositol into the media will have a direct inhibitory effect in the enzyme and thus lowering the levels of PS.[99] On the other hand, controlled PA lipid supplementation to *S. cerevisiae* cells can be performed since this lipid is known to stimulate PSS enzyme activity.[199, 200] DGPP phosphatase can also be manipulated in *S. cerevisiae* since its regulation is known to increase the affinity of PS synthase to CDP-DAG.[201] Either method could potentially stimulate PSS enzyme activity in the presence of our azido serine probes and improve timescale of metabolic labeling and analysis.

Soluble lipid substrates like $SerN_3$ probes may not accumulate properly at the ER where PS is synthesized so metabolic labeling experiments could also benefit from directed organelle delivery of precursors using organelle targeting moieties. Several research groups have utilized organelle-targeting moieties like sulfonate, triphenylphosphine (TPP), or toluenesulfonamide to drive key precursors to the PM[202] or the yeast vacuole,[203] the mitochondrion,[204] and the ER,[205] respectively. This would however require further synthesis to attach organelle directing groups to the precursor probe and its subsequent cleavage. Nevertheless, a future direction for this project would be to leverage this technique to maximize the chances for $SerN_3$ probes to encounter its synthase enzyme for subsequent metabolic conversion, thereby enhancing lipid metabolic labeling.

Finally, pursuing *in vivo* applications using these serine probes, such as detecting over time or real-time imaging analysis, will be an exciting extension of this work. As such, while TLC and LCMS analysis can identify labeled lipid products over time, these techniques cannot provide information on subcellular localization and cannot be done *in vivo*; however, in conjunction with fluorescence microscopy our approach will likely provide a useful tool for tracking the biosynthesis and flux of important lipids inside cells. To our knowledge, this is the first account of a clickable serine probe for phospholipid labeling, particularly for PS, a lipid known to act as a marker on the outer surfaces of diseased cells such as in cancer.

2.6 General Experimental and Synthetic Procedures

2.6.1 General Experimental

Materials: Reagents and solvents were generally purchased from Acros, Aldrich or Fisher Scientific and used as received. All lipid standards, L-*α*-Phosphatidylcholine (mixed isomers from chicken egg), L-*α*-phosphatidic acid (sodium salt from chicken eggs), 1,2-dioleoyl-*sn*-glycero-3-phosphoethanolamine, and 1,2-distearoyl-*sn*-glycero-3-phospho-L-serine, were purchased from Avanti Polar Lipids, Inc. *O-tert*-Butyl-L-serine *tert*-butyl ester hydrochloride (**2.1**), *N-(tert*-Butoxycarbonyl)-L-serine (**2.4**), 1,3-dibromopropane, *O-tert*-Butyl-D-serine methyl ester hydrochloride (**2.6**), N-(*tert*-Butoxycarbonyl)-D-serine monohydrate, and 3-azidopropylamine were purchased from Fisher Scientific. Dibenzocyclooctyne-cyanine (**Cy3-DBCO**) was obtained from Sigma Aldrich. AFDye™ 647 DBCO (AF647-DBCO or Cy5-DBCO) was purchased from Click Chemistry Tools. Dry solvents were obtained from a Pure solvent delivery system purchased from

Innovative Technology, Inc. CellBright® Red (#30023) was purchased from Biotium. Column chromatography was performed using 230-400 mesh silica gel purchased from Sorbent Technologies. NMR spectra were obtained using Varian Mercury 300, 500, and 600 spectrometers. Mass spectra were obtained with a JEOL DART-AccuTOF mass spectrometer and Waters Synapt G2-Si electrospray ionization mass spectrometer with a quadrupole-time-of-flight mass analyzer (Milford, MA). Optical rotation values were obtained using a Perkin-Elmer 241 polarimeter. Ultrapure water was purified via a Millipore water system (≥ 18 MΩ·cm triple water purification system). 4-Ethynyl-*N*-ethyl-1,8-napththalimide was synthesized as previously reported.[206] Thin-layer chromatography (TLC) glass plates, pre-coated 0.25 mm silica gel without fluorescent indicator (20x20cm) were purchased from Sorbent Technologies (Norcross, GA).

***Saccharomyces cerevisiae* Cell Growth**: *S. cerevisiae* TRY 181 (wild-type, uraΔhisΔ) strain cells were streaked or spread on YPD (1% yeast extract, 2% peptone, 2% dextrose, 2% agar) plates from inoculum and incubated at 30 ^{o}C, and single colonies were seen after ~24 h. Next, from a single colony, a loop of cells was added to 5 mL 2% galactose minimal medium into a glass cell culture tube and incubated at 30 ^{o}C at 225 rpm with good aeration overnight to an optical density of ~1.5. Galactose minimal media (2%, YNB, galactose as a carbon source) was made by adding the following: 6.7 g of Yeast Nitrogen Base (without amino acids), 20 mg uracil, 20 mg L-histidine, and 20 g galactose dissolved in 1000 mL Milli-Q water and filtered via presterilized Millipore vacuum filtration system to which ~20 mL aliquot was poured out into a Falcon tube to prevent contamination.

Treatment of L-serine and D-serine Probes in *S. cerevisiae*: Overnight cultures growing in 2% galactose medium were diluted to an OD_{600} (optical density) of 0.2 in fresh medium along with probes **N-L-SerN$_3$** or **C-L-SerN$_3$** (or controls **N-D-SerN$_3$** or **C-D-SerN$_3$**) to a final concentration of 1.5 mM (stock solutions in Milli-Q water stored at 4-0°C). Cells were incubated for 10-12 h until the OD_{600} value reached ~1.0 or at late-log phase, not exceeding an OD_{600} of 1.5 to avoid autofluorescence from yeast cells due to diauxic shift. For good aeration, the medium constituted no more than one-fifth of the total tube volume, and growth was carried out in a shaking incubator at 225 rpm. Next, the cell solution was collected in a 10 mL conical vial and centrifuged at 10,000 *x*g for 5 min at 4-0°C followed by washing with 10 mL of cold water. The rinse step was repeated twice with a final spin down at 3000 *x*g. Samples were immediately used while kept on ice 4-0°C for fluorescence microscopy or immediately fixed for flow cytometry studies.

Fluorescence Imaging of Labeled Lipids in *S. cerevisiae*: After cell harvest and washing steps, *S. cerevisiae* cells were resuspended in 1X PBS (pH = 7.47), diluted to an OD_{600} = 0.6/mL, and incubated with **Cy3-DBCO** clickable dye (in Milli-Q stock) to a final concentration of 1 µM. Samples were covered with foil for 1 h at rt with shaking. The cells were spun down (5000 *x*g) and the top dye solution was removed. The cells were finally washed with water, vortexed, and spun down (5000 *x*g) a total of three times. After the final rinse, cells were fixed (3.7 PFA%) for 15 min at rt. Further centrifugation (5000 *x*g for 3 min) for supernatant removal and resuspension in 1X PBS gave fixed yeast samples. For microscopy studies, 3 µL of cell culture were mounted onto microscope slides and covered with a coverslip, immobilized with acrylic nailpolish and visualized under a confocal microscope (Leica SP8 White Light Laser Confocal microscope).

Samples were excited at 554 nm and fluorescence was collected between 559-620 nm with a HyD detector. The laser strength, gain and offset settings were kept constant. All images acquired on *S. cerevisiae* cells were taken after a zoom factor of 6 or 8 was applied and as a Z-stack of 7-14 z-slices with 1.0 µm increments, after which lightning deconvolution was applied through Leica Application Suite (LAS) V4.4 software. All sample and control images were processed the same way using FIJI (v.2.1.0/1.53c) and Adobe Photoshop (v.22.3.0).

Colocalization with CellBrite® Red DiD Membrane Dye: After SPAAC and washing of excess **Cy3-DBCO**, cells were resuspended in 1X PBS and incubated with DiD (Biotium, CellBright® Red, #30023) for 10 minutes as per manufacturer's instructions. Cells were washed three times with 1X PBS (pH = 7.47), and finally resuspended in 1X PBS. Samples were excited at 554 nm and fluorescence was collected between 559-620 nm for Cy3 with a HyD detector. For DiD fluorescence, samples were excited at 644nm, collecting fluorescence between 656-670nm. All images were taken after a zoom factor of 12 was applied and as a Z-stack. Pearson's correlation coefficient was acquired from deconvolved images using FIJI's Coloc2 plugin: FIJI (v.2.1.0/1.53c) by selecting ROIs from 30 cells per replicate (**Figure 2.4**).

Flow Cytometry: Samples for flow cytometry were first fixed (3.7% PFA), incubated with AFDye™ 647 DBCO for 1.5 hrs (1 µM final concentration in OD_{600} = 0.6/mL cell suspension), and washed in similar fashion as samples for fluorescence microscopy. After washing and centrifugation, cell pellets were resuspended in 600 µL PBS and kept on ice for flow cytometry with FACSCalibur LSR II flow cytometer (Becton Dickinson). After exclusion of debris (FSC-A vs SSC-A plot) and gating

for single cells (FSC-W vs FSC-A), AFDye™ 647 DBCO fluorescence intensity was recorded in the APC channel. Flow cytometry data were obtained for 50,000-60,000 gated events per sample. Replicates were analyzed on the same day and data analysis was performed using FlowJo software (v.10.11 FlowJo LLC, OR, USA). Unstained cells were also prepared for a representative negative population in each run. For unstained controls, probe-supplemented yeast samples were only fixed and not incubated with click-dye. For every flow cytometry experiment, samples were also viewed under the confocal microscope, excited at 633 nm, and fluorescence was collected between 651-671nm with a HyD detector. FACSCalibur LSR II flow cytometer use was assisted by Trevor Hancock from Dr. Tim Sparer's lab.

***In vitro* PS Synthase Assay:** Membrane extracts collected from wild-type *Candida albicans* strain, SC5314, were used for the *in vitro* PS synthase assay. The cells were grown and broken as previously described.[189] The cell lysate was cleared by centrifuging at 2000 x g, 4°C for 5 min, and the crude membrane was collected by spinning the resulting supernatant at 27,000 x g, 4°C for 30 min. The pellets were resuspended in 0.1 M Tris-Cl pH 7.5, 5 mM BME, 10% glycerol, and the total protein concentration was measured using Bio-Rad Protein Assay. A total of 0.5 mg membrane protein was used in each reaction with 50 mM Tris-HCl, pH 7.5, 0.1% Triton X-100, 0.5 mM $MnCl_2$, and 0.1 mM CDP-DAG (Avanti Polar Lipids, Alabaster, AL, USA) in a total volume of 100 µL. The reaction mixture was incubated with the final concentrations of 0, 1, 5, 10, or 25 mM of serine analog **N-L-SerN_3** or **C-L-SerN_3** at 4°C for 30 min before the start of the reaction. Then, 0.5 mM L-serine spiked with 5% (by volume) [^{3}H] L-serine (30,500 cpm/nmol) was added into the assay mixture to initiate the reaction, and PS synthase activity (nmol/mg) was measured by

monitoring the incorporation of [^{3}H] L-serine in the chloroform phase (for product phosphatidylserine) via a scintillation counter. A thirty-minute time point was chosen for single point assays, following a prior procedure.[189, 195] Statistical analysis was performed on Graphpad Prism 9.1.

Lipid Extraction: The lipid extraction was performed following a modified Bligh and Dyer method.[196] Briefly, frozen cells in 2 mL Eppendorf tubes were warmed to rt and resuspended in 500 µL of chloroform and 100 µL of methanol. Samples were vortexed for 30 s and centrifuged at 5000 *x*g for 5 min. The supernatant was transferred to a new Eppendorf tube. The methanol-chloroform extraction was repeated once more, and the collected supernatant was collected into a new tube. To the supernatant, 300 µL of chloroform was added and mixed manually for 30 s. 600 µL of 0.1% AcOH in MQ water was added and gently mixed at rt for 30 s. Centrifugation at 5000 *x*g for 5 minutes afforded a biphasic liquid phase. The upper (aqueous) phase was transferred, and the lower (organic) phase was transferred into a new tube using solvent-rinsed pipet tips. The final chloroform extraction was repeated to the aqueous phase. Next, the whole organic phase (collected from 2 extraction steps) was centrifuged for 5 min at 3000 *x*g at rt and dried under nitrogen. Collected extracts were dried with a steady N_2 stream. Lipid extracts that were used directly for LCMS were stored at 0°C, while lipid extracts used for CuAAC were kept at rt or immediately subjected to click reaction.

CuAAC for Fluorescence-based Thin Layer Chromatography: CuAAC was performed following a prior procedure.[107] Lipid extracts were resuspended in 16µL $CHCl_3$. For the preparation of the

8.60 mM Cu(I) click solution, 3.80 mg Cu(I)$(MeCN)_4BF_4$ was dissolved in 605 µL acetonitrile and 800 uL of ethanol. 200 µL of this copper solution was combined with 10 µL of 4-Ethynyl-*N*-ethyl-1,8-napththalimide dye (22.5 µM in $CHCl_3$/MeOH) as the click mix and vortexed for 30 s. The click mix (30 µL) was added to lipid extracts (suspended in 16 µL $CHCl_3$), as well as to aliquots of unmetabolized serine probe stocks (0.5 mM). The clicked samples were flushed with N_2, vortexed, spun down, and then incubated on a 42°C water bath for 16 h. After CuAAC incubation, the clicked samples were vortexed and spun down (3000 *x*g). For TLC, clicked samples were loaded onto a thin-layer chromatography (TLC) plate in 5 µL increments (40 µL total lipid extracts), with drying in between each addition. Lipid samples were separated by TLC using glass plates of pre-coated 0.25 mm silica gel without fluorescent indicator (20 x 20 cm). The spots were dried with a heat gun prior to the addition of phospholipid standards: 2-4 µL of PS, PC, PA, and PE standards (3-5 mM in $CHCl_3$/MeOH). Next, the TLC plate was developed in an eluant mixture of chloroform/methanol/water/acetic acid (65:25:4:1, v/v/v/v) until an R_f of 0.6 had been reached. The plate was air dried for an hour and then developed with 1:1 cyclohexane/ethyl acetate. The TLC plate was visualized using an iPhone camera (true color images) or a UV-365nm Transilluminator (Figure 4B, Figure S8). The clicked spots were marked with a lead pencil to differentiate later from the spots due to primulin staining of lipids. The TLC plate was also captured using a Geldoc with a SYBR Green emission filter (grayscale images not shown). The plates were then dipped in primulin stain (5 mg primulin per 100 mL 9:1 acetone/water) and then imaged again and processed using ImageJ.

Mass Spectrometry: The dried residues from extraction were resuspended in 100 µL of methanol. LC-HRMS analysis was performed using a Thermo Scientific Exploris™ 120 mass spectrometer equipped with an electrospray ionization probe (ESI) coupled to a Vanquish UPLC system. Separations were carried out under the following chromatographic conditions using a Thermo Accucore C18 column (2.6 µm, 100Å, 100 x 3 mm) operating at a flow rate of 0.200 mL • min^{-1} following a 2 µL injection. Separations were run using mobile phase A: 10 mM ammonium formate in 60:40 acetonitrile:water and mobile phase B: 10 mM ammonium formate in 90:10 isopropanol:acetonitrile. Column and sample temperature were kept at 45°C and 4°C, respectively. The gradient was programmed as follows: 0-2 min, 30% B; 2-3 min, 30-40% B; 3-7 min, 40-50% B; 7-8 min, 50-60% B; 8-9 min, 60-62.5% B; 9-10 min, 62.5-65.0% B; 10-12 min, 65-68% B; 12-13 min, 68-78% B; 13-14 min, 70.0-72.5% B; 14-16 min, 72.5-75.0 min; 16-20.5 min, 75-80% B; 20.5-23 min, 80-98% B; 23-28 min, 98% B; 28-32 min, 98-100% B; 32-34 min, 100-90% B; 34-40 min, 90-30% B. The mass spectrometer was operated under the following tune parameters: Positive ion (V): 3400; Negative ion (V): 2000; Sheath gas (arb): 20; Aux gas (arb): 7; Sweep gas (arb): 1; Ion transfer tube temp (°C): 350; Vaporizer temp (°C): 400. For full scan acquisition, the instrument was operated under the following parameters: Orbitrap resolution: 120000; Scan range: 100-3000 m/z; RF Lens (%): 70; Maximum injection time: 100 ms, Microscans: 1. For data dependent acquisition, the instrument was operated under the following parameters: Isolation window: 1.2 m/z; Orbitrap resolution: 30,000; Maximum injection time: 22 ms; Microscans: 1. HCD collision energies were normalized and stepped to 20, 50 and 75%. Raw files were converted to mzML files and full scan data was evaluated using MAVEN software. For peak identification, retention times were compared with respect to natural lipid of the same lipid

species. N_3-labeled lipids were identified (C12 isotope as parent peak) comparing the exact mass (±5 ppm) to a generated compound list.

2.6.2 Synthetic Procedures and Characterization Data

2.6.2.1 General procedure for the synthesis of N-L-SerN_3 and N-D-SerN_3.

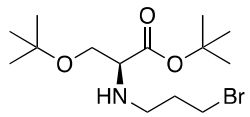

2.2

***tert*-Butyl *N*-(3-bromopropyl)-*O*-(*tert*-butyl)-*L*-serinate (2.2)**. *O-tert*-butyl-L-serine ester *tert*-butyl hydrochloride was washed with saturated sodium bicarbonate solution (25 mL) and extracted with methylene chloride (3 x 25 mL). The organic layer was washed with saturated sodium chloride solution and dried over magnesium sulfate. The solvent was removed with a rotary evaporator and then placed under high vacuum for 3 hours to give *tert*-Butyl *O-(tert*-butyl)-L-serinate (**2.1**, 0.672 g, 3.10 mmol) as a light-yellow oil. Dry *N*,*N*-dimethylformamide (15 mL) was added to the reaction mixture, which was flushed with N_2. Potassium carbonate (0.855 g, 6.19 mmol) was added and the solution was stirred for 30 minutes. Dibromopropane (0.315 mL, 3.09 mmol) was then added and the solution was refluxed at 55°C and stirred for 22 h. Cold purified water (200 mL) was added and the solution was extracted with methylene chloride (3 x 25 mL). The collected organic layer was washed with brine and dried over magnesium sulfate, followed by three rounds of methylene chloride addition and rotary evaporation before placing under high vacuum. The crude (light yellow-orange syrup) bromopropyl-serine intermediate **(2.2)** was used without further purification.

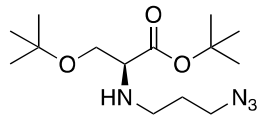

2.3

***tert*-Butyl *N*-(3-azidopropyl)-*O*-(*tert*-butyl)-*L*-serinate (2.3).** To a stirred solution of crude **2.2** (0.629 g, 1.86 mmol) in 40 mL *N*,*N*-dimethylformamide was added *N*-methyl morpholinium chloride (0.282 g, 2.05 mmol) and the reaction was allowed to stir for 45 min at 35°C under inert atmosphere. An excess of sodium azide (0.158 g, 2.43 mmol) was added and the reaction was allowed to stir overnight at 65°C. Cold purified water (80 mL) was added to quench the mixture, followed by extraction with methylene chloride (3 x 35 mL). When insoluble solids persisted, the crude mixture was gravity filtered through filter paper and rinsed with *N*,*N*-dimethylformamide. The resulting crude was concentrated and then washed with water (50 mL). The yellow organic phase was washed with a brine solution and dried with magnesium sulfate. After filtering off the drying agent, the solvent was removed through rotary evaporation and high vacuum. The resulting crude sample was purified through silica gel column chromatography using gradient elution of 25-60% ethyl acetate/hexanes. The desired product (**2.3**) was isolated as a light-yellow oil (33.5 mg, 1.12 mmol, 60% yield), as confirmed by: TLC (R_f = 0.54 40% ethyl acetate/hexanes; ninhydrin stain); ^{1}H NMR (300 MHz, $CDCl_3$) δ3.56 – 3.41 (m, 2H), 3.37 – 3.30 (m, 2H), 3.18 (d, *J* = 0.7 Hz, 1H), 2.80 – 2.69 (m, 1H), 2.61 – 2.50 (m, 1H), 1.93 – 1.79 (s, 1H), 1.79 – 1.64 (m, 2H), 1.45 – 1.43 (s, 9H), 1.13 – 1.11 (s, 9H). ^{13}C NMR (126 MHz, $CDCl_3$)**:** δ 172.63, 80.92, 72.88, 63.18, 62.22, 49.41, 45.07, 29.44, 28.10, 27.33. ESI-TOF-MS $[M+H]^+$ calculated for $C_{14}H_{29}N_4O_3$: 301.2234; found: 301.2249.

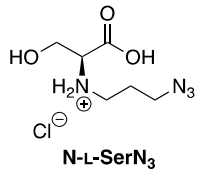

N-L-SerN$_3$

(*S*)-3-azido-*N*-(1-carboxy-2-hydroxyethyl)propan-1-aminium chloride (N-L-SerN$_3$). Compound **2.3** (33.5 mg, 1.12 mmol) was dissolved in 1,4-dioxane (1.5 mL) and treated with 8 M hydrochloric acid (11.2 mL), and the mixture was allowed to stir for 8 h at 70°C. The reaction mixture was then dropped to 0°C in an ice bath and methanol (6.0 mL) was added to dilute the mixture. The solvent was then removed with a rotary evaporator through an azeotrope with toluene at 60°C, followed by placement under high vacuum. A C_{18} silica column was preconditioned through treatment with 100% MeOH followed by 50%MeOH/H_2O. Reverse-phase column chromatography with elution using 50% MeOH/H_2O provided **N-L-SerN$_3$** (94.8 mg, 0.502 mmol, 45% yield) as a light-yellow to clear oil as confirmed by: Reverse-phase C_{18} TLC (R_f = 0.80, 50% MeOH/H_2O; ninhydrin stain); $[\alpha]^{24}_D$ +5.66° (c = 0.62, H_2O);^{1}H NMR (300 MHz, CD_3OD) δ 4.19 (s, 1H), 4.05 (t, *J* = 3.6 Hz, 2H), 3.87 (s, 1H), 3.51 (t, *J* = 6.4 Hz, 2H), 3.19 (dd, *J* = 9.0, 6.6 Hz, 2H), 2.00 (h, *J* = 6.4 Hz, 2H).^{13}C NMR (126 MHz, CD_3OD) δ 171.53, 65.21, 62.00, 56.42, 47.84, 29.21. ESI-TOF-MS $[M+H]^+$ calculated for $C_6H_{13}N_4O_3$: 189.0982; found: 189.0986.

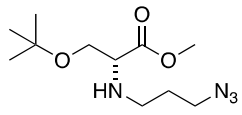

2.6

Methyl *N*-(3-azidopropyl)-*O*-(*tert*-butyl)-*D*-serinate (2.6). The procedures for compounds **(2.2)** and **(2.3)** were followed using O-*tert*-butyl-D-serine methyl ester hydrochloride as starting

material to give **2.6** as a light-yellow oil as confirmed by: TLC (R_f = 0.46, 50% ethyl acetate/hexanes; ninhydrin, brown); ^{1}H NMR (500 MHz, $CDCl_3$) δ 3.71 (s, 3H), 3.58 – 3.51 (m, 2H), 3.39 – 3.31 (dt, 2H), 2.79 – 2.74 (dt, J = 11.6, 6.8 Hz, 1H), 2.60 – 2.54 (dt, J = 11.6, 7.0 Hz, 1H), 1.76 – 1.71 (m, J = 6.8 Hz, 2H), 1.12 (s, 9H); ^{13}C NMR (126 MHz, $CDCl_3$**):** δ 173.72, 73.20, 62.97, 61.91, 51.71, 49.39, 45.17, 29.38, 27.31 HRMS-DART $[M+H]^+$ calculated for $C_{11}H_{23}N_4O_3$: 259.17647; found: 259.15118.

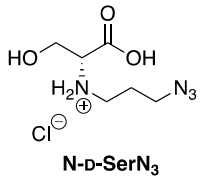

N-D-SerN$_3$

(*R*)-3-azido-*N*-(1-carboxy-2-hydroxyethyl)propan-1-aminium chloride (N-D-SerN$_3$). A solution of **2.6** in water (5 mL) was treated with 8 M hydrochloric acid (11.2 mL) and the mixture was allowed to stir for 8 h at 70°C. For the deprotection of the methyl ester, the solution was stirred for two more days at 90°C. The workup and chromatography procedure for **2.3** was followed to give **N-D-SerN$_3$** as a light-yellow to clear oil. $[\alpha]^{24}_D$ -5.70**°** (c = 0.62**,** H_2O); The ^{1}H and ^{13}C NMR spectra for the product **N-D-SerN$_3$** did not differ from those of **N-L-SerN$_3$**.

2.6.2.2 General procedure for the synthesis of C-L-SerN$_3$ and C-D-SerN$_3$

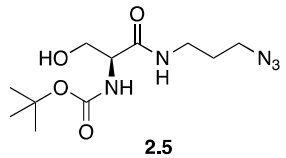

2.5

***tert*-Butyl (*S*)-(1-((3-azidopropyl)amino)-3-hydroxy-1-oxopropan-2-yl)carbamate (2.5)** *N-(tert-*Butoxycarbonyl)-L-serine **(2.4)** (65.4 mg, 0.319 mmol) was dissolved in 10 mL dichloromethane

at 0°C under argon. To this was added a solution of hydroxybenzotriazole (HOBt, 45 mg, 0.333 mmol) and O-(benzotriazol-1-yl)-*N*,*N*,*N*′,*N*′-tetramethyluronium hexa-fluorophosphate (HBTU, 121 mg, 0.319 mmol) in methylene chloride. After 1 min, a mixture containing 3-azidopropylamine (60 µL, 0.611 mmol) dissolved in 6 mL dichloromethane with diisopropylethylamine (150 µL, 0.861 mmol) was added, which was then allowed to warm to rt and stirred for 48 h under argon. The reaction was then cooled, and 40 mL cold DI water was used to quench the reaction while stirring for 3 min. The bottom methylene chloride phase was collected, washed with brine, and dried over sodium sulfate, while the remaining aqueous layer was extracted with ethyl acetate (3 x 25 mL), washed with brine, and dried over magnesium sulfate. Filtration and concentration gave a clear oil. Column chromatography using a gradient elution of 2-9% Methanol/ CH_2Cl_2 gave a final white solid (46.8 mg, 0.163 mmol, 51%). TLC (R_f = 0.43 in 7%MeOH/ CH_2Cl_2; ninhydrin stain), ^{1}H NMR (500 MHz, CD_3OD) δ 4.06 (t, J = 5.2 Hz, 1H), 3.72 (dd, J = 5.3, 3.9 Hz, 2H), 3.36 (t, J = 6.8 Hz, 2H), 3.27 (ddt, J = 20.2, 13.5, 6.7 Hz, 2H), 1.82 – 1.70 (m, 2H), 1.45 (s, 9H). ^{13}C NMR (126 MHz, CD_3OD) δ 171.97, 156.32, 79.44, 61.81, 56.87, 48.58, 36.33, 28.23, 27.25. HRMS-DART: $[M+H]^+$ calculated for $C_{11}H_{22}N_5O_4$: 288.1489; found: 288.1367; $[M-C_4H_9+H]^+$ calculated for $C_7H_{14}N_5O_4$, 232.1040; found, 232.0800; [M-t-butyl-O-CO+H]$^+$ calculated for $C_6H_{14}N_5O_2$ calculated: 188.1142; found: 188.09274.

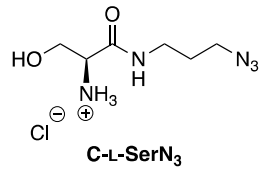

C-L-SerN$_3$

(*S*)-1-((3-Azidopropyl)amino)-3-hydroxy-1-oxopropan-2-aminium chloride (C-L-SerN$_3$). In a 100 mL RBF, compound **2.5** (46.8 mg, 0.163 mmol) was dissolved in methanol (30 mL). Hydrochloric

acid (5.0 mL of an 8 M solution in methanol) was added dropwise and the reaction mixture was allowed to stir for 12 h at 50 °C. The reaction was then cooled using an ice water bath and diluted with 6 mL methanol. The mixture was then concentrated to remove solvents under high vacuum. Deprotection was confirmed by normal-phase TLC (R_f = 0.78 in 50%MeOH/H_2O; ninhydrin, purple). Reverse-phase column C_{18} chromatography (50% methanol/water as eluent) afforded **C-L-SerN$_3$** as a clear, colorless crystal (24.0 mg, 0.128 mmol, 79%). $[\alpha]^{24}_D$ = + 9.54 (c = 0.30, H_2O); ^{1}H NMR (500 MHz, CD_3OD) δ 3.93 (m, 2H), 3.82 (dd, *J* = 12.4, 7.5 Hz, 1H), 3.38 (t, J = 6.7 Hz, 2H), 3.33 (d, J = 6.8 Hz, 2H), 1.79 (p, *J* = 6.7 Hz, 2H). ^{13}C NMR (126 MHz, CD_3OD) δ 166.88, 60.29, 54.88, 48.55, 36.57, 28.18. ESI-TOF-MS $[M+H]^+$ calculated for $C_6H_{14}N_5O_2$ calculated, 188.1142; detected, 188.1151.

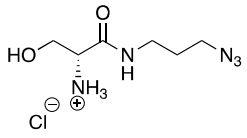

C-D-SerN$_3$

(*R*)-1-((3-Azidopropyl)amino)-3-hydroxy-1-oxopropan-2-aminium chloride (C-D-SerN$_3$). The procedures for **(2.5)** and its deprotection were followed using N-(*tert*-Butoxycarbonyl)-D-serine monohydrate as starting material. $[\alpha]^{24}_D$ = - 9.60 (c = 0.30, H_2O); The ^{1}H and ^{13}C NMR spectra for the product **C-D-SerN$_3$** did not differ from that of **C-L-SerN$_3$**.

Chapter 3. Harnessing clickable acylated glycerol probes as chemical tools for tracking glycerolipid metabolism

The scientific data used in this Chapter has been published by the authors: Ancajas, C. F.; Carr, A. J.; Lou, J.; Sagar, R.; Zhou, Y.; Reynolds, T.; Best, M. D., Harnessing Clickable Acylated Glycerol Probes as Chemical Tools for Tracking Glycerolipid Metabolism. *Chem. Eur. J.* e202300417. Former Best Group member A.J. Carr synthesized all probes shown in Figure 3.2, except for compound **C_4-MEG-N_3,** which was synthesized by current member J. Lou. Y. Zhou assisted with the growth of yeast cells. Otherwise, experiments were performed by C.F. Ancajas. M.D. Best and T. Reynolds contributed to oversight of the project.

3.1 Abstract

While the goal of the prior chapter is the targeted labeling of one phospholipid and its metabolites by introducing the click handle at the lipid headgroup, in this chapter, we are pursuing a complementary approach of propagating the click handle within target lipid classes. Herein we report the use of clickable monoacylglycerol (MAG) analogs (**C_n-MAG-N_3**) as probes that would more broadly label glycerophospholipids. In our design, we strategically incorporated the azide tag onto the glycerol region such that the click tag would not be removed through processes including acyl chain and headgroup remodeling. These **C_n-MAG-N_3** probes contain acyl chains of different lengths (n = 4, 10, 12, 14, 16, 18, and 18:1) and this Chapter recounts how they resulted in widely variable cell imaging and cytotoxicity profiles. For instance, MAG probes containing medium-chain C10 and C12 tails were not tolerated by *S. cerevisiae* and resulted in growth suppression. We focused on a probe bearing a short acyl chain (**C_4-MAG-N_3**) which was

better tolerated and displayed favorable fluorescence imaging at the plasma membrane. Fluorescence-based TLC and LCMS methods confirmed that **C_4-MAG-N_3** infiltrated natural lipid biosynthetic pathways to produce click-tagged versions of both neutral and phospholipid products. Alternatively, strategic blocking of the glycerol *sn*-3 position in probe **C_4-MEG-N_3** served to deactivate phospholipid tagging and focus labeling on neutral lipids. This work shows that lipid metabolic labeling profiles can be tuned based on probe structures and provides valuable tools for evaluating alterations to lipid metabolism in cells.

3.2 Background and motivation

A common lipid metabolic labeling approach has focused on labeling specific phospholipid structures using clickable probe analogs of substrates that map onto the headgroups of target glycerophospholipids[207] including PC,[88, 109, 154] PA,[112, 155, 198] PS,[208] PI[117] and glycophosphatidylinositol (GPI) anchors.[159, 209] This bioorthogonal strategy also extends to labeling ceramide or other sphingolipids.[128, 210] However, a complementary strategy would enable the labeling of broader families of glycerolipids to obtain a snapshot of changes in lipid metabolism in response to different cellular processes. Such an approach would be comparable to biorthogonal non-canonical amino acid tagging (BONCAT), which has been beneficial for analyzing changes in global protein synthesis.[211] One method that enables broad lipid labeling utilizes click-tagged fatty acid (FA) precursors to infiltrate the hydrophobic regions of different lipid structures, an approach that has commonly been applied to scrutinize FA metabolism, β oxidation,[212] and total lipid profiling.[107] With regard to glycerolipid labeling, a drawback of this approach is that the tag can be removed through acyl chain remodeling and FAs are also diverted

into structures other than phospholipids, such as through posttranslational protein lipidation.[106,213]

In order to obtain broader snapshots of glycerolipid metabolism, the glycerol scaffold of lipids provides an attractive motif for metabolic labeling since this region is conserved within glycerolipids. Therefore, probes can be developed to target general glycerolipid biosynthesis in a manner by which the clickable tag will not be excised if an acyl chain or lipid headgroup is modified through metabolism. Herein we introduce azide-tagged glycerol and monoacylglycerol (MAG) probes as a distinct avenue for lipid tracing. Since MAGs are short-lived and common intermediates for glycolipid and glycerophospholipid biosynthesis,[99] we hypothesized that they could provide an avenue for accessing end-product lipids- an interesting pursuit when studying lipid biosynthesis and flux.

Also, clickable MAG probes have not, to our knowledge, been leveraged as an exogenous biorthogonal chemical reporter for the synergistic analysis and visualization of global glycerolipid flux. Moreover, implementation of MAG probes may also allow access to free glycerol analogs, which is a strategy that has previously been utilized for metabolic engineering studies.[214, 215] Once fed to live cells, MAG probes can be incorporated into lipid metabolism or be cleaved by esterase enzyme to generate azido-glycerol (**Figure 3.1**, top right panel). Due to these attributes, we set out to explore the efficacy of clickable glycerol and MAG probes for glycerolipid metabolic labeling. Various analytical and imaging techniques will aid in confirming the labeled lipids from the MAG analogs following investigation on each probe's toxicity profile for the organism of interest.

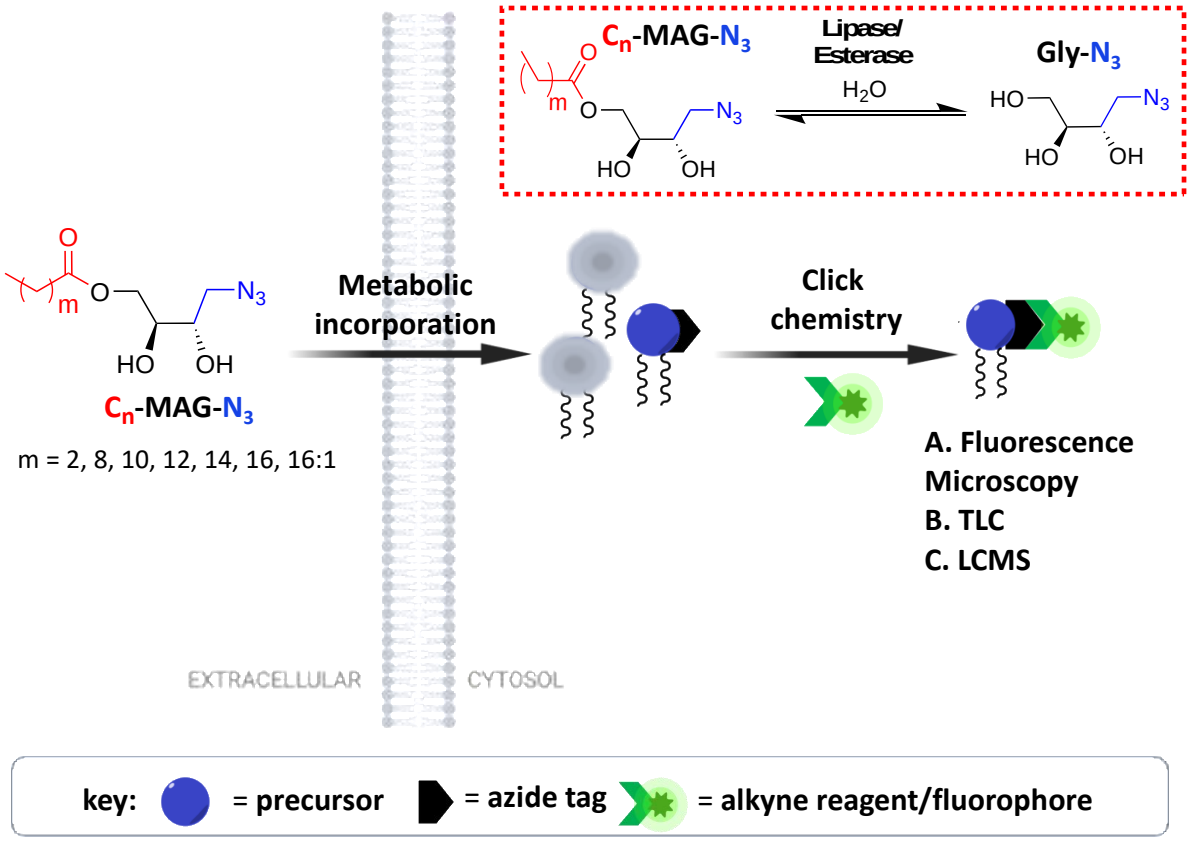

Figure 3.1. Chemical tagging of monoacylglycerol for labeling glycerolipid products. Clickable MAG probes (**C_n-MAG-N_3**) are designed to infiltrate natural lipid biosynthetic pathways to potentially produce click-tagged versions of both neutral and phospholipid products. Cellular lipases/esterases can cleave the synthetic acyl chains to give glycerol (red dashed box).

3.3 Panel of azido-mag probes and an azido-glycerol probe

To explore glycerolipid labeling, we developed a series of azide-tagged probes of glycerol as well as MAGs bearing different lengths of acyl chains attached to oxygen. The azide tag was specifically chosen to enable imaging applications through post-derivatization via the strain-promoted azide-alkyne cycloaddition (SPAAC) through reaction with cyclooctyne-containing reagents. The core design features a glycerol derivative, **Gly-N_3** (**Figure 3.2**), in which an azidomethylene moiety is appended at the *sn*-1 position in place of a hydrogen atom on the glycerol backbone. This approach draws from previous phospholipid probes the Best Group developed that retained protein binding properties despite the addition of the azidomethylene tag.[216,217] Along with **Gly-N_3**, a panel of MAG derivatives containing a single FA tail appended to the *sn*-3 position (**C_n-MAG-N_3**, where n denotes the total number of carbons in the acyl chain) was also synthesized. This includes analogs with varying acyl chain lengths ranging from short (**C_4-MAG-N_3**), to medium (**C_{10}-MAG-N_3**, **C_{12}-MAG-N_3**, **C_{14}-MAG-N_3**), and long (**C_{16}-MAG-N_3**, **C_{18}-MAG-N_3** and unsaturated, **$C_{18:1}$-MAG-N_3**) (**Figure 3.2**). These MAG probes were explored as an avenue for improving cell-permeability, after which the acyl chain could be hydrolyzed by intracellular lipases/esterases to manipulate acyl chains.[218, 219] Finally, we additionally developed **C_4-MEG-N_3** as an alternate probe for comparison in which the *sn*-3 alkyl chain is attached via an ether linkage to block hydrolytic cleavage by hydrolytic enzymes. The **Gly-N_3** and **C_n-MAG-N_3** compounds were synthesized by former Best Group member Dr. Adam J. Carr while probe **C_4-MEG-N_3** and additional samples of **C_4-MAG-N_3** were synthesized Dr. Jinchao Lou.[220]

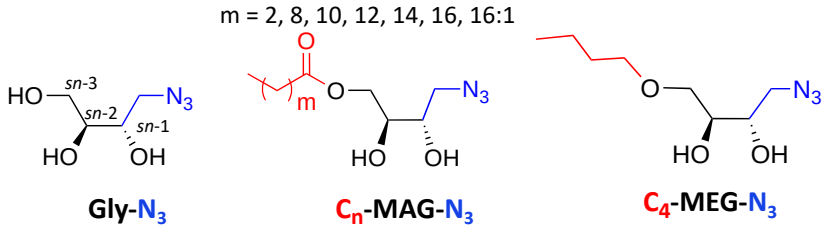

Figure 3.2. Structures of azide-tagged glycerol probe Gly-N_3, MAG probes of type C_n-MAG-N_3, and ether-linked probe C_4-MEG-N_3. Synthetically added tails are shown in red with FA tails of varying lengths and the methylene azide tag is drawn in blue. Strategic blocking of the glycerol sn-3 position is possible with probe **C_4-MEG-N_3** to potentially deactivate phospholipid tagging and focus labeling on neutral lipids.

3.4 Evaluation of probe cellular labeling properties

3.4.1 Previous research contributions

Prior to my joining the Best Group, Dr. Adam Carr had initially performed cellular labeling experiments with the **Gly-N_3** probe as well as the medium- and long-chain **C_n-MAG-N_3** probes into growing yeast cultures in 2% glycerol media. Lipid extraction and TLC experiments revealed that **C_{14}-MAG-N_3** probe generated the best extent of labeling when it resulted in strong labeled lipid spots even at 0.25 mM concentration. TLC studies also revealed **C_{10}-MAG-N_3** and **C_{12}-MAG-N_3** probes to exhibit considerable fluorescent spots correspoinding to labeled neutral lipids when grown in the same conditions (log-phase incubation and glycerol growth media). These experiments also suggested that 1 mM probe concentrations were needed to observe clear/strong labeled lipid spots on the TLC plate. However, the growth of yeast cultures in glycerol media was slow. This entailed dilution of initial seed cultures and re-inoculation into glycerol media, spanning ~5 days, before the MAG analogs could even be incubated.

However, Dr. Carr's work also showed preliminary evidence that growing probes in 2% galactose media instead of glycerol resulted in labeled lipids spots on TLC.[221] Thus, my initial aim was to perform cellular labeling experiments utilizing galactose as the carbon source for efficient labeling protocols. The next sections will reveal how these probes fared as precursors for incorporation into lipid metabolism by investigating the labeled lipid content and conducting fluorescence microscopy experiments along with other analytical techniques.

3.4.2 Fluorescence microscopy and flow cytometry studies with Gly-N_3 and MAG-N_3

To study metabolic labeling using **Gly-N_3** and **MAG-N_3** probes, we once again employed the yeast *S. cerevisiae,* which has proven to be a valuable model system for eukaryotic lipid metabolism.[222, 223] Moreover, glycerol kinase from *S. cerevisiae* has previously been shown to tolerate unnatural modification of its glycerol substrate.[224]

We began evaluation of cellular labeling activities by conducting fluorescence microscopy experiments resulting from treatment of cells with probe, followed by SPAAC with a clickable fluorescent reagent. In detail, cells were grown in 2% galactose synthetic media and then incubated with 1 mM of **Gly-N_3** and **MAG-N_3** derivatives. The media was removed and cells were washed, followed by addition of formaldehyde (3.7%) solution for fixation. Azide-bearing lipids were then labeled through conjugation to DBCO-Cy3 via SPAAC, washes were performed to remove unreacted dye, and cell labeling was visualized using confocal fluorescence microscopy. In these experiments, initial glycerol analog **Gly-N_3** did not show evidence of incorporation into cells since signal from cells treated with 1mM **Gly-N_3** was not more intense when compared to negative control cells not treated with **Gly-N_3** (**Figure 3.3**). These results suggested that **Gly-N_3** probe was either not effective at infiltrating metabolic pathways to label glycerolipids or that cell entry of this compound was unsuccessful when cells are grown in galactose media.

On the contrary, cellular fluorescence images resulting from **C_n-MAG-N_3** probe treatment showed widely variable signal strength and localization depending upon the length of the acyl chain. In particular, **C_4-MAG-N_3** primarily resulted in fluorescence that was localized at the periphery of cells (**Figure 3.4A**). This was noted as a positive since our goal was to label glycerolipids, many of which are localized at cellular plasma membranes. It is important to note

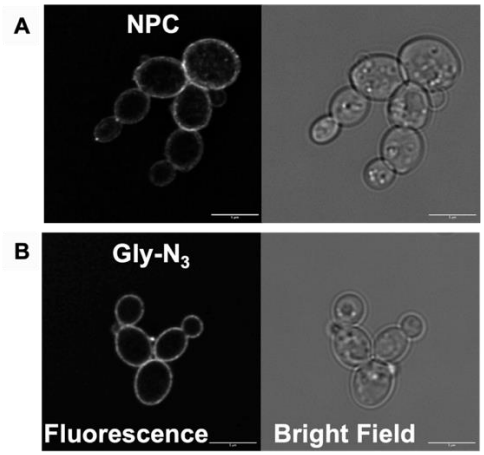

Figure 3.3. Fluorescence micrographs of S. cerevisiae cells treated with 1 mM Gly-N_3. Cells were incubated with **Gly-N_3** (50 µL stock in 99% ethanol) or without probe (50 µL ethanol) were grown for 12 hrs and were fixed and clicked with DBCO-Cy3 fluorophore. Cellular fluorescence images of Cy3 fluorescence did not show significantly increased fluorescence for cells treated with **Gly-N_3** (**B**) compared to untreated cells (**A**). Scale bar indicates 5 µm.

that the localization of the observed signal may be impacted by the accessibility of the dye reagent (DBCO-Cy3), which could enhance labeling of the plasma membrane as the first point of contact. It is also possible that lipids could remain mobile after fixing cells, since, our fixation methods (PFA) only reacts to crosslink amine-containing lipid-fluorophore conjugates, leaving other lipids mobile, and thus could impact localization. Nevertheless, the results show that **C_4-MAG-N_3** is effective at labeling cells.

On the contrary, probes with longer acyl chains yielded variable fluorescence patterns. For MAG probes bearing intermediate length chains (**C_{10}-MAG-N_3**, **C_{12}-MAG-N_3**), we instead observed diffuse cytosolic staining (**Figure 3.4C, D**). We speculated that this signal profile may result from cell death, since it is characteristic for the plasma membranes of dead yeast cells to rupture, which may lead to accumulation of excess dye.[225]

Interestingly, further increasing of chain length in the probe **C_{14}-MAG-N_3** (**Figure 3.4E**) culminated in a return to fluorescence localized at the cell periphery, although the resulting signal was rather weak compared to that resulting from **C_4-MAG-N_3** treatment. Meanwhile, MAG probe containing palmitic acid tail, **C_{16}-MAG-N_3**, showed fluorescence at the cytosol (**Figure 3.4F**). Besides the enhanced cytosolic fluorescence, brightfield images for capric **C_{10}-MAG-N_3** and lauric **C_{12}-MAG-N_3** probes showed inconsistent cell morphology and sizes, while probe **C_{16}-MAG-N_3** displayed ruptured cytosol, which is another necrotic marker. We investigated this possibility further via cytotoxicity experiments that will be described in the next section. Probe **$C_{18:1}$-MAG-N_3** instead resulted in fluorescent clumps within cells (**Figure 3.4G**) and was further investigated via colocalization experiments (*See Section 3.6*).

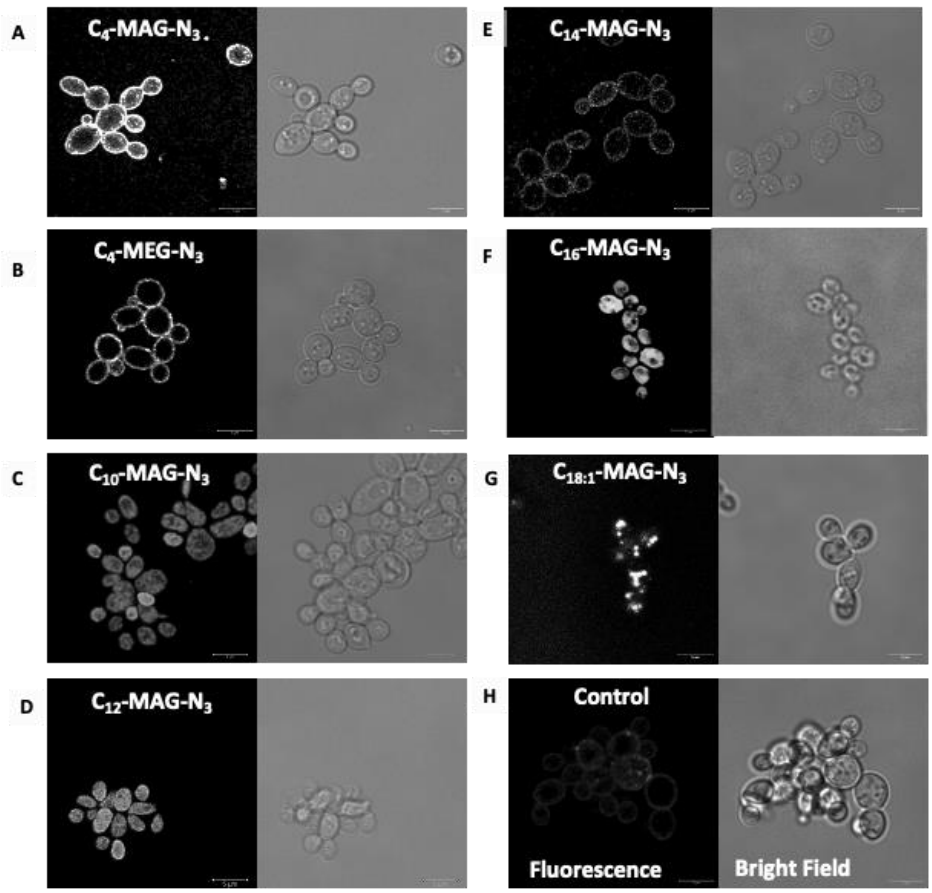

Figure 3.4. Fluorescence micrographs of cell labelling with C_n-MAG-N_3 probes and C_4-MEG-N_3. S. cerevisiae cells were treated with 1.0 mM of either **C_4-MAG-N_3** (**A**), **C_4-MEG-N_3** (**B**), **C_{10}-MAG-N_3** (**C**), **C_{12}-MAG-N_3** (**D**), **C_{14}-MAG-N_3** (**F**), **C_{16}-MAG-N_3** (**F**), **$C_{18:1}$-MAG-N_3** (**G**), or ethanol (**H**) from the initial OD_{600} of 0.2 and incubated for 12 hrs. After removal of media and washing steps, cells were then fixed and click-labeled with 1 µM DBCO-Cy3, washed to remove unreacted dye, and subjected to confocal microscopy. In each panel, the left image shows fluorescence while the right side provides a bright field image. Images are representative of n = 180 fluorescing cells from 6 biological replicates. Scale bars indicate 5 µm.

Based on the promising labeling properties we observed for **C_4-MAG-N_3**, we next compared this to imaging resulting from ether-linked derivative **C_4-MEG-N_3**. We expected that the ether-linked chain at the *sn*-3 position in the latter probe would disable cleavage by esterase enzymes, which we hypothesized would preclude metabolic labeling of phospholipid biosynthesis due to the unavailability of the *sn*-3 hydroxyl group for phosphorylation and headgroup introduction. We found that confocal images resulting from **C_4-MEG-N_3** exhibited signal localization that was similar to **C_4-MAG-N_3** but appeared to be significantly less intense (**Figure 3.4B**). This difference was quantified by flow cytometry, which confirmed diminished fluorescence using **C_4-MEG-N_3** probe compared to **C_4-MAG-N_3** (**Figure 3.5**). This fluorescence analysis thus served as the first clue that **C_4-MEG-N_3** probe was less efficient at labeling compared to **C_4-MAG-N_3**.

It should be noted that due to instrumental wavelength filters, flow cytometry experiments were performed via SPAAC with a different clickable reagent (AF647-DBCO). The results from these experiments provided initial evidence in line with our hypothesis by suggesting that probe **C_4-MEG-N_3** is less effective at metabolic labeling compared to **C_4-MAG-N_3** probe, which will be discussed further through subsequent TLC and MS experiments.

We also quantified fluorescence signal for long chain **C_n-MAG-N_3** probes (**Figure 3.6**). No significant difference in fluorescence intensity between **C_{14}-MAG-N_3** and control samples was observed. This was surprising since TLC experiments conducted by Dr. Carr indicated this probe to be the most efficient at labeling. However, the discrepency is likely due to the difference in carbon sources used for growing the cells.

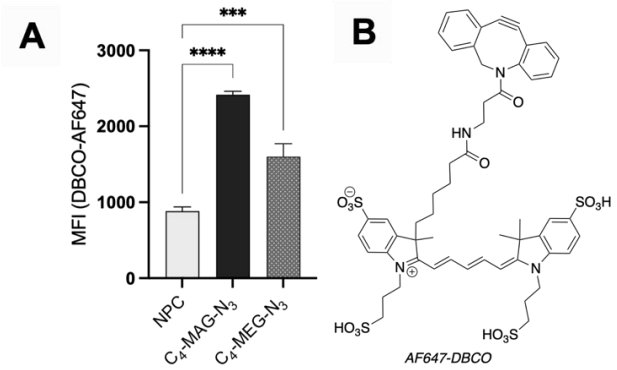

Figure 3.5. Flow cytometry analysis of S. cerevisiae cells incubated with C_4-MAG-N_3 and C_4-MEG-N_3. Quantification of fluorescence intensity (Mean fluorescent intensity, MFI) for cells labeled by **C_4-MAG-N_3** and **C_4-MEG-N_3** was performed by flow cytometry (**A**) after SPAAC with clickable dye AF647-DBCO (**B**). Error bars represent standard errors from 6 biological replicates. Significance was determined by Brown-Forsythe and Welch's ANOVA test (*** p = 0.0001; **** = p <0.0001) via GraphPad Prism.

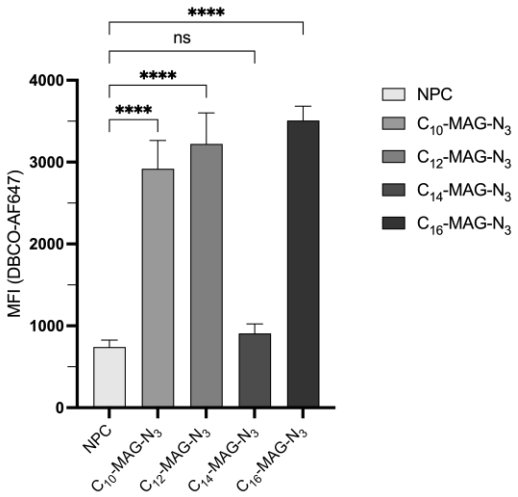

Figure 3.6. Flow cytometry analysis of S. cerevisiae cells incubated with medium chain and long chain C_n-MAG-N_3 probes. Quantification of fluorescence intensity (Mean fluorescent intensity, MFI) for **C_n-MAG-N_3** and probes **C_{10}**, **C_{12}**, **C_{14}**, and **C_{16}** was measured and analyzed by flow cytometry after SPAAC with clickable dye AF647-DBCO. Error bars represent standard errors from 6 biological replicates. Biological replicates were analyzed on the same day. Significance was determined by Brown-Forsythe and Welch's ANOVA test (ns = not significant; **** = p <0.0001) via GraphPad Prism.

3.4.3 Cytotoxicity studies for azido-MAG probes

Since we had speculated that certain probes were affecting cell viability, we next moved to study cytotoxicity effects of probes that produced fluorescent signal. To do so, *S. cerevisiae* cells were grown in galactose media in the presence of 1 mM of each probe and cell density (OD_{600}) was measured at 0, 12, 14, and 24 hour time points. We observed that MAG probes with medium chain fatty acid tails (**C_{10}-MAG-N_3**, **C_{12}-MAG-N_3**), which had resulted in intense cytoplasmic fluorescence signal and exhibited significantly higher fluorescence compared to control (Flow cytometry results, **Figure 3.6**), indeed abrogated cell growth since OD_{600} maintained at lag phase around 0.2 or 0.4 (**Figure 3.7**). This phenomenon is in line with prior literature reports that *S. cerevisiae* cells are known to undergo a pro-apoptotic mechanism upon exogenous treatment with MAGs with medium acyl chain length.[226,227] Interestingly, **C_{16}-MAG-N_3** probe containing the palmitoyl tail, which also exhibited similar cytosolic fluorescence, displayed minimal growth suppression (**Figure 3.7A**). While palmitoyl glycerol has been shown to be toxic in rodent models,[228, 229] previous studies in *S. cerevisiae* showed no lipotoxic effects of palmitoyl MAG, and instead displayed MGl2p or MAG lipase activity preference for C-16 acyl chain length instead.[219] Nevertheless, our results imply that either **C_{16}-MAG-N_3** probe itself or esterase-cleaved palmitic acid from the probe causes some cellular growth repression over time. Otherwise, the **C_4-MAG-N_3**, **C_{14}-MAG-N_3**, **C_{18}-MAG-N_3**, **$C_{18:1}$-MAG-N_3**, and **C_4-MEG-N_3** analogs enabled log-phase cell growth that was in range of no probe control cells (**NPC**). Moreover, the calculated doubling times (Dts) from the growth curves (14 hrs) for **C_4-MAG-N_3** and **C_4-MEG-N_3** were not significantly different from that of untreated cells (**Figure 3.7B**).

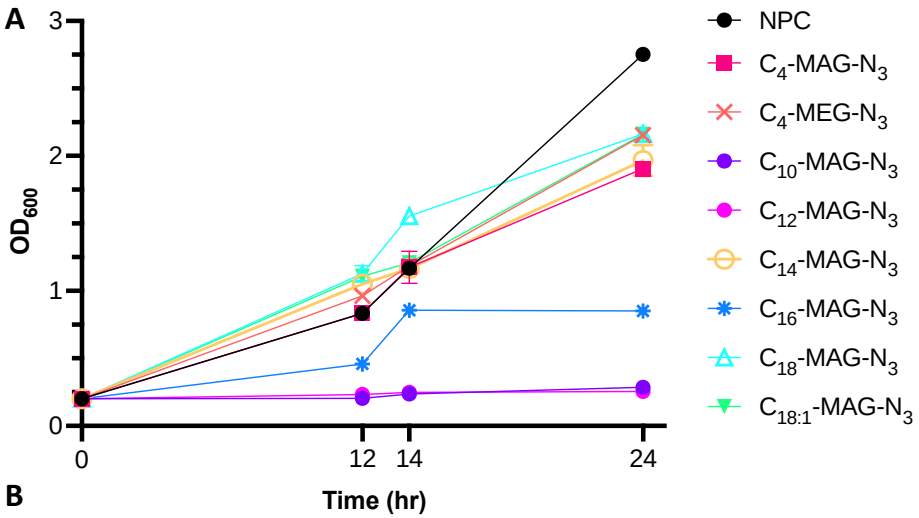

B

Sample	doubling time (hr)	14 hrs		
NPC	5.497	**Dunnett's T3 multiple comparisons test**	**p-value**	**Significance**
C_4-MAG-N_3	5.490	NPC vs. C_4-MAG-N_3	0.9995	ns
C_4-MEG-N_3	5.440	NPC vs. C_4-MEG-N_3	0.9330	ns

Figure 3.7. Growth of S. cerevisiae cells in the presence of 1.0mM C_n-MAG-N_3 probes. A. Growth curves for cells treated with different MAG probes. Cells growing at log-phase were diluted to an initial OD_{600} of 0.2 and incubated with 1.0 mM of each **C_n-MAG-N_3** analog as well as **C_4-MEG-N_3** in 2% galactose media. Cell densities were measured at 12, 14, and 24 hour time points. **B.** Doubling times calculated from growth curves (14 hr) in the presence of **C_4-MAG-N_3** and **C_4-MEG-N_3.** Doubling times for either probe was shown to not be significantly different from untreated cells. Statistical analysis was performed using Welch ANOVA test and the post-hoc analysis compares each **C_4-MAG-N_3** and **C_4-MEG-N_3** to control (ns: not significant).

3.5 Investigating classes and species of labeled lipids from C_4-MAG-N_3 and C_4-MEG-N_3

3.5.1 Fluorescence-based TLC reveals labeling of phospholipid and neutral lipid classes

We next set out to confirm glycerolipid labeling and investigate the lipid classes that are labeled by the C_4-containing probes, which we selected for further analysis based on their favorable imaging properties. We initially performed thin-layer chromatography (TLC) analysis by extracting lipids from cells incubated with either **C_4-MAG-N_3** or **C_4-MEG-N_3**, grown for 12 or 24 hrs. Lipid extracts were then subjected to fluorescence labeling via copper-catalyzed azide-alkyne cycloaddition (CuAAC) with ethynylnaphthalimide "naphth", a nonpolar fluorogenic reagent that minimally impacts R_f of lipids, followed by analyzing via TLC separation (**Scheme 3.1**). These probes are expected to label both non-polar (i.e. TAG/DAG) and polar (i.e. glycerophospholipid) products (see summary of potential products in **Figure 3.8**).

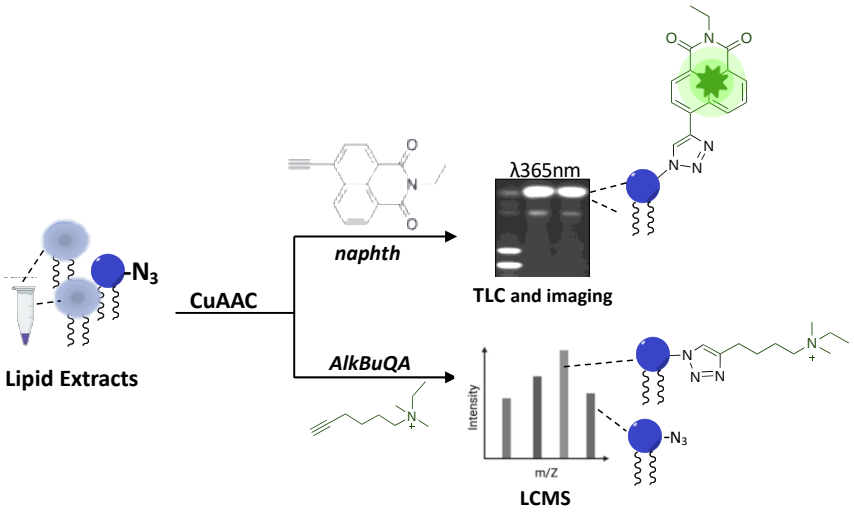

Scheme 3.1. General experimental outline for fluorescence-based TLC and MS analysis via CuAAC. S. cerevisiae cells were incubated with 1.0 mM **C_n-MAG-N_3** or **C-MEG-N_3** for 12 hrs, harvested, washed, and subjected to a lipid extraction and CuAAC protocol with either naphth dye for TLC separation and visualization or with an alkyne quaternary ammonium reagent, **AlkBuQA**, for LCMS analysis.

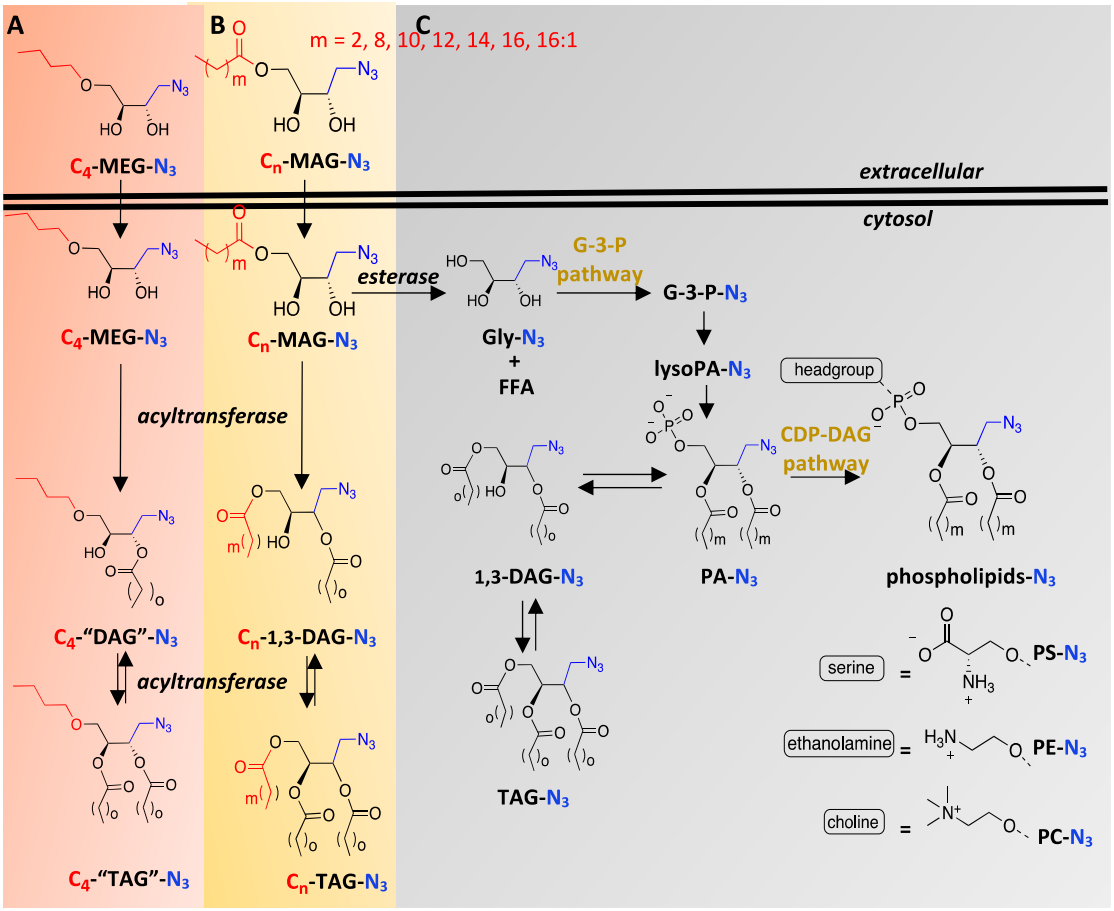

Figure 3.8. A simplified representation of lipid biosynthetic transformations in S. cerevisiae indicating potential glycerolipid products from C_4-MAG-N_3 or C_4-MEG-N_3 probe. Synthetically added tails are shown in red, biosynthetically added FA tail of varying lengths (m) are drawn in black, and the methylene azide tag is indicated by blue font. **A.** Acyltransferases can convert **C_4-MEG-N_3** into "DAG" and "TAG". Note that the C_4-ether is counted as one tail (ie: C_4-ether + fatty acyl tail = "DAG"). **B.** Labeled nonpolar lipids can be produced from acyltransferase activity from **C_4-MAG-N_3**. **C.** Alternatively, labeled neutral lipids can be accessed from the glycerol-3-phosphate (G-3-P) pathway. From **C_4-MAG-N_3**, MAG lipase/esterase activity can result in glycerol-N_3 (Gly-N_3) and free fatty acid (FFA). Then, through the cytidine diphosphate diacylglycerol (CDP-DAG) pathway, labeled phospholipids can be produced. Note that the pathways illustrated do not encompass all lipid transformations.[99, 218]

We conducted TLC analysis to separate and visualize labeled products using a two-step elution method through a combination of polar and then non-polar eluants. As shown in **Figure 3.9**, **C_4-MAG-N_3** treatment led to the appearance of fluorescent bands observed in fluorescent images that appeared close to commercial standards for both non-polar lipids (MAG, R_f = 0.79 and DAG, R_f = 0.84-0.92, non-polar) as well as two phospholipid classes (PC, R_f = 0.34 and PS, R_f = 0.28). New spots correlating with PC and PS were only observed when cells were harvested at log phase, which indicates that labeled lipids undergo rapid turnover. The R_f values for commercial standards of the appropriate lipids are listed on the left side of **Figure 3.9**, with arrows pointing toward their position. The R_f values for new spots are shown on the right side of each TLC image. These new spots appear slightly lower than commercial standards, which can be explained since these probes are modified via CuAAC with naphth dye. The timeline of labeled lipid turnover was investigated in pulse-chase labeling experiments (*Section 3.5.3*).

Treatment with **C_4-MEG-N_3** led to similar high R_f spots that were comparable to commercial standard for DAG (R_f = 0.84-0.92, lanes 6-7, **Figure 3.9B**). In contrast, there were no clear bands corresponding to polar lipids (R_f < 0.60) resulting from cells grown with **C_4-MEG-N_3**. These results support our hypothesis that **C_4-MAG-N_3** would be effective for labeling phospholipids while this activity would be deactivated for **C_4-MEG-N_3** by irreversibly blocking the *sn*-3 position where the phospholipid headgroup would reside.

While probe **C_4-MAG-N_3** produced TLC bands that correlate with phospholipids, it is important to note that these spots were faint, particularly in comparison to bands for labeled products that overlap with neutral lipids. This suggests that **C_4-MAG-N_3** is less effective as a

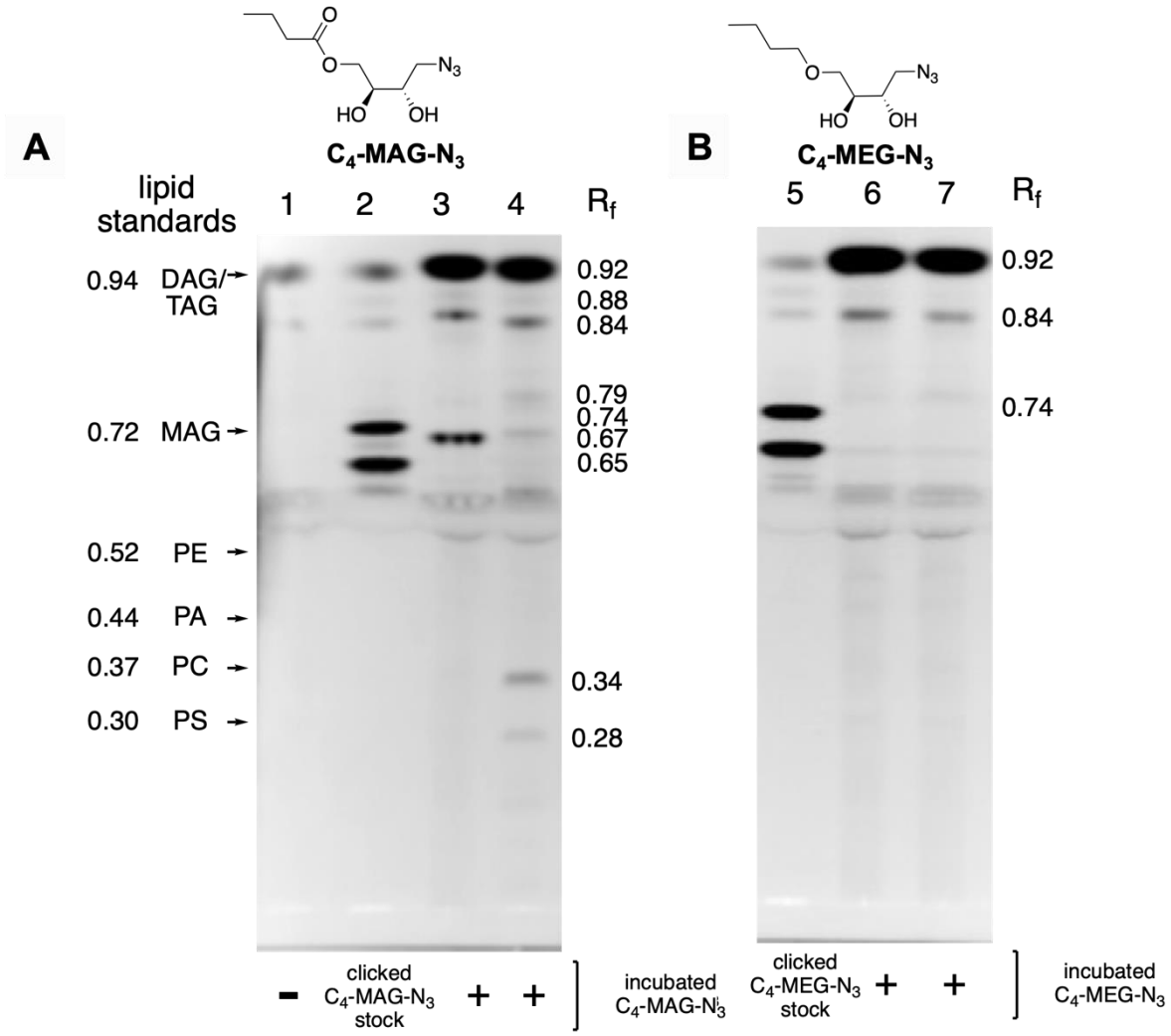

Figure 3.9. TLC image showing C_4-MAG-N_3 labels neutral lipids and phospholipids while C_4-MEG-N_3 labels only neutral lipids. Lipids were extracted and subjected to CuAAC reaction with ethynylnaphthalimide "naphth". Clicked extracts were loaded onto a TLC plate for lipid separation by elution with chloroform/methanol/water/acetic acid and then cyclohexane/ethyl acetate and then analyzed by fluorescence imaging. **A)** Lane 1 contained no probe control lipid extracts. Lane 2 was loaded with a stock of **C_4-MAG-N_3** that was clicked with naphth. Lanes 3 and 4 were naphth-clicked lipid extracts from yeast incubated with **C_4-MAG-N_3**. Lane 3 contained lipids isolated from 24-hr incubation while lane 4 contained lipids obtained from 12-hr incubation. The R_f values and positions of lipid standards for DAG (16:0/16:0), MAG (18:1), and different phospholipids are indicated with arrows on the left side of the figure (viewed after primulin staining). R_f values for new spots are shown on the right side of each image. **B)** TLC plate representing click-derived fluorescence from lipid extracts when S. cerevisiae cells were incubated with 1.0 mM **C_4-MEG-N_3**. Lane 5 was loaded with a stock of **C_4-MEG-N_3** that was clicked with naphth. Lanes 6 and 7 contained lipids from 24-hr and 12-hr incubation, respectively.

substrate for enzymes that produce phospholipids, perhaps because the added azidomethylene tag is problematic for these particular enzymes. On the contrary, probe **C_4-MEG-N_3** can be seen as advantageous since our data support that this probe bypasses the labeling of phospholipids altogether but retains robust labeling of neutral lipids. Therefore, this strategy is expected to be beneficial for focusing metabolic labeling within the family of neutral lipids including DAG and TAG products.

3.5.2 LCMS analysis confirms labeling of several lipid classes by C_4-MAG-N_3

To further characterize the identities of potential labeled products (see **Figure 3.8**), we additionally performed MS analysis after whole-cell lipid extraction. For this purpose, azide-tagged lipids were post-derivatized through CuAAC reaction with *N*-ethyl-*N*,*N*-dimethylhex-5-yn-1-aminium (**AlkBuQA**) to enhance LCMS detection, as described in previous reports,[112,230] followed by LCMS analysis (**Scheme 3.1**). After lipid extract sample preparation (Hanson and Lester method),[231] LC/MS experiments were run by Katarina Jones at the BSMMSC. Cells treated with **C_4-MAG-N_3** yielded mass peaks corresponding to a range of labeled lipids including both phospholipids (**Table 3.1**; PA, PS, PE, PC; representative mass spectra shown in **Figure 3.10**) and neutral lipids. Unclicked azide-labeled glycerophospholipids were detected as [M+H]+ and [M+NH_4]+ species under positive ESI conditions and were detected as [M-H]- or [M+FA-H]- species under negative mode. In all cases, mass peaks were observed from replicate samples from **C_4-MAG-N_3**-treated cells and masses were not observed for untreated/NPC samples.

Table 3.1. Detected mass peaks corresponding to labeled phospholipid products from cells incubated with C_4-MAG-N_3 probe. Lipids are listed as either the unclicked product (mN_3) or click-derived product (mAlkQA). Derivatized (AlkQA) lipids were detected as [M]+. (mN_3 = methylene azide, mAlkQA= methylene alkyne quaternary ammonium, FA = formic acid). Retention times (native RT) for native lipid are included.

adduct	PA lipid species	Calculated mass	Detected mass	Error (ppm)	RT	native RT	native lipid	adduct
[M-H]-	(36:0)PAmN3	758.5454	758.5459	0.66	12.98	13.68	(36:0)PA	[M-H]-
[M-H]-	(34:1)PAmN3	728.4984	728.4993	1.24	13.98	13.27	(34:1)PA	[M-H]-
[M-H]-	(34:0)PAmN3	730.5141	730.5151	1.37	13.57	12.56	(34:0)PA	[M-H]-
[M]+	(36:2)PAmAlkQA	909.6804	909.6796	0.88	12.07	13.38	(36:2)PA	[M+H]+
[M]+	(16:1)LPAmAlkQA	617.4037	617.4012	4.05	6.42	--	(16:1)LPA	[M+H]+

adduct	PS lipid species	Calculated mass	Detected mass	Error (ppm)	RT	native RT	native lipid	adduct
[M-H]-	(34:2)PSmN3	813.5148	813.5125	-2.83	11.17	11.44	(34:2)PS	[M-H]-
[M-H]-	(34:1)PSmN3	815.5305	815.5294	-1.35	11.23	11.27	(34:1)PS	[M-H]-

adduct	PE lipid species	Calculated mass	Detected mass	Error (ppm)	RT	native RT	native lipid	adduct
[M-H]-	(36:1)PEmN3	799.5720	799.5696	-3.00	12.07	12.54	(36:1)PE	[M-H]-
[M-H]-	(34:0)PEmN3	773.5563	773.5545	-2.33	14.80	14.97	(34:0)PE	[M-H]-
[M-H]-	(32:1)PEmN3	743.5093	743.5074	-2.56	11.50	12.63	(32:1)PE	[M-H]-
[M+NH4]+	(34:0)PEmN3	792.5974	792.5998	3.03	9.43	10.54	(34:0)PE	[M+NH4]+
[M+NH4]+	(30:0)PEmN3	736.5348	736.5319	-3.94	11.47	10.86	(30:0)PE	[M+NH4]+

adduct	PC lipid species	Calculated mass	Detected mass	Error (ppm)	RT	native RT	native lipid	adduct
[M+FA-H]-	(36:2)PCmN3	885.6087	885.6064	-2.60	11.45	13.6	(36:2)PC	[M+FA-H]-
[M+FA-H]-	(30:1)PCmN3	803.5305	803.5273	-3.98	9.07	10.82	(30:1)PC	[M+FA-H]-
[M+FA-H]-	(28:1)PCmN3	775.4992	775.4971	-2.71	8.67	9.01	(28:1)PC	[M+FA-H]-
[M]+	(36:0)PCmAlkQA	998.8008	998.8035	2.70	19.8	16.06	(36:0)PC	[M+H]+
[M+NH4]+	(32:1)PCmN3	804.5974	804.5984	1.24	9.69	9.28	(32:1)PC	[M+NH4]+

A.

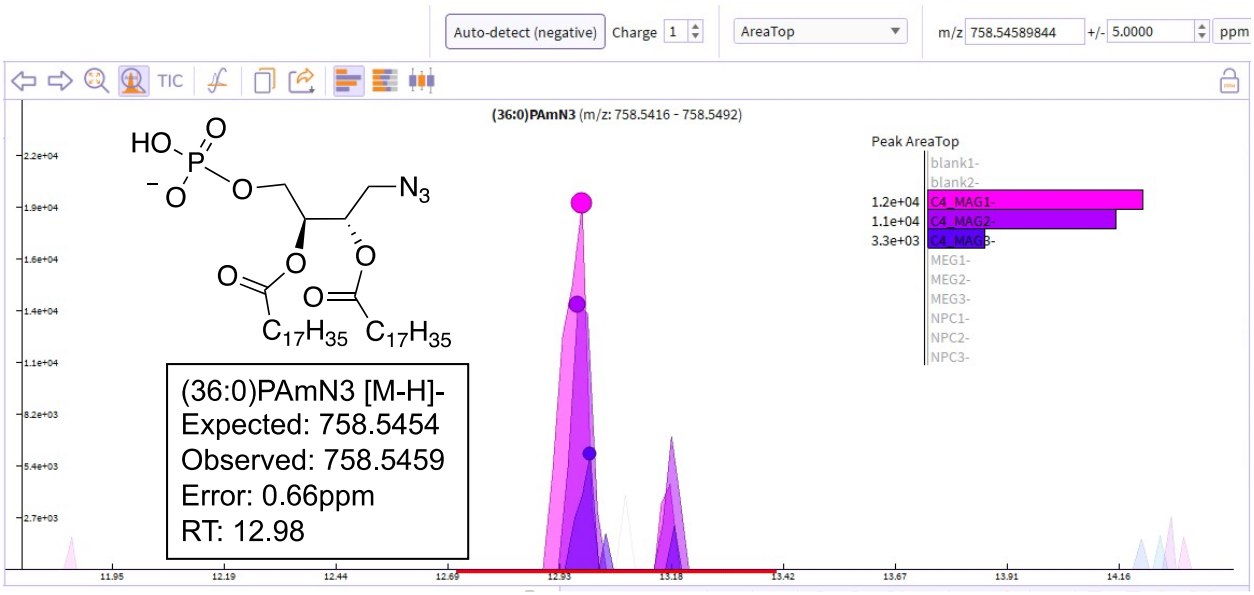

B.

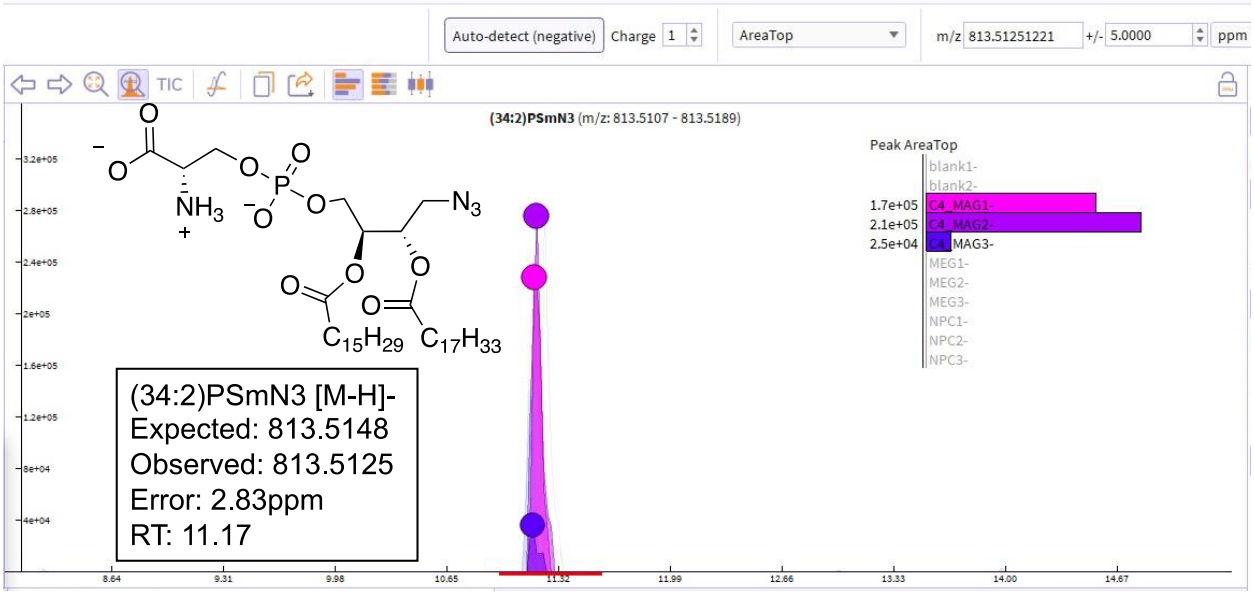

Figure 3.10. Representative mass spectra for click-tagged phospholipid products of probe C_4-MAG-N_3. Products were detected by liquid chromatography mass spectrometry (LCMS) Structures are shown that match the detected mass peak for each labeled lipid. The colored inset shows plots of peak areas and depicts three replicate samples treated with probe **C_4-MAG-N_3** (pink/purple, C4_MAG), **C_4-MEG-N_3** (light blue, MEG), or without probe (yellow, NPC). **A**) PA, **B**) PS, **C**) PE, **D**) PC. If a mass peak only showed in **C_4-MAG-N_3**-treated cells, then this confirmed that this species was N_3-labeled lipid species. Labeled lipids were identified (C12 isotope as parent peak) comparing the exact mass (±5 ppm) to a generated compound list.

C.

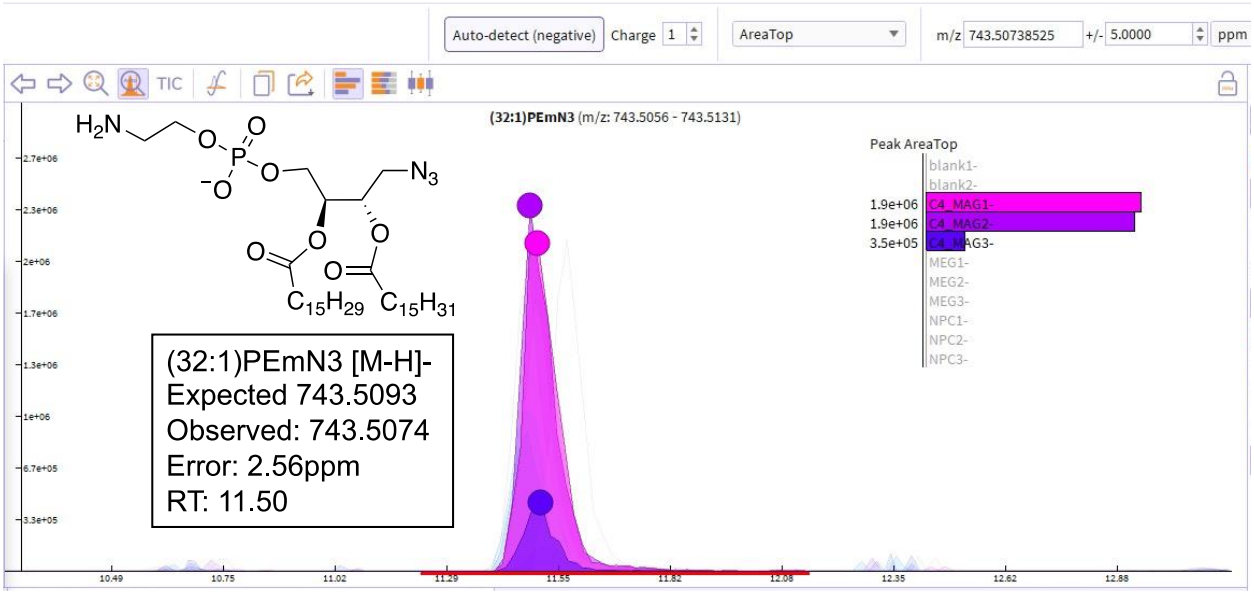

D.

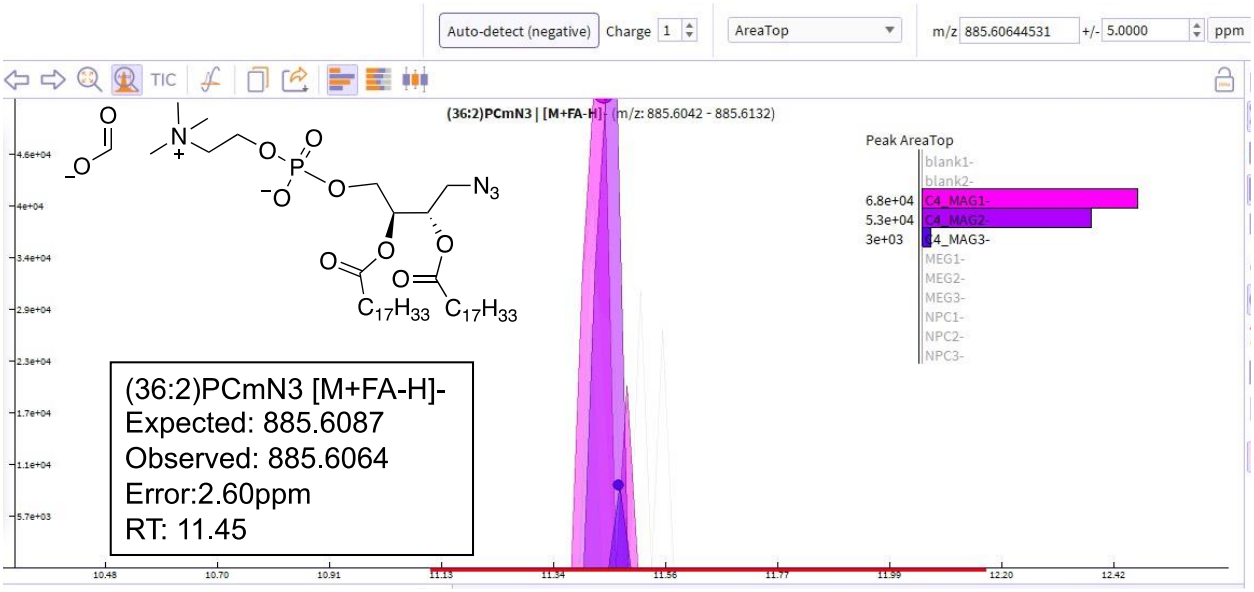

Figure 3.10. (continued)

A.

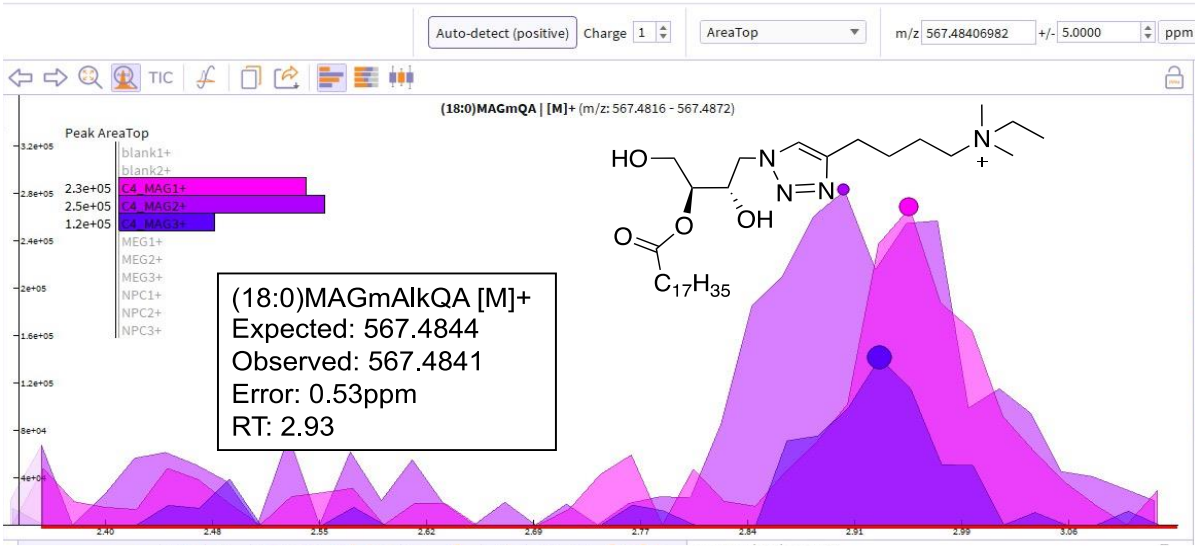

B.

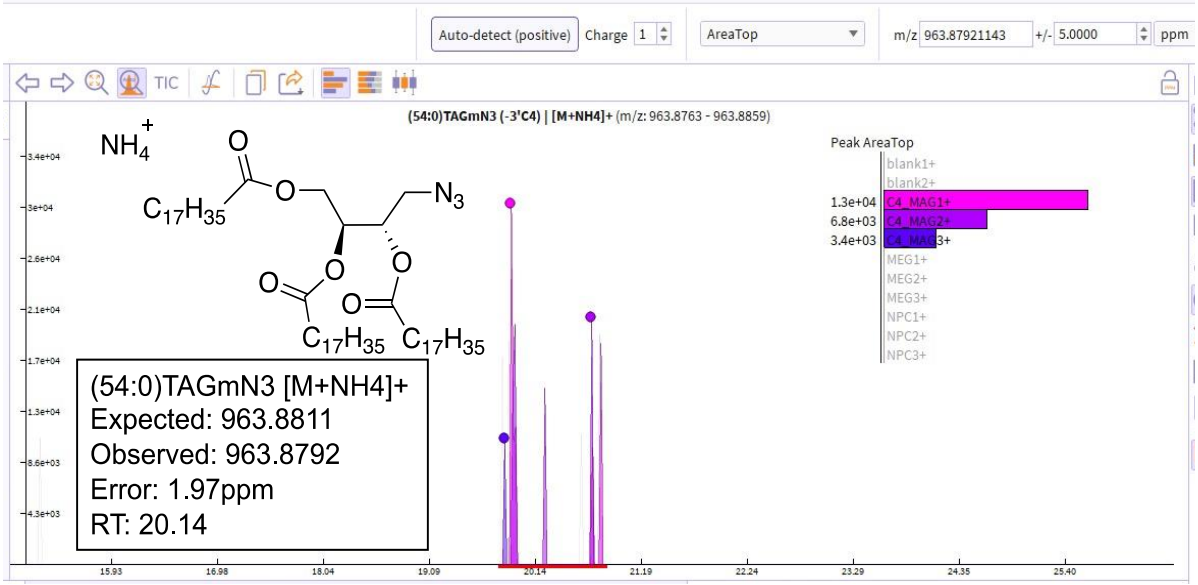

Figure 3.11. Representative mass spectra for click-tagged neutral lipid products of probe C_4-MAG-N_3. Products were detected by liquid chromatography mass spectrometry (LCMS) Structures are shown that match the detected mass peak for each labeled lipid. The colored inset shows plots of peak areas and depicts two replicate samples treated with probe **C_4-MAG-N_3** (pink/purple, C4_MAG), **C_4-MEG-N_3** (light blue, MEG) or without probe (yellow, NPC). **A**) MAG, **B**) TAG.

Labeled neutral lipids were also observed from **C_4-MAG-N_3**-treated cells (**Table 3.2**; MAG, DAG, and TAG; representative mass spectra shown in **Figure 3.11**). In our analysis, while we detected products resulting from the click reaction with **AlkBuQA**, masses corresponding to unclicked lipids (mN_3) were still detected from the same samples. Labeled lipids containing the azido-methylene tag were detected in both positive and negative ESI conditions. Azide-labeled (mN3) MAGs, DAGs, and TAGs were detected under positive ESI conditions as [M+H]+ or $[M+NH_4]$+, while clicked lipids (mAlkQA) were only detected as [M]+.

The masses of detected lipids correspond to lipids were the C4-acyl chain has been cleaved off and metabolized to other lipid products, particularly phospholipids. However, masses corresponding to unmetabolized **C_4-MAG-N_3** probe was still observed for 12 hours (data not shown). This is the first indication that butyrate hydrolysis may affect the efficiency of probe uptake into lipid metabolism.

On the contrary, **C_4-MEG-N_3** treatment was found to result in mass peaks correlating with labeled neutral lipids (**Table 3.3**; DAG and TAG; representative mass spectra shown in **Figure 3.12**), but not phospholipids. Labeled products were detected as N_3-lipids where the ether tag is retained and a FA has been acylated. In all cases, mass peaks were not observed for untreated/NPC samples. Neutral lipids were detected as the click-derived product (mAlkQA). We also found that derivatization with **AlkBuQA** enhanced the detection of labeled DAG lipids. These results further support our expectation that **C_4-MAG-N_3** labels a broad range of neutral lipids and phospholipids while blocking the *sn*-3 position of **C_4-MEG-N_3** would deactivate phospholipid labeling.

Table 3.2. Mass peaks corresponding with labeled neutral lipid products detected in positive ion mode from cells incubated with C_4-MAG-N_3 probe. Lipids are listed as either the unclicked product (mN_3) or click-derived product (mAlkQA).

adduct	glycerolipid species	Calculated mass	Detected mass	Error (ppm)	RT	native RT	native lipid	adduct
[M]+	(18:0)MAGmAlkQA	567.4844	567.4841	-0.53	2.93	5.23	(18:0)MAG	[M+H]+
[M+H]+	(34:2)DAGmN3	648.531	648.5309	-0.15	13.73	14.79	(34:2)DAG	[M+H]+
[M+NH4]+	(54:0)TAGmN3	963.8811	963.8792	-1.97	20.14	20.91	(54:0)TAG	[M+NH4]+
[M+NH4]+	(52:3)TAGmN3	873.7402	873.7401	-0.11	19.84	22.07	(52:3)TAG	[M+NH4]+
[M+NH4]+	(50:2)TAGmN3	903.7872	903.7835	-4.09	21.60	21.99	(50:2)TAG	[M+NH4]+

Table 3.3. Detected labeled neutral lipid products in positive ion mode from cells incubated with C_4-MEG-N_3 probe. Note C_4-ether is counted as one tail (ie: C_4-ether + fatty acyl tail = "DAG").

adduct	glycerolipid species	Calculated mass	Detected mass	Error (ppm)	RT	native RT	native lipid	adduct
[M]+	MEG(4:0/18:1)"DAG"mAlkQA	621.5313	621.5309	-0.64	2.93	3.67	(18:1)MAG	[M+NH4]+
[M]+	MEG(4:0/18:0)"DAG"mAlkQA	623.5470	623.5463	-1.12	5.56	5.23	(18:0)MAG	[M+NH4]+
[M]+	MEG(4:0/16:1)"DAG"mAlkQA	593.5001	593.4998	-0.51	3.18	4.46	(16:1)MAG	[M+NH4]+
[M]+	MEG(4:0/16:1/16:1)"TAG"mAlkQA	829.7141	829.7155	1.69	22.03	21.60	(48:2)TAG	[M+NH4]+
[M]+	MEG(4:0/18:1/18:1)"TAG"mAlkQA	885.7767	885.7788	2.37	22.71	21.99	(50:2)TAG	[M+NH4]+

A.

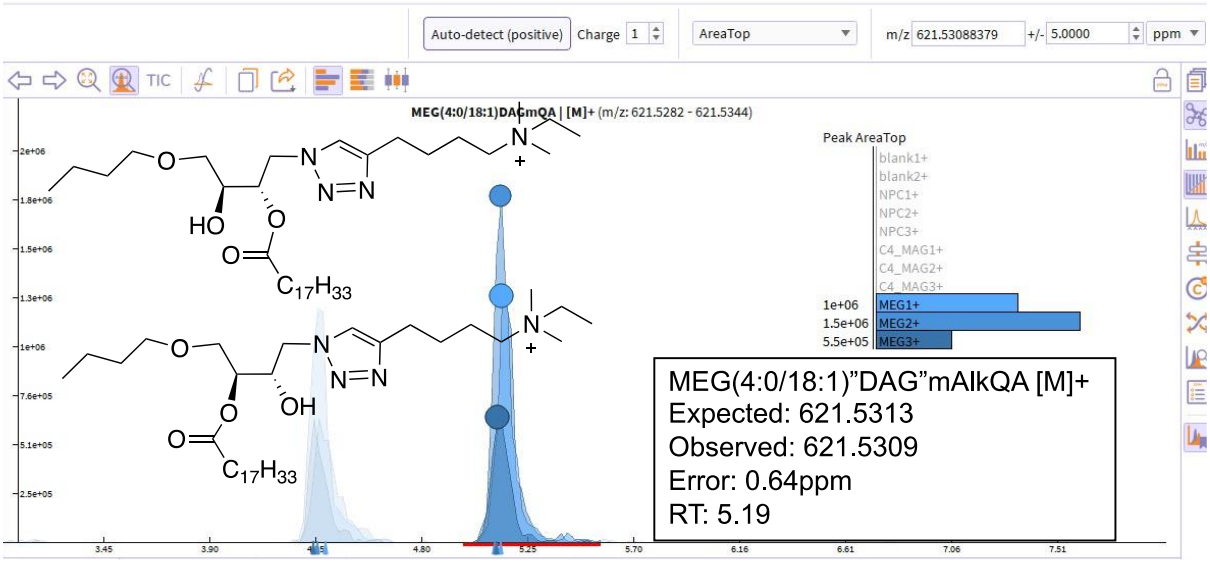

Figure 3.12. Representative mass spectra for click-tagged neutral lipid products of probe C_4-MEG-N_3. Products were detected by LCMS. The colored inset shows plots of peak areas and depicts two replicate samples treated with probe **C_4-MAG-N_3** (pink/purple, C4_MAG), **C_4-MEG-N_3** (light blue, MEG), or without probe (yellow, NPC). **A-B**) "DAG" and **C**) "TAG".

B.

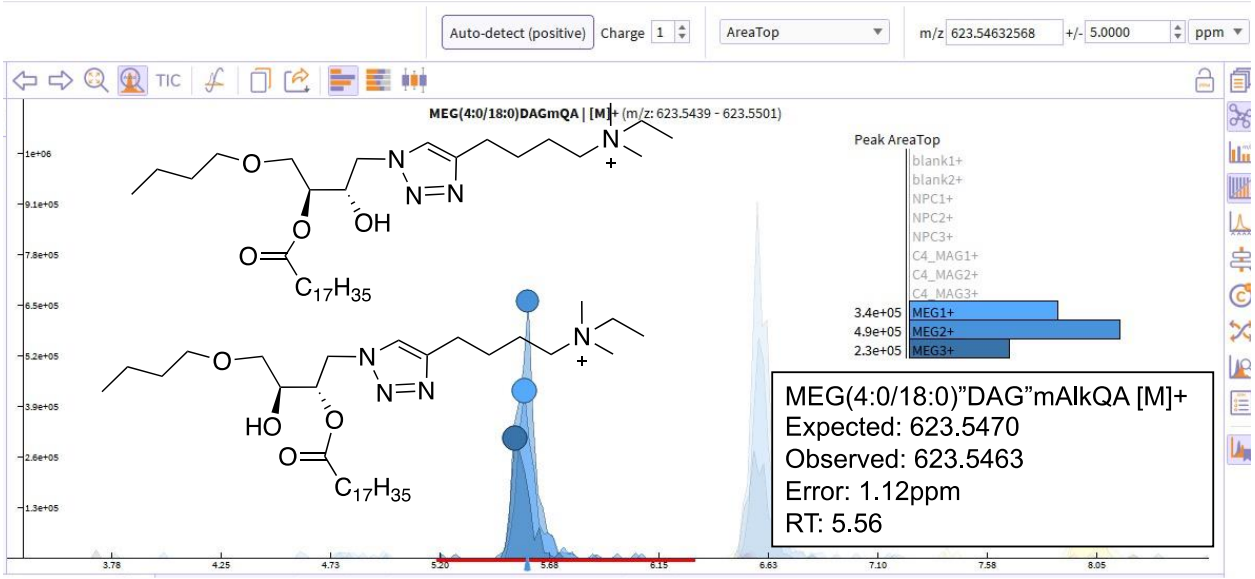

C.

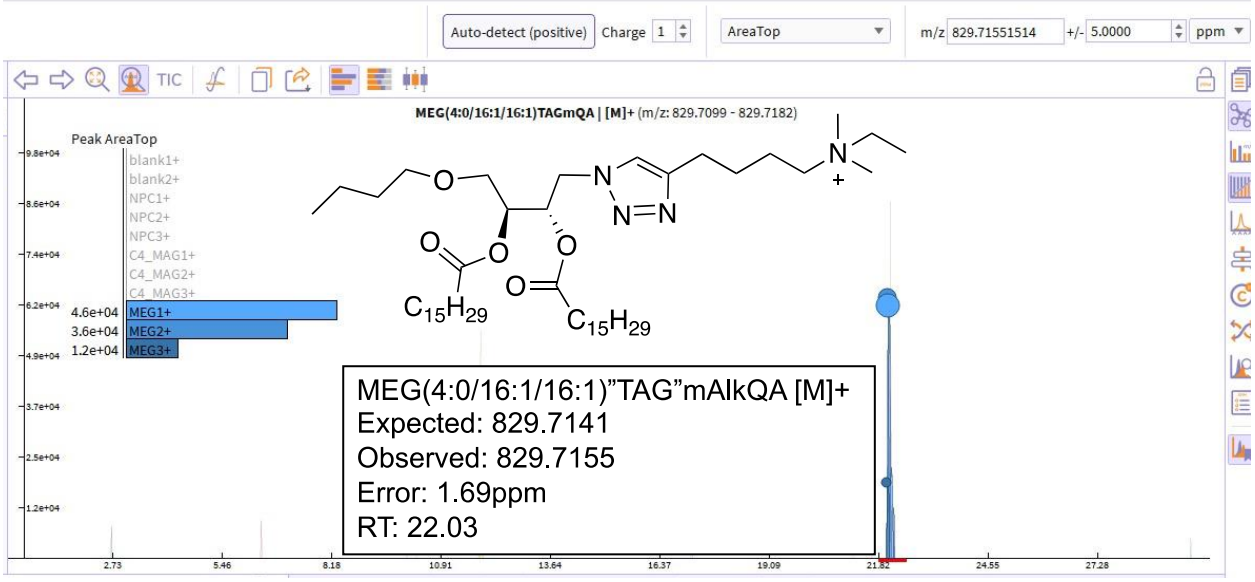

Figure 3.12. (continued)

3.5.3 Pulse-chase labeling studies with C_4-MAG-N_3

Our initial TLC results show phospholipid labeling only during log phase (12 hours), which is abrogated in stationary phase (24 hours). While normal phospholipid enzyme activity is maximal during exponential phase of cell growth,[197] these initial TLC results of "no phospholipid labeling" after 24 hr **C_4-MAG-N_3** incubation suggest that labeled lipids undergo rapid metabolism by which they are decomposed. Another likely phenomenon leading to the disappearance of bands after 24 hrs is that the yeast cells may be overloaded due to the constant presence of probe in the media. To investigate these possibilities and to gain more information on lipid turnover, we performed pulse-chase labeling experiments. For each pulse-chase experiment, we incubated cells at OD_{600} of ~0.1 with 1.0mM of **C_4-MAG-N_3**, and after the indicated pulse period, replaced the media with fresh media without probe and removed chase aliquots at 0, 2, 4, and 8 hrs.

We found that a 1 hr pulse period followed by 0, 2, 4, and 8hr chase did not result in clearly defined labeled bands through TLC analysis. We hypothesize that this result may be attributed to slow hydrolysis of butyrates[232, 233] by esterase enzymes and/or slow incorporation into labeled products such that labeling experiments may require longer probe incubation times.[234] Therefore, we performed 5 hr and 10 hr pulse periods and found that a 5 hr pulse period until mid-log phase of OD~0.4 was sufficient to observe bands via TLC (**Figure 3.13**). With these 5-hour incubation pulse-chase studies, we observed labeled spots corresponding to labeled phospholipids (R_f = 0.16, 0.20, 0.36, lanes 1-4, **Figure 3.13 A**) and neutral lipids (R_f = 0.60, 0.64, 0.80, 0.83, lanes 1-4, **Figure 3.13 A**) for all chase aliquots, indicating that these labeled lipids were stable over time (5 hr pulse, 8 hr chase).

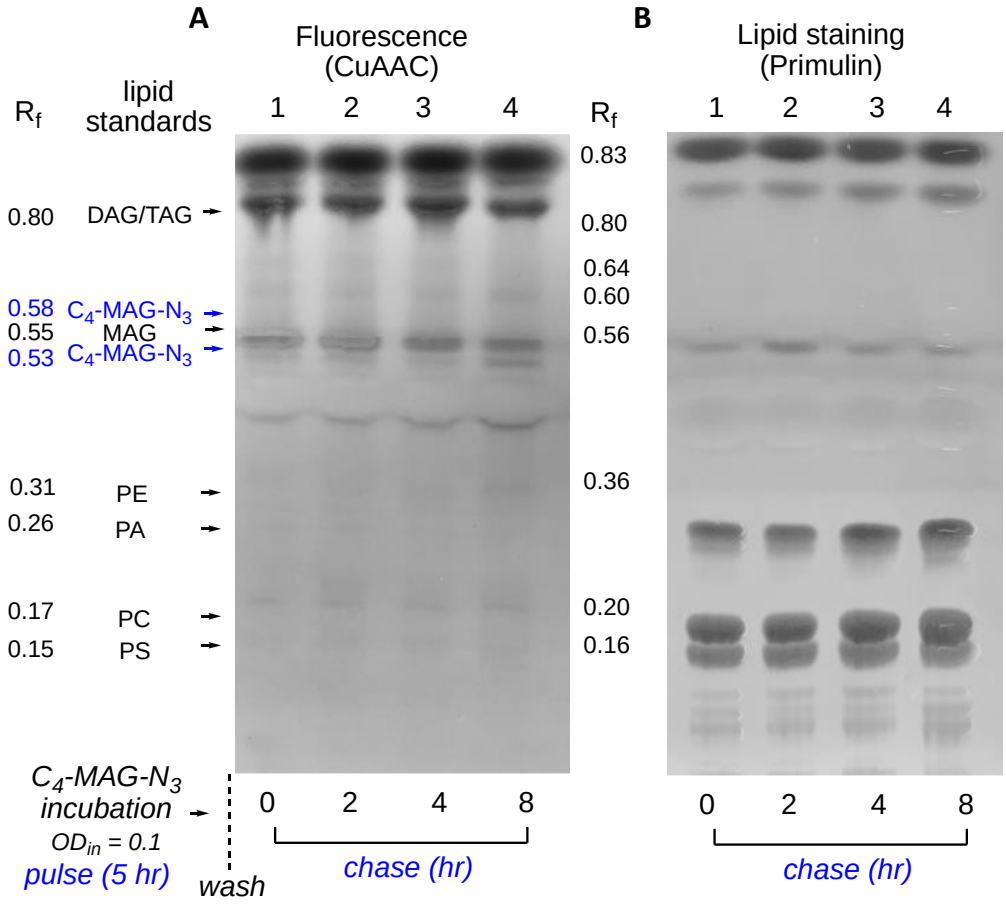

Figure 3.13. Representative TLC image for three trials of 5-hour pulse period and subsequent chase analysis (t = 0, 2, 4, 8 hrs). A. Cells were diluted to OD_{600} of ~0.1 and grown in the presence of 1.0 mM **C_4-MAG-N_3**. Cells were harvested after mid-log phase was reached (OD_{600} of ~0.4) and media was washed off. Cells were re-incubated in fresh media without probe and allowed to grow until aliquots were taken for chase (t = 0, 2, 4, 8hrs) analysis and lipid extraction. Each TLC pulse-chase experiment was run in triplicates (3 TLC plates per pulse period). **B.** The same TLC plate but imaged after primulin staining to indicate native lipid spots and lipid standards. Phospholipid labeling is observed (plate A, lanes 1-4, R_f = 0.16, 0.20, 0.36) with R_f values similar commercial lipid standards of PS, PC, and PE . Considerable neutral lipid labeling (R_f = 0.60, 0.64, 0.80) is also indicated. Note that the R_f values vary from that of Figure 3.9 since these experiments were run on a new batch of TLC plates. Lipid standards are included for each TLC run/plate to identify and compare lipid classes.

We unfortunately observed only very faint bands for labeled phospholipids after the probe was washed for the chase period. For experiments with 10 hr pulse periods, we observed similar faint phospholipid bands and all three TLC trials resulted in consistent results (**Figure 3.14**). Similar to 5-hr pulse experiments, the 10-hr pulse incubation resulted in labeled bands that did not disappear over time (over chase periods), indicating stable labeled lipids under these conditions. However, while both phospholipid and neutral lipid spots were observed, the spots corresponding to labeled phospholipids were faint especially when compared to neutral lipid bands. Thus, these pulse-chase results from 5 or 10 hr pulse periods likely suggest that phospholipid-modifying enzymes are affected to a greater extent by the addition of the azide tag.

3.6 Investigating labeled lipids from long-chain probes, C_{18}-MAG-N_3 and $C_{18:1}$-MAG-N_3.

3.6.1 Fluorescence microscopy and lipid droplet colocalization studies

Given that probe **$C_{18:1}$-MAG-N_3** was previously observed to exhibit fluorescence imaging patterns that are reminiscent of lipid droplets during studies employing Cy3 clickable dye, we were interested to know whether or not **$C_{18:1}$-MAG-N_3** exclusively labeled neutral lipids, which are the major constituents of lipid droplets (LDs).[10] To explore this possibility, we performed fluorescence imaging co-localization studies. To assess whether fluorescence lipid metabolic labeling co-localizes with lipid droplets in yeast, we compared fluorescence resulting from click chemistry conjugation (AF647-DBCO) to the signal for Nile Red (NR), a known yeast lipid droplet marker.[235] For these fluorescence microscopy experiments, AF647-DBCO was once again used for SPAAC since NR dye and DBCO-Cy3 are excitable by the same diode laser at ~550 nm.

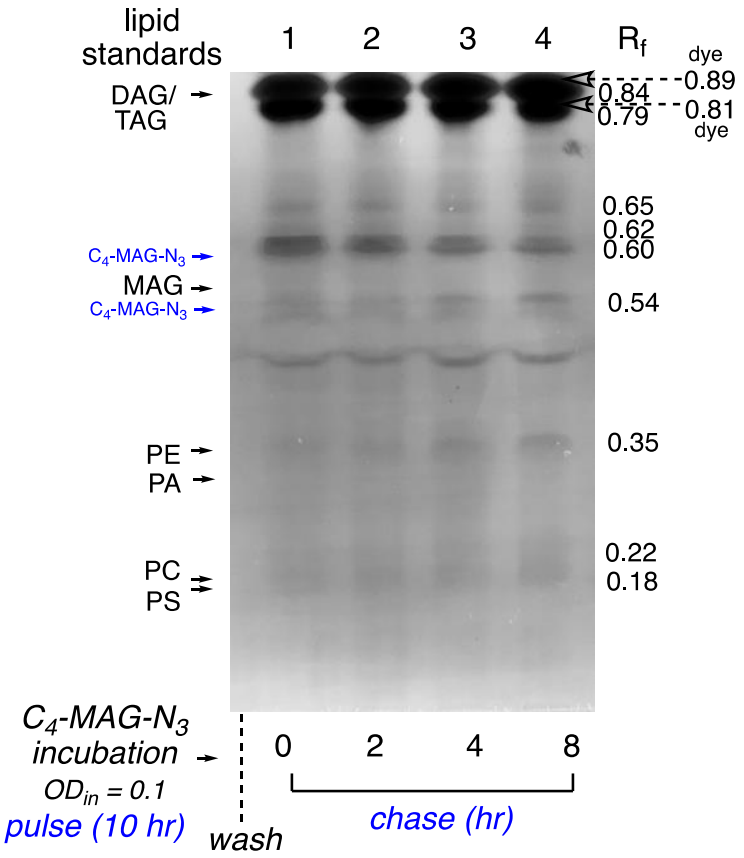

Figure 3.14. Representative TLC images for 10-hour pulse experiments. Cells were diluted to OD_{600} of ~0.1. grown in the presence of 1.0mM **C_4-MAG-N_3** and harvested after log phase was reached (**10 hours**) and media was washed off. Cells were re-incubated in fresh media without probe and allowed to grow until aliquots were taken for chase (t = 0, 2, 4, 8hrs) analysis and lipid extraction. Some faint phospholipid labeling is observed after 10 hr pulse incubation of probe (R_f = 0.18,0.22, 0.35) while neutral lipid labeling is also shown (R_f = 0.65,0.79, 0.84).

During experiments the internal fluorescent clumps were not reproducible when cells grown with 1.0 mM of **$C_{18:1}$-MAG-N_3** were clicked with AF647-DBCO dye (**Figure 3.15A**). While we observed fluorescent clumps from these studies, they were either localized on the plasma membrane or associated outside the cell for single-stained (DBCO) cells. This was also the case for **$C_{18:1}$-MAG-N_3** -incubated cells that were both clicked with AF647-DBCO and stained with NR. As observed in **Figure 3.15B**, Cy5 fluorescence was observed outside of regions of fluorescence due to NR staining, and thus, no colocalization. These results suggest that probe **$C_{18:1}$-MAG-N_3** does not result in fluorescent signal that co-localizes with lipid droplets. One possible explanation for the inconsistent fluorescence signals between click reactions with Cy3-DBCO and AF647-DBCO dyes could be the inaccessibility of AF647-DBCO in labeling LDs since it is a triply-sulfonated dye and is highly hydrophilic. Utilizing a non-sulfonated cyclooctyne dye with an excitation wavelength outside of NR should be sought after for follow-up colocalization experiments.

We also quantified fluorescence after SPAAC using flow cytometry for **$C_{18:1}$-MAG-N_3** and the saturated (stearate) analog **C_{18}-MAG-N_3** and found that the latter was not significantly more fluorescent than control (**Figure 3.15C**). We hypothesized that the saturated C_{18} probe was not incorporated for metabolic labeling because there was no observed fluorescence after click conugation (microscopy and flow cytometry) and that this probe also resulted in insoluble clumps when spiked onto cell cultures (**Figure 3.15D**). All in all, these microscopy experiments did not validate nor negate the possibility for **$C_{18:1}$-MAG-N_3** labeling LDs. While **C_{18}-MAG-N_3** probe may not be a stuitable reporter for labeling, **$C_{18:1}$-MAG-N_3** probe needs to be explored through different means such as by analysis and isolation of its lipid content by solvent extraction methods.

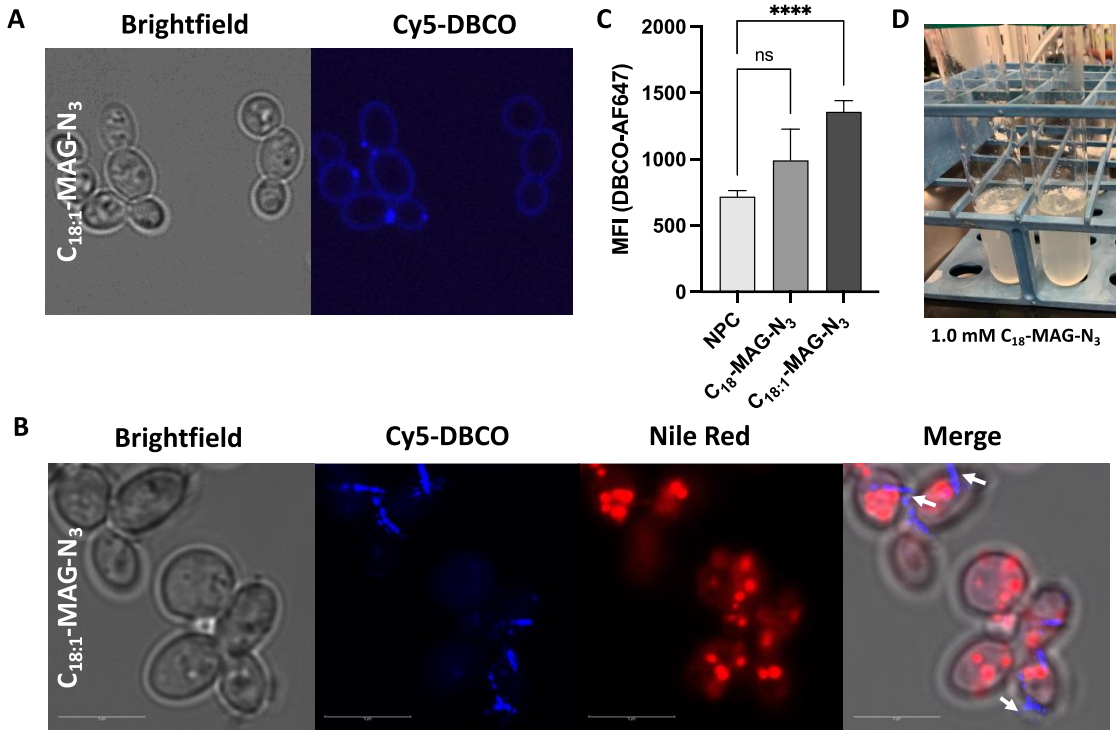

Figure 3.15. Analysis of cellular labeling by long-chain proes C_{18}-MAG-N_3 and $C_{18:1}$-MAG-N_3 in S. cerevisiae cells. Yeast cells were incubated for 12 hrs with 1.0 mM **C_{18}-MAG-N_3** or **$C_{18:1}$-MAG-N_3** (log-phase). Harvested cells were then fixed and clicked with **DBCO-AF647** or **Cy5-DBCO** fluorophore. **A.** Faint plasma-membrane staining from **$C_{18:1}$-MAG-N_3**. **B.** Colocalization analysis of click-based fluorescence from **$C_{18:1}$-MAG-N_3** with Nile Red dye (NR). S. cerevisiae cells were grown with **$C_{18:1}$-MAG-N_3**, followed by click with DBCO-Cy5 (2 µM), and incubation with Nile Red (5ug/mL NR per 5 × 10^6 cells), which localizes at lipid droplets. After sequential scanning, the two channels for Cy5 and NR fluorescence were merged and shown in the left column. Scale bars indicate 5µm **C.** Quantification of fluorescence intensity (Mean fluorescent intensity, MFI) for **C_{18}-MAG-N_3** and **$C_{18:1}$-MAG-N_3** by flow cytometry with clickable dye AF647-DBCO. Biological replicates were analyzed on the same day. Significance was determined by Brown-Forsythe and Welch's ANOVA test (ns = not significant; **** = p <0.0001) via GraphPad Prism **D.** Image of insoluble **C_{18}-MAG-N_3** in yeast cell culture.

3.6.2 TLC and LCMS analysis on lipid extracts from $C_{18:1}$-MAG-N_3

Since fluorescence analysis after click with a sulfonated dye was not feasible for lipid droplet analysis, we moved on to extract and analyze the lipid content from cells incubated with **$C_{18:1}$-MAG-N_3**. Thus, to explore the possibility of labeling neutral lipids by **$C_{18:1}$-MAG-N_3** probe, we sought to perform similar TLC and LCMS analysis as before. Lipid extracts (Hanson and Lester method) from cells incubated with probe were subjected to CuAAC with naphth for TLC and **AlkBuQA** for LCMS lipidomics analysis. After lipid extract sample preparation, samples were handed to Katarina Jones at the BSMMSC for LC/MS. For TLC, labeled fluorescent spots were observed that match DAG or TAG (**Figure 3.16A**, R_f = 0.87, 0.83, lanes 2* and 3*). Meanwhile, no fluorescent spots were observed on the polar regions on the TLC plate (R_f < 0.60, not shown). LCMS analysis also revealed labeling of DAG and TAG species (**Table 3.4**, **Figure 3.17**). We observed N_3-labeled lipids as well as **AlkBuQA**-derivatized lipid masses that correspond to major lipid species found in yeast, namely oleic and palmitic FA species (**Table 3.4**). Thus, TLC and LCMS results indicate that **$C_{18:1}$-MAG-N_3** probe labels neutral lipids. Acyltransferases could append extra FA tails onto **$C_{18:1}$-MAG-N_3** probe that is left uncleaved to generate labeled DAG and TAG.

However, literature precedents suggest that *S. cerevisiae* utilize oleic acid as a carbon source to be stored into lipid droplets or to utilize exogenous oleic acid amounts for increased total phospholipid and neutral content.[236] Esterase/lipase activity could preferencially cleave **$C_{18:1}$-MAG-N_3** probe to release oleic acid, leading to an undesirable effect of increased natural (unlabeled) lipid content. Indeed, qualitative TLC analysis showed that the presence of **$C_{18:1}$-MAG-N_3** probe resulted in increased natural lipid content compared to control extracts without probe. As shown in **Figure 3.16B**, no probe control lane 4 displays lower primulin area whereas

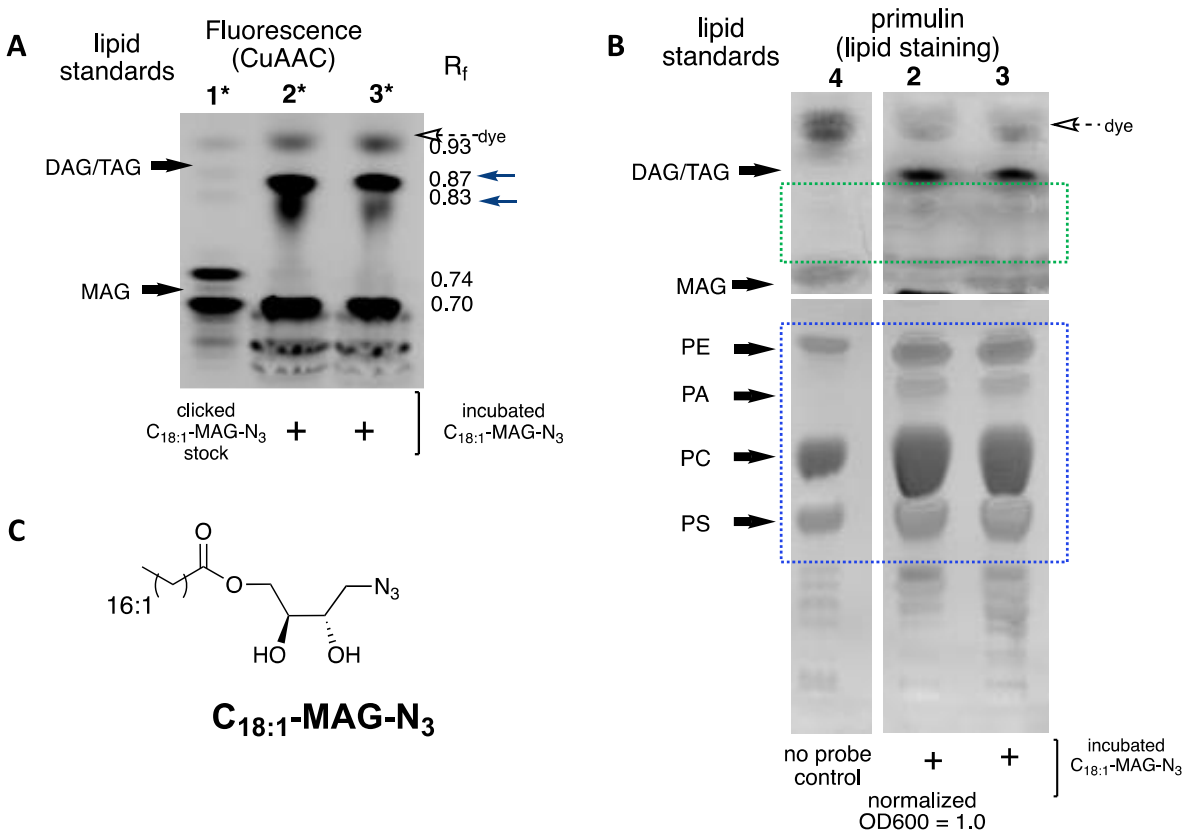

Figure 3.16. TLC plate representing clicked lipid extracts from cells incubated with $C_{18:1}$-MAG-N_3 (12 hours). Lipids were extracted and subjected to CuAAC reaction with ethynylnaphthalimide "naphth", loaded onto TLC lanes and then eluted. Lane 1* was loaded with a stock of **$C_{18:1}$-MAG-N_3** that was clicked with naphth. Lanes 2 and 3 are replicate samples of naphth-clicked lipid extracts from log-growth yeast incubated with **$C_{18:1}$-MAG-N_3**. **A.** The TLC image on the left shows spots corresponding to neutral lipids (R_f > 0.60) and the positions of lipid standards DAG (16:0/16:0) and MAG (18:1) are indicated. R_f values for new spots are shown on the right side of each image. Distinct spots on lanes 2* and 3* (R_f = 0.83, 0.87)which are faint or not observed in lane 1* (probe-only) indicate neutral lipid labeling. **B.** TLC image on the right shows the same TLC run as **A** but depicts spots after primulin staning for viewing natural lipids. Note that the plate has been excised for clarity. Blue dashed box: compare phospholipid staining wherein the area of primulin staining are greater in Lanes 2 and 3 (where lipid extracts from **$C_{18:1}$-MAG-N_3**-incubated cells were loaded) than in lane 4, where no probe control lipid extracts were added. Green dashed box shows darker primulin stained areas in lanes 2 and 3 compared to no probe control lane 4. **C.** Structure of **$C_{18:1}$-MAG-N_3**.

Table 3.4. List of detected labeled neutral lipids (DAG and TAG) from $C_{18:1}$-MAG-N_3 lipid extracts.

adduct	DAG lipid species	Calculated mass	Detected mass	Error (ppm)	RT	native RT	native lipid	adduct
[M+NH4]+	(18:1/18:1)DAGmN3	693.5888	693.5892	0.58	16.26	16.11	(18:1/18:1)DAG	[M+NH4]+
[M]+	(18:1/18:1)DAGmAlkQA	829.7141	829.7129	-1.45	12.76	16.11	(18:1/18:1)DAG	[M]+
[M]+	(18:1/18:0)DAGmAlkQA	831.7297	831.7288	-1.08	13.82	18.48	(18:1/18:0)DAG	[M]+
[M]+	(18:1/16:1)DAGmAlkQA	801.6827	801.6817	-1.25	11.59	14.77	(18:1/16:1)DAG	[M]+
[M+NH4]+	(18:1/16:0)DAGmN3	667.5732	667.5726	-0.90	16.20	15.91	(18:1/16:0)DAG	[M+NH4]+
[M]+	(18:1/16:0)DAGmAlkQA	803.6984	803.6973	-1.37	12.70	15.91	(18:1/16:0)DAG	[M]+
[M]+	(18:1/14:1)DAGmN3	637.5262	637.5248	-2.20	7.40	13.54	(18:1/14:1)DAG	[M]+
[M]+	(18:1/14:1)DAGmAlkQA	773.6514	773.6496	-2.33	10.20	13.54	(18:1/14:1)DAG	[M]+
[M]+	(18:1/14:0)DAGmAlkQA	775.6671	775.6652	-2.45	11.45	14.86	(18:1/14:0)DAG	[M]+
adduct	**TAG lipid species**	**Calculated mass**	**Detected mass**	**Error (ppm)**	**RT**	**native RT**	**native lipid**	**adduct**
[M+NH4]+	(48:2)TAGmN3 [M+NH4]+	875.7559	875.7546	-1.48	13.97	21.6	(48:2)TAG	[M+NH4]+
[M+NH4]+	(50:1)TAGmN3 [M+NH4]+	905.8029	905.8004	-2.76	18.10	22.43	(50:1)TAG	[M+NH4]+
[M+NH4]+	(52:2)TAGmN3 [M+NH4]+	875.7559	875.7546	-1.48	13.97	22.39	(52:2)TAG	[M+NH4]+
[M+NH4]+	(52:3)TAGmN3 [M+NH4]+	873.7402	873.7388	-1.60	13.35	22.07	(52:3)TAG	[M+NH4]+
[M+NH4]+	(54:1)TAGmN3 [M+NH4]+	961.8655	961.863	-2.60	20.28	22.01	(54:1)TAG	[M+NH4]+
[M+NH4]+	(54:2)TAGmN3 [M+NH4]+	959.8498	959.8467	-3.23	19.38	21.59	(54:2)TAG	[M+NH4]+

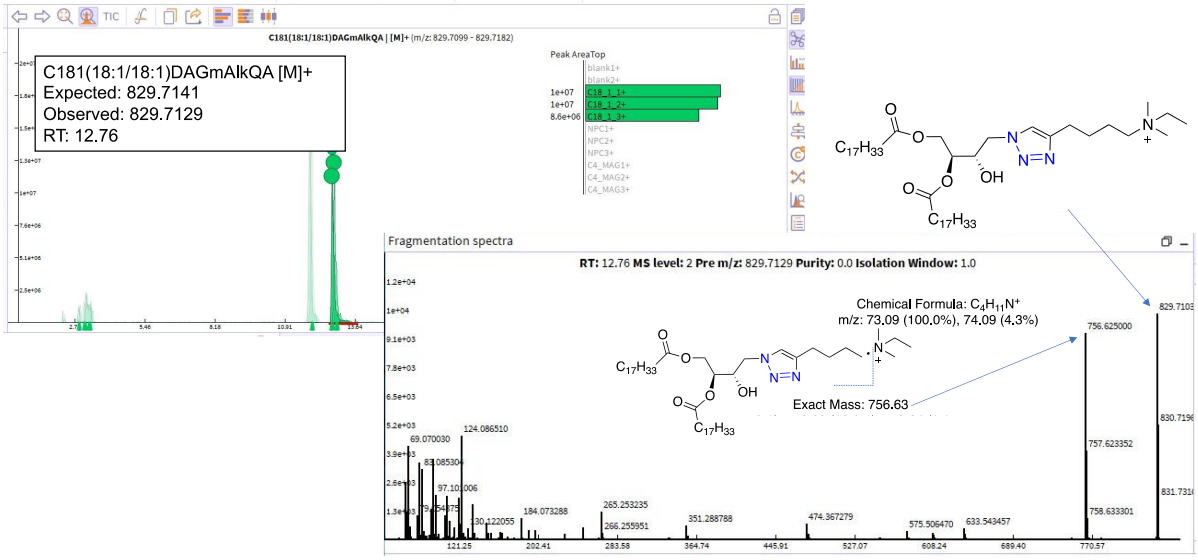

Figure 3.17. Representative mass spectrum for click-tagged neutral lipid products of probe $C_{18:1}$-MAG-N_3. Products were detected by liquid chromatography mass spectrometry (LCMS) Structures are shown that match the detected mass peak for each labeled lipid. Also shown are the assigned fragments in the MS/MS spectrum. The colored inset shows plots of peak areas and depicts two replicate samples treated with probe **$C_{18:1}$-MAG-N_3** (green, C18_1), **C_4-MAG-N_3** (pink/purple, C4_MAG), **C_4-MEG-N_3** (light blue, MEG), or without probe (yellow, NPC). Labeled lipids were identified (C12 isotope as parent peak) comparing the exact mass (±5 ppm) to a generated compound list.

the lanes loaded with lipid exracts from **$C_{18:1}$-MAG-N_3**-supplemented yeast cells (lane 2 and 3) displayed darker and greater area of primulin staining. Although this analysis was qualitative, the observation was consistent between duplicate TLC plate trials, indicating that the oleate acylglycerol probe was likely upregulating phospholipid content (**Figure 3.16B**, blue dashed box) and neutral lipid content (**Figure 3.16B**, green dashed box). Future studies should investigate the extent of lipid remodeling caused by exogenous addition of this probe by performing quantitative LCMS preparation and lipidomic analysis. The optimal concentration of **$C_{18:1}$-MAG-N_3** where it does not affect lipid levels could also be explored.

All in all, initial fluorescence microscopy results with DBCO-Cy3, as well as both CuAAC-TLC results and MS analysis, all point to **$C_{18:1}$-MAG-N_3** as a probe that effectively labels neutral lipids. However, the probe also likely increased oleic acid content in the cell and lead to an increase of (unlabeled) native lipid. This could have a deleterious impacts on the yeast or unnaturally alter lipid metabolism, making **$C_{18:1}$-MAG-N_3** unsuitable as a reporter for metabolic labeling under these conditions (1.0mM probe and 2% galactose synthetic minimal media).

3.7 Conclusions and future outlook

In this work, a series of azide-tagged MAG probes was assessed for lipid metabolic labeling properties. While **Gly-N_3** did not exhibit increased fluorescence compared to control, we found that each **C_n-MAG-N_3** probe resulted in a distinct fluorescence pattern and variable cytotoxicity. The short chain **C_4-MAG-N_3** probe in particular was found to successfully infiltrate lipid metabolism and result in fluorescence at the plasma membrane. Labeled lipid classes were identified using TLC separation and further characterized down to lipid species resolution using

LCMS. In line with our expectations, probe **C_4-MAG-N_3,** resulted in the labeling of both neutral lipids and phospholipids (albeit the latter less effectively), while our data show that **C_4-MEG-N_3** exclusively labeled neutral lipids, which we attribute to blocking of the *sn*-3 position. Currently, the extent of phospholipid labeling using clickable MAG probes is somewhat limited, suggesting that methylene azide may affect enzymes for phosphate addition. A possible drawback may be the strict requirements for multi-step enzyme processes that convert glycerol-N_3 (after MAG hydrolysis) to PA-N_3, which is ultimately the central metabolite for phospholipid synthesis in yeast. In the next section in Chapter 4, we summarize our efforts towards a probe that mimics PA, which is designed as an alternate route towards global labeling of glycerophospholipids.

Overall, this work showcases the potential of broadly labeling glycerolipids in cells using probe **C_4-MAG-N_3**, while probes of type **C_4-MEG-N_3** could be particularly advantageous for focusing the metabolic labeling of neutral lipids. Additionally, we have shown that the portfolio of labeled lipids can be controlled through subtle modifications to the structures of probes that act as mimics of biosynthetic precursors. In this case, we can collectively study how these labeled lipids fluctuate in bulk assays.

3.8 General Experimental and Synthetic Procedures

3.8.1 Synthetic Procedures

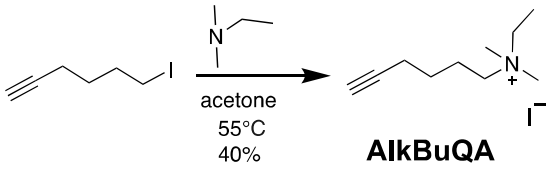

AlkBuQA

Synthesis of click reagent N-ethyl-N,N-dimethylhex-5-yn-1-aminium (**AlkBuQA**). In a 50mL RBF, 6-iodohex-1-yne (0.600 mL, 6.07 mmol) and dimethylethylamine (0.79 mL 7.2 mmol) were

dissolved in acetone (20 mL) to give a light-yellow mixture. A condenser was fitted to the RBF and the reaction mixture was allowed to stir for 12 h at 55 °C. The reaction was concentrated to remove volatiles to give a yellow crude. The crude was dissolved in minimum amount of CH_2Cl_2, to which addition of cold diethyl ether resulted in white precipitate which were filtered and rinsed with diethyl ether to give the product as the iodide salt (40%). ^{1}H NMR (500 MHz, $CDCl_3$) δ 3.63 (d, *J* = 22.5 Hz, 4H), 3.33 (s, 6H), 2.32 (s, 2H), 2.04 (s, 1H), 1.88 (s, 2H), 1.64 (s, 2H), 1.41 (s, 3H). ^{13}C NMR (126 MHz, $CDCl_3$) δ 82.97, 77.37, 77.32, 70.07, 63.20, 60.02, 51.05, 24.62, 21.57, 17.94, 8.87. ESI-TOF-MS $[M]^+$ calcd for $C_{10}H_{20}N$, 154.1590; detected, 154.1601.

3.8.2 Materials

All lipid standards, L-*α*-phosphatidylcholine (mixed isomers from chicken egg), L-*α*-phosphatidic acid (sodium salt from chicken eggs), and 1,2-dioleoyl-*sn*-glycero-3-phosphoethanolamine, were purchased from Avanti Polar Lipids, Inc. NMR spectra were obtained using Varian Mercury 300, 500, and 600 MHz spectrometers. Mass spectra were obtained with a JEOL DART-AccuTOF mass spectrometer or a Waters Synapt G2-Si electrospray ionization mass spectrometer with a quadrupole-time-of-flight mass analyzer (Milford, MA). Dibenzocyclooctyne-cyanine (DBCO-Cy3) was obtained from Sigma Aldrich. AFDye^{TM} 647 DBCO (AF647-DBCO) was purchased from Click Chemistry Tools. 4-Ethynyl-*N*-ethyl-1,8-napththalimide was synthesized as previously reported.[206] Thin-layer chromatography (TLC) glass plates, pre-coated 0.25 mm silica gel without fluorescent indicator (20x20cm) were purchased from Sorbent Technologies (Norcross, GA)

3.8.3 Methods

Yeast Strains and Culture Conditions: *S. cerevisiae* TRY 181 (wild-type, uraΔhisΔ) cells were streaked on YPD (1% yeast extract, 2% peptone, 2% dextrose, 2% agar) plates and grown at 30 ^{o}C. A loop of cells was inoculated into fresh 2% synthetic medium as the preculture. 2% minimal media (YNB) was prepared by combining the following: 6.7g of yeast nitrogen base (w/o AAs), 20 mg uracil, 20 mg L-histidine, and 20 g galactose dissolved in 1 L Milli-Q water and filtered via a pre-sterilized Millipore vacuum filtration system. All cells were grown in liquid medium at 30 ^{o}C in a 225 rpm shaker. After ~18 h, cells from the seed culture were diluted back to an initial OD_{600} of 0.2 in fresh media and supplemented with either **Gly-N_3**, **C_n-MAG-N_3**, **C_4-MEG-N_3** or ethanol in an equivalent concentration (5 mL total volume with growth media) until harvest. For growth curve studies, an aliquot was taken at designated timepoints for OD measurement (**Figure 3.7**). For *in vivo* metabolic labeling, cells were harvested at 12 hours (12 and 24 hours for TLC) by centrifugation (3000 x g for 5 min at 4-0°C) to remove growth media. After removal of growth media, the cells were washed three times with Milli-Q water (pelleted at 3000 x g, 5 min for each wash). MAG-N_3 probe stocks were kept in ethanol (100 mM or 50 mM) so MAG-N_3 addition into 5 mL cultures did not exceed 10% by volume to prevent leaky membranes and to ensure no detrimental effects on the growth of *S. cerevisia*e.[237] For pulse-chase TLC assays, cells were grown at total volume required for 4-5 aliquot removals. Initial media containing **C_4-MAG-N_3** was removed at the indicated pulse timepoint and was replaced with fresh media before cells were again incubated at 30 ^{o}C for chase. 5-10mL aliquots were removed per chase timepoint and subjected to lipid extraction procedures as indicated (**Figure 3.13** and **3.14**). An aliquot at the 0th hour was also kept for analysis.

SPAAC and Fluorescence Microscopy: Washed cells were fixed for 15 min (3.7% PFA in PBS). Fixed cells were washed with 1x PBS and resuspended in 5 mL 1x PBS. 1 mL cell suspension (diluted to an OD_{600} of 0.60/mL) was transferred to a fresh tube and incubated with DBCO-Cy3 clickable dye (1 µM final concentration in Milli-Q) for 1 hr at rt. The cells were finally washed with Milli-Q, vortexed, and spun down (5000 *x*g) a total of three times. Finally, resuspension in 1mL 1x PBS (pH = 7.4) gave clicked yeast samples. Cell culture samples (3 µL) were mounted onto microscope slides and covered with a coverslip, immobilized with acrylic nail polish and visualized under a confocal microscope (Leica SP8 White Light Laser Confocal microscope) using a 63x oil objective. The samples were imaged by differential interference contrast (DIC) to first locate the cells and a zoom factor of 6 or 8 was applied to properly view the yeast cells. Then, samples were excited at 554 nm and fluorescence images were collected between 559-620nm with a HyD detector. The laser strength, gain, and offset settings were kept constant between samples. All images acquired on *S. cerevisiae* cells were taken as a Z-stack of 7-14 z-slices with 1.0µm increments, after which lightning deconvolution was applied through Leica Application Suite (LAS) V4.4 software. Images were processed the same way using FIJI (v.2.1.0/1.53c).

Quantification of Fluorescence Intensity by Flow Cytometry: Samples for flow cytometry were first fixed (3.7% PFA in PBS), incubated with AFDye™ 647 DBCO (2 µM in from 0.11 mM stock in Milli-Q), and washed in similar fashion as samples for fluorescence microscopy. After washing and centrifugation, cells were diluted to an OD_{600} of 0.06 or 1.1 x 10^6 cells/mL, centrifuged (200 x g for 3 min), and the resulting pellets were resuspended in 1 mL of 1X PBS buffer and kept on ice for flow cytometry with FACSCalibur LSR II flow cytometer (Becton Dickinson). After exclusion

of debris (FSC-A vs SSC-A plot) and gating for single cells (FSC-W vs FSC-A), AFDye™ 647 DBCO fluorescence intensity was recorded in the APC channel. Flow cytometry data were obtained for 50,000-60,000 gated events per sample. For unstained controls, probe-supplemented yeast samples were only fixed and not incubated with click-dye and were prepared each run for a representative negative population. Biological replicates were analyzed on the same day and analysis was performed using FlowJo software (v.10.11 FlowJo LLC, OR, USA). For flow cytometry experiments, samples were also viewed under the confocal microscope, excited at 633 nm, and fluorescence was collected between 651-671nm with a HyD detector. Statistical analysis was performed on Graphpad Prism 9.1. FACSCalibur LSR II flow cytometer use was assisted by Trevor Hancock from Dr. Tim Sparer's lab.

SPAAC and Nile Red Staining: Washed cells were fixed for 15 min (3.7% PFA in PBS). Fixed cells were washed with 1x PBS and resuspended in 5 mL 1x PBS. 1 mL cell suspension (diluted to an OD_{600} of 1.0/mL) was transferred to a fresh tube and incubated with AFDye™ 647 DBCO clickable dye (2 µM final concentration in Milli-Q) for 1.5 hr at rt. The cells were finally washed with Milli-Q, vortexed, and spun down (5000 *x*g) a total of three times and resuspended in 1mL 1x PBS (pH = 7.4). An aliquot (250 µL) was set aside for Nile Red staining. 1 µL Nile Red Nile Red solution in acetone was added to this aliquot. Nile Red was prepared ahead at the following concentration: 5 µg/mL Nile Red per $5x10^6$ cells.[235] Each sample was vortexed immediately and incubated for 5 min. Cell culture samples were washed two times with 1X PBS, resuspended in 100 µL PBS and were mounted onto microscope slides (3 µL) and covered with a coverslip, immobilized with acrylic nail polish and visualized under a confocal microscope (Leica SP8 White Light Laser

Confocal microscope) using a 63x oil objective. The samples were imaged by differential interference contrast (DIC) to first locate the cells and a zoom factor of 6 or 8 was applied to properly view the yeast cells. For 2-color sequential scanning, samples were excited at 515 nm and fluorescence images were collected between 558-620nm for NR fluorescence and excited at 643 nm, and fluorescence was collected between 651-671nm (HyD detector) (**Figure 3.15**).

Lipid Extraction for Mass Spectrometry and Fluorescence-based Thin Layer Chromatography: The lipid extraction method followed a prior procedure with minor modification.[231] Log phase samples (15 mL volume) were placed on ice and cold trichloroacetic acid (TCA) solution was added to a final 5% concentration for an hour incubation. Growth media and TCA suspension were removed and then cells were centrifuged and washed 3 times with MQ water. Cells were either used directly for lipid extraction or stored at -20 °C. Cells warmed to rt were resuspended in 1 mL lipid extraction mix of (15/15/5/1/0.018) 95% EtOH/H_2O/diethyl-ether/pyridine/4.2 N NH_4OH aqueous solution. Samples were vortexed for 1 minute and then incubated for 15 minutes at 55°C. This extraction was repeated once more for a total of two times. Collected extracts were dried with a steady N_2 stream. Lipid extracts were resuspended in 16 µL $CHCl_3$. For the preparation of the 8.60 mM Cu(I) click solution, 3.80 mg Cu(I)$(MeCN)_4BF_4$ was dissolved in 605 µL acetonitrile and 800 µL of ethanol. 200 µL of this copper solution was combined with 10 µL of *N*-ethyl-*N*,*N*-dimethylhex-5-yn-1-aminium or **AlkBuQA** (100 mM in MeOH) or 10 µL of 4-ethynyl-*N*-ethyl-1,8-naphthalimide dye "naphth" (22.5 µM in $CHCl_3$/MeOH) as the click mix and vortexed for 30 s. The click mix (30 µL) was added to lipid extracts (suspended in 16 µL $CHCl_3$), as well as to aliquots of unmetabolized **C_n-MAG-N_3** probe stocks (0.5 mM). The clicked samples were

flushed with N_2, vortexed, spun down, and then incubated on a 42 °C water bath for 16 h. After CuAAC incubation, the clicked samples were vortexed and spun down (4,600 x g). For mass spectrometry, samples were diluted with 30 µL of $CHCl_3$/MeOH/H_2O (73:23:3) prior to LCMS. For TLC, clicked samples were loaded onto a thin-layer chromatography (TLC) plate in 5 µL increments (40 µL total lipid extracts), with drying in between each addition. Lipid samples were separated by TLC using glass plates of pre-coated 0.25 mm silica gel without fluorescent indicator (20 x 20 cm). The spots were dried with a heat gun prior to the addition of phospholipid standards: 2-4 µL of PS, PC, PA, DOPE, MAG and DAG standards (3-5 mM in $CHCl_3$/MeOH). The plate was once again dried with a slow stream of nitrogen and then developed in a solvent mixture of chloroform/methanol/water/acetic acid (65:25:4:1, v/v/v/v) until an Rf or 0.6. The plate was air-dried for an hour and then developed with 1:1 cyclohexane/ethyl acetate.[238] Next, the TLC plate was imaged using a Geldoc with a SYBR Green emission filter processed using ImageJ (LUT inverted). The "click" spots were marked with a lead pencil to differentiate later from the spots due to primulin staining. The plate was dipped in primulin stain (5 mg primulin per 100 mL 9:1 acetone/water) and then imaged again (primulin-stained image not shown).

Ultra-High Performance Liquid Chromatography High Resolution Mass Spectrometry (UHPLC-HRMS)[239] **and Analysis:** An UltiMate 3000 ultra-high performance liquid chromatography system (UHPLC, Dionex, Sunnyvale, CA) was used to inject 10 µL of sample onto a CORTECS C18 column (90 Å, 2.7 µm, 2.1 mm × 150 mm; Waters) controlled at 40 °C. Mobile phase A was 60:40 acetonitrile/water with 10 mM ammonium formate as a buffer and 0.1% formic acid while mobile phase B consisted of 90:10 2-propanol/acetonitrile with 10 mM ammonium formate as a buffer

and 0.1% formic acid. The gradient used follows: *t* = 0 min: 32% solvent B flow rate of 0.30 ml/min, *t* = 1.5 min: 32% solvent B flow rate 0.4 ml/min, *t* = 2.5 min: 45% solvent B flow rate 0.4 ml/min, *t* = 5 min: 52% solvent B flow rate 0.3 ml/min, *t* = 8.0 min 58% solvent B flow rate 0.3 ml/min, *t* = 11.0 min 68% solvent B flow rate 0.4 ml/min, *t* = 14.0 min 75% mobile phase B flow rate of 0.4 ml/min, *t* = 18.0 min 80% solvent B flow rate of 0.4 mL/min, *t* = 21 98% solvent B flow rate 0.45 ml/min, *t* = 25.0 min 32% solvent B flow rate 0.3 ml/min until equilibration at 30 min. Eluent was introduced to the mass spectrometer via an electrospray ionization (ESI) source, with the following parameters: sheath gas 30 (arbitrary units), aux gas 8 (arbitrary units), sweep gas 3 (arbitrary units), spray voltage 3 kV, capillary temperature 300 °C. Mass analysis was performed using an Exactive Plus (Thermo Scientific, Waltham, MA) mass spectrometer operated in dual polarity mode. Masses were detected in full scan mode within a scan range of 100–1,500 *m/z*, operated at a resolution of 140,000, with an automatic gain control target of (AGC) of 3×10^6 ions, and a maximum IT time of 100 ms. Full scan data was complemented with all ion fragmentation data at a resolution of 35,000 utilizing 35 eV collisional energy. Raw files were converted to mzML files using MS convert and full scan data was evaluated using El MAVEN software. For peak identification, retention times of labeled lipids were compared with respect to natural lipid of the same lipid species. Labeled lipids (from a generated compound list) were identified (C12 isotope as parent peak) based on their accurate mass (±5 ppm).

Chapter 4. Development of bioactivatable and clickable phosphatidic acid probes as new chemical reporters for glycerophospholipids

4.1 Abstract

Dysregulation of lipids contributes to human diseases[22-24] and unnatural lipid production and regulation have been heavily linked with certain cancers.[25, 26] Motivated by these observations, scientists are increasingly interested in probing the lipidome, especially by monitoring changes in the lipidome at the onset of such diseases. For a long time, researchers have relied heavily on isotope labeling in combination with mass spectrometry to study lipid flux. More recently the use of alkyne fatty acids as precursors that infiltrate the lipidome to uncover lipid metabolism has been well-mined. However, despite the utility of alkyne tracers, this pursuit has some downsides, namely, that terminal alkynes are not as amenable to SPAAC for *in vivo* applications, and that it is susceptible to fatty-acid remodeling which could confound analysis. For these reasons, we have sought to utilize azide as the bioorthogonal tag and append this to the glycerol backbone of glycerolipid probe structures since this tag is suitable for bioconjugation via SPAAC.

Toward this end, azido acylglycerol precursor probes were designed and analyzed in their capabilities to label yeast glycerolipids (Chapter 3). However, azido-MAG probes showed limited labeling of phospholipids and thus led us to speculate that this resulted from the high stringency for kinase enzymes in accepting these probes as substrates for conversion to phospholipids. The PA design described in this chapter is expected to circumvent the phosphorylation step required for phospholipid biosynthesis since the initial probes would already contain the phosphate moiety. Thus, we hypothesize that an azido-PA derivative could be more effective at labeling

glycerophospholipids. Azido-PA as a synthetic target is also critical since in yeast, PA is a precursor for TAG and all phospholipids, while in mammalian systems, PA also acts as a central metabolite. Finally, designing a suitable lipid tool that could potentially achieve global glycerolipid labeling would be advantageous for detecting changes in the totality of glycerolipid biosynthesis in response to different stimuli.

4.2 Background and motivation for probe design

Considering the previous results utilizing azido-MAG probes, we hypothesize that an azide-tagged PA mimic may exhibit increased potential as an alternative route for accessing global glycerophospholipid labeling. We are motivated by the fact that a PA probe would already include the key phosphate group that would need to be added to the previously described MAG probes. Therefore, we hypothesize that an azido-PA probe that bypasses the phosphorylation step required as an entry point to phospholipid synthesis could improve phospholipid labeling. Additionally, PA is an ideal target for metabolic labeling studies since it acts as a central metabolite for lipid biosynthesis in both simple and complex eukaryotes. However, since PA molecules are negatively charged at physiological pH, it is important for PA probes to be prepared in a form that enables membrane permeability. To circumvent this problem, we sought to synthesize probe **SATE-C_4-PA-N_3**, in which the phosphate group is masked as a neutral bioactivatable *S*-acetyl-thioethyl (SATE) group that is removed after cell entry (**Figure 4.1A, B**). Following cellular delivery, the azido-PA analog is expected to hijack phospholipid and neutral lipid biosynthetic pathways to be leveraged for metabolic labeling of a variety of lipid classes (**Figure 4.1C**).

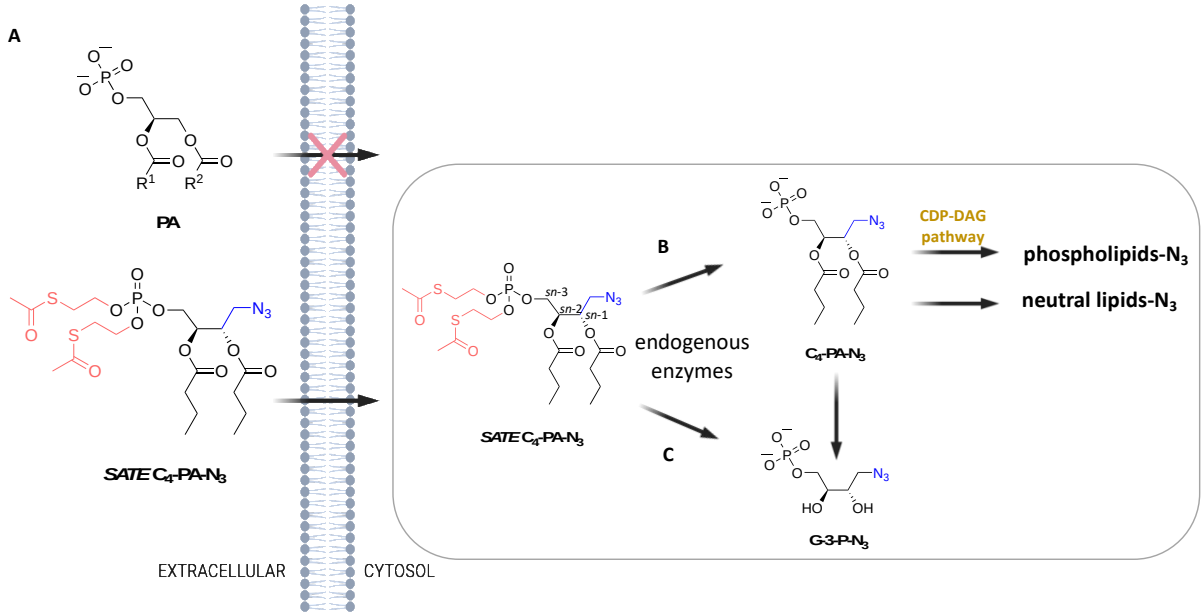

Figure 4.1. Predicted hydrolysis of SATE-C_4-PA-N_3 probe upon cellular entry and its lipid products in S. cerevisiae. **A.** PA lipid precursor design is based on a pro-drug type approach via masking phosphate charges with SATE and permit cell entry. **B.** Endogenous esterases can cleave **SATE-C_4-PA-N_3** to release the "active" lipid **C_4-PA-N_3**. This metabolite can be directly incorporated into the CDP-DAG pathway to label phospholipids or be esterified to generate neutral lipids like MAG, DAG, and TAG. **C. C_4-PA-N_3** butyrate tails can be cleaved (2 more rounds of cleavage) to give **G-3-P-N_3**.

4.2.1 Biolabile masking groups

The impermeant nature of some phospholipid analogs has precluded their exogenous delivery into cells. Unless endocytosis, active transport, or vesicle delivery and fusion is involved, this has particularly posed a challenge for lipids that carry multiple charges (either from the headgroup or from the phosphate groups) in their structures. However, a clever strategy utilizing bioactivatable groups has allowed for such phosphate charges to be masked and then unveiled following cell entry.[234, 240] Biolabile groups such as acytoxymethyl (AM)[241] and *S*-acetyl-thioethyl (SATE) have been previously utilized to mask charges of lipid phosphate groups. A butanoyl (Bt) group has also been attached to alcohol groups to reduce hydrophilicity.[241, 242] These bioactivatable groups essentially function through a prodrug approach, rendering the phospholipid "inactive" until intracellular enzymes cleave the protecting group, thereby liberating the active compound/metabolite (**Figure 4.2**). We have chosen SATE to be incorporated into our design because AM ester hydrolysis has long been known to release the potentially toxic byproduct formaldehyde, and while information about the products generated from SATE hydrolysis and their cellular effects is still lacking[234]

4.2.2 Examples of phospholipids with bioactivatable or photoactivatable masking groups

Our approach is inspired by successful strategies utilizing protecting groups for masking phosphate charges of phosphate-containing lipids.[243] This includes lipid analogs in which the phosphate charge is masked such as derivatives of PA, phosphatidylinositol-3,4,5-triphosphate ($PI(3,4,5)P_3$), DAGs, or sphingolipids. Before diving into specific examples however, it is important

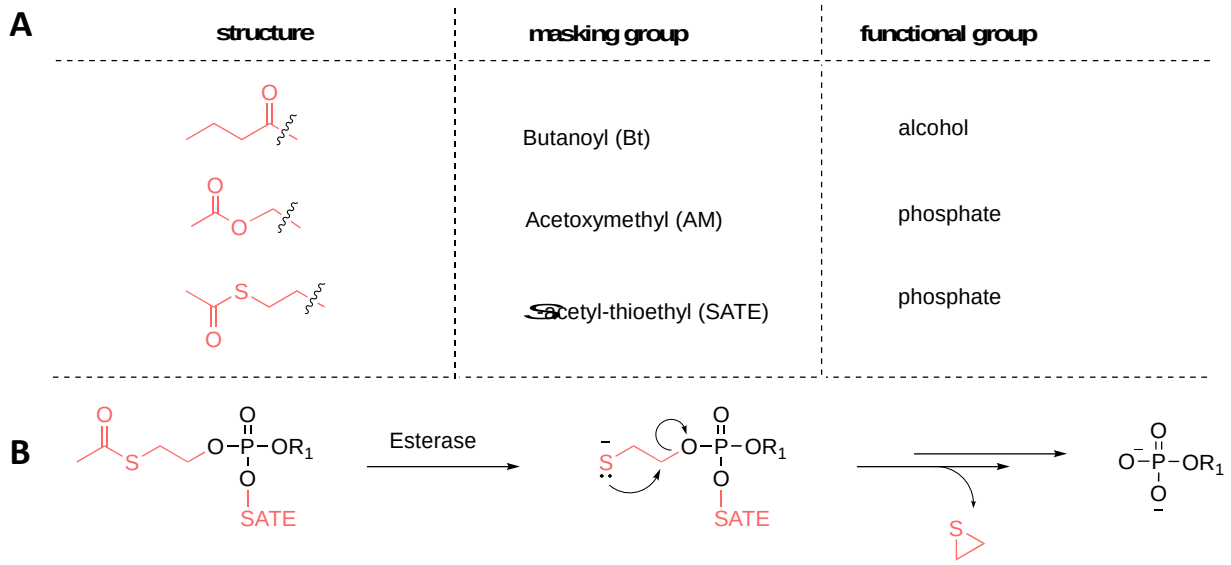

Figure 4.2. Biolabile protecting groups used for masking phosphate moieties. A. Structures of protecting groups and the general functional group they mask. **B.** Mechanism of thioester hydrolysis showing that thioester bond breakage occurs, resulting in the unstable 2-mercaptoethyl phosphotriester, which decomposes and releases thiirane and the active compound of interest.

to point out that these lipid analogs could be masked by either a 'bioactivatable' or 'photoactivatable' group. The distinction between these protecting groups should be made clear since caged, photoactivatable groups allow for spatial and temporal control of lipid release upon UV light application, whereas bioactivatable groups rely on natural enzymatic processes. While the development of photocaged lipid probes was perhaps originally pursued as an alternative to the use of ester protecting groups, which are prone to uncontrolled enzymatic hydrolysis,[241] many lipid surrogates actually contain both features (**Figure 4.3**).[243]

In an interesting example, Mentel and coworkers developed cell-permeable PI(3,4,5)P_3 lipid derivatives where the phosphate groups were masked with AM esters and the hydroxyls were masked with butyrates (**Figure 4.3A**). For the photolabile caged derivative, **cgdiC$_8$PIP$_3$/AM**, one of the AM esters was replaced with coumarin. Citir and coworkers utilized both caged **cgdiC$_8$PIP$_3$/AM** and uncaged **diC$_8$PIP$_3$/AM** and found that butyrates that mask the hydroxy groups remained intact much longer than the AM groups that masked the phosphate groups,[232] which was consistent with previous literature indicating that AM esters are removed much faster than butyrates for cell-permeable nucleotide derivatives.[233] However, the downside associated with lipids masked using more than one caging group or with multiply-charged lipids is that this may lead to a generally reduced uncaging efficiency to access the 'active' lipid. An additional example to highlight is a caged derivative of PA, **NiBnzPA/SATE**, wherein the two phosphate charges are masked by an SATE group and a photolabile nitrobenzyl ester (**Figure 4.3B**).[242] However, beyond the report for synthetic contribution, the work towards this PA lipid design has not been amenable for *in vivo* applications in studying PA lipid metabolism and its effects in cellular signaling.

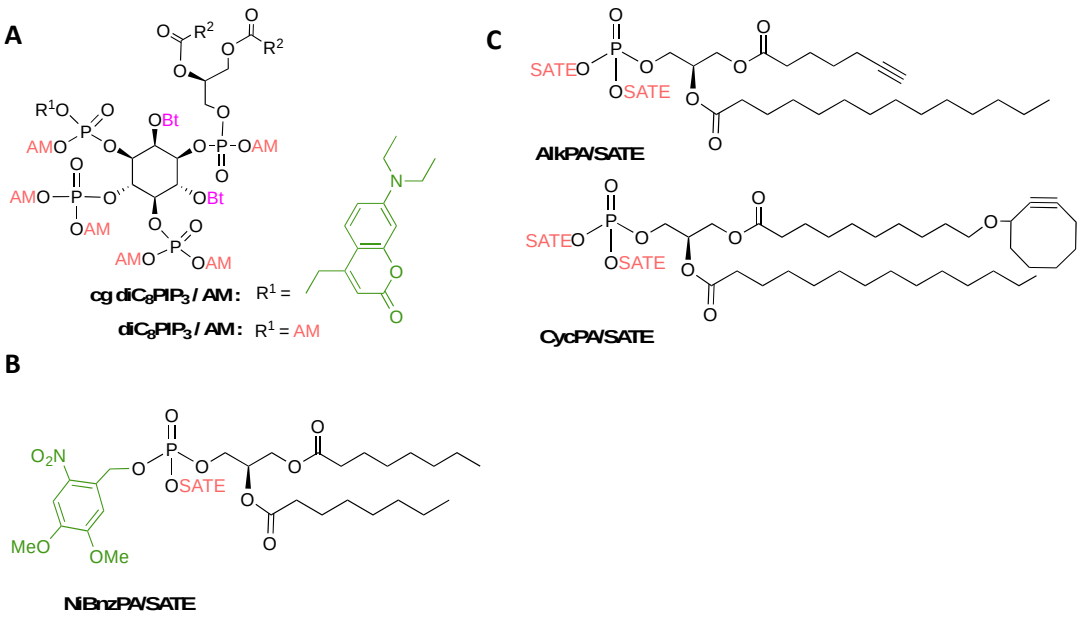

Figure 4.3. Examples of previously reported photoactivatable or bioactivatable phospholipids. **A**. Structures of membrane-permeable derivatives of PI(3,4,5)P_3: caged **cgdiC$_8$PIP$_3$/AM** and non-caged **diC$_8$PIP$_3$/AM**. The caged derivative was masked with photoactivatable 7-diethylamino-4-methylenehydroxy coumarin. R^2=C_7H_{15}, AM=acetoxymethyl, Bt=butanoyl. **B** and **C.** Membrane-permeable derivatives of PA lipid with the click tag added as either as a terminal alkyne for CuAAC, or as a cyclooctyne for SPAAC. Caging group colors: green, photocleavable moiety; pink, alcohol hydrophobic masking group; peach, phosphate charge masking group.

A study by Neef and Schultz introduced PA lipid derivatives containing both a clickable tag and bioactivatable groups to mask phosphate group charges the clickable group was introduced at the terminus of the fatty acyl chain (**Figure 4.3C**).[244] They were able to image different pools of lipids generated from each lipid analog. Most of the caged compounds in literature are simply to designed to release a signaling lipid, altering its own intracellular concentration and resulting in downstream effects.[149, 245] While purposely increasing target lipid concentration could be the goal for such studies, it is ideal in precursor metabolic labeling projects for for the probe to result in minimal interference with lipid pathways and enzyme activities. Thus, deviations in natural lipid metabolism should be investigated for samples with or without the masked compound.

4.2.3 Design of azido-PA probe and expected pathway to lipid products

Based on the azido-MAG probe design in Chapter 3, we envisioned a PA lipid mimic to contain the same methylene azide unit attached at the *sn*-1 position, since this labeling approach was found to be successful for infiltrating lipid products. For the fatty acyl chains of the PA probe, we selected short-chain butyrate derivatives to control the hydrophilicity of this compound and because our LCMS results with **C_4-MAG-N_3** probe suggested labeled lipids from butyrate hydrolysis.[220] SATE groups will be installed at each of the phosphate groups, resulting in the phosphotriester moieties of probe structure **SATE-C_4-PA-N_3**. Generation of an SATE-protected PA derivative usually entails coupling of a phosphoramidite reagent already containing the SATE group (**Figure 4.4**).[242, 244] In our work, we follow the same synthetic procedure as well as propose another route to generate a SATE-masked PA derivative which will be expanded in the next section.

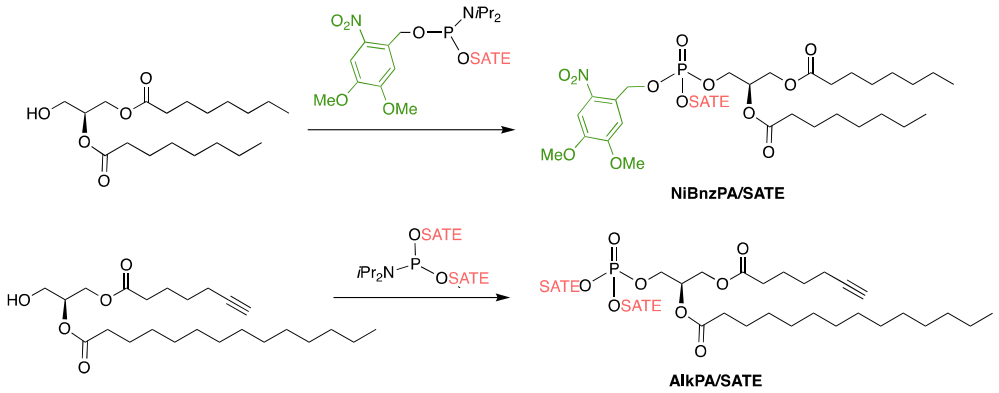

Figure 4.4. Common approach of using a phosphoramidite precursor for the synthesis of membrane-permeant, SATE-protected PA derivatives.

4.3 Synthesis of SATE-protected azido-PA lipid

Two routes have been simultaneously pursued for the synthesis of **SATE-C_4-PA-N_3**, which are shown in **Scheme 4.1** and **Scheme 4.2**. The route in **Scheme 4.1** follows the generic installment of SATE groups by reaction of bis-SATE phosphoramidite intermediate **4.43** with the glycerol backbone, except that instead of coupling with DAG,[242, 244] the two acyl chains will be introduced after phosphoramidite coupling**.** In the other proposed route, the *S*-acyl-thioethyl group is installed at a later stage in the synthesis (**Scheme 4.2**). This alternate route would also enable access to **C_4-PA-N_3** as the unmasked version of **SATE-C_4-PA-N_3**, which can be employed as a control probe for future cellular labeling studies.

Both routes utilize protected azidoglycerol compound **4.3** as a common intermediate, which was synthesized using a previously reported literature procedure.[217] The route begins with protection of the diol group in diethyl-L-tartrate as a cyclopentylidene acetal through reaction with cyclopentanone. This was then followed by reduction of the ester groups with lithium aluminum hydride to give the resulting 1,4-diol **4.1**. The diol was mono-tosylated by careful stoichiometric control of potassium iodide in the presence of silver oxide to give **4.2**. After which the azide tag is installed by substitution of the tosyl group using sodium azide in the presence of crown ether. From here, two separate routes were explored to install the phosphate headgroup. In the first route, 1,4-azidoalcohol **4.3** was coupled with a known SATE phosphoramidite precursor, which must be freshly prepared (**Scheme 4.1**).[246] However, a few issues were encountered for the attempts of synthesizing phosphotriester **4.4**, such as inconsistent yields of thioesterethanol **4.41** and instability of the SATE-phosphoramidite precursor **4.42** (synthesized and provided by Best lab member Jinchao).

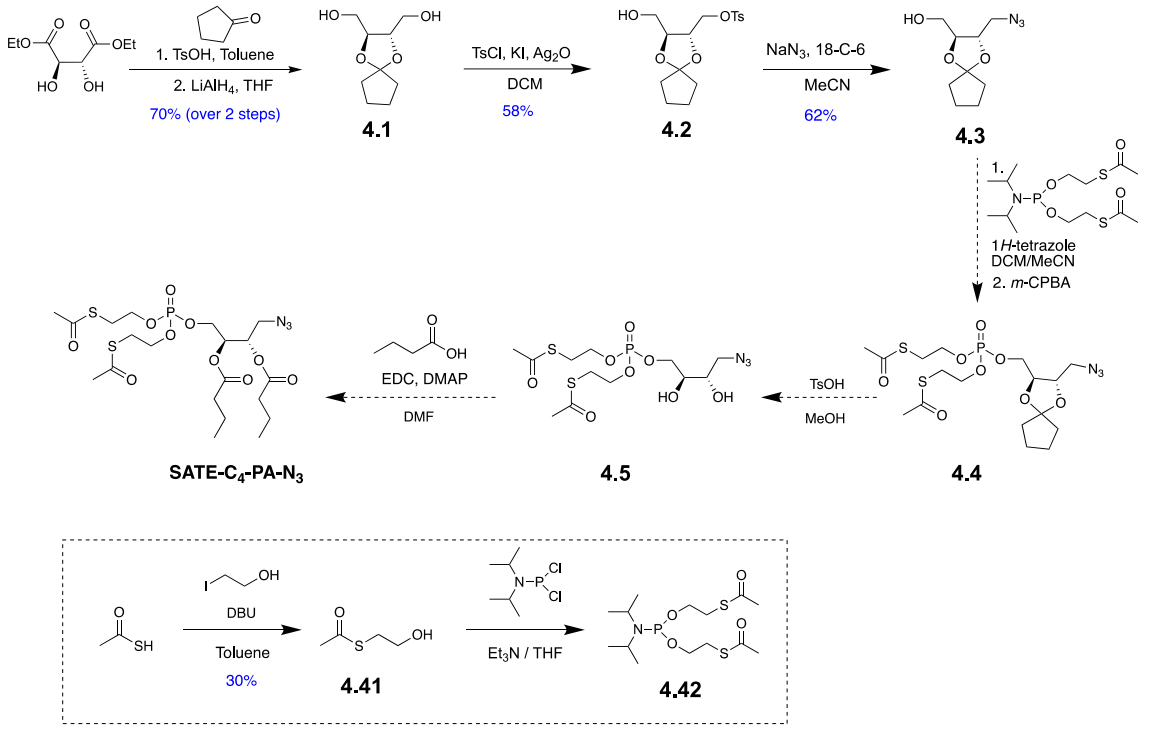

Scheme 4.1. Initial synthetic route for SATE-C_4-PA-N_3.

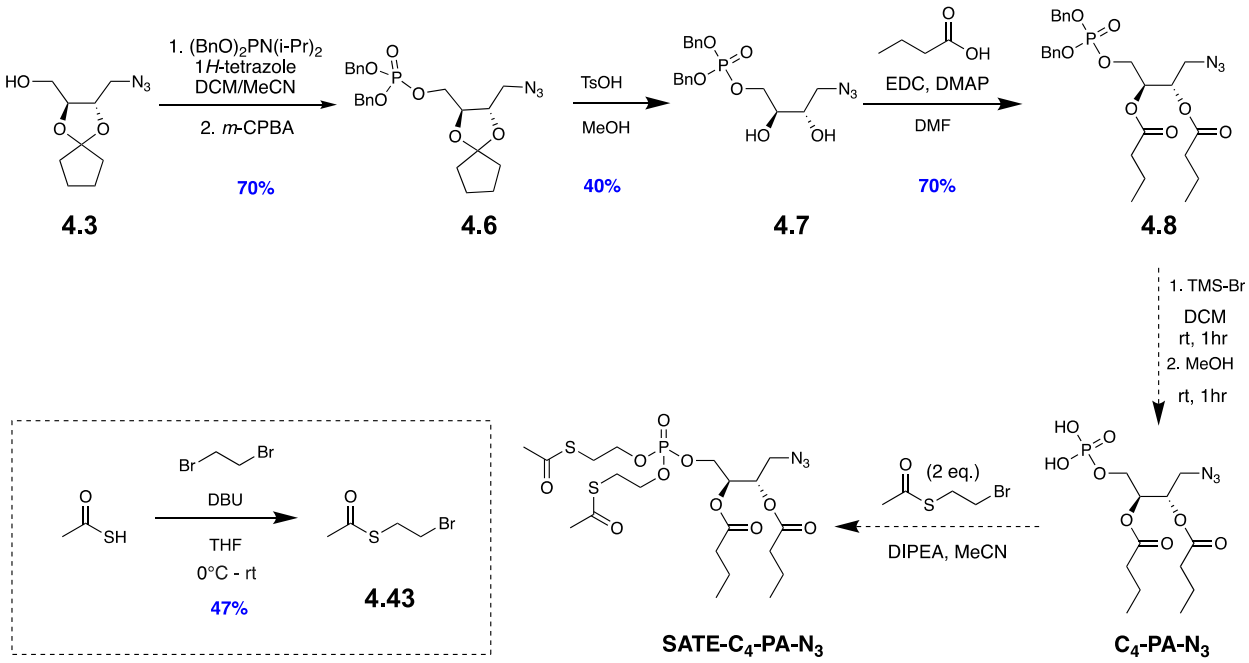

Scheme 4.2. Alternative synthetic route for SATE-C_4-PA-N_3, which enables synthetic access to free phosphate probe C_4-PA-N_3.

Meanwhile, we pursued a different strategy involving ester coupling to add the C_4 tails prior to installment of the SATE groups (**Scheme 4.2**). In this route, coupling of azidoalcohol **4.3** with dibenzyl *N,N*-diisopropylphosphoramidite and subsequent oxidation with *m*-CPBA afforded intermediate **4.6**. Then, the cyclopentylidene acetal protecting group was removed under mildy acidic conditions with *p*-toluenesulfonic acid (*p*-TsOH) for esterification with butyric acid to give **4.8**. Deprotection of the dibenzyl groups was attempted using either bromotrimethylsilane or iodotrimethylsilane to afford free phosphate **C_4-PA-N_3** to no success. SATE groups could be added to free phosphate **C_4-PA-N_3** by alkylation with bromoethyl thioacetate **4.44**. Facile synthesis of **4.44** was possible by reacting thioacetic acid with 1,2-dibromoethane.

4.4 Conclusions and future work

Compared to established methods of tracing lipids (ie: using clickable fatty acid precursors, isotope labeling, etc.), our approach offers a new avenue for global mapping of lipid remodeling since the placement of the methylene azide tag is at the glycerol backbone which is conserved throughout glycerolipids and phospholipids. While the tag placement is the same as the MAG-N_3 probes in Chapter 3, herein we introduce **SATE-C_4-PA-N_3** which is specifically designed to hijack the biosynthesis of phospholipids via the CDP-DAG pathway. The probe is also unique in that the phosphate charges are masked with an SATE protecting group which is readily cleaved by endogenous esterases to release a PA lipid mimic.

Once **SATE-C_4-PA-N_3** is synthesized, the future directions for this project would be to confirm its suitability as a bioorthogonal precursor amenable for cellular studies and subsequent lipid content analysis. We will work to first confirm the general stability of this probe in cell

culture conditions and to test its toxicity in yeast. Once we obtain optimal probe dosage in cell cultures, we will perform SPAAC with fluorescent cyclooctyne to visualize the lipid products via fluorescence microscopy. We expect the fluorescence to be localized at the plasma membrane as well as internal membranes since this probe is hypothesized to label neutral lipids and glycerphospholipids. Then we will also perform lipid extraction on cells with or without **SATE-C_4-PA-N_3** to analyze and identify the lipid classes and species it labels.

We also propose an *in vitro* study to determine that can serve as a substrate for esterase enzyme. To confirm esterase cleavage of the **SATE-C_4-PA-N_3** probe, we can incubate this with commercially available esterases, look for ester hydrolysis products by MS, and compare products with buffer controls or negative controls like heat-killed enzyme. Another interesting future direction would be to explore the metabolism of the butyrate byproduct, an area less explored for masked lipid analogs.

4.5 Synthesis Procedures and Characterization Data

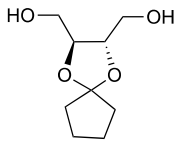

4.1

((2*S*,3*S*)-1,4-Dioxaspiro[4.4]nonane-2,3-diyl)dimethanol (**4.1**). Following a previously published procedure,[217] a solution of diethyl-L-tartrate (4.10 g, 19.88 mmol), *p*-toluenesulfonic acid (0.388 g, 22.5 mmol), and cyclopentanone (8.7 mL, 83.2 mmol) in toluene (110mL) was warmed to 100°C. The solution was stirred in a 250 mL flask fitted with a Dean-Stark trap and condenser. The light-yellow solution was allowed to stir overnight and then quenched with 400 mg of solid

sodium bicarbonate. The solution was stirred for 30 minutes, filtered to remove solids, and concentrated under vacuum to give a viscous yellow crude. The crude solution was dissolved in tetrahydrofuran (THF) and transferred to a syringe for dropwise addition. Into a 250 mL RBF, lithium aluminum hydride ($LiAlH_4$, 2.2 g, 58 mmol) was slowly added, cooled to 0°C, and suspended in 40 mL THF. The crude mixture was slowly added (dropwise) to the flask containing $LiAlH_4$ over 45 min. The solution was allowed to stir at 0°C for 40 more minutes before warming to rt. After 1 hour, the mixture was cooled to 0°C and quenched with 2.5 mL water, 2.5 mL 10% sodium hydroxide (aq), and 5 mL water then warmed to rt. The solution was stirred for 1 hour, dried with magnesium sulfate, filtered, and concentrated using rotary evaporation to give an oily crude mixture. The crude was purified by flash column chromatography on silica gel (25/35/45% ethyl acetate/hexanes to 100% EtOAc) to afford 1,4-diol **4.1** (2.62 g, 13.9 mmol, 70% yield) as confirmed by: TLC (R_f = 0.30, 100% EtOAc/Hex; KM_nO_4 stained); HRMS-DART: $[M+H]^+$ Calculated for $C_9H_{17}O_4$: 189.1127; Found: 189.0779; $[M-H_2O]^+$ Calculated for $C_9H_{15}O_3$: 171.10; Found: 171.071. NMR data matched a previous report.

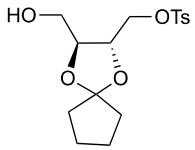

4.2

((2*S*,3*S*)-3-(Hydroxymethyl)-1,4-dioxaspiro[4.4]nonan-2-yl)methyl 4-methylbenzenesulfonate (**4.2**). Compound **4.2** was synthesized according to the previous report with slight modifications.[217] In a 100 mL RBF under Ar, 1,4-diol **4.1** (1.82 g, 9.67 mmol), Ag_2O (1.41 g, 6.08 mmol), TsCl (2.15 g, 11.3 mmol) and KI (01.29 g, 7.77 mmol) were added into a 100 mL RBF under

Ar and dissolved with 25 mL anhydrous CH_2Cl_2. The solution was stirred for 12 hours at rt. The solution was filtered twice through a 5-cm SiO_2 column to remove Ag_2O and rinsed with 50 mL EtOAc. The filtrate was concentrated under reduced pressure and subjected to silica gel column chromatography. The crude material was then purified by silica gel chromatography by packing SiO_2 column with 100% hexanes, then eluting with solvent gradient 20/30/40/50% EtOAc/Hex to yield the mono-tosylated product **4.2** as a clear oil (1.92 g, 5.61 mmol, 58% yield) as confirmed by: TLC (R_f = 0.58, 50% EtOAc/Hexane; KM_nO_4 stained, UV active); HRMS-DART $[M+H]^+$ Calculated for $C_{16}H_{22}O_6S_1$: 343.120986; Found: 343.20807. NMR data matched previous reports.

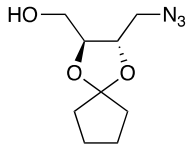

4.3

((2*S*,3*S*)-3-(Azidomethyl)-1,4-dioxaspiro[4.4]nonan-2-yl)methanol (4.3). Compound **4.2** (1.92 g, 5.61 mmol), NaN_3 (1.09 g, 16.8 mmol) and 18-crown-6 (0.592 g, 2.24 mmol) were weighed into a 100 mL RBF under Ar and dissolved with 30 mL anhydrous MeCN. The RBF was then fitted with a condenser and stirred at 80°C for 2 days. The solution was cooled to rt, filtered through a 4 cm layer of celite, and rinsed with 50 mL EtOAc. The crude was concentrated and then purified by silica gel chromatography using the gradient 10/20/30/40/50% EtOAc/Hex (0.741 g, 3.47 mmol, 62%) to afford **4.3** as a clear oil as confirmed by: TLC (R_f = 0.53, 50% EtOAc/Hex; KM_nO_4 stained, not UV active); ^{1}H NMR (500 MHz, $CDCl_3$) δ 3.96 – 3.78 (m, 2H), 3.72 – 3.50 (m, 2H), 3.40 (dd, *J* = 13.0, 4.3 Hz, 1H), 3.25 (dd, *J* = 13.0, 5.3 Hz, 1H), 2.05 (s, 1H), 1.83 – 1.47 (m, 8H). ^{13}C NMR (126 MHz, $CDCl_3$) δ 119.71, 78.42, 75.85, 61.90, 51.91, 37.20, 37.11, 23.37, 23.17. HRMS-DART: $[M-N_2+H]^+$ Calculated for $C_9H_{16}N_3O_3$: 186.1130; Found: 186.1150.

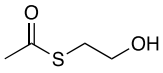

4.41

***S*-(2-Hydroxyethyl) ethanethioate** (**4.41**). To an oven-dried 100 mL RBF, thioacetic acid (0.93 mL, 13.13 mmol) was dissolved in 15 mL toluene. The solution was stirred under Argon atmosphere and place in an ice bath. DBU (1.98 mL, 13.11 mmol) was added to give a yellow-orange solution, after which 2-iodoethanol (0.90 mL, 10.5 mmol) was added. A white suspension was observed and the solution turned from orange to a yellow. The reaction was stirred at rt overnight. For workup, the mixture was diluted with 40 mL of CH_2Cl_2 and 120 mL H_2O. The mixture was transferred to a separatory funnel, and the organic layer was collected. The remaining aqueous layer was washed with 2 x 30 mL CH_2Cl_2. The collected organic layer was washed with H_2O and brine then dried over sodium sulfate. After filtration to remove solids, volatiles were removed under vacuum. The crude was dissolved in CH_2Cl_2 and loaded onto a SiO_2 column (packed with 100% hexanes). Flash column chromatography was performed using elution gradient: 10/15/20/25/30% EtOAc/Hex, to give **4.41** (0.473 g, 3.94 mmol, 30% yield) as a light-yellow oil as confirmed by: TLC (R_f = 0.22, 25% EtOAc/Hexane; KM_nO_4 stained, UV active); ^{1}H NMR (500 MHz, $CDCl_3$) δ3.60 (q, 2H), 3.42 (t, 1H) , 2.94 (t, 2H), 2.24 (s, 3H). ^{13}C NMR (126 MHz, $CDCl_3$) δ 196.42, 61.21, 31.70, 30.50. HRMS-DART: $C_4H_9O_2S^+$ $[M+H]^+$ expected: 121.0318, found: 121.0075 and $[M-H_2O]^+$ Calculated: 103.0212; Found: 103.0016.

Compounds **4.6** to **4.7** were synthesized as previously reported.[217]

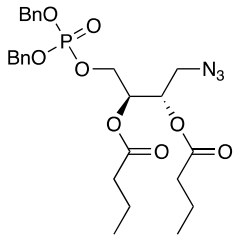

4.8

(2*S*,3*S*)-1-Azido-4-((bis(benzyloxy)phosphoryl)oxy)butane-2,3-diyl dibutyrate (**4.8**). To an oven-dried 50 mL RBF, was added, (*2S,3S*)-4-azido-2,3-dihydroxybutyl dibenzyl phosphate (**4.7**) (142 mg, 0.348 mmol), EDC (680 mg, 3.55 mmol) and anhydrous CH_2Cl_2 (12 mL). After 5 minutes, butyric acid (0.095 mL, 3.55 mmol) and DMAP (42.5 mg, 1.18 mmol) were added. The solution was then stirred room temperature overnight. For workup, the solution was diluted with 10 mL EtOAc and 10 mL CH_2Cl_2. The cloudy solution was poured through a silica plug and rinsed with 30 mL EtOAc. Volatiles were removed under a high vacuum. Flash column chromatography with elution gradient of 10-80%ethylacetate/hexane gave **4.8** in 56% yield (107 mg) as a clear oil as confirmed by: TLC (R_f = 0.53, 50% EtOAc/Hexane; KM_nO_4 stained, UV active); ^{1}H NMR (500 MHz, $CDCl_3$) δ 7.34 (t, *J* = 1.3 Hz, 8H), 5.27 – 5.13 (m, 2H), 5.02 (dt, *J* = 8.7, 2.8 Hz, 4H), 4.00 (ddd, *J* = 11.5, 6.7, 4.9 Hz, 1H), 3.31 (dd, *J* = 13.3, 5.4 Hz, 1H), 2.38 – 2.19 (m, 4H), 1.62 (dh, *J* = 12.3, 7.4 Hz, 4H), 0.92 (dt, *J* = 9.3, 7.4 Hz, 6H). ^{13}C NMR (126 MHz, $CDCl_3$) δ 172.47, 172.41, 135.56, 135.50, 128.66, 128.62, 128.02, 127.98, 69.95, 69.89, 69.72, 69.62, 69.58, 65.09, 65.05, 50.55, 35.85, 18.25, 13.56 . (*with impurities: ethyl acetate peaks) ^{31}P NMR (202 MHz, $CDCl_3$) δ 1.14.

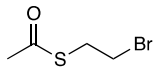

4.43

***S*-(2-Bromoethyl) ethanethioate** (**4.43**). To an oven-dried 50 mL RBF, thioacetic acid (1.23 mL, 17.5 mmol) was dissolved in anhydrous THF. DBU (2.61 mL, 17.5 mmol) was added to give an orange solution, after which dibromoethane (3.10 mL, 36mmol) was added. A white suspension was observed and the solution was stirred at rt for 7 hrs. For workup, the cloudy mixture was filtered through a 4 cm layer of celite and rinsed with 40mL of CH_2Cl_2. Volatiles were removed under a high vacuum. Flash column chromatography with elution gradient of 5/8/10% EtOAc-Hex gave **4.43** in 47% yield (1.51 g) as a light-yellow oil as confirmed by: TLC (R_f = 0.60, 15% EtOAc-Hex; KM_nO_4 stained, UV active). ^{1}H NMR (500 MHz, $CDCl_3$) δ3.34 (t, 2H), 3.30 (t, 2H), 2.34 (s, 3H). ^{13}C NMR (126 MHz, $CDCl_3$) δ 194.23, 31.22, 30.53, 30.04. HRMS-DART: $C_4H_8BrOS^+$ [M+H]+ expected: 182.95, found: 182.93 and 184.93.

Chapter 5. Design and synthesis of yeast phosphatidylserine synthase inhibitors for covalent labeling of the enzyme active site

5.1 Background and motivation

The structures and active sites of PS synthase enzymes that catalyze the biosynthesis of PS varies depending on the organism. For example, Pss1p and Pss2p are the mammalian PS synthases, which catalyzes the headgroup exchange of choline and ethanolamine from PC to PS and PE to PS, respectively. Meanwhile, Cho1p (gene name: *CHO1*) is the fungal PS synthase, which catalyzes the synthesis of PS from CDP-DAG and L-serine with CMP as the byproduct. Consequently, Cho1p is required for the virulence of *Candida albicans*. Since this enzyme is absent in humans, inhibitors that deactivate this enzyme would serve as potential drug targets against the fungal infection candidiasis. However, neither the serine binding site of the *C. albicans* PS synthase nor the crystal structure of the protein itself have been completely uncovered.[195, 247] Unveiling the protein's structure would be crucial for rational drug design. In collaboration with Yue Zhou in the lab of Todd Reynolds in the UT Microbiology department, we designed serine and cysteine analogs that could covalently interact with the enzyme and enable us to map the residues of the active site. We chose to modify serine since this is the enzyme's natural substrate. Additionally, we explored cysteine analogs due to their structural similarity to serine, with the difference being the presence of sulfur instead of oxygen. In this chapter, we highlight our rationale for the analogs and our efforts towards their synthesis.

5.2 Design and synthesis of analogs for probing PS synthase active site composition

We designed small molecule serine and cysteine analogs to contain an electrophilic tag that is reactive towards any electron-rich amino acid residues that are in proximity when bound to the PS synthase active site. Electrophiles such as alkyl bromides can be attached via a propyl linker appended to cysteine (X = S) or serine (X = O) (**Figure 5.1A**). The placement of the trap also avoids the modification at the amino acid *C*- and *N*-termini. Our initial goal is to perform the same approach for activity-based protein profiling[248, 249] with the probe inhibitors to reveal the enzyme's core residues that link to them. A second bifunctional analog bears an azide reporter tag, which can be leveraged for fluorescence imaging by click reaction with fluorescent dye, either for imaging *in vivo* or for SDS-PAGE gels. The latter can help profile the enzyme by directly performing click reaction within cell lysates following incubation of the inhibitor probe and a simple read-out can be conducted by gel electrophoresis and fluorescence analysis of bands (**Figure 5.1B**). With the azide tag, affinity chromatography can also be utilized to enrich labeled proteins or peptide fragments following protein digestion. In detail, once the inhibitor is incubated with cellular materials and covalently links with the enzyme (via electrophilic trap), the linked enzymes can be profiled after click reaction with a biotin alkyne. The biotin can permit enrichment with streptavidin, followed by enzyme digestion to generate fragments for LC-MS analysis. The bromopropylcysteine **Cys-5a** has previously been shown to be a good candidate for serine active site inhibition.[250] Thus, the next goal is to synthesize the bifunctional **Cys-5b** probe to enable click chemistry for enrichment of the residues.

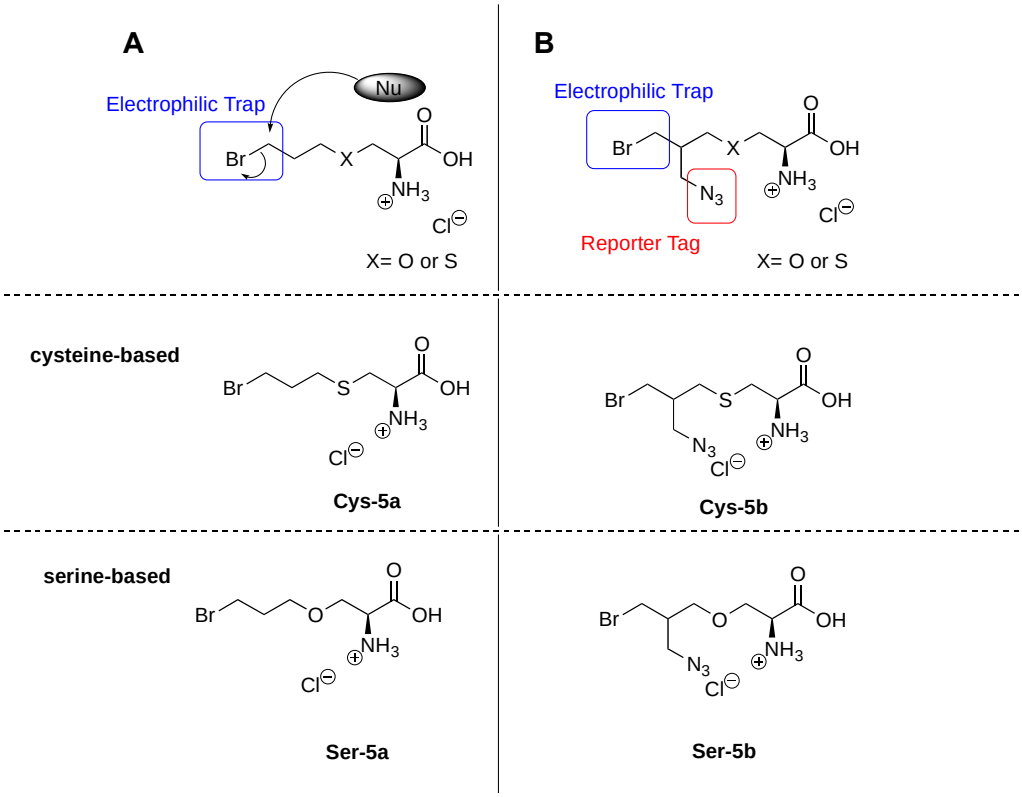

Figure 5.1. Design of serine and cysteine analogs to probe the PS synthase active site by electrophilic trapping and bioorthogonal ligation chemistry.

5.2.1 Synthesis of S-bromopropylcysteine

The synthesis of bromopropylcysteine **Cys-5a**, which was previously synthesized by Best lab member Dr. Tanei Ricks, began with Boc-protected L-cysteine methyl ester (**Scheme 5.1**). This procedure is based on Fiore and coworkers' work on *S*-glycopeptide synthesis.[251] Alkyl halide substitution of dibromopropane from the nucleophilic sulfur afforded **5.1**. The next step should be a facile deprotection of the Boc (*tert*-butyl carbamate) and methyl protecting groups, but proved to exhibit synthetic drawbacks when attempting previously utilized deprotection conditions with hydrochloric acid (HCl) in aqueous solution. Even after 24 hours of stirring at 70°C, **5.1** was not completely deprotected and instead retained the methyl ester (**Cys-5a-ester**) when analyzed by TLC and ^{1}H NMR. We initially attempted to stir unprotected **Cys-5a-ester** in aqueous sodium hydroxide solution for 3 hours, but this resulted in the same ester intermediate. This was likely due to insolubility of **5.1** in aqueous solution so this protected intermediate was instead dissolved in dioxane and stirred with HCl (4M in dioxane) to access S-bromopropylcysteine **Cys-5a**. Complete methyl ester deprotection was also possible after three days of stirring **5.1** in HCl solution at 90°C**.**

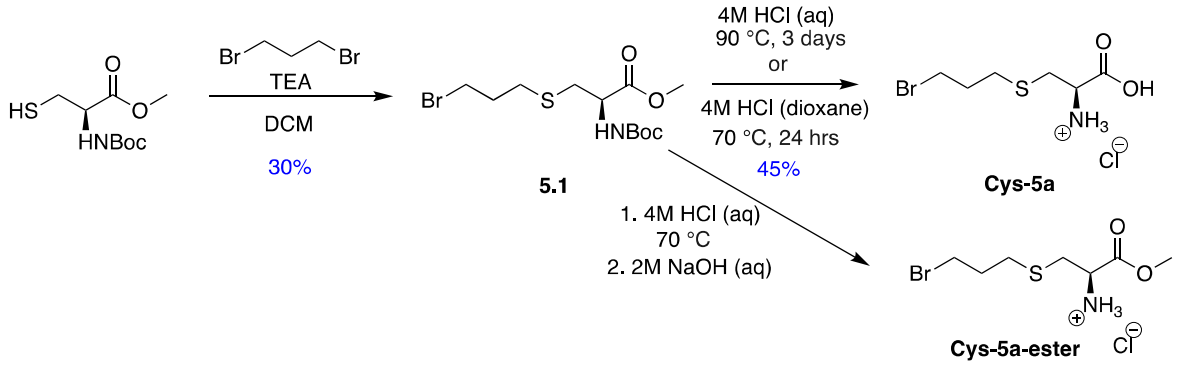

Scheme 5.1. Synthesis of bromopropylcysteine Cys-5a analog bearing the electrophilic tag.

5.2.2 Synthesis of bifunctional bromopropylazidomethylcysteine and the dibromoazide precursor

We then pursued synthesis of bifunctional cysteine analog **Cys-5b**, which along with the electrophilic trap, includes an additional azide linker (Scheme 5.2). The synthesis begins once more with *N*-Boc-L-cysteine methyl ester and thiolate activation by triethylamine. Alkylation of the starting cysteine with dibromoazide **5.5** afforded protected **5.2**. Subsequent deprotection is expected to result in the desired **Cys-5b** bifunctional analog.

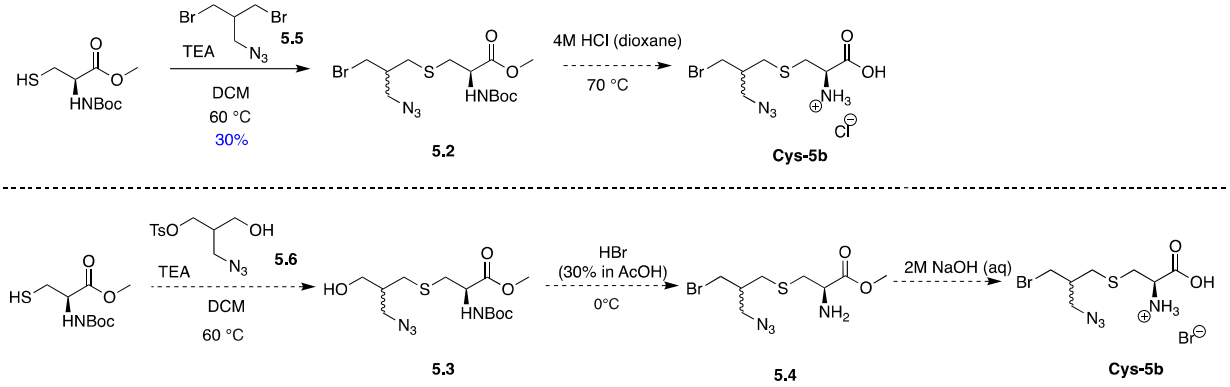

Scheme 5.2. Synthesis of azidobromopropylcysteine **Cys-5b**.

Mono-tosylated diol intermediate **5.51** was prepared from commercially available acetonide protected glycerol, followed by tosylation and acetonide deprotection (Scheme 5.3). Then, the tosyl group was substituted with azide using sodium azide in the presence of crown ether to give azide **5.52**. The next step was to prepare tosyl-functionalized intermediate **5.53** for bromide substitution to the desired precursor 1,3-dibromopropane-2-methylazide **5.5**, but conversion of the two alcohol groups to tosyl groups was low-yielding. However, the byproduct, monotosylated **5.6**, was utilized as another precursor for an alternative route in the synthesis of bifunctional **Cys-5b** (Scheme 5.2, bottom panel).

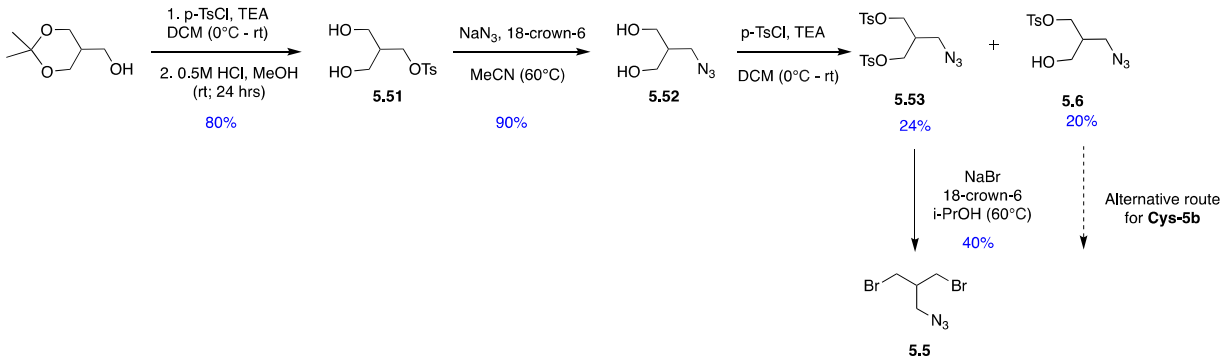

Scheme 5.3. Synthesis of 1,3-dibromopropane-2-methylazide.

5.3 Conclusion

For a full elucidation of the PS synthase active site, the sequences that code for this protein must be determined. Towards this end, ongoing work by collaborator Yue Zhou in the lab of Dr. Reynolds in the UTK Microbiology Department is aimed at uncovering the structure of the Cho1p enzyme for *C. albicans* and analyzing the predicted serine binding motif.[195] Our contribution to this investigation entails designing inhibitor probes that covalently interact with the PS synthase for this organism. Toward this end, we have synthesized **Cys-5a**, a cysteine analog equipped with an electrophilic trap, as well as the protected version of **Cys-5b**, the bifunctional cysteine derivative that contains an azide tag for further derivatization. The next step following synthesis is to incubate these analogs into cells, generate cell lysates, and conduct LC-MS/MS to reveal the core nucleophile residue that covalently binds to the analog. However, experiments can also be conducted *in vitro* with the isolated enzyme.[247] The experimental design would be to incubate these analogs with isolated PS synthase enzyme, along with CDP-DAG substrate and conduct LC-MS/MS. Doing so will reveal and verify the predicted core nucleophile residue that covalently binds to the cysteine analog. Finally, it is important to note that this bromopropyl

electrophilic trap has a broad application in terms of what nucleophile "attacks" it. This is resolved with the "specificity" portion of the probe, which is its core serine or cysteine structure, designed to be close to the L-serine substrate of PS synthase enzyme. In this case, the **Cys-5a** and bifunctional **Cys-5b** analog can serve as a "broad spectrum" probe for enzymes similar to PS synthase, adding to the set of chemical probes for active site profiling.

5.4 Synthesis Procedures and Characterization Data

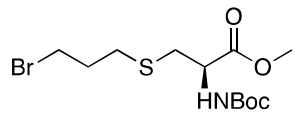

5.1

***S*-(3-Bromopropyl)-*N*-(*tert*-butoxycarbonyl)-*L*-cysteinate (5.1).** To a solution of methyl (*tert*-butoxycarbonyl)-L-cysteine methyl ester (480 µL, 2.33 mmol) in CH_2Cl_2 (20 mL) were added Et_3N (1.2 mL, 4.50 mmol) and 1,3-dibromopropane (1.05 mL, 10.3 mmol). The clear solution was allowed to stir at room temperature for one day. For workup, 50 mL CH_2Cl_2 was added to dilute the solution, which was then washed with H_2O (2 x 25 mL), and the collected organic layer was dried (Na_2SO_4), concentrated, and placed under a high vacuum overnight. Flash column chromatography with elution gradient of 10/12/14% EtOAc/Hex gave a pure product in 30% yield (244 mg) as a clear viscous substance as confirmed by TLC (R_f = 0.41, 20% EtOAc/Hex; ninhydrin stain); ^{1}H NMR (300 MHz, $CDCl_3$) δ5.34, 4.48, 3.72, 3.44, 2.92, 2.64, 2.04, 1.40*;* ^{13}C NMR (75 MHz, $CDCl_3$) δ 171.38, 155.04, 80.10, 53.30, 52.52, 34.47, 32.05, 31.80, 30.82, 28.26.

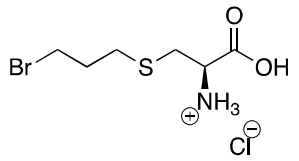

Cys-5a

2-((3-Bromopropyl)thio)-1-carboxyethan-1-aminium chloride (**Cys-5a**). 4M HCl in dioxane (25 mL) was slowly added to a 100 mL RBF containing the protected S-bromopropylcysteine **5.1** (1.27 g, 3.57 mmol, suspended in dioxane). The resulting light yellow solution was fitted with an oven-dried condenser, flushed with nitrogen and heated at 70°C and stirred for 1 day to give a dirty-yellow solution. After TLC monitoring (disappearance of bottom spot in reverse-phase TLC), excess acid was removed under reduced pressure, diluted with water (105 mL), and washed with 2 x 10 mL of diethyl ether. The collected aqueous layer was concentrated with heating to give a dirty-white salt. The collected salt was washed with diethyl ether (vortexed to disperse clumps) several times until no longer yellow and filtered. The collected dirty-white powder was placed under reduced pressure. Reverse-phase flash chromatography was employed using C18 syringe column with nitrogen gas as pressure, with elution gradient of 10/20/40/50/60% MeOH/water to give white powder as a pure product in 45% yield (0.573 mg, 1.61 mmol) as confirmed by: Reverse-Phase TLC (R_f = 0.80 in 50%MeOH/water; purple in ninhydrin stain); ^{1}H NMR (500 MHz, CD_3OD) δ 4.23 (dd, *J* = 7.2, 4.4 Hz, 1H), 3.69 (t, *J* = 6.3 Hz, 2H), 3.19 (dd, *J* = 14.8, 4.4 Hz, 1H), 3.08 (dd, *J* = 14.8, 7.2 Hz, 1H), 2.78 (td, *J* = 7.1, 1.4 Hz, 2H), 2.10 – 2.01 (m, 2H); ^{13}C NMR (126 MHz, d_2o) δ 175.35, 53.50, 43.60, 31.87, 31.16, 28.32.; DART-MS: $[M+H]^+$ for $C_6H_{12}BrNO_2$ calculated, 243.98; detected, 243.94.

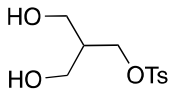

5.51

3-Hydroxy-2-(hydroxymethyl)propyl 4-methylbenzenesulfonate (5.51). To a solution of (2,2-dimethyl-1,3-dioxan-5-yl)methanol (1.00 mL, 6.84 mmol) in CH_2Cl_2 was added Et_3N (1.35 mL, 10.2 mmol) in portions. After stirring at rt for 5 min, *p*-TsCl (1.95 g, 10.26 mmol) was added in portions and the solution was allowed to react for 5 hours. For work-up, the solution was poured into 0.5 M HCl and extracted with 3 x 25mL of CH_2Cl_2. The collected organic layer was washed with 25 mL water and 25 mL of brine, one time each. The product was dried over sodium sulfate and concentrated to give a clear oil. This intermediate product was used without further purification and diluted with 10 mL MeOH. Next, 0.5 M HCl (25mL) was added to the solution in portions, whereby a white powder crashed out after every addition. The solution was stirred overnight and subsequently neutralized with $NaHCO_3$. The crude solution was filtered through celite and solvent was removed under reduced pressure. The yellow oil was subjected to column chromatography using the elution gradient 100%hexane to 25/50/75/80% EtOAc/Hex. The product was collected as a clear oil at a 74% yield over two steps (1.314g, 5.05mmol) as confirmed by: TLC (R_f = 0.50 in 100%EtOAc; $KMnO_4$ stain), ^{1}H NMR (500 MHz, CD_3OD): δ 7.77 (s, 2H), 7.44(s, 2H), 4.12 (s, 2H), 3.55 (s, 4H), 2.44 (s, 3H), 1.95 (s, 1H). ^{13}C NMR (126 MHz, CD_3OD): δ 145.09, 132.87, 129.68, 127.60, 68.47, 58.92, 43.44, 20.20.

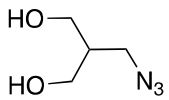

5.52

2-(Azidomethyl)propane-1,3-diol (5.52). The intermediate 3-hydroxy-2-(hydroxymethyl)propyl 4-methylbenzenesulfonate (1.314g, 5.05mmol) and 18-Crown-6 (0.438, 1.34mmol) were dissolved in MeCN and stirred for two minutes. 3 equivalents of NaN_3 (1.846g, 28.4mmol) were added to the solution, which was fitted with a condenser and an Argon balloon for overnight stirring at 85°C. The murky white crude solution was allowed to cool to rt before filtration through a 3 cm layer of celite and rinses with ethyl acetate. Solvents were removed under reduced pressure and the collected light brown oil residue was run through column chromatography using the solvent gradient 25/50/75% EtOAc/Hex. The collected fractions from fraction 20-27 was not UV active and collected for analysis. The product isolated gave a 90% yield (0.601g, 4.58mmol) as confirmed by: TLC (R_f = 0.35 in 100%EtOAc; $KMnO_4$ stain), ^{1}H NMR (500 MHz, CD_3OD) δ 3.80 – 3.70 (m, 4H), 3.45 (d, J = 6.6 Hz, 2H), 2.93 (s, 2H), 2.00 – 1.88 (m, 1H).^{13}C NMR (126 MHz, CD_3OD) δ62.50, 50.17, 42.29. HRMS-DART: $[M+H]^+$ calculated for $C_4H_9N_3O_2$: 132.1191, found: 133.09192; $[M-N_2+H]^+$ calculated for $C_4H_9N_1O_2$: 104.1057; Found: 104.06893.

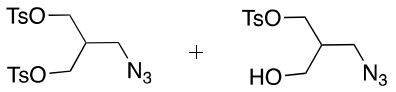

5.53 **5.6**

2-(Azidomethyl)propane-1,3-diyl bis(4-methylbenzenesulfonate) (ditosylated product **5.53) and 3-Azido-2-(hydroxymethyl)propyl 4-methylbenzenesulfonate (**monotosylated product **5.6).** To a solution of 2-(azidomethyl)propane-1,3-diol (**5.52**) (0.5268 g, 4.01 mmol) was added 1.35 equivalents of triethylamine (760 uL, 5.45 mmol) in 5mL of CH_2Cl_2. Next, 4 equivalents of *p*-toluene sulfonyl chloride (3.058 g, 16.01 mmol) were added in increments, after which the

remaining CH_2Cl_2 was added (25mL total). After stirring at rt for 24 hours, the solution was poured into a 0.5M HCl (aq) solution and extracted three times with 25mL of CH_2Cl_2. The collected organic layer was washed with water twice and then once with saturated sodium chloride solution (aq). This was followed by drying with sodium sulfate and filtration through a funnel fitted with cotton. The organic solvents were removed under reduced pressure to give a clear oil. Flash column chromatography using the solvent gradient 5/10/15/20% EtOAc/Hex gave the ditosylated product **(5.53)** as a clear oil in a 24% yield (0.428g, 0.974mmol). The mono-tosylated product **(5.6)** was also isolated in a 20% yield (0.225g, 0.789mmol) with an Rf value of 0.77 in 75%EtOAc/Hex. Formation of the ditosylated product **(5.53)** was confirmed by: TLC R_f=0.85 in 75%EtOAc-hexanes; $KMnO_4$ stain), ^{1}H NMR (500 MHz, cdcl$_3$) δ 7.77 – 7.74 (m, 4H), 7.38 – 7.34 (m, 4H), 3.98 (d, J = 5.8 Hz, 4H), 3.37 (d, J = 6.3 Hz, 2H), 2.46 (s, 6H), 2.22 (p, J = 6.0 Hz, 1H).^{13}C NMR (126 MHz, $CDCl_3$) δ 145.39, 132.15, 130.06, 127.93, 66.67, 48.30, 38.40, 21.68. Formation of the monotosylated product (5.6) was confirmed by: TLC (R_f = 0.77 in 75% EtOAc/Hex; $KMnO_4$ stain), ^{1}H NMR (500 MHz, $CDCl_3$) δ 7.82 – 7.76 (m, 2H), 7.39 – 7.34 (m, 2H), 4.10 (d, J = 5.7 Hz, 2H), 3.70 – 3.61 (m, 2H), 3.47 – 3.36 (m, 2H), 2.45 (s, 3H), 2.14 – 2.03 (m, 1H).^{13}C NMR (126 MHz, cdcl$_3$) δ 145.21, 132.46, 130.00, 127.92, 67.98, 60.15, 49.22, 40.70, 21.66.

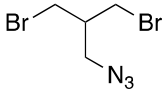

5.5

1-Azido-3-bromo-2-(bromomethyl)propane (5.5). Sodium bromide (0.270g, 2.24mmol) was partially dissolved in acetone, after which the intermediate 2-(azidomethyl)propane-1,3-diyl bis(4-methylbenzenesulfonate (0.428g, 0.974mmol) **(5.53)** was added and stirred overnight at

55°C. Within 4 hours, the solution turned murky white, with the reaction TLC showing formation of the mono-substituted product. (R_f=0.67 in 30% EtOAc/Hex; UV, $KMnO_4$ staining). After 24 hours, di-substituted product was observed as a faint spot in the TLC of an aliquot (R_f = 0.80 in 30% EtOAc/Hex, $KMnO_4$ stain). An additional 2 equivalents of NaBr were introduced to the reaction flask and the solution was allowed to react for 24 more hours at 75°C. After a total of two days, the solution was cooled to rt and the solvent was removed under reduced pressure to give a heterogeneous mixture of oil and white solids. The white salts were filtered off, giving a light yellow oil. The crude was subjected to flash column chromatography using the solvent gradient, 3/5/8/12% EtOAc-hexanes to give the product as a light yellow oil (40.5mg, 0.157mmol, 16%) as confirmed by TLC Rf=0.80 in 10%EtOAc-hexanes; $KMnO_4$ stain), ^{1}H NMR (500 MHz, $CDCl_3$) δ 3.54 (dd, *J* = 6.4, 4.5 Hz, 4H), 2.24 (hept, *J* = 5.9 Hz, 2H), 1.25 (s, 1H).^{13}C NMR (126 MHz, $CDCl_3$) δ 151.91, 42.28, 32.58.

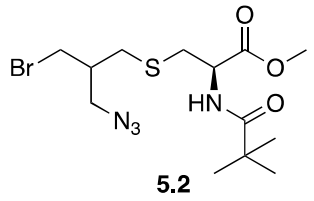

5.2

Methyl *S*-(3-azido-2-(bromomethyl)propyl)-*N*-(*tert*-butoxycarbonyl)cysteinate (5.2). To a solution of methyl (*tert*-butoxycarbonyl)-*L*-cysteine methyl ester *or S*-Butenyl L-cysteine (32.3 uL, 0.157 mmol) in CH_2Cl_2 (20 mL) were added Et_3N (43.7 uL, 0.314 mmol) and 1,3-dibromopropane-2-methylazide (**5.5**) (40.5 mg, 0.157 mmol). The clear solution stirred at room temperature for one day. For workup the solution was washed with H_2O (2 x 15 mL), and the collected organic layer was dried (Na_2SO_4), and concentrated, and placed under a high vacuum overnight. Flash

chromatography with elution gradient of 100% hexanes - 10/15/20/30% EtOAc/Hex gave a pure product in 30% yield (19.4 mg, 0.047 mmol) as a clear viscous substance as confirmed by: TLC (R_f = 0.50, 20% EtOAc/Hex; ninhydrin stain); ^{1}H NMR (500 MHz, $CDCl_3$) δ 6.15 (s, 1H), 5.72 (s, 1H), 3.82 (s, 3H), 3.66 (s, 2H), 3.55 (s, 2H), 3.54 (s, 2H), 3.48 (s, 1H), 2.24 (s, 2H), 1.48 (d, *J* = 0.9 Hz, 9H); ^{13}C NMR (126 MHz, $CDCl_3$) δ 164.44, 131.27, 105.15, 52.85, 51.91, 51.16, 43.80, 42.29, 32.56, 31.68, 28.23.

Chapter 6. Conclusions

Lipids are attractive targets for imaging and tracing since they are responsible for many essential biological functions. One powerful experimental platform that has emerged takes advantage of the chemical reporter strategy where click-tagged substrates are fed to live cells for cellular uptake and incorporation into lipid biosynthetic pathways, resulting in the production of tagged versions of lipid targets. In this dissertation, we highlighted a series of novel and non-toxic substrate mimics that generates traceable lipids either for a particular pathway or for several lipid biosynthesis routes. Control of labeled lipid targets was possible via organic synthesis and attachment of the click tag through the headgroup or the glycerol backbone.

In Chapter 2, we focused on PS as a lipid target since it plays many roles in intracellular processes and its extrafacial exposure poses it as a biomarker. Our method takes advantage of headgroup tagging of PS's precursor, L-Serine by modifying its N- or C- terminus. It was determined that **N-L-SerN$_3$** labels PS, PE, and PC lipids, thus presenting itself as a new metabolic reporter probe for the PS → PE → PC CDP-DAG pathway in *S. cerevisiae*. Meanwhile, current microscopy and LCMS results point to **C-L-SerN$_3$** as a selective PS label. Visualization of labeled lipids from these serine precursors was possible through SPAAC with click-partner cyanine dye; however, our current methodology relies on fixation which cannot offer information on movement and trafficking of lipid products. Future work should tackle *in vivo* tracking of functionalized lipids following SPAAC. Nevertheless, our experiments revealed these serine probes to label PS lipid products and coincide with expected PS lipid localization for yeast at the PM and budding sites.

In Chapters 3 and 4, metabolic precursors wherein the clickable tag is appended to the glycerol backbone's *sn*-1 position are presented. In Chapter 3, mass-spectrometry based analysis revealed that **C_4-MAG-N_3** labels phospholipids (PS, PE, PC, PA) and neutral lipids (MAG, DAG, TAG). The labeled lipids were visualized and enriched at the PM where bulk phospholipids are expected to be localized. However, pulse-chase assays and TLC revealed that distribution or propagation of the azide tag was 'uneven' among these lipid classes. Nevertheless, our analysis showcase the importance for investigating lipid product turnover and *how well* the azide label is propagated into various lipid classes, especially since lipids are subject to multi-enzyme pathways. One concern is that the azide-modified glycerol is restrictive as a phosphatidyl group acceptor. We confront this problem with the synthesis of a PA lipid mimic, **SATE-C_4-PA-N_3**, as a precursor which contains a phosphate group.

As with many metabolic labeling platforms, it can be challenging to focus selectivity for a lipid class which can be lamented from the intertwined lipid metabolic network and the use of precursors that are mimics of "multivariable" substrates of different enzymes. Fortunately, there exists many tools in fields of biology and chemistry to perform validation assays. For example, MS and lipidomics can provide clarity on identities of labeled lipid products, and mutant cell lines lacking a specific enzyme that will convert lipid products and subsequent abrogation of signal can give confidence to the hypothesis that the precursor labels the intended lipid product(s). Another concern of this technique is the lack of efficiency for metabolic labeling and strategies are needed to maximize the chances of precursors to locate its enzyme for conversion. To overcome this, substantial future work should focus on attaching organelle-targeting moieties onto precursors to bias delivery to sites of lipid synthesis.

While majority of of the experiments conducted in this dissertation utilized yeast (*S. cerevisiae and C. albicans*), we should seek to examine the utility of our precursor probes in other cell lines and higher eukaryotes to broaden their potential scope of applications. For example, extrafacial exposure of azide-tagged PS can be exploited for targeted delivery applications in cancer cells. In another instance, azido-MAG probes with different acyl chain lengths could have varied toxicity effects when exogenously added in other cells/organisms.

In summary, the work presented in this dissertation highlights the synthesis and use of clickable precursors aimed for labeling a specific lipid class and for labeling bulk glycerolipids and glycerophospholipids in cells. In terms of broader applications, specific labeling of a lipid class can be exploited to uncover its metabolic interactors and elucidate its transport and trafficking within cells. On the other hand, several different pathways can be studied at a time using the same clickable lipid precursor. All in all, we expect these probes to be valuable chemical tools for visualizing lipids, studying lipid remodeling, and discerning how lipid metabolism shifts in cells in response to different stimuli and biological processes. The interdisciplinary techniques showcased in this dissertation is also a testament to the broader world of lipid science whereby researchers across various disciplines work together to elucidate and answer outstanding questions in lipidomics and lipid cell biology.

References

1. Sunshine, H.; Iruela-Arispe, M. L., Membrane lipids and cell signaling. *Curr Opin Lipidol* **2017,** *28* (5), 408-413.
2. Sprong, H.; van der Sluijs, P.; van Meer, G., How proteins move lipids and lipids move proteins. *Nat Rev Mol Cell Biol* **2001,** *2* (7), 504-13.
3. Cho, W.; Stahelin, R. V., Membrane-protein interactions in cell signaling and membrane trafficking. *Annu Rev Biophys Biomol Struct* **2005,** *34*, 119-51.
4. Jiang, H.; Zhang, X.; Chen, X.; Aramsangtienchai, P.; Tong, Z.; Lin, H., Protein Lipidation: Occurrence, Mechanisms, Biological Functions, and Enabling Technologies. *Chem Rev* **2018,** *118* (3), 919-988.
5. Morita, S.-y.; Ikeda, Y., Regulation of membrane phospholipid biosynthesis in mammalian cells. *Biochemical Pharmacology* **2022,** *206*, 115296.
6. Fahy, E.; Subramaniam, S.; Brown, H. A.; Glass, C. K.; Merrill, A. H., Jr.; Murphy, R. C.; Raetz, C. R. H.; Russell, D. W.; Seyama, Y.; Shaw, W.; Shimizu, T.; Spener, F.; van Meer, G.; VanNieuwenhze, M. S.; White, S. H.; Witztum, J. L.; Dennis, E. A., A comprehensive classification system for lipids¹. *Journal of Lipid Research* **2005,** *46* (5), 839-861.
7. Shevchenko, A.; Simons, K., Lipidomics: coming to grips with lipid diversity. *Nat. Rev. Mol. Cell Biol.* **2010,** *11* (8), 593-598.
8. Liebisch, G.; Fahy, E.; Aoki, J.; Dennis, E. A.; Durand, T.; Ejsing, C. S.; Fedorova, M.; Feussner, I.; Griffiths, W. J.; Köfeler, H.; Merrill, A. H., Jr.; Murphy, R. C.; O'Donnell, V. B.; Oskolkova, O.; Subramaniam, S.; Wakelam, M. J. O.; Spener, F., Update on LIPID MAPS classification, nomenclature, and shorthand notation for MS-derived lipid structures. *Journal of Lipid Research* **2020,** *61* (12), 1539-1555.
9. Welte, M. A., Expanding roles for lipid droplets. *Curr Biol* **2015,** *25* (11), R470-81.
10. Athenstaedt, K., Nonpolar Lipids in Yeast: Synthesis, Storage, and Degradation. In *Biogenesis of Fatty Acids, Lipids and Membranes*, Geiger, O., Ed. Springer International Publishing: Cham, 2019; pp 363-373.
11. Wakelam, M. J. O., Diacylglycerol – when is it an intracellular messenger? *Biochimica et Biophysica Acta (BBA) - Molecular and Cell Biology of Lipids* **1998,** *1436* (1), 117-126.
12. Shi, Y.; Cheng, D., Beyond triglyceride synthesis: the dynamic functional roles of MGAT and DGAT enzymes in energy metabolism. *Am J Physiol Endocrinol Metab* **2009,** *297* (1), E10-8.
13. Zadoorian, A.; Du, X.; Yang, H., Lipid droplet biogenesis and functions in health and disease. *Nature Reviews Endocrinology* **2023,** *19*, 443-459.
14. van Meer, G.; Voelker, D. R.; Feigenson, G. W., Membrane lipids: where they are and how they behave. *Nature Reviews Molecular Cell Biology* **2008,** *9* (2), 112-124.
15. Vance, J. E., Historical perspective: phosphatidylserine and phosphatidylethanolamine from the 1800s to the present. *J Lipid Res* **2018,** *59* (6), 923-944.
16. Blagović, B.; Mesarić, M.; Marić, V.; Rupčić, J., Characterization of lipid components in the whole cells and plasma membranes of baker's Yeast. *Croatica Chemica Acta* **2005,** *78*, 479-484.
17. Blagović, B.; Rupčić, J.; Mesarić, M.; Georgiú, K.; Marić, V., Lipid Composition of Brewer's Yeast. *Food Technology and Biotechnology* **2001,** *39*, 175-181.

18. Sapar, M. L.; Ji, H.; Wang, B.; Poe, A. R.; Dubey, K.; Ren, X.; Ni, J.-Q.; Han, C., Phosphatidylserine Externalization Results from and Causes Neurite Degeneration in Drosophila. *Cell Reports* **2018,** *24* (9), 2273-2286.
19. Hodgkin, M. N.; Pettitt, T. R.; Martin, A.; Michell, R. H.; Pemberton, A. J.; Wakelam, M. J. O., Diacylglycerols and phosphatidates: which molecular species are intracellular messengers? *Trends Biochem. Sci* **1998,** *23* (6), 200-204.
20. Pendaries, C.; Tronchère, H.; Plantavid, M.; Payrastre, B., Phosphoinositide signaling disorders in human diseases. *FEBS Lett* **2003,** *546* (1), 25-31.
21. van Meer, G.; de Kroon, A. I. P. M., Lipid map of the mammalian cell. *Journal of Cell Science* **2011,** *124* (1), 5-8.
22. Snaebjornsson, M. T.; Janaki-Raman, S.; Schulze, A., Greasing the Wheels of the Cancer Machine: The Role of Lipid Metabolism in Cancer. *Cell Metabolism* **2020,** *31* (1), 62-76.
23. Wymann, M. P.; Schneiter, R., Lipid signalling in disease. *Nat Rev Mol Cell Biol* **2008,** *9* (2), 162-76.
24. Santos, C. R.; Schulze, A., Lipid metabolism in cancer. *The FEBS Journal* **2012,** *279* (15), 2610-2623.
25. Pischon, T.; Nöthlings, U.; Boeing, H., Obesity and cancer: Symposium on 'Diet and cancer'. *Proceedings of the Nutrition Society* **2008,** *67* (2), 128-145.
26. Adams, K. F.; Schatzkin, A.; Harris, T. B.; Kipnis, V.; Mouw, T.; Ballard-Barbash, R.; Hollenbeck, A.; Leitzmann, M. F., Overweight, Obesity, and Mortality in a Large Prospective Cohort of Persons 50 to 71 Years Old. *New England Journal of Medicine* **2006,** *355* (8), 763-778.
27. Rosing, J.; Bevers, E.; Comfurius, P.; Hemker, H.; van Dieijen, G.; Weiss, H.; Zwaal, R., Impaired factor X and prothrombin activation associated with decreased phospholipid exposure in platelets from a patient with a bleeding disorder. *Blood* **1985,** *65* (6), 1557-1561.
28. van den Eijnde, S. M.; Boshart, L.; Baehrecke, E. H.; De Zeeuw, C. I.; Reutelingsperger, C. P.; Vermeij-Keers, C., Cell surface exposure of phosphatidylserine during apoptosis is phylogenetically conserved. *Apoptosis* **1998,** *3* (1), 9-16.
29. Sharma, B.; Kanwar, S. S., Phosphatidylserine: A cancer cell targeting biomarker. *Seminars in Cancer Biology* **2018,** *52*, 17-25.
30. Prescher, J. A.; Bertozzi, C. R., Chemistry in living systems. *Nature Chemical Biology* **2005,** *1* (1), 13-21.
31. Cairns, R. A.; Harris, I. S.; Mak, T. W., Regulation of cancer cell metabolism. *Nature Reviews Cancer* **2011,** *11* (2), 85-95.
32. Best, M. D., Click chemistry and bioorthogonal reactions: unprecedented selectivity in the labeling of biological molecules. *Biochem.* **2009,** *48* (28), 6571-84.
33. Devaraj, N. K., The Future of Bioorthogonal Chemistry. *ACS Central Science* **2018,** *4* (8), 952-959.
34. Sletten, E. M.; Bertozzi, C. R., Bioorthogonal chemistry: fishing for selectivity in a sea of functionality. *Angew Chem Int Ed Engl* **2009,** *48* (38), 6974-98.
35. Sletten, E. M.; Bertozzi, C. R., From Mechanism to Mouse: A Tale of Two Bioorthogonal Reactions. *Accounts of Chemical Research* **2011,** *44* (9), 666-676.
36. Bumpus, T. W.; Baskin, J. M., Greasing the Wheels of Lipid Biology with Chemical Tools. *Trends in biochemical sciences* **2018,** *43* (12), 970-983.

37. Kuerschner, L.; Thiele, C., Tracing Lipid Metabolism by Alkyne Lipids and Mass Spectrometry: The State of the Art. *Frontiers in Molecular Biosciences* **2022,** *9*.
38. Chiu, D.-C.; Baskin, J. M., Imaging and Editing the Phospholipidome. *Accounts of Chemical Research* **2022,** *55* (21), 3088-3098.
39. Ecker, J.; Liebisch, G., Application of stable isotopes to investigate the metabolism of fatty acids, glycerophospholipid and sphingolipid species. *Prog. Lipid Res.* **2014,** *54*, 14-31.
40. Wegener, G.; Kellermann, M. Y.; Elvert, M., Tracking activity and function of microorganisms by stable isotope probing of membrane lipids. *Curr. Opin. Biotechnol.* **2016,** *41*, 43-52.
41. Foster, D. W.; Katz, J., The distribution of tritium in fatty acids synthesized from tritiated glucose and tritiated water by rat adipose tissue. *Biochimica et Biophysica Acta (BBA) - Lipids and Lipid Metabolism* **1966,** *125* (3), 422-427.
42. Jungas, R. L., Fatty acid synthesis in adipose tissue incubated in tritiated water. *Biochemistry* **1968,** *7* (10), 3708-3717.
43. Batista Silva, W.; Daloso, D. M.; Fernie, A. R.; Nunes-Nesi, A.; Araújo, W. L., Can stable isotope mass spectrometry replace radiolabelled approaches in metabolic studies? *Plant Science* **2016,** *249*, 59-69.
44. Kim, I.-Y.; Park, S.; Jang, J.; Wolfe, R. R., Quantifications of Lipid Kinetics In Vivo Using Stable Isotope Tracer Methodology. *J Lipid Atheroscler* **2020,** *9* (1), 110-123.
45. Rampler, E.; Coman, C.; Hermann, G.; Sickmann, A.; Ahrends, R.; Koellensperger, G., LILY-lipidome isotope labeling of yeast: in vivo synthesis of 13C labeled reference lipids for quantification by mass spectrometry. *Analyst* **2017,** *142* (11), 1891-1899.
46. Triebl, A.; Wenk, M. R., Analytical Considerations of Stable Isotope Labelling in Lipidomics. *Biomolecules* **2018,** *8* (4).
47. Berry, K. A. Z.; Hankin, J. A.; Barkley, R. M.; Spraggins, J. M.; Caprioli, R. M.; Murphy, R. C., MALDI Imaging of Lipid Biochemistry in Tissues by Mass Spectrometry. *Chem. Rev.* **2011,** *111* (10), 6491-6512.
48. Bowman, A. P.; Heeren, R. M. A.; Ellis, S. R., Advances in mass spectrometry imaging enabling observation of localised lipid biochemistry within tissues. *Trends Anal. Chem.* **2019,** *120*.
49. Murphy, R. C.; Hankin, J. A.; Barkley, R. M., Imaging of lipid species by MALDI mass spectrometry. *J. Lipid Res.* **2009,** *50*, S317-S322.
50. Elvington, S. M.; Bu, F.; Nichols, J. W., Fluorescent, Acyl Chain-labeled Phosphatidylcholine Analogs Reveal Novel Transport Pathways across the Plasma Membrane of Yeast*. *J. Biol.Chem.* **2005,** *280* (49), 40957-40964.
51. Hanson, P. K.; Grant, A. M.; Nichols, J. W., NBD-labeled phosphatidylcholine enters the yeast vacuole via the pre-vacuolar compartment. *J. Cell Sci.* **2002,** *115* (Pt 13), 2725-33.
52. Smith, B. A.; O'Neil, E. J.; Lampkins, A. J.; Johnson, J. R.; Lee, J. J.; Cole, E. L.; Smith, B. D., Evaluation of fluorescent phosphatidylserine substrates for the aminophospholipid flippase in mammalian cells. *J Fluoresc* **2012,** *22* (1), 93-101.
53. Laguerre, A.; Schultz, C., Novel lipid tools and probes for biological investigations. *Curr. Opin. Cell Biol.* **2018,** *53*, 97-104.

54. Kean, L. S.; Fuller, R. S.; Nichols, J. W., Retrograde lipid traffic in yeast: identification of two distinct pathways for internalization of fluorescent-labeled phosphatidylcholine from the plasma membrane. *J Cell Biol* **1993,** *123* (6 Pt 1), 1403-19.
55. Varandas, P. A. M. M.; Cobb, A. J. A.; Segundo, M. A.; Silva, E. M. P., Emergent Glycerophospholipid Fluorescent Probes: Synthesis and Applications. *Bioconjug. Chem.* **2020,** *31* (3), 417-435.
56. Maekawa, M.; Fairn, G. D., Molecular probes to visualize the location, organization and dynamics of lipids. *J Cell Sci* **2014,** *127* (Pt 22), 4801-12.
57. Shaner, N. C.; Patterson, G. H.; Davidson, M. W., Advances in fluorescent protein technology. *Journal of Cell Science* **2007,** *120* (24), 4247-4260.
58. Lemmon, M. A., Membrane recognition by phospholipid-binding domains. *Nat. Rev. Mol. Cell Biol.* **2008,** *9* (2), 99-111.
59. Gillooly, D. J.; Morrow, I. C.; Lindsay, M.; Gould, R.; Bryant, N. J.; Gaullier, J.-M.; Parton, R. G.; Stenmark, H., Localization of phosphatidylinositol 3-phosphate in yeast and mammalian cells. *The EMBO Journal* **2000,** *19* (17), 4577-4588.
60. Best, M. D., Click Chemistry and Bioorthogonal Reactions: Unprecedented Selectivity in the Labeling of Biological Molecules. *Biochemistry* **2009,** *48* (28), 6571-6584.
61. Sletten, E. M.; Bertozzi, C. R., Bioorthogonal Chemistry: Fishing for Selectivity in a Sea of Functionality. *Angew. Chem., Int. Edit.* **2009,** *48* (38), 6974-6998.
62. Sletten, E. M.; Bertozzi, C. R., From Mechanism to Mouse: A Tale of Two Bioorthogonal Reactions. *Acc. Chem. Res.* **2011,** *44* (9), 666-676.
63. Devaraj, N. K., The Future of Bioorthogonal Chemistry. *ACS Cent. Sci.* **2018,** *4* (8), 952-959.
64. Kolb, H. C.; Finn, M. G.; Sharpless, K. B., Click chemistry: Diverse chemical function from a few good reactions. *Angew. Chem., Int. Edit.* **2001,** *40* (11), 2004-+.
65. Hein, J. E.; Fokin, V. V., Copper-catalyzed azide-alkyne cycloaddition (CuAAC) and beyond: new reactivity of copper(I) acetylides. *Chem. Soc. Rev.* **2010,** *39* (4), 1302-1315.
66. Meldal, M.; Tornoe, C. W., Cu-catalyzed azide-alkyne cycloaddition. *Chem. Rev.* **2008,** *108* (8), 2952-3015.
67. Rostovtsev, V. V.; Green, L. G.; Fokin, V. V.; Sharpless, K. B., A stepwise Huisgen cycloaddition process: Copper(I)-catalyzed regioselective "ligation" of azides and terminal alkynes. *Angew. Chem., Int. Edit.* **2002,** *41* (14), 2596-+.
68. Tornoe, C. W.; Christensen, C.; Meldal, M., Peptidotriazoles on solid phase: 1,2,3 - triazoles by regiospecific copper(I)-catalyzed 1,3-dipolar cycloadditions of terminal alkynes to azides. *J. Org. Chem.* **2002,** *67* (9), 3057-3064.
69. Kohn, M.; Breinbauer, R., The Staudinger ligation - A gift to chemical biology'. *Angew. Chem., Int. Edit.* **2004,** *43* (24), 3106-3116.
70. Nilsson, B. L.; Kiessling, L. L.; Raines, R. T., Staudinger ligation: A peptide from a thioester and azide. *Org. Lett.* **2000,** *2* (13), 1939-1941.
71. Saxon, E.; Armstrong, J. I.; Bertozzi, C. R., A "traceless" Staudinger ligation for the chemoselective synthesis of amide bonds. *Org. Lett.* **2000,** *2* (14), 2141-2143.
72. van Berkel, S. S.; van Eldijk, M. B.; van Hest, J. C. M., Staudinger Ligation as a Method for Bioconjugation. *Angew. Chem., Int. Edit.* **2011,** *50* (38), 8806-8827.

73. Saxon, E.; Bertozzi, C. R., Cell surface engineering by a modified Staudinger reaction. *Science* **2000,** *287* (5460), 2007-2010.
74. Chang, P. V.; Chen, X.; Smyrniotis, C.; Xenakis, A.; Hu, T. S.; Bertozzi, C. R.; Wu, P., Metabolic Labeling of Sialic Acids in Living Animals with Alkynyl Sugars. *Angew. Chem. Int. Edit.* **2009,** *48* (22), 4030-4033.
75. Laughlin, S. T.; Bertozzi, C. R., Metabolic labeling of glycans with azido sugars and subsequent glycan-profiling and visualization via Staudinger ligation. *Nat. Protocols* **2007,** *2* (11), 2930-2944.
76. Tiwari, V. K.; Mishra, B. B.; Mishra, K. B.; Mishra, N.; Singh, A. S.; Chen, X., Cu-Catalyzed Click Reaction in Carbohydrate Chemistry. *Chem. Rev.* **2016,** *116* (5), 3086-3240.
77. El-Sagheer, A. H.; Brown, T., Click chemistry with DNA. *Chem. Soc. Rev.* **2010,** *39* (4), 1388-1405.
78. Gierlich, J.; Burley, G. A.; Gramlich, P. M. E.; Hammond, D. M.; Carell, T., Click chemistry as a reliable method for the high-density postsynthetic functionalization of alkyne-modified DNA. *Org. Lett.* **2006,** *8* (17), 3639-3642.
79. Gramlich, P. M. E.; Wirges, C. T.; Manetto, A.; Carell, T., Postsynthetic DNA Modification through the Copper-Catalyzed Azide-Alkyne Cycloaddition Reaction. *Angew. Chem., Int. Edit.* **2008,** *47* (44), 8350-8358.
80. Seo, T. S.; Li, Z. M.; Ruparel, H.; Ju, J. Y., Click chemistry to construct fluorescent oligonucleotides for DNA sequencing. *J. Org. Chem.* **2003,** *68* (2), 609-612.
81. Johnson, J. A.; Lu, Y. Y.; Van Deventer, J. A.; Tirrell, D. A., Residue-specific incorporation of non-canonical amino acids into proteins: recent developments and applications. *Curr. Opin. Chem. Biol.* **2010,** *14* (6), 774-780.
82. Kiick, K. L.; Saxon, E.; Tirrell, D. A.; Bertozzi, C. R., Incorporation of azides into recombinant proteins for chemoselective modification by the Staudinger ligation. *Proc. Natl. Acad. Sci. U.S.A.* **2002,** *99* (1), 19-24.
83. Liu, C. C.; Schultz, P. G., Adding New Chemistries to the Genetic Code. In *Annu. Rev. Biochem.*, Kornberg, R. D.; Raetz, C. R. H.; Rothman, J. E.; Thorner, J. W., Eds. 2010; Vol. 79, pp 413-444.
84. Ngo, J. T.; Tirrell, D. A., Noncanonical Amino Acids in the Interrogation of Cellular Protein Synthesis. *Acc. Chem. Res.* **2011,** *44* (9), 677-685.
85. Wang, L.; Brock, A.; Herberich, B.; Schultz, P. G., Expanding the genetic code of Escherichia coli. *Science* **2001,** *292* (5516), 498-500.
86. Bumpus, T. W.; Baskin, J. M., Greasing the Wheels of Lipid Biology with Chemical Tools. *Trends Biochem. Sci.* **2018,** *43* (12), 970-983.
87. Jao, C. Y.; Nedelcu, D.; Lopez, L. V.; Samarakoon, T. N.; Welti, R.; Salic, A., Bioorthogonal Probes for Imaging Sterols in Cells. *ChemBioChem* **2015,** *16* (4), 611-617.
88. Jao, C. Y.; Roth, M.; Welti, R.; Salic, A., Metabolic labeling and direct imaging of choline phospholipids in vivo. *Proc. Natl. Acad. Sci. U.S.A.* **2009,** *106* (36), 15332-15337.
89. Jewett, J. C.; Bertozzi, C. R., Cu-free click cycloaddition reactions in chemical biology. *Chem. Soc. Rev.* **2010,** *39* (4), 1272-1279.
90. Agard, N. J.; Prescher, J. A.; Bertozzi, C. R., A strain-promoted 3+2 azide-alkyne cycloaddition for covalent modification of blomolecules in living systems. *J. Am. Chem. Soc.* **2004,** *126* (46), 15046-15047.

91. Baskin, J. M.; Prescher, J. A.; Laughlin, S. T.; Agard, N. J.; Chang, P. V.; Miller, I. A.; Lo, A.; Codelli, J. A.; Bertozzi, C. R., Copper-free click chemistry for dynamic in vivo imaging. *Proc. Natl. Acad. Sci. U.S.A.* **2007,** *104* (43), 16793-16797.
92. Soriano Del Amo, D.; Wang, W.; Jiang, H.; Besanceney, C.; Yan, A. C.; Levy, M.; Liu, Y.; Marlow, F. L.; Wu, P., Biocompatible copper(I) catalysts for in vivo imaging of glycans. *J Am Chem Soc* **2010,** *132* (47), 16893-9.
93. Presolski, S. I.; Hong, V.; Cho, S. H.; Finn, M. G., Tailored ligand acceleration of the Cu-catalyzed azide-alkyne cycloaddition reaction: practical and mechanistic implications. *J Am Chem Soc* **2010,** *132* (41), 14570-6.
94. Wu, H. X.; Devaraj, N. K., Inverse Electron-Demand Diels-Alder Bioorthogonal Reactions. *Topics Curr. Chem.* **2016,** *374* (1).
95. Oliveira, B. L.; Guo, Z.; Bernardes, G. J. L., Inverse electron demand Diels-Alder reactions in chemical biology. *Chem. Soc. Rev.* **2017,** *46* (16), 4895-4950.
96. Selvaraj, R.; Fox, J. M., trans-Cyclooctene - a stable, voracious dienophile for bioorthogonal labeling. *Curr. Opin. Chem. Biol.* **2013,** *17* (5), 753-760.
97. Best, M. D.; Zhang, H. L.; Prestwich, G. D., Inositol polyphosphates, diphosphoinositol polyphosphates and phosphatidylinositol polyphosphate lipids: Structure, synthesis, and development of probes for studying biological activity. *Nat. Prod. Reports* **2010,** *27* (10), 1403-1430.
98. Vance, J., Phospholipid synthesis and transport in mammalian cells. *Traffic* **2015,** *16* (1), 1-18.
99. Henry, S. A.; Kohlwein, S. D.; Carman, G. M., Metabolism and regulation of glycerolipids in the yeast Saccharomyces cerevisiae. *Genetics* **2012,** *190* (2), 317-349.
100. Atkinson, K. D.; Jensen, B.; Kolat, A. I.; Storm, E. M.; Henry, S. A.; Fogel, S., Yeast mutants auxotrophic for choline or ethanolamine. *Journal of Bacteriology* **1980,** *141* (2), 558-564.
101. Trotter, P. J.; Pedretti, J.; Yates, R.; Voelker, D. R., Phosphatidylserine Decarboxylase 2 of Saccharomyces cerevisiáe: CLONING AND MAPPING OF THE GENE, HETEROLOGOUS EXPRESSION, AND CREATION OF THE NULL ALLELE (∗). *Journal of Biological Chemistry* **1995,** *270* (11), 6071-6080.
102. Kuerschner, L.; Thiele, C., Multiple bonds for the lipid interest. *Biochim. Biophys. Acta* **2014,** *1841* (8), 1031-1037.
103. Thiele, C.; Papan, C.; Hoelper, D.; Kusserow, K.; Gaebler, A.; Schoene, M.; Piotrowitz, K.; Lohmann, D.; Spandl, J.; Stevanovic, A.; Shevchenko, A.; Kuerschner, L., Tracing Fatty Acid Metabolism by Click Chemistry. *ACS Chem. Biol.* **2012,** *7* (12), 2004-2011.
104. Robichaud, P. P.; Poirier, S. J.; Boudreau, L. H.; Doiron, J. A.; Barnett, D. A.; Boilard, E.; Surette, M. E., On the cellular metabolism of the click chemistry probe 19-alkyne arachidonic acid. *J. Lipid Res.* **2016,** *57* (10), 1821-1830.
105. Hang, H. C.; Linder, M. E., Exploring Protein Lipidation with Chemical Biology. *Chem. Rev.* **2011,** *111* (10), 6341-6358.
106. Hang, H. C.; Wilson, J. P.; Charron, G., Bioorthogonal Chemical Reporters for Analyzing Protein Lipidation and Lipid Trafficking. *Acc. Chem. Res.* **2011,** *44* (9), 699-708.
107. Thiele, C.; Wunderling, K.; Leyendecker, P., Multiplexed and single cell tracing of lipid metabolism. *Nat. Methods* **2019,** *16* (11), 1123-1130.

108. Bieber, L. L.; Newburgh, R. W., The incorporation of dimethylaminoethanol and dimethylaminoisopropyl alcohol into Phormia regina phospholipids*. *Journal of Lipid Research* **1963,** *4* (4), 397-401.
109. Jao, C. Y.; Roth, M.; Welti, R.; Salic, A., Biosynthetic Labeling and Two-Color Imaging of Phospholipids in Cells. *ChemBioChem* **2015,** *16* (3), 472-476.
110. Fu, H. X.; Li, Y. R.; Sun, L. B.; He, P.; Duan, X. R., Ratiometric Fluorescence Azide-Alkyne Cycloaddition for Live Mammalian Cell Imaging. *Anal. Chem.* **2015,** *87* (22), 11332-11336.
111. Bumpus, T. W.; Baskin, J. M., A Chemoenzymatic Strategy for Imaging Cellular Phosphatidic Acid Synthesis. *Angew. Chem., Int. Edit.* **2016,** *55* (42), 13155-13158.
112. Bumpus, T. W.; Baskin, J. M., Clickable Substrate Mimics Enable Imaging of Phospholipase D Activity. *ACS Cent. Sci.* **2017,** *3* (10), 1070-1077.
113. Liang, D. J.; Wu, K. N.; Tei, R.; Bumpus, T. W.; Ye, J.; Baskin, J. M., A real-time, click chemistry imaging approach reveals stimulus-specific subcellular locations of phospholipase D activity. *Proc. Natl. Acad. Sci. U.S.A.* **2019,** *116* (31), 15453-15462.
114. Bumpus, T. W.; Liang, F. J.; Baskin, J. M., Ex Uno Plura: Differential Labeling of Phospholipid Biosynthetic Pathways with a Single Bioorthogonal Alcohol. *Biochemistry* **2018,** *57* (2), 226-230.
115. Lu, L. L.; Gao, J.; Guo, Z. W., Labeling Cell Surface GPIs and GPI-Anchored Proteins through Metabolic Engineering with Artificial Inositol Derivatives. *Angew. Chem., Int. Edit.* **2015,** *54* (33), 9679-9682.
116. Jaiswal, M.; Zhu, S. Y.; Jiang, W. J.; Guo, Z. W., Synthesis and evaluation of N-alpha,N-epsilon-diacetyl-l-lysine-inositol conjugates as cancer-selective probes for metabolic engineering of GPIs and GPI-anchored proteins. *Org. Biomol. Chem.* **2020,** *18* (15), 2938-2948.
117. Ricks, T. J.; Cassilly, C. D.; Carr, A. J.; Alves, D. S.; Alam, S.; Tscherch, K.; Yokley, T. W.; Workman, C. E.; Morrell-Falvey, J. L.; Barrera, F. N.; Reynolds, T. B.; Best, M. D., Labeling of Phosphatidylinositol Lipid Products in Cells through Metabolic Engineering by Using a Clickable myo-Inositol Probe. *ChemBioChem* **2019,** *20* (2), 172-180.
118. Hirata, M.; Watanabe, Y.; Ishimatsu, T.; Ikebe, T.; Kimura, Y.; Yamaguchi, K.; Ozaki, S.; Koga, T., Synthetic Inositol Trisphosphate Analogs and Their Effects on Phosphatase, Kinase, and the Release of Ca2+*. *Journal of Biological Chemistry* **1989,** *264* (34), 20303-20308.
119. Hirata, M.; Yanaga, F.; Koga, T.; Ogasawara, T.; Watanabe, Y.; Ozaki, S., Stereospecific recognition of inositol 1,4,5-trisphosphate analogs by the phosphatase, kinase, and binding proteins. *Journal of Biological Chemistry* **1990,** *265* (15), 8404-8407.
120. Ozaki, S.; Watanabe, Y.; Ogasawara, T.; Hirata, M.; Kanematsu, T., Synthesis and biological properties of 2-substituted myo-inositol 1,4,5-trisphosphate analogues directed toward affinity chromatography and photoaffinity labeling. *Carbohydrate Research* **1992,** *234*, 189-206.
121. Watanabe, Y.; Hirata, M.; Ogasawara, T.; Koga, T.; Ozaki, S., Synthesis and characterization of a photoaffinity probe possessing biotinyl and azidobenzoyl moieties for IP-3-affiniated protein. *Bioorganic & Medicinal Chemistry Letters* **1991,** *1* (8), 399-402.
122. Ausmus, A. P.; Hogue, M.; Snyder, J. L.; Rundell, S. R.; Bednarz, K. M.; Banahene, N.; Swarts, B. M., Ferrier Carbocyclization-Mediated Synthesis of Enantiopure Azido Inositol Analogues. *J. Org. Chem.* **2020,** *85* (5), 3182-3191.

123. Pasari, S.; Ismail, S. M.; Wenk, M. R.; Lear, M. J., Preparation of azide biosynthetic surrogates of myo-inositol. *Tetrahedron Letters* **2015,** *56* (20), 2597-2601.
124. Sandbhor, M. S.; Key, J. A.; Strelkov, I. S.; Cairo, C. W., A Modular Synthesis of Alkynyl-Phosphocholine Headgroups for Labeling Sphingomyelin and Phosphatidylcholine. *J. Org. Chem.* **2009,** *74* (22), 8669-8674.
125. Alecu, I.; Tedeschi, A.; Behler, N.; Wunderling, K.; Lamberz, C.; Lauterbach, M. A. R.; Gaebler, A.; Ernst, D.; Van Veldhoven, P. P.; Al-Amoudi, A.; Latz, E.; Othman, A.; Kuerschner, L.; Hornemann, T.; Bradke, F.; Thiele, C.; Penno, A., Localization of 1-deoxysphingolipids to mitochondria induces mitochondrial dysfunction. *J. Lipid Res.* **2017,** *58* (1), 42-59.
126. Dauner, M.; Batroff, E.; Bachmann, V.; Hauck, C. R.; Wittmann, V., Synthetic Glycosphingolipids for Live-Cell Labeling. *Bioconjugate Chem.* **2016,** *27* (7), 1624-1637.
127. Shen, L.; Cai, K. M.; Yu, J.; Cheng, J. J., Novel Liposomal Azido Mannosamine Lipids on Metabolic Cell Labeling and Imaging via Cu-Free Click Chemistry. *Bioconjugate Chem.* **2019,** *30* (9), 2317-2322.
128. Knittel, C. H.; Devaraj, N. K., Bioconjugation Strategies for Revealing the Roles of Lipids in Living Cells. *Acc Chem Res* **2022,** *55* (21), 3099-3109.
129. Punt, J. M.; van der Vliet, D.; van der Stelt, M., Chemical Probes to Control and Visualize Lipid Metabolism in the Brain. *Accounts of Chemical Research* **2022,** *55* (22), 3205-3217.
130. Huang, L.-L.; Nie, W.; Zhang, J.; Xie, H.-Y., Cell-Membrane-Based Biomimetic Systems with Bioorthogonal Functionalities. *Accounts of Chemical Research* **2020,** *53* (1), 276-287.
131. Huang, L.-L.; Lu, G.-H.; Hao, J.; Wang, H.; Yin, D.-L.; Xie, H.-Y., Enveloped Virus Labeling via Both Intrinsic Biosynthesis and Metabolic Incorporation of Phospholipids in Host Cells. *Analytical Chemistry* **2013,** *85* (10), 5263-5270.
132. Zhao, X.; Shen, Y.; Adogla, E. A.; Viswanath, A.; Tan, R.; Benicewicz, B. C.; Greytak, A. B.; Lin, Y.; Wang, Q., Surface labeling of enveloped virus with polymeric imidazole ligand-capped quantum dots via the metabolic incorporation of phospholipids into host cells. *Journal of Materials Chemistry B* **2016,** *4* (14), 2421-2427.
133. Luo, Z.; Loja, M.; Farwell, D. G.; Luu, Q. C.; Donald, P. J.; Amott, D.; Gandour-Edwards, R.; Nitin, N., High-Resolution Optical Molecular Imaging of Changes in Choline Metabolism in Oral Neoplasia. *Translational Oncology* **2013,** *6* (1), 33-41.
134. Luo, Z.; Samadzadeh, K. M.; Nitin, N., Rapid assessment of drug resistance of cancer cells to gefitinib and carboplatin using optical imaging. *Analytical Biochemistry* **2016,** *504*, 50-58.
135. Luo, Z.; Tikekar, R. V.; Samadzadeh, K.; Nitin, N., Optical molecular imaging approach for rapid assessment of response of individual cancer cells to chemotherapy. *Journal of Biomedical Optics* **2012,** *17* (10), 106006.
136. Lu, G.; Zuo, L.; Zhang, J.; Zhu, H.; Zhuang, W.; Wei, W.; Xie, H.-Y., Two-step tumor-targeting therapy via integrating metabolic lipid-engineering with in situ click chemistry. *Biomater. Sci.* **2020,** *8* (8), 2283-2288.
137. Xiong, K.; Wei, W.; Jin, Y.; Wang, S.; Zhao, D.; Wang, S.; Gao, X.; Qiao, C.; Yue, H.; Ma, G.; Xie, H.-Y., Biomimetic Immuno-Magnetosomes for High-Performance Enrichment of Circulating Tumor Cells. *Advanced Materials* **2016,** *28* (36), 7929-7935.
138. Rao, L.; Meng, Q.-F.; Huang, Q.; Wang, Z.; Yu, G.-T.; Li, A.; Ma, W.; Zhang, N.; Guo, S.-S.; Zhao, X.-Z.; Liu, K.; Yuan, Y.; Liu, W., Platelet–Leukocyte Hybrid Membrane-Coated

Immunomagnetic Beads for Highly Efficient and Highly Specific Isolation of Circulating Tumor Cells. *Advanced Functional Materials* **2018,** *28* (34), 1803531.
139. Zhang, F.; Wu, L.; Nie, W.; Huang, L.; Zhang, J.; Li, F.; Xie, H.-Y., Biomimetic Microfluidic System for Fast and Specific Detection of Circulating Tumor Cells. *Analytical Chemistry* **2019,** *91* (24), 15726-15731.
140. Zhang, L.; Min, W., Bioorthogonal chemical imaging of metabolic changes during epithelial-mesenchymal transition of cancer cells by stimulated Raman scattering microscopy. *J Biomed Opt* **2017,** *22* (10), 1-7.
141. Li, X.; Li, Y.; Jiang, M.; Wu, W.; He, S.; Chen, C.; Qin, Z.; Tang, B. Z.; Mak, H. Y.; Qu, J. Y., Quantitative Imaging of Lipid Synthesis and Lipolysis Dynamics in Caenorhabditis elegans by Stimulated Raman Scattering Microscopy. *Analytical Chemistry* **2019,** *91* (3), 2279-2287.
142. Iyoshi, S.; Cheng, J. L.; Tatematsu, T.; Takatori, S.; Taki, M.; Yamamoto, Y.; Salic, A.; Fujimoto, T., Asymmetrical distribution of choline phospholipids revealed by click chemistry and freeze-fracture electron microscopy. *ACS Chem. Biol.* **2014,** *9* (10), 2217-2222.
143. Ngo, J. T.; Adams, S. R.; Deerinck, T. J.; Boassa, D.; Rodriguez-Rivera, F.; Palida, S. F.; Bertozzi, C. R.; Ellisman, M. H.; Tsien, R. Y., Click-EM for imaging metabolically tagged nonprotein biomolecules. *Nature Chemical Biology* **2016,** *12* (6), 459-465.
144. Li, C.; Key, J. A.; Jia, F.; Dandapat, A.; Hur, S.; Cairo, C. W., Practical Labeling Methodology for Choline-Derived Lipids and Applications in Live Cell Fluorescence Imaging. *Photochemistry and Photobiology* **2014,** *90* (3), 686-695.
145. Merklinger, E.; Schloetel, J.-G.; Spitta, L.; Thiele, C.; Lang, T., No Evidence for Spontaneous Lipid Transfer at ER–PM Membrane Contact Sites. *The Journal of Membrane Biology* **2016,** *249* (1), 41-56.
146. Soltysik, K.; Ohsaki, Y.; Tatematsu, T.; Cheng, J.; Fujimoto, T., Nuclear lipid droplets derive from a lipoprotein precursor and regulate phosphatidylcholine synthesis. Nat Commun. 2019; 10 (1): 473.
147. Zhang, P.; Dong, B.; Zeng, E.; Wang, F.; Jiang, Y.; Li, D.; Liu, D., In Vivo Tracking of Multiple Tumor Exosomes Labeled by Phospholipid-Based Bioorthogonal Conjugation. *Analytical Chemistry* **2018,** *90* (19), 11273-11279.
148. Jiang, Y.; Wang, L.; Zhang, P.; Liu, X.; Di, H.; Yang, J.; Liu, S.-L.; Pang, D.-W.; Liu, D., Chemoenzymatic Labeling of Extracellular Vesicles for Visualizing Their Cellular Internalization in Real Time. *Analytical Chemistry* **2020,** *92* (2), 2103-2111.
149. Haberkant, P.; Holthuis, J. C. M., Fat & fabulous: Bifunctional lipids in the spotlight. *Biochimica et Biophysica Acta (BBA) - Molecular and Cell Biology of Lipids* **2014,** *1841* (8), 1022-1030.
150. Haberkant, P.; Raijmakers, R.; Wildwater, M.; Sachsenheimer, T.; Brügger, B.; Maeda, K.; Houweling, M.; Gavin, A.-C.; Schultz, C.; van Meer, G.; Heck, A. J. R.; Holthuis, J. C. M., In Vivo Profiling and Visualization of Cellular Protein–Lipid Interactions Using Bifunctional Fatty Acids. *Angew. Chem. Int. Ed.* **2013,** *52* (14), 4033-4038.
151. Haberkant, P.; Stein, F.; Höglinger, D.; Gerl, M. J.; Brügger, B.; Van Veldhoven, P. P.; Krijgsveld, J.; Gavin, A.-C.; Schultz, C., Bifunctional Sphingosine for Cell-Based Analysis of Protein-Sphingolipid Interactions. *ACS Chem. Bio.* **2016,** *11* (1), 222-230.
152. Best, M. D., Global approaches for the elucidation of phosphoinositide-binding proteins. *Chemistry and Physics of Lipids* **2014,** *182*, 19-28.

153. Best, M. D.; Rowland, M. M.; Bostic, H. E., Exploiting Bioorthogonal Chemistry to Elucidate Protein–Lipid Binding Interactions and Other Biological Roles of Phospholipids. *Accounts of Chemical Research* **2011,** *44* (9), 686-698.
154. Wang, D.; Du, S.; Cazenave-Gassiot, A.; Ge, J.; Lee, J. S.; Wenk, M. R.; Yao, S. Q., Global Mapping of Protein-Lipid Interactions by Using Modified Choline-Containing Phospholipids Metabolically Synthesized in Live Cells. *Angew. Chem. Int. Ed.* **2017,** *56* (21), 5829-5833.
155. Bumpus, T. W.; Baskin, J. M., A Chemoenzymatic Strategy for Imaging Cellular Phosphatidic Acid Synthesis. *Angew. Chem. Int. Ed.* **2016,** *55* (42), 13155-13158.
156. Liang, D. J.; Wu, K. N.; Tei, R.; Bumpus, T. W.; Ye, J.; Baskin, J. M., A real-time, click chemistry imaging approach reveals stimulus-specific subcellular locations of phospholipase D activity. *Proc. Natl. Acad. Sci., U.S.A.* **2019,** *116* (31), 15453-15462.
157. Lu, L. L.; Gao, J.; Guo, Z. W., Labeling cell surface GPIs and GPI-anchored proteins through metabolic engineering with artificial inositol derivatives. *Angew. Chem., Int. Ed.* **2015,** *54* (33), 9679-9682.
158. Jaiswal, M.; Zhu, S.; Jiang, W.; Guo, Z., Synthesis and evaluation of N(α),N(ε)-diacetyl-l-lysine-inositol conjugates as cancer-selective probes for metabolic engineering of GPIs and GPI-anchored proteins. *Org Biomol Chem* **2020,** *18* (15), 2938-2948.
159. Craig, K. C.; Guo, Z., Design and synthesis of 4-azido-phosphatidylinositol as a potential probe for metabolic engineering of glycosylphosphatidylinositol on cells. *J. Carbohydr. Chem.* **2022,** *41*, 238 - 248.
160. Stace, C. L.; Ktistakis, N. T., Phosphatidic acid- and phosphatidylserine-binding proteins. *Biochim. Biophys. Acta* **2006,** *1761* (8), 913-926.
161. van Genderen, H. O.; Kenis, H.; Hofstra, L.; Narula, J.; Reutelingsperger, C. P. M., Extracellular annexin A5: Functions of phosphatidylserine-binding and two-dimensional crystallization. *Biochim. Biophys. Acta* **2008,** *1783* (6), 953-963.
162. Andree, H. A. M.; Stuart, M. C. A.; Hermens, W. T.; Reutelingsperger, C. P. M.; Hemker, H. C.; Frederik, P. M.; Willems, G. M., Clustering of Lipid-Bound Annexin-V May Explain Its Anticoagulant Effect. *J. Biol. Chem.* **1992,** *267* (25), 17907-17912.
163. Cederholm, A.; Frostegard, J., Annexin A5 as a novel player in prevention of atherothrombosis in SLE and in the general population. In *Autoimmunity, Pt D*, 2007; Vol. 1108, pp 96-103.
164. Rand, J. H.; Wu, X. X.; Quinn, A. S.; Chen, P. J. P.; McCrae, K. R.; Bovill, E. G.; Taatjes, D. J., Human monoclonal antiphospholipid antibodies disrupt the annexin A5 anticoagulant crystal shield on phospholipid bilayers - Evidence from atomic force microscopy and functional assay. *Am. J. Pathol.* **2003,** *163* (3), 1193-1200.
165. Cederholm, A.; Sul, J.; von Landenberg, P.; Frostegard, J., Annexin A5 in cardiovascular disease and antiphospholipid syndrome: A novel mechanism. *Clin. Exp. Rheumatol.* **2007,** *25* (2), 143-143.
166. Hanshaw, R. G.; Smith, B. D., New reagents for phosphatidylserine recognition and detection of apoptosis. *Bioorg. Med. Chem.* **2005,** *13* (17), 5035-5042.
167. Balasubramanian, K.; Schroit, A. J., Aminophospholipid asymmetry: A matter of life and death. *Annu. Rev. Physiol.* **2003,** *65*, 701-734.

168. Yeung, T.; Gilbert, G. E.; Shi, J.; Silvius, J.; Kapus, A.; Grinstein, S., Membrane phosphatidylserine regulates surface charge and protein localization. *Science* **2008,** *319* (5860), 210-213.
169. Zwaal, R. F. A.; Comfurius, P.; Bevers, E. M., Surface exposure of phosphatidylserine in pathological cells. *Cell. Mol. Life Sci.* **2005,** *62* (9), 971-988.
170. Vermes, I.; Haanen, C.; Steffens-Nakken, H.; Reutellingsperger, C., A novel assay for apoptosis Flow cytometric detection of phosphatidylserine expression on early apoptotic cells using fluorescein labelled Annexin V. *Journal of Immunological Methods* **1995,** *184* (1), 39-51.
171. Birge, R. B.; Boeltz, S.; Kumar, S.; Carlson, J.; Wanderley, J.; Calianese, D.; Barcinski, M.; Brekken, R. A.; Huang, X.; Hutchins, J. T.; Freimark, B.; Empig, C.; Mercer, J.; Schroit, A. J.; Schett, G.; Herrmann, M., Phosphatidylserine is a global immunosuppressive signal in efferocytosis, infectious disease, and cancer. *Cell Death & Differentiation* **2016,** *23* (6), 962-978.
172. Ran, S.; Downes, A.; Thorpe, P. E., Increased exposure of anionic phospholipids on the surface of tumor blood vessels. *Cancer Res.* **2002,** *62* (21), 6132-6140.
173. Cheng, X.; Li, L.; Thorpe, P. E.; Yopp, A. C.; Brekken, R. A.; Huang, X., Antibody-Mediated Blockade of Phosphatidylserine Enhances the Antitumor Effect of Sorafenib in Hepatocellular Carcinomas Xenografts. *Annals of Surgical Oncology* **2016,** *23* (5), 583-591.
174. De, M.; Ghosh, S.; Sen, T.; Shadab, M.; Banerjee, I.; Basu, S.; Ali, N., A Novel Therapeutic Strategy for Cancer Using Phosphatidylserine Targeting Stearylamine-Bearing Cationic Liposomes. *Molecular Therapy - Nucleic Acids* **2018,** *10*, 9-27.
175. N'Guessan, K. F.; Patel, P. H.; Qi, X., SapC-DOPS – a Phosphatidylserine-targeted Nanovesicle for selective Cancer therapy. *Cell Communication and Signaling* **2020,** *18* (1), 6.
176. Alam, S. Development of New Methods for Liposomal Drug Delivery and the Labeling of Cellular Lipids. Dissertation, University of Tennessee, Knoxville, 2016.
177. Chang, W.; Fa, H.; Xiao, D.; Wang, J., Targeting phosphatidylserine for Cancer therapy: prospects and challenges. *Theranostics* **2020,** *10* (20), 9214-9229.
178. Chen, Y. L.; Montedonico, A. E.; Kauffman, S.; Dunlap, J. R.; Menn, F. M.; Reynolds, T. B., Phosphatidylserine synthase and phosphatidylserine decarboxylase are essential for cell wall integrity and virulence in Candida albicans. *Mol. Microbiol.* **2010,** *75* (5), 1112-32.
179. Cassilly, C. D.; Reynolds, T. B., PS, It's Complicated: The Roles of Phosphatidylserine and Phosphatidylethanolamine in the Pathogenesis of Candida albicans and Other Microbial Pathogens. *J Fungi (Basel)* **2018,** *4* (1).
180. Fairn, G. D.; Hermansson, M.; Somerharju, P.; Grinstein, S., Phosphatidylserine is polarized and required for proper Cdc42 localization and for development of cell polarity. *Nat. Cell Biol.* **2011,** *13* (12), 1424-1430.
181. Billcliff, P. G.; Lowe, M., Inositol lipid phosphatases in membrane trafficking and human disease. *Biochem. J.* **2014,** *461*, 159-175.
182. Vance, J. E.; Tasseva, G., Formation and function of phosphatidylserine and phosphatidylethanolamine in mammalian cells. *Biochim. Biophys. Acta* **2013,** *1831* (3), 543-554.
183. Tatsuta, T.; Scharwey, M.; Langer, T., Mitochondrial lipid trafficking. *Trends Cell Biol.* **2014,** *24* (1), 44-52.
184. Balla, T., Phosphoinositides: Tiny lipids with giant impact on cell regulation. *Physiol. Rev.* **2013,** *93* (3), 1019-1137.

185. Di Paolo, G.; De Camilli, P., Phosphoinositides in cell regulation and membrane dynamics. *Nature* **2006,** *443* (7112), 651-657.
186. Frasch, S. C.; Bratton, D. L., Emerging roles for lysophosphatidylserine in resolution of inflammation. *Prog. Lipid Res.* **2012,** *51* (3), 199-207.
187. Eisenberg, T.; Buttner, S., Lipids and cell death in yeast. *FEMS Yeast Res.* **2014,** *14* (1), 179-197.
188. Alam, S. Development of New Methods for Liposomal Drug Delivery and the Labeling of Cellular Lipids. Dissertation, University of Tennessee, Knoxville, 2016.
189. Cassilly, C. D.; Farmer, A. T.; Montedonico, A. E.; Smith, T. K.; Campagna, S. R.; Reynolds, T. B., Role of phosphatidylserine synthase in shaping the phospholipidome of Candida albicans. *FEMS Yeast Res.* **2017,** *17* (2), 1-8.
190. Hans, M. A.; Heinzle, E.; Wittmann, C., Free intracellular amino acid pools during autonomous oscillations in Saccharomyces cerevisiae. *Biotechnol. Bioeng.* **2003,** *82* (2), 143-51.
191. Zinser, E.; Sperka-Gottlieb, C. D.; Fasch, E. V.; Kohlwein, S. D.; Paltauf, F.; Daum, G., Phospholipid synthesis and lipid composition of subcellular membranes in the unicellular eukaryote Saccharomyces cerevisiae. *J Bacteriol* **1991,** *173* (6), 2026-34.
192. Tuller, G.; Nemec, T.; Hrastnik, C.; Daum, G., Lipid composition of subcellular membranes of an FY1679-derived haploid yeast wild-type strain grown on different carbon sources. *Yeast* **1999,** *15* (14), 1555-64.
193. Klug, L.; Daum, G., Yeast lipid metabolism at a glance. *FEMS Yeast Research* **2014,** *14* (3), 369-388.
194. Kim, D.; Stoldt, S.; Weber, M.; Jakobs, S.; Belov, V. N.; Hell, S. W., A Bright Surprise: Live-Cell Labeling with Negatively Charged Fluorescent Probes based on Disulfonated Rhodamines and HaloTag. *Chemistry–Methods* **2023,** *n/a* (n/a), e202200076.
195. Zhou, Y.; Cassilly, C. D.; Reynolds, T. B., Mapping the Substrate-Binding Sites in the Phosphatidylserine Synthase in Candida albicans. *Front. Cell. Infect. Microbiol.* **2021,** *11* (1281), 1-17.
196. Bligh, E. G.; Dyer, W. J., A rapid method of total lipid extraction and purification. *Can. J. Biochem. Physiol.* **1959,** *37* (8), 911-7.
197. Cottrell, S. F.; Getz, G. S.; Rabinowitz, M., Phospholipid accumulation during the cell cycle in synchronous cultures of the yeast, Saccharomyces cerevisiae. *J. Biol. Chem.* **1981,** *256* (21), 10973-10978.
198. Liang, D.; Wu, K.; Tei, R.; Bumpus, T. W.; Ye, J.; Baskin, J. M., A real-time, click chemistry imaging approach reveals stimulus-specific subcellular locations of phospholipase D activity. *Proc Natl Acad Sci U.S.A* **2019,** *116* (31), 15453.
199. Bae-Lee, M.; Carman, G., Regulation of yeast phosphatidylserine synthase and phosphatidylinositol synthase activities by phospholipids in Triton X-100/phospholipid mixed micelles. *Journal of Biological Chemistry* **1990,** *265* (13), 7221-7226.
200. Carman, G. M.; Han, G. S., Regulation of phospholipid synthesis in yeast. *J Lipid Res* **2009,** *50 Suppl* (Suppl), S69-73.
201. Oshiro, J.; Rangaswamy, S.; Chen, X.; Han, G.-S.; Quinn, J. E.; Carman, G. M., Regulation of the DPP1-encoded Diacylglycerol Pyrophosphate (DGPP) Phosphatase by Inositol and Growth Phase. *The Journal of Biological Chemistry* **2000,** *275*, 40887 - 40896.

202. Nadler, A.; Yushchenko, D. A.; Müller, R.; Stein, F.; Feng, S.; Mulle, C.; Carta, M.; Schultz, C., Exclusive photorelease of signalling lipids at the plasma membrane. *Nature Communications* **2015,** *6* (1), 10056.
203. Girik, V.; Feng, S.; Hariri, H.; Henne, W. M.; Riezman, H., Vacuole-Specific Lipid Release for Tracking Intracellular Lipid Metabolism and Transport in Saccharomyces cerevisiae. *ACS Chem. Bio.* **2022,** *17* (6), 1485-1494.
204. Feng, S.; Harayama, T.; Chang, D.; Hannich, J. T.; Winssinger, N.; Riezman, H., Lysosome-targeted photoactivation reveals local sphingosine metabolism signatures. *Chemical Science* **2019,** *10* (8), 2253-2258.
205. Qiao, L.; Shao, X.; Gao, S.; Ming, Z.; Fu, X.; Wei, Q., Research on endoplasmic reticulum-targeting fluorescent probes and endoplasmic reticulum stress-mediated nanoanticancer strategies: A review. *Colloids Surf B Biointerfaces* **2021,** *208*, 112046.
206. Ast, S.; Rutledge, P. J.; Todd, M. H., Reversing the Triazole Topology in a Cyclam-Triazole-Dye Ligand Gives a 10-Fold Brighter Signal Response to Zn2+ in Aqueous Solution. *Eur. J. Inorg. Chem.* **2012,** (34), 5611-5615.
207. Ancajas, C. F.; Ricks, T. J.; Best, M. D., Metabolic labeling of glycerophospholipids via clickable analogs derivatized at the lipid headgroup. *Chem. Phys. Lipids* **2020,** *232*, 104971.
208. Ancajas, C. F.; Alam, S.; Alves, D. S.; Zhou, Y.; Wadsworth, N. M.; Cassilly, C. D.; Ricks, T. J.; Carr, A. J.; Reynolds, T. B.; Barrera, F. N.; Best, M. D., Cellular Labeling of Phosphatidylserine Using Clickable Serine Probes. *ACS Chem. Bio.* **2023**.
209. Lu, L.; Gao, J.; Guo, Z., Labeling Cell Surface GPIs and GPI-Anchored Proteins through Metabolic Engineering with Artificial Inositol Derivatives. *Angew. Chem. Int. Ed.* **2015,** *54* (33), 9679-9682.
210. Gallion, L. A.; Wang, Y.; Massaro, A.; Yao, M.; Petersen, B. V.; Zhang, Q.; Huang, W.; Carr, A. J.; Zhang, Q.; Allbritton, N. L., "Fix and Click" for Assay of Sphingolipid Signaling in Single Primary Human Intestinal Epithelial Cells. *J. Anal. Chem.* **2022,** *94* (3), 1594-1600.
211. Dieterich, D. C.; Lee, J. J.; Link, A. J.; Graumann, J.; Tirrell, D. A.; Schuman, E. M., Labeling, detection and identification of newly synthesized proteomes with bioorthogonal non-canonical amino-acid tagging. *Nat Protoc* **2007,** *2* (3), 532-40.
212. Thiele, C.; Papan, C.; Hoelper, D.; Kusserow, K.; Gaebler, A.; Schoene, M.; Piotrowitz, K.; Lohmann, D.; Spandl, J.; Stevanovic, A.; Shevchenko, A.; Kuerschner, L., Tracing Fatty Acid Metabolism by Click Chemistry. *ACS Chem. Bio.* **2012,** *7* (12), 2004-2011.
213. Ticho, A. L.; Malhotra, P.; Manzella, C. R.; Dudeja, P. K.; Saksena, S.; Gill, R. K.; Alrefai, W. A., S-acylation modulates the function of the apical sodium-dependent bile acid transporter in human cells. *J.Biol.Chem.* **2020,** *295* (14), 4488-4497.
214. Toya, Y.; Ohashi, S.; Shimizu, H., Optimal 13C-labeling of glycerol carbon source for precise flux estimation in Escherichia coli. *J. Biosci. Bioeng.* **2018,** *125* (3), 301-305.
215. Yuzawa, T.; Shirai, T.; Orishimo, R.; Kawai, K.; Kondo, A.; Hirasawa, T., (13)C-metabolic flux analysis in glycerol-assimilating strains of Saccharomyces cerevisiae. *J. Appl. Microbiol.* **2021,** *67* (4), 142-149.
216. Smith, M. D.; Gong, D.; Sudhahar, C. G.; Reno, J. C.; Stahelin, R. V.; Best, M. D., Synthesis and Convenient Functionalization of Azide-Labeled Diacylglycerol Analogues for Modular Access to Biologically Active Lipid Probes. *Bioconjug. Chem.* **2008,** *19* (9), 1855-1863.

217. Smith, M. D.; Sudhahar, C. G.; Gong, D.; Stahelin, R. V.; Best, M. D., Modular synthesis of biologically active phosphatidic acid probes using click chemistry. *Mol. BioSyst.* **2009,** *5* (9), 962-972.
218. Heier, C.; Taschler, U.; Rengachari, S.; Oberer, M.; Wolinski, H.; Natter, K.; Kohlwein, S. D.; Leber, R.; Zimmermann, R., Identification of Yju3p as functional orthologue of mammalian monoglyceride lipase in the yeast Saccharomycescerevisiae. *Biochim. Biophys. Acta.* **2010,** *1801* (9), 1063-71.
219. Selvaraju, K.; Gowsalya, R.; Vijayakumar, R.; Nachiappan, V., MGL2/YMR210w encodes a monoacylglycerol lipase in Saccharomyces cerevisiae. *FEBS Lett.* **2016,** *590* (8), 1174-86.
220. Ancajas, C.; Carr, A. J.; Lou, J.; Sagar, R.; Zhou, Y.; Reynolds, T.; Best, M. D., Harnessing Clickable Acylated Glycerol Probes as Chemical Tools for Tracking Glycerolipid Metabolism. *Chemistry – A European Journal n/a* (n/a), e202300417.
221. Carr, A. Synthesis and Application of Biomimetic Probes for Investigating Protein-Lipid Interactions and Lipid Metabolism. Dissertation, University of Tennessee, Knoxville, 2018.
222. Singh, P., Budding Yeast: An Ideal Backdrop for In vivo Lipid Biochemistry. *Front. Cell Dev. Biol.* **2016,** *4*, 156.
223. Santos, A. X. S.; Riezman, H., Yeast as a model system for studying lipid homeostasis and function. *FEBS Lett.* **2012,** *586* (18), 2858-2867.
224. Crans, D. C.; Whitesides, G. M., Glycerol kinase: substrate specificity. *J. Am. Chem. Soc.* **1985,** *107* (24), 7008-7018.
225. Carmona-Gutierrez, D.; Eisenberg, T.; Büttner, S.; Meisinger, C.; Kroemer, G.; Madeo, F., Apoptosis in yeast: triggers, pathways, subroutines. *Cell Death Differ.* **2010,** *17* (5), 763-773.
226. Strandberg, K. L.; Peterson, M. L.; Lin, Y. C.; Pack, M. C.; Chase, D. J.; Schlievert, P. M., Glycerol monolaurate inhibits Candida and Gardnerella vaginalis in vitro and in vivo but not Lactobacillus. *Antimicrob. Agents Chemother.* **2010,** *54* (2), 597-601.
227. Clitherow, K. H.; Binaljadm, T. M.; Hansen, J.; Spain, S. G.; Hatton, P. V.; Murdoch, C., Medium-Chain Fatty Acids Released from Polymeric Electrospun Patches Inhibit Candida albicans Growth and Reduce the Biofilm Viability. *ACS Biomater. Sci. Eng.* **2020,** *6* (7), 4087-4095.
228. Schnitzer-Polokoff, R.; Tove, S. B., Toxicity of rac-1(3)-palmitoyl glycerol in weanling mice. *J Nutr* **1979,** *109* (8), 1358-67.
229. Trumbo, P. R.; Meuten, D. J.; King, M. W.; Tove, S. B., Toxicity of palmitoyl glycerol to mice: depression of thyroid function. *J Nutr* **1987,** *117* (10), 1780-7.
230. Santa, T.; Al-Dirbashi, O. Y.; Fukushima, T., Derivatization reagents in liquid chromatography/electrospray ionization tandem mass spectrometry for biomedical analysis. *Drug Discov. Ther.* **2007,** *1* (2), 108-18.
231. Hanson, B. A.; Lester, R. L., The extraction of inositol-containing phospholipids and phosphatidylcholine from Saccharomyces cerevisiae and Neurospora crassa. *J. Lipid. Res.* **1980,** *21* (3), 309-15.
232. Citir, M.; Müller, R.; Hauke, S.; Traynor-Kaplan, A.; Schultz, C., Monitoring the cellular metabolism of a membrane-permeant photo-caged phosphatidylinositol 3,4,5-trisphosphate derivative. *Chemistry and Physics of Lipids* **2021,** *241*, 105124.

233. Bartsch, M.; Zorn-Kruppa, M.; Kühl, N.; Genieser, H.-G.; Schwede, F.; Jastorff, B., Bioactivatable, Membrane-Permeant Analogs of Cyclic Nucleotides as Biological Tools for Growth Control of C6 Glioma Cells. **2003,** *384* (9), 1321-1326.
234. Schultz, C., Prodrugs of biologically active phosphate esters. *Bioorganic & Medicinal Chemistry* **2003,** *11* (6), 885-898.
235. Rostron, K. A.; Rolph, C. E.; Lawrence, C. L., Nile red fluorescence screening facilitating neutral lipid phenotype determination in budding yeast, Saccharomyces cerevisiae, and the fission yeast Schizosaccharomyces pombe. *Antonie van Leeuwenhoek* **2015,** *108* (1), 97-106.
236. Grillitsch, K.; Connerth, M.; Köfeler, H.; Arrey, T. N.; Rietschel, B.; Wagner, B.; Karas, M.; Daum, G., Lipid particles/droplets of the yeast Saccharomyces cerevisiae revisited: lipidome meets proteome. *Biochim Biophys Acta* **2011,** *1811* (12), 1165-76.
237. Cabral, M. G.; Viegas, C. A.; Sá-Correia, I., Mechanisms underlying the acquisition of resistance to octanoic-acid-induced-death following exposure of Saccharomyces cerevisiae to mild stress imposed by octanoic acid or ethanol. *Arch. Microbiol.* **2001,** *175* (4), 301-307.
238. Xu, G.; Waki, H.; Kon, K.; Ando, S., Thin-Layer Chromatography of Phospholipids and Their Lyso Forms: Application to Determination of Extracts from Rat Hippocampal CA1 Region. *Microchem. J.* **1996,** *53* (1), 29-33.
239. Woodall, B. M.; Harp, J. R.; Brewer, W. T.; Tague, E. D.; Campagna, S. R.; Fozo, E. M., Enterococcus faecalis Readily Adapts Membrane Phospholipid Composition to Environmental and Genetic Perturbation. *Front. Microbiol.* **2021,** *12*, 616045.
240. Subramanian, D.; Laketa, V.; Müller, R.; Tischer, C.; Zarbakhsh, S.; Pepperkok, R.; Schultz, C., Activation of membrane-permeant caged PtdIns(3)P induces endosomal fusion in cells. *Nat Chem Biol* **2010,** *6* (5), 324-6.
241. Mentel, M.; Laketa, V.; Subramanian, D.; Gillandt, H.; Schultz, C., Photoactivatable and Cell-Membrane-Permeable Phosphatidylinositol 3,4,5-Trisphosphate. *Angewandte Chemie International Edition* **2011,** *50* (16), 3811-3814.
242. Dinkel, C.; Wichmann, O.; Schultz, C., Versatile reagents to introduce caged phosphates. *Tetrahedron Letters* **2003,** *44* (6), 1153-1155.
243. Höglinger, D.; Nadler, A.; Schultz, C., Caged lipids as tools for investigating cellular signaling. *Biochimica et Biophysica Acta (BBA) - Molecular and Cell Biology of Lipids* **2014,** *1841* (8), 1085-1096.
244. Neef, A. B.; Schultz, C., Selective Fluorescence Labeling of Lipids in Living Cells. *Angew Chem Int Ed Engl* **2009,** *48* (8), 1498-1500.
245. Höglinger, D.; Nadler, A.; Haberkant, P.; Kirkpatrick, J.; Schifferer, M.; Stein, F.; Hauke, S.; Porter, F. D.; Schultz, C., Trifunctional lipid probes for comprehensive studies of single lipid species in living cells. *Proc. Natl. Acad. Sci. U.S.A.* **2017,** *114* (7), 1566-1571.
246. Lefebvre, I.; Perigaud, C.; Pompon, A.; Aubertin, A.-M.; Girardet, J.-L.; Kirn, A.; Gosselin, G.; Imbach, J.-L., Mononucleoside Phosphotriester Derivatives with S-Acyl-2-thioethyl Bioreversible Phosphate-Protecting Groups: Intracellular Delivery of 3'-Azido-2',3'-dideoxythymidine 5'-Monophosphate. *Journal of Medicinal Chemistry* **1995,** *38* (20), 3941-3950.
247. Zhou, Y.; Syed, J. H.; Semchonok, D. A.; Wright, E.; Kyrilis, F. L.; Hamdi, F.; Kastritis, P. L.; Bruce, B. D.; Reynolds, T. B., Solubilization, purification, and characterization of the hexameric form of phosphatidylserine synthase from Candida albicans. *Journal of Biological Chemistry* **2023**, 104756.

248. Cravatt, B. F.; Wright, A. T.; Kozarich, J. W., Activity-based protein profiling: from enzyme chemistry to proteomic chemistry. *Annu Rev Biochem* **2008,** *77*, 383-414.
249. Wright, M. H.; Sieber, S. A., Chemical proteomics approaches for identifying the cellular targets of natural products. *Natural Product Reports* **2016,** *33* (5), 681-708.
250. Ricks, T. J. Design and synthesis of analogs of myo-inositol, serine, and cysteine to enable chemical biology studies. Dissertation, University of Tennessee, Knoxville, 2017.
251. Fiore, M.; Lo Conte, M.; Pacifico, S.; Marra, A.; Dondoni, A., Synthesis of S-glycosyl amino acids and S-glycopeptides via photoinduced click thiol–ene coupling. *Tetrahedron Letters* **2011,** *52*, 444-447.

Appendix

NMR and Mass spectra

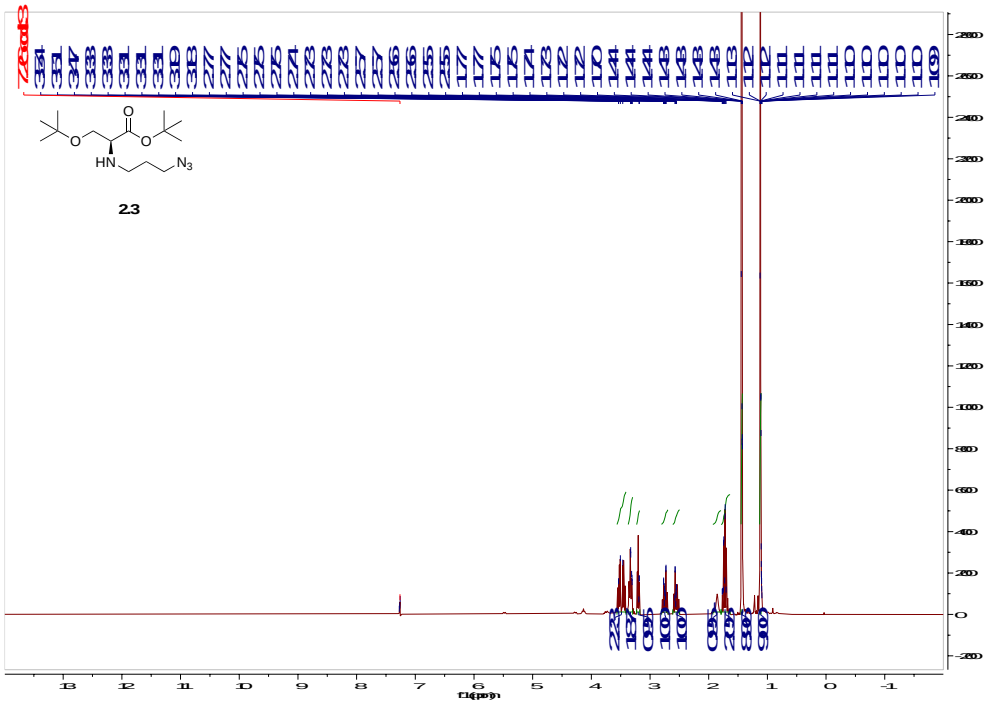

Spectrum A1. ^{1}H NMR of compound 2.3.

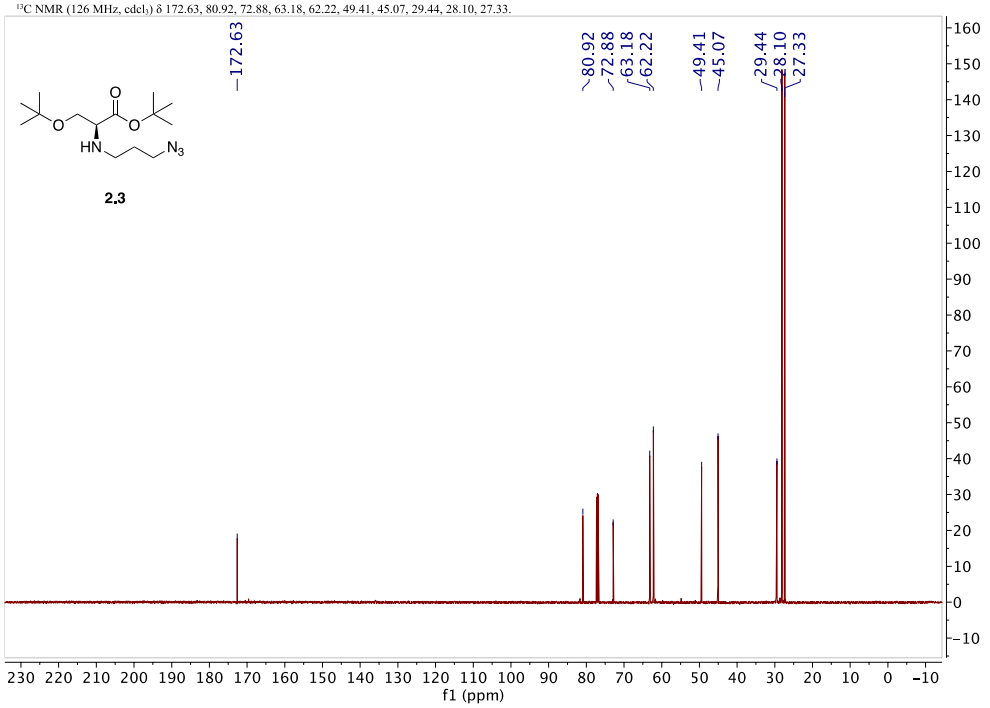

Spectrum A2. ^{13}C NMR of compound 2.3.

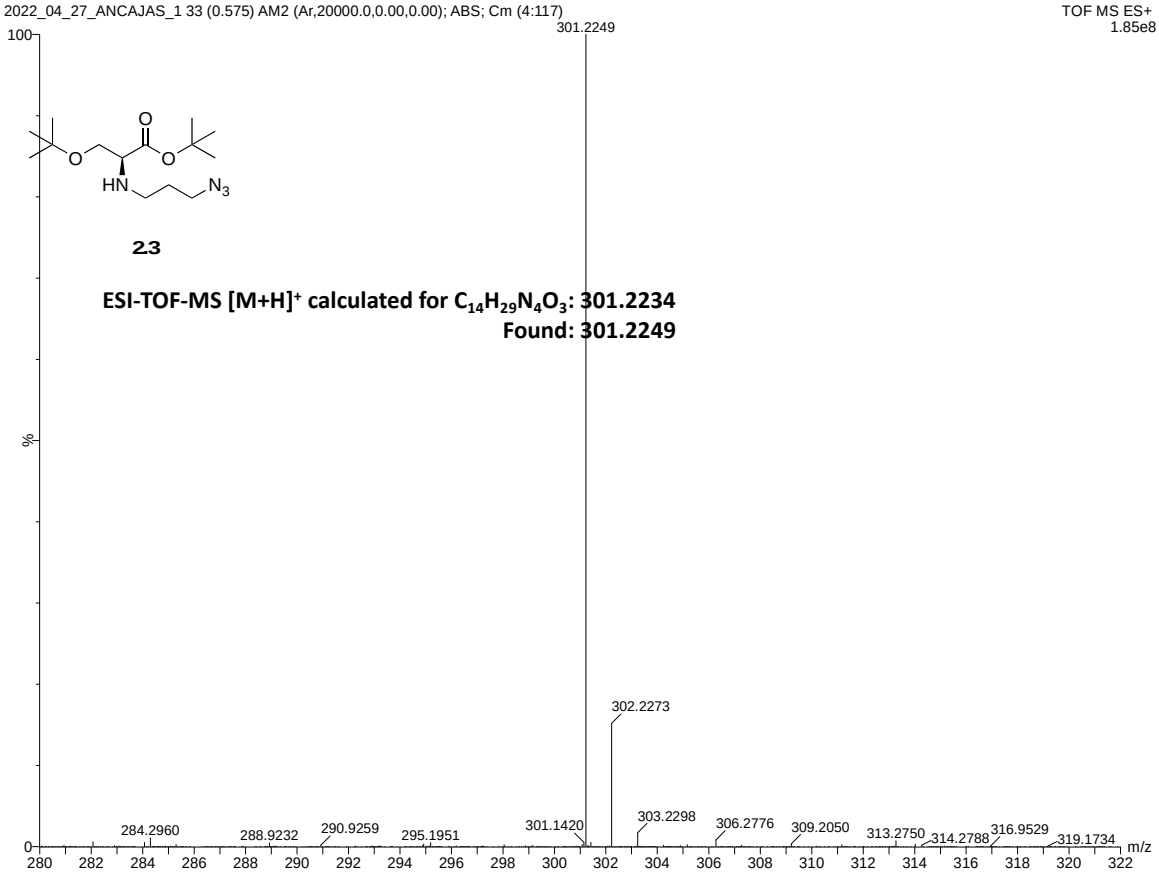

Spectrum A3. ESI-TOF-MS of compound 2.3.

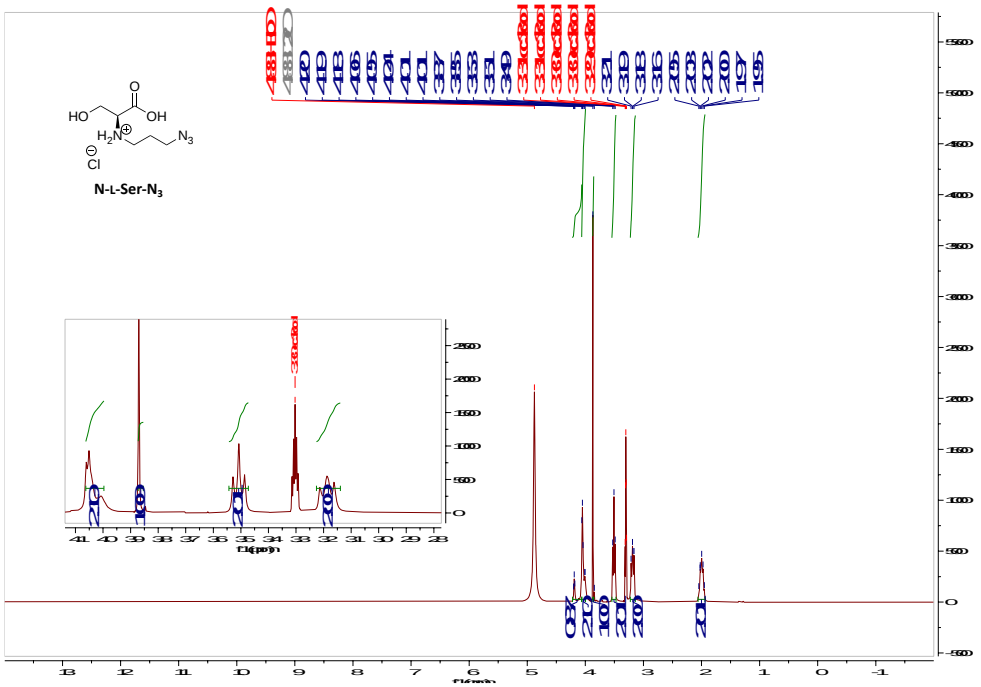

Spectrum A4. ^{1}H NMR of compound N-L-Ser-N$_3$.

^{13}C NMR (126 MHz, cdcl$_3$) δ 171.53, 65.21, 62.00, 56.42, 47.84, 29.21.

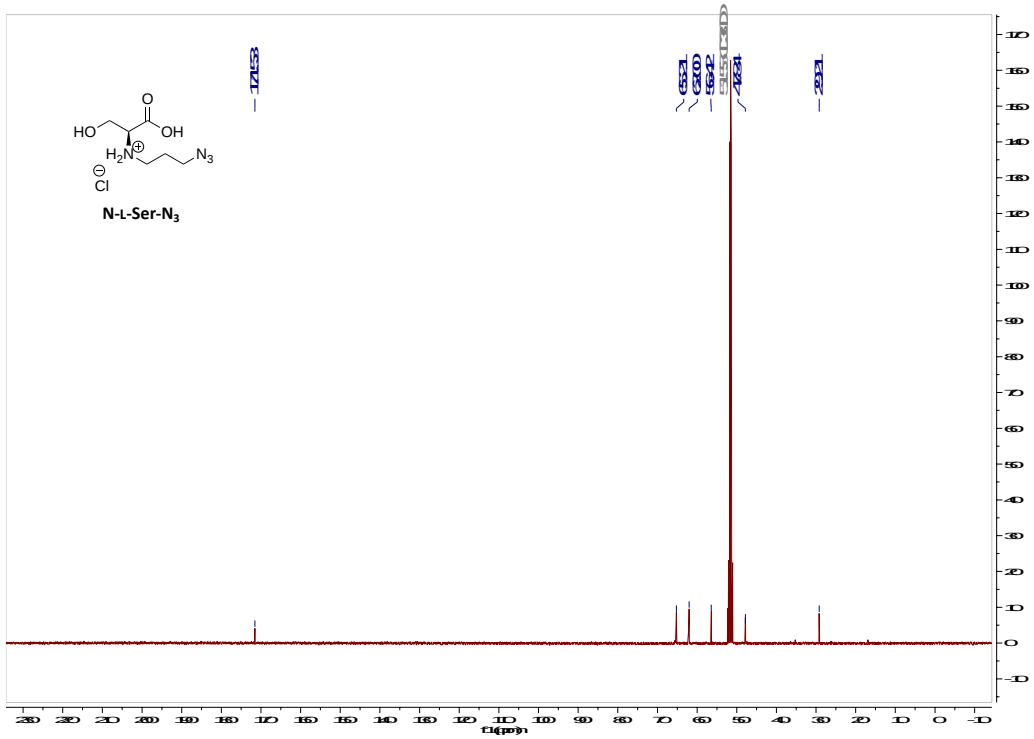

Spectrum A5. ^{13}C NMR of compound N-L-Ser-N$_3$.

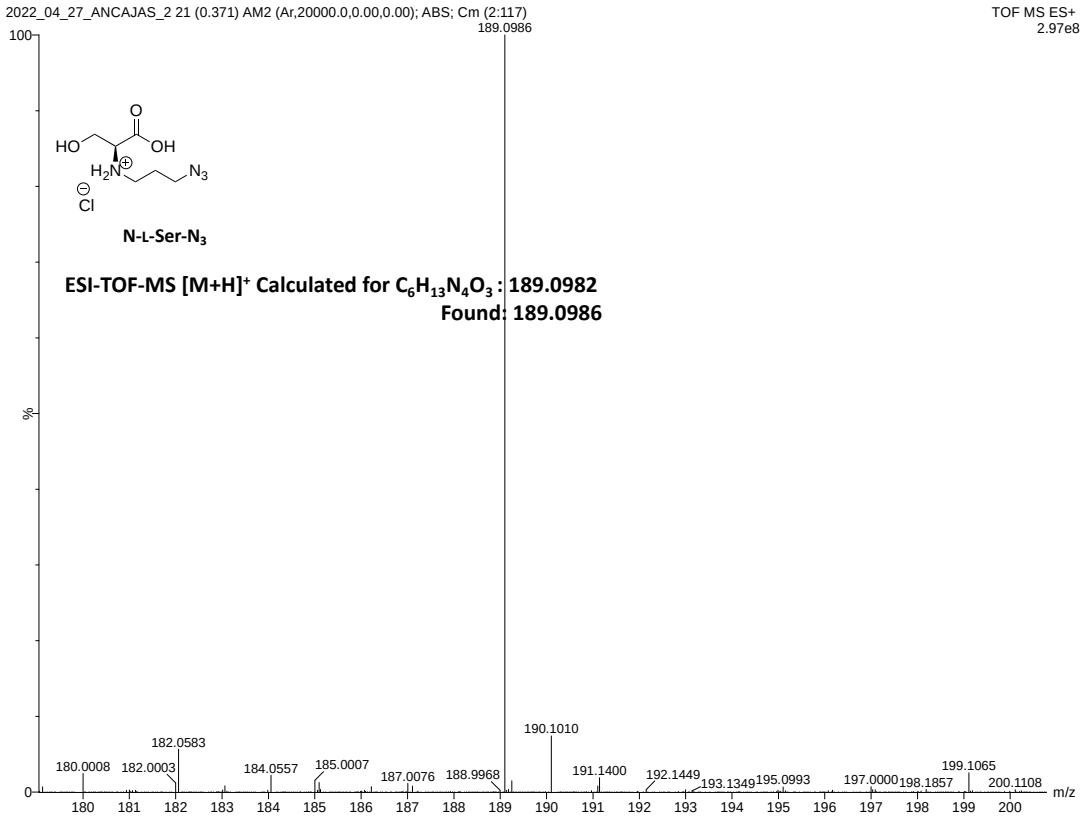

Spectrum A6. ESI-TOF-MS of compound N-L-Ser-N_3.

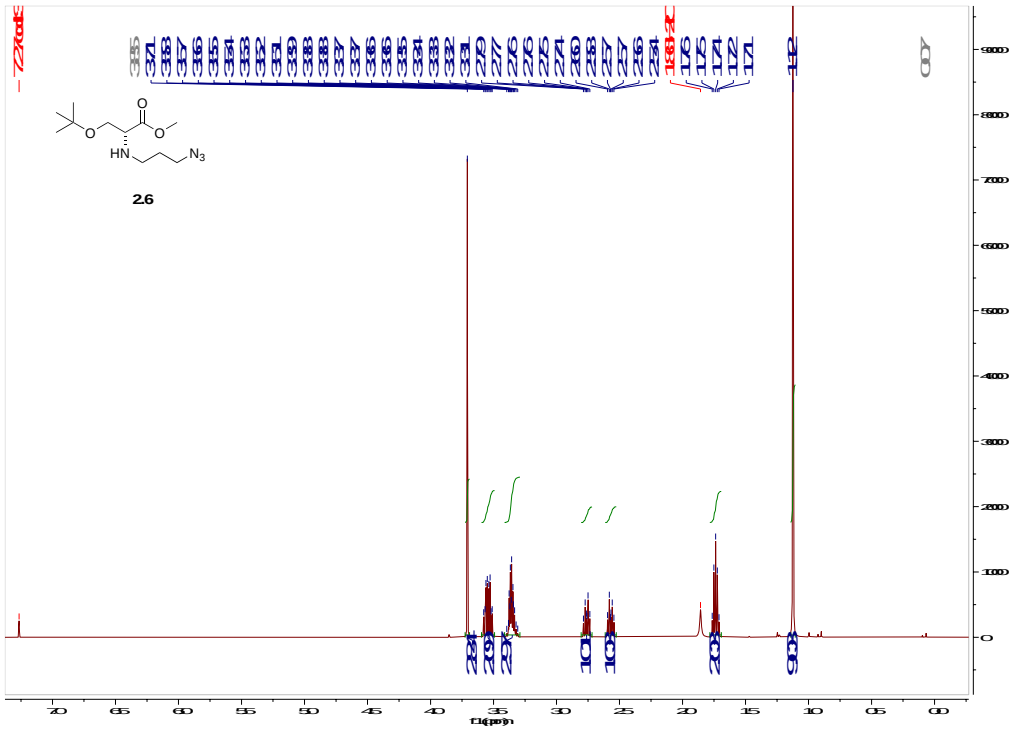

Spectrum A7. ^{1}H NMR of compound 2.6.

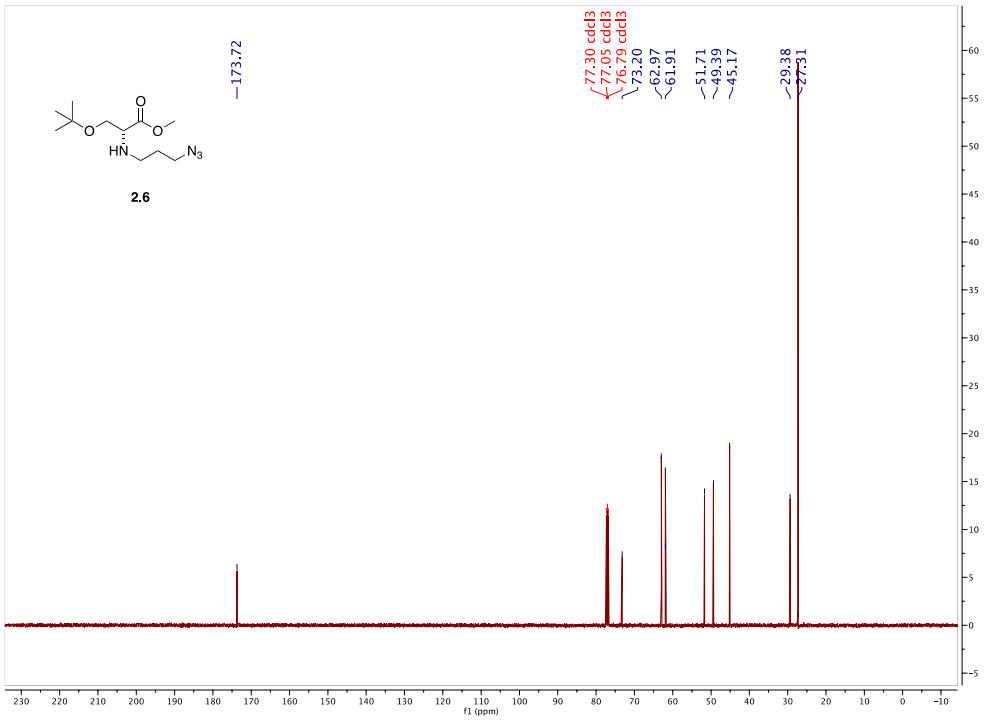

Spectrum A8. ^{13}C NMR of compound 2.6.

MS[1];0.676; / ESI+ / 220426_BEST_CAFA_tbuOMeNDserN3

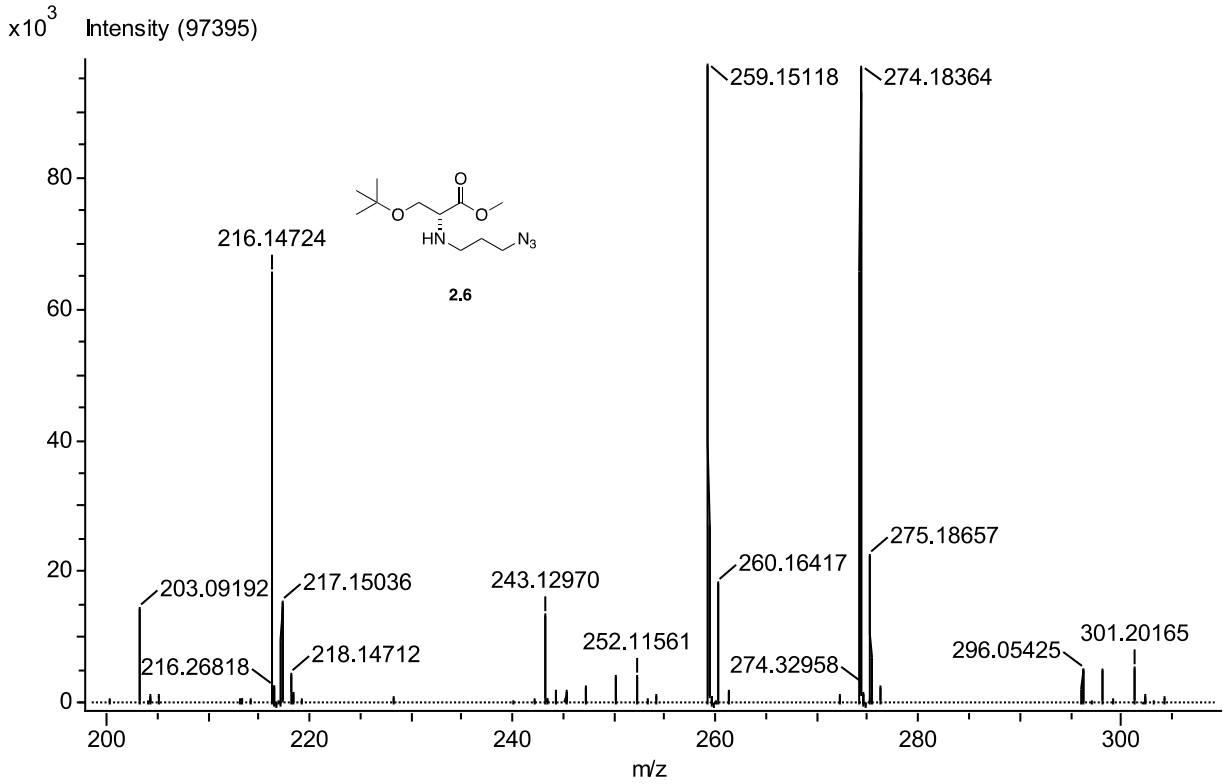

Spectrum A9. HRMS-DART of compound 2.6.

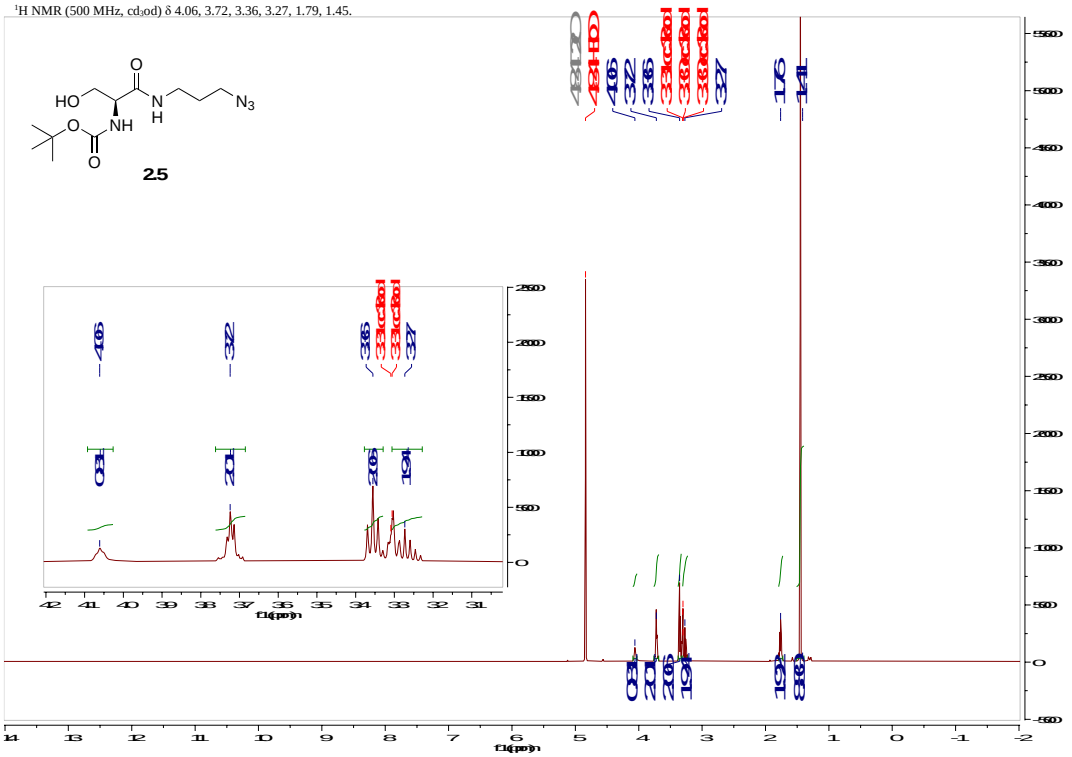

Spectrum A10. ^{1}H NMR of compound 2.5.

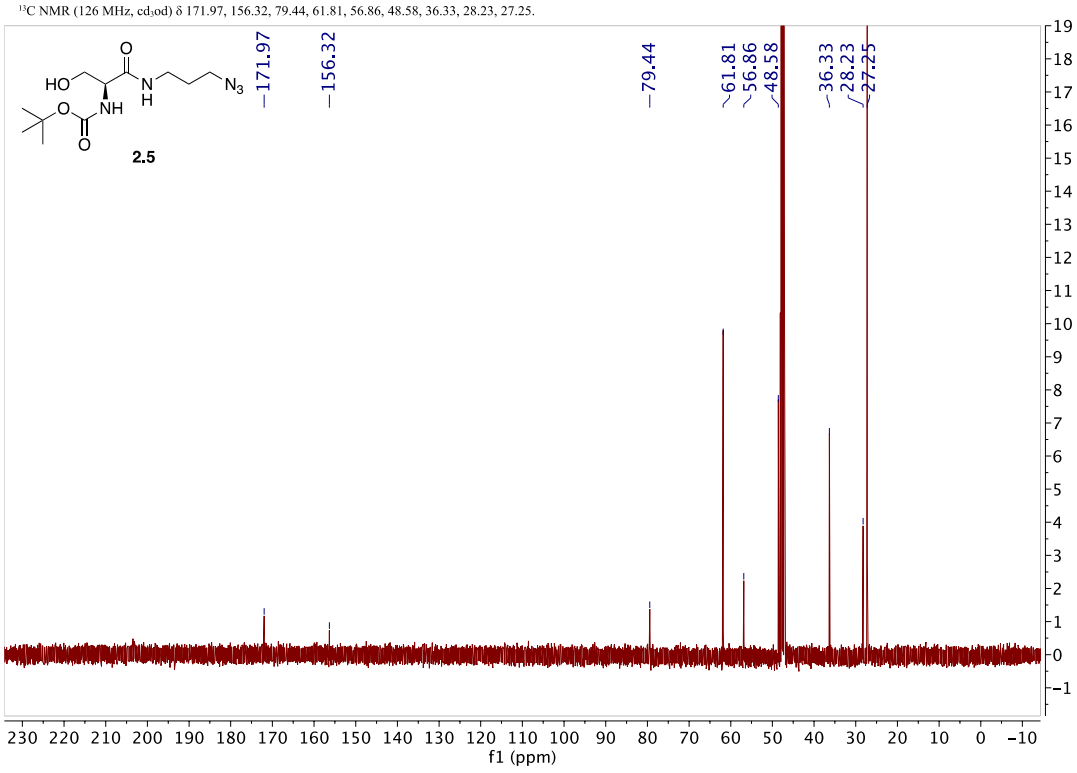

Spectrum A11. ^{13}C NMR of compound 2.5.

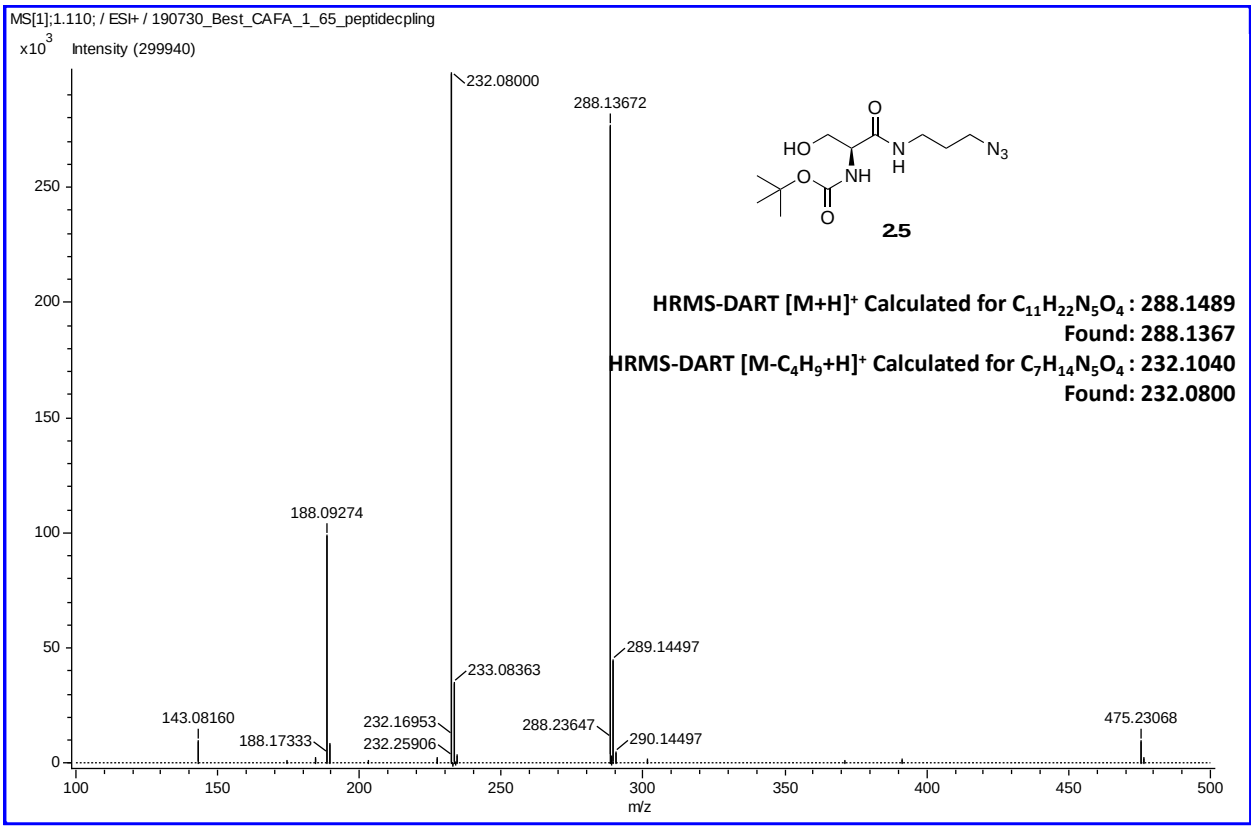

Spectrum A12. HRMS-DART MS of compound 2.5.

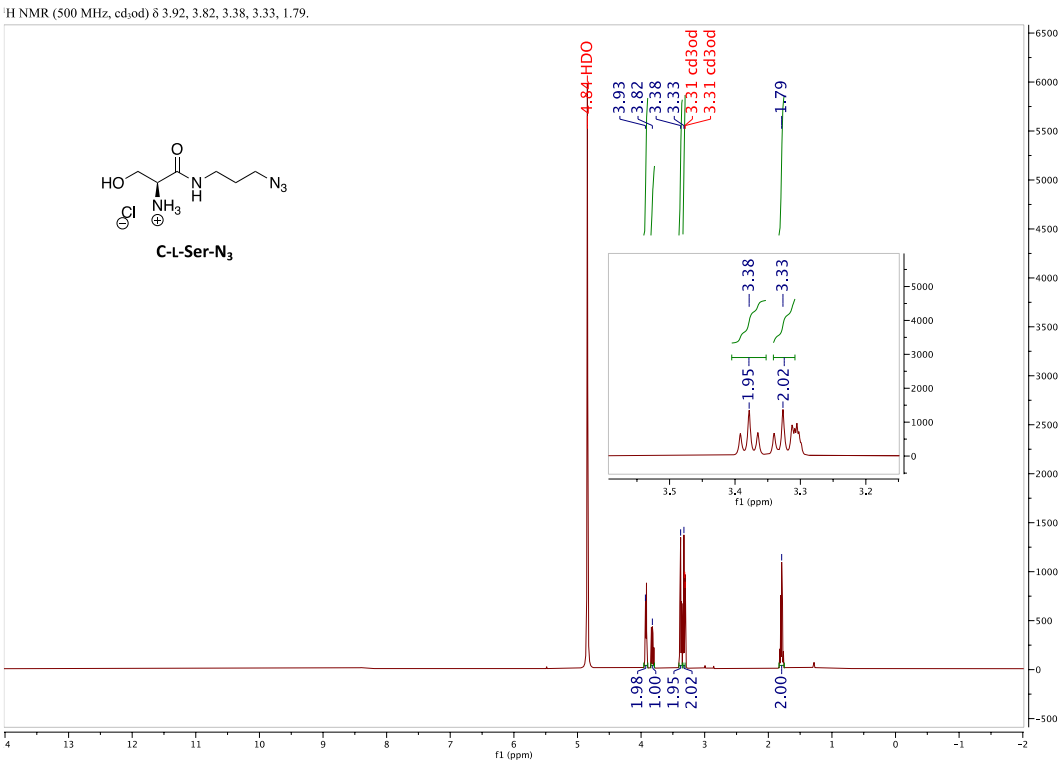

Spectrum A13. ^{1}H NMR of compound C-L-Ser-N$_3$.

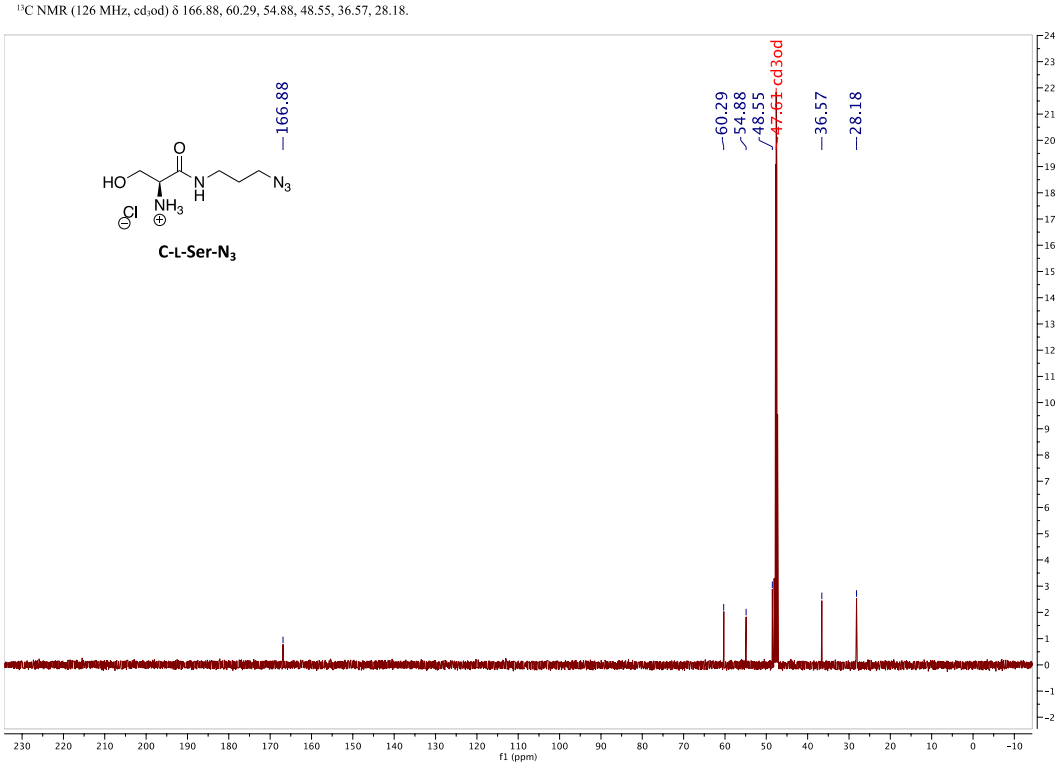

Spectrum A14. ^{13}C NMR of compound C-L-Ser-N$_3$.

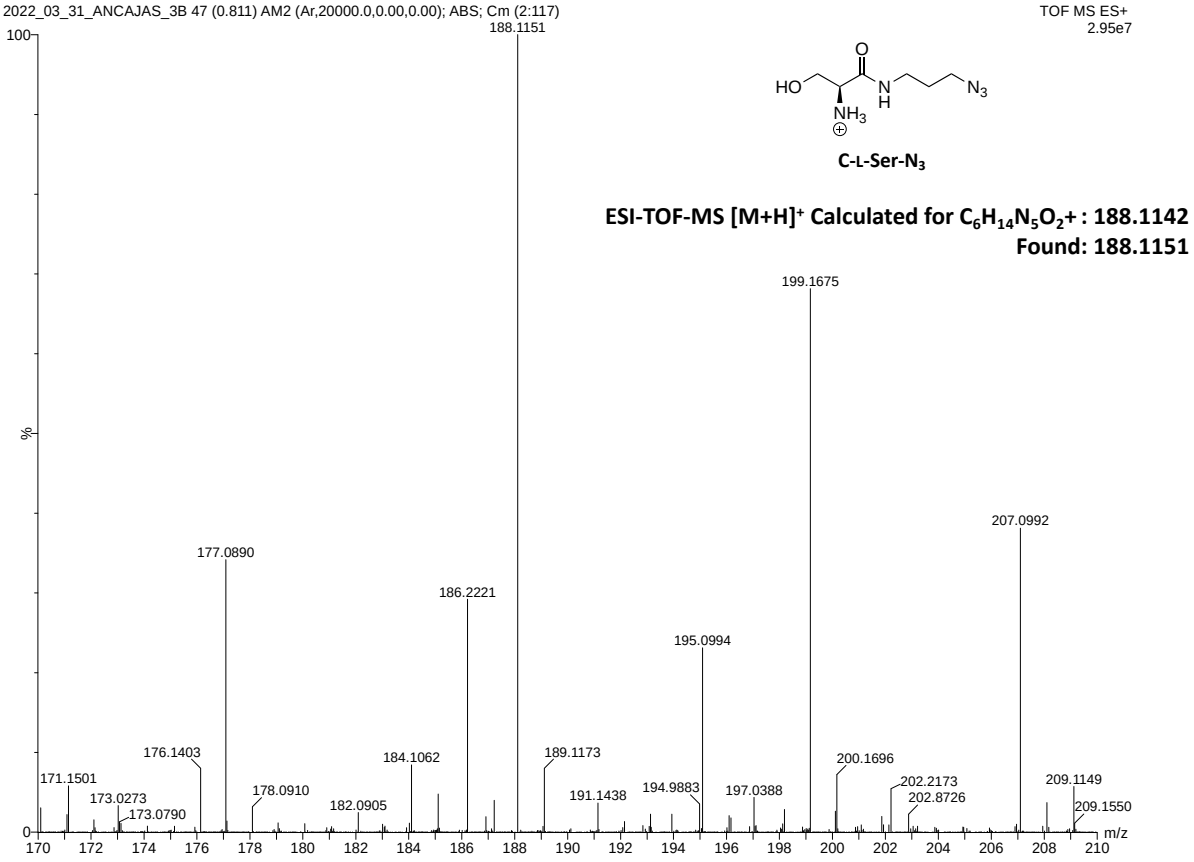

Spectrum A15. ESI-TOF-MS of compound C-L-Ser-N_3.

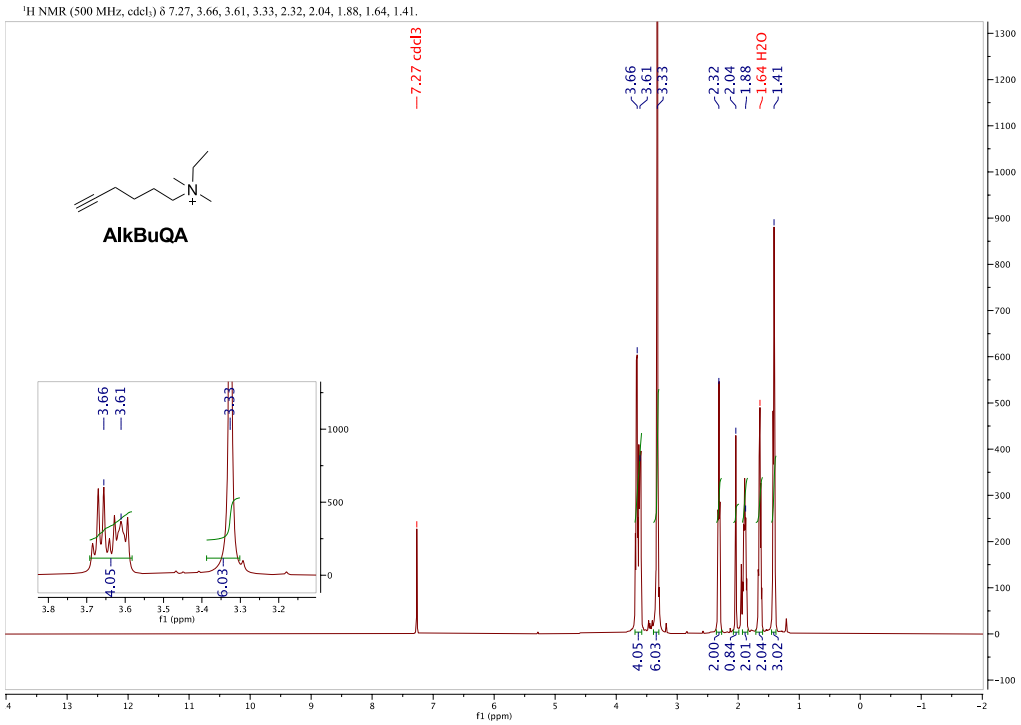

Spectrum A16. ^{1}H NMR of compound AlkBuQA.

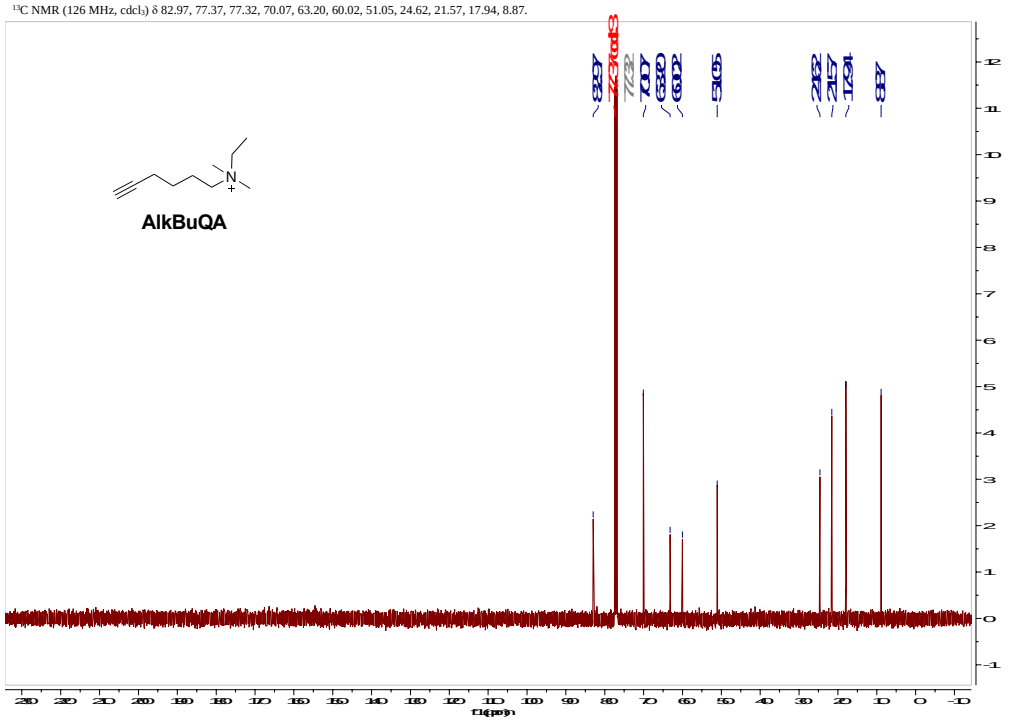

Spectrum A17. ^{13}C NMR of compound AlkBuQA.

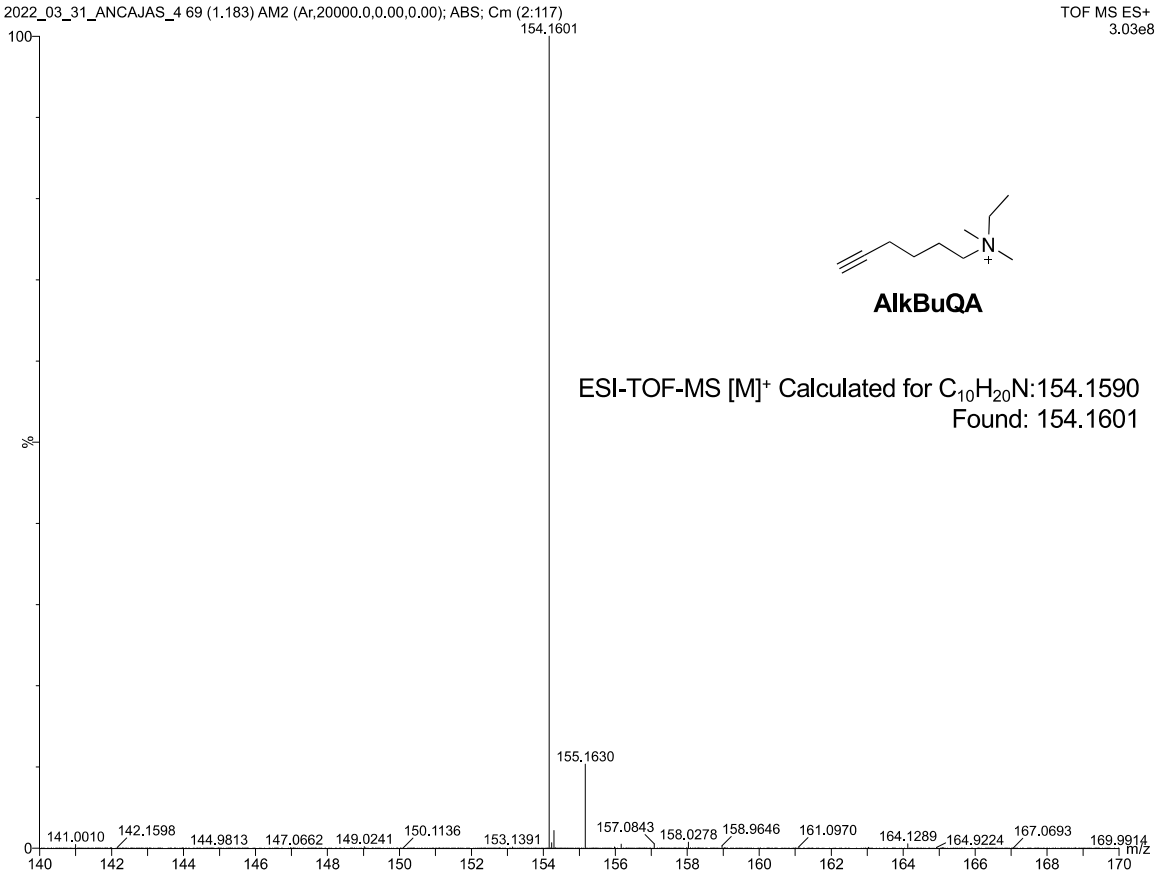

Spectrum A18. ESI-TOF-MS of compound AlkBuQA.

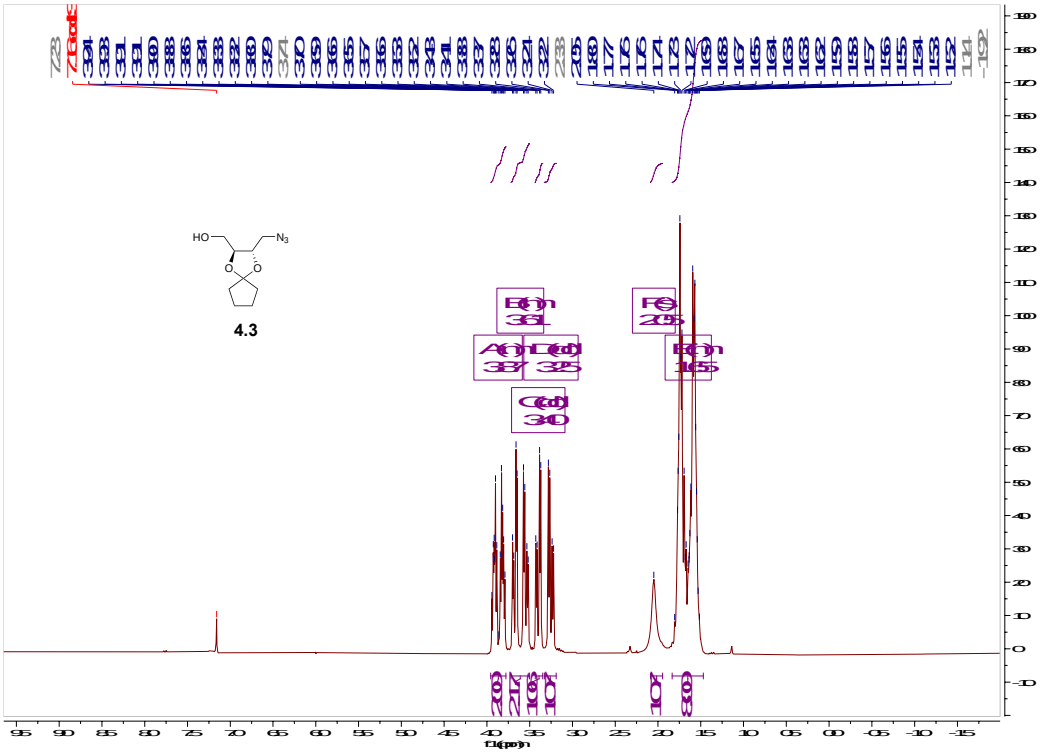

Spectrum A19. ^{1}H NMR of compound 4.3.

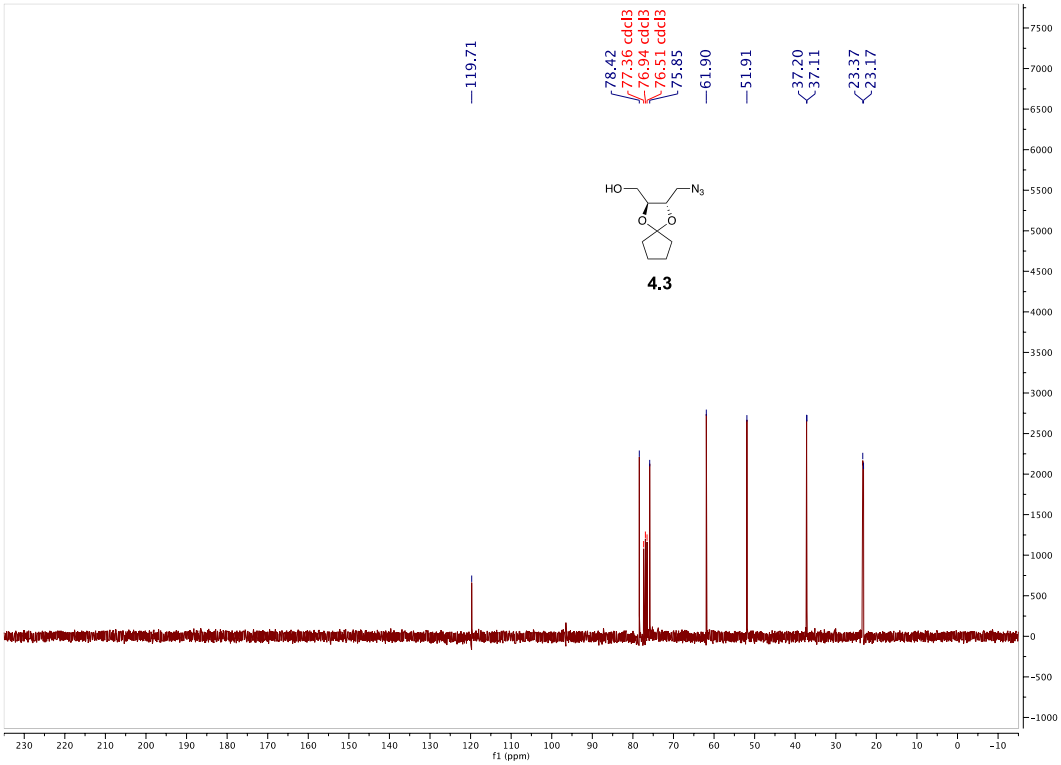

Spectrum A20. ^{13}C NMR of compound 4.3.

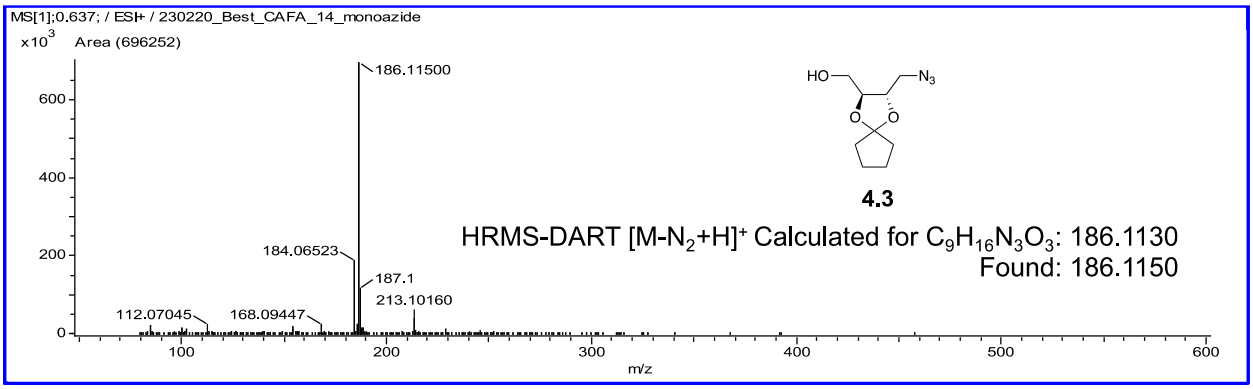

Spectrum A21. HRMS-DART of compound 4.3.

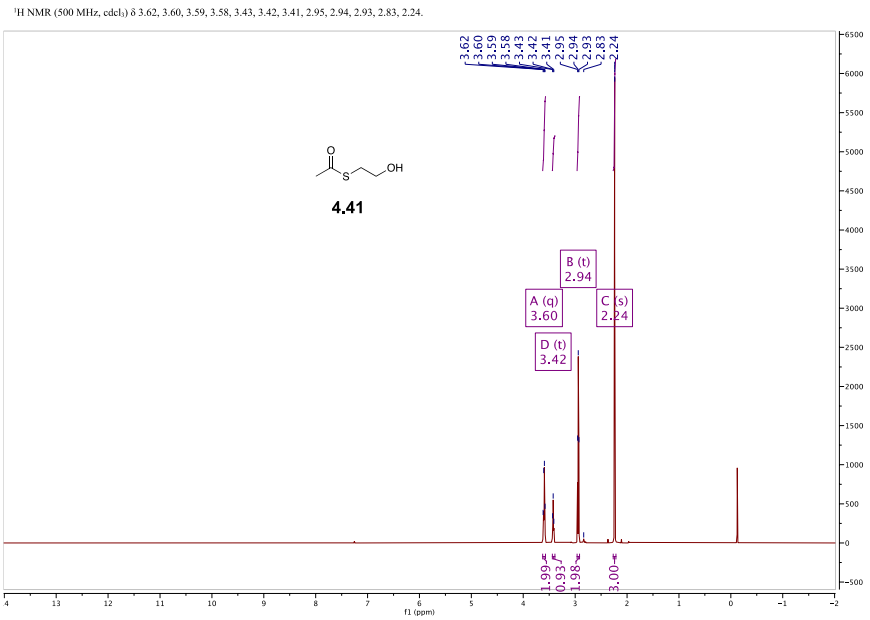

Spectrum A22. ^{1}H NMR of compound 4.41.

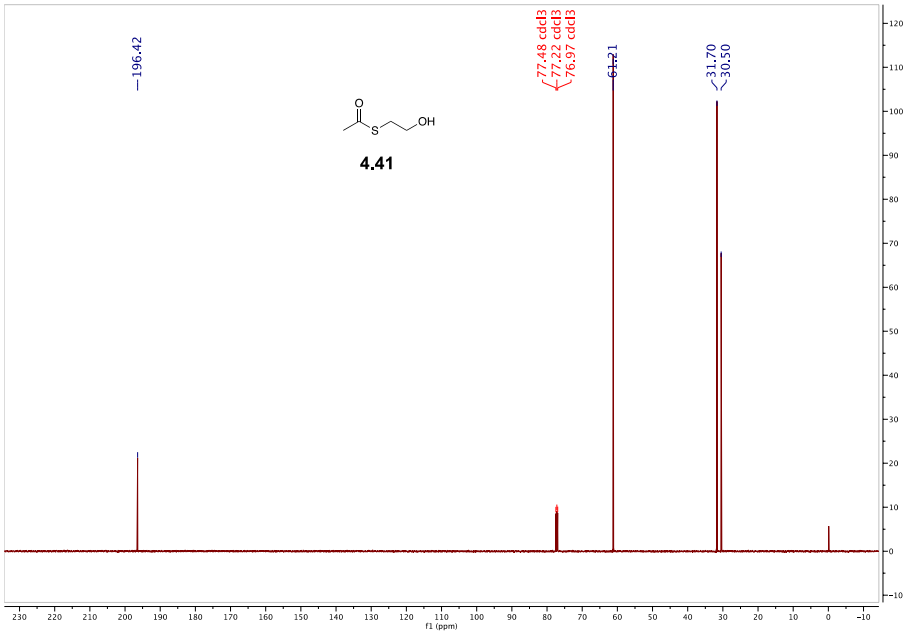

Spectrum A23. ^{13}C NMR of compound 4.41.

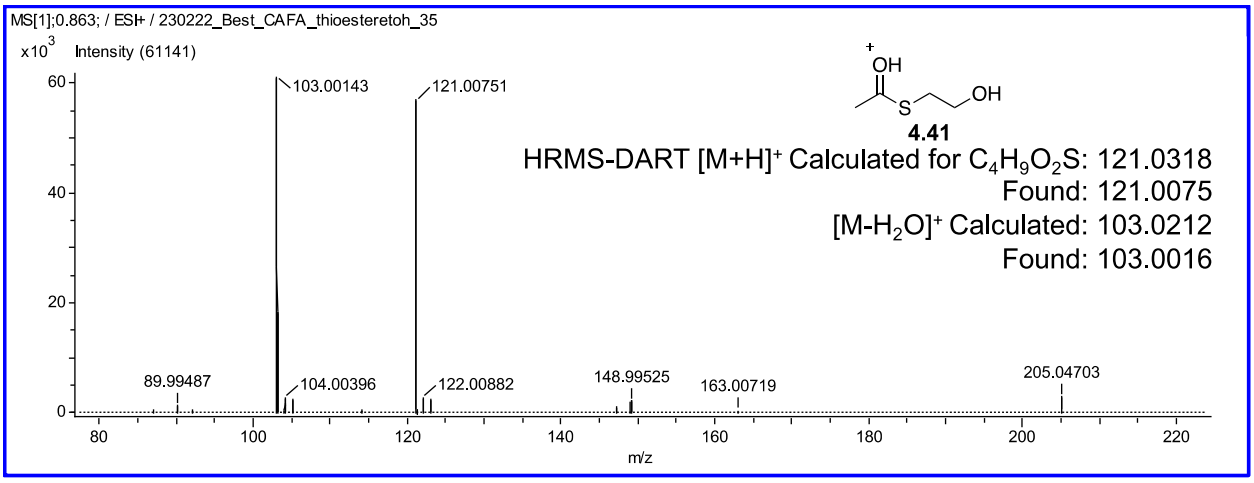

Spectrum A24. HRMS-DART of compound 4.41.

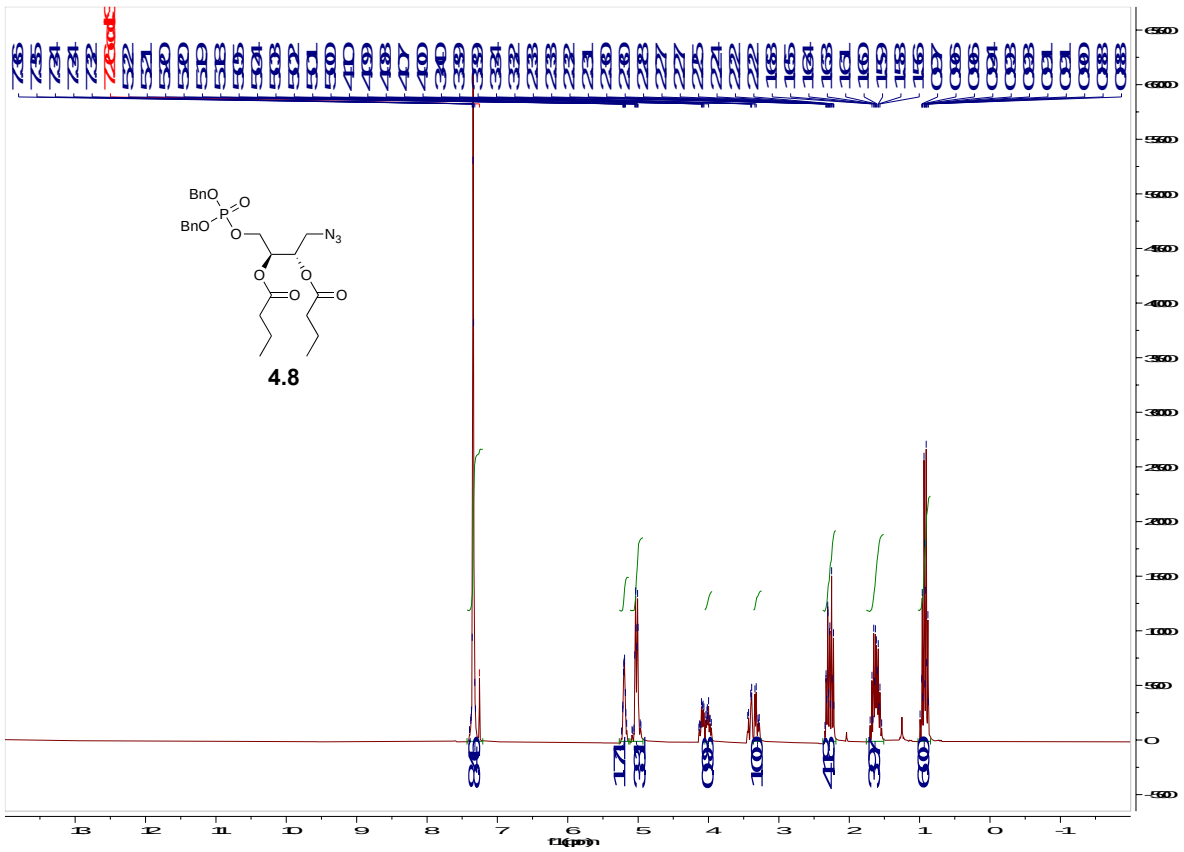

Spectrum A25. ^{1}H NMR of compound 4.8.

^{13}C NMR (126 MHz, cdcl$_3$) δ 172.47, 172.41, 135.56, 135.50, 128.66, 128.62, 128.02, 127.98, 69.95, 69.89, 69.72, 69.62, 69.58, 65.09, 65.05, 50.55, 35.85, 18.25, 13.56.

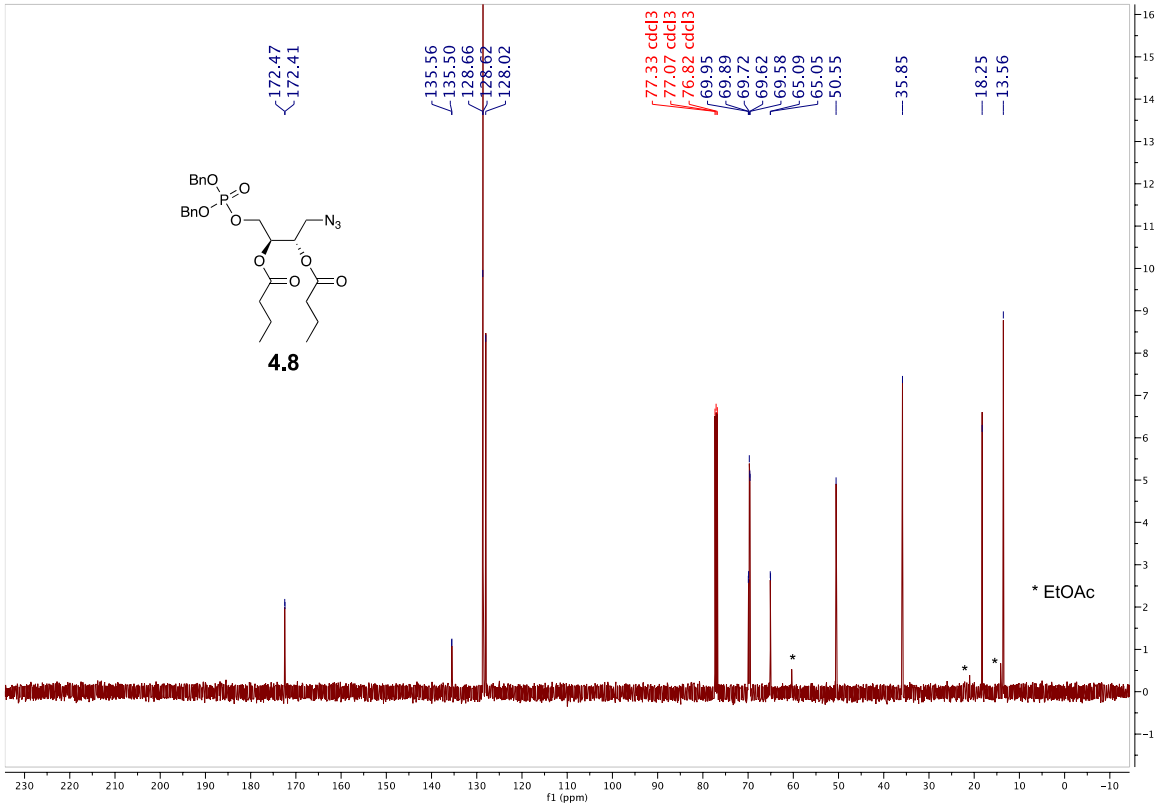

Spectrum A26. ^{13}C NMR of compound 4.8.

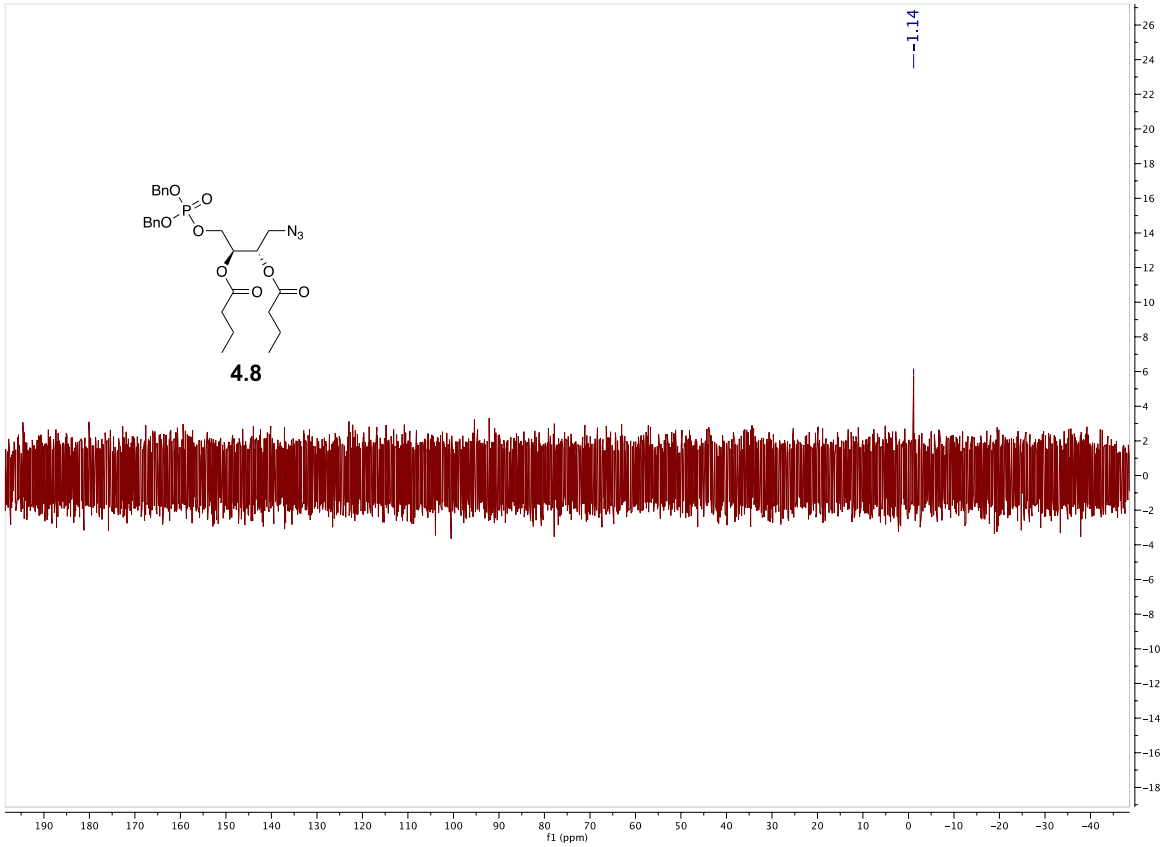

Spectrum A27. ^{31}P NMR of compound 4.8.

^{1}H NMR (500 MHz, cdcl$_3$) δ 3.36, 3.36, 3.35, 3.34, 3.34, 3.34, 3.33, 3.33, 3.33, 3.21, 3.21, 3.20,

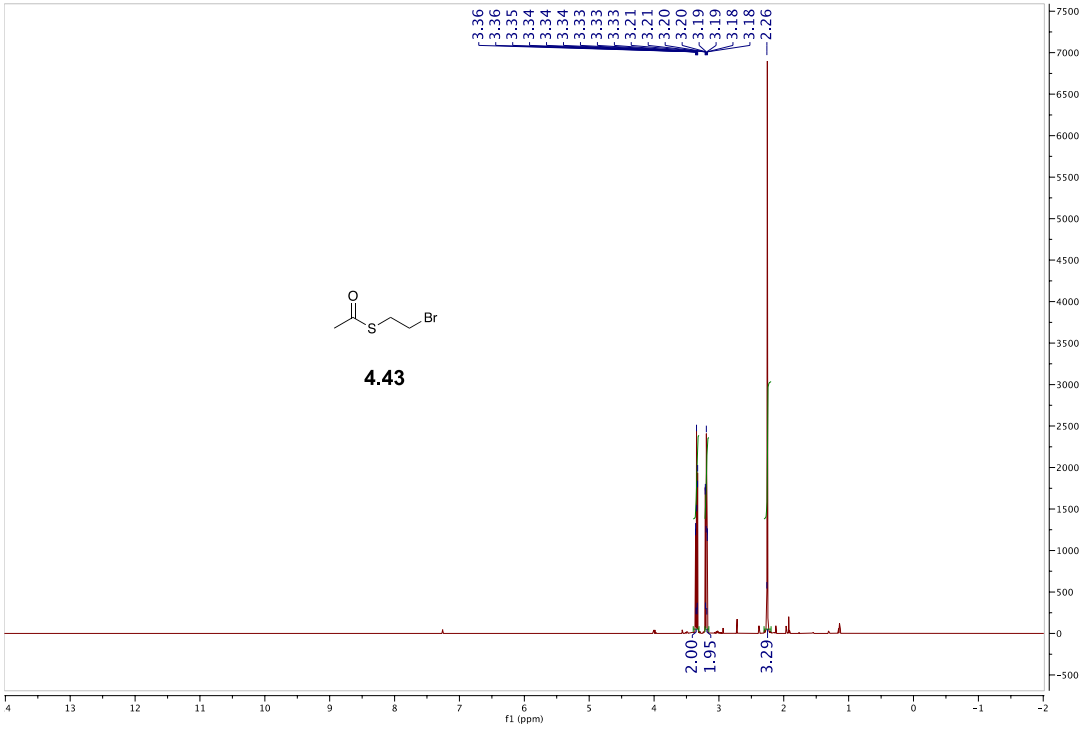

Spectrum A28. ^{1}H NMR of compound 4.43.

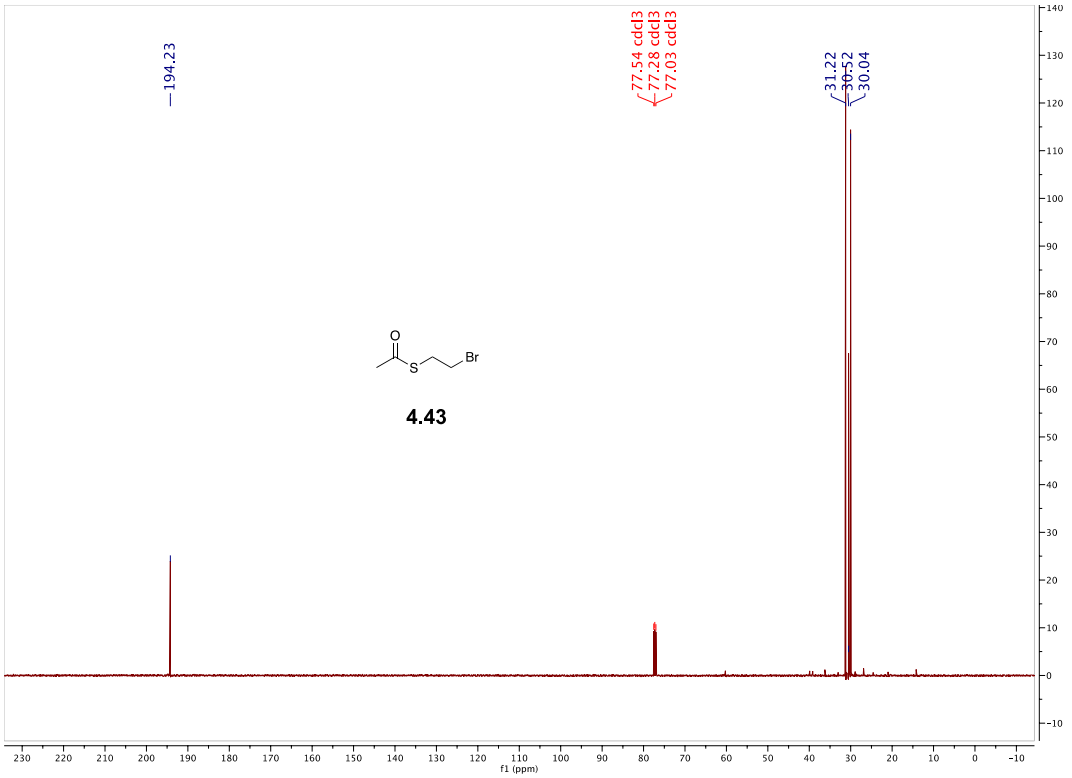

Spectrum A29. ^{13}C NMR of compound 4.43.

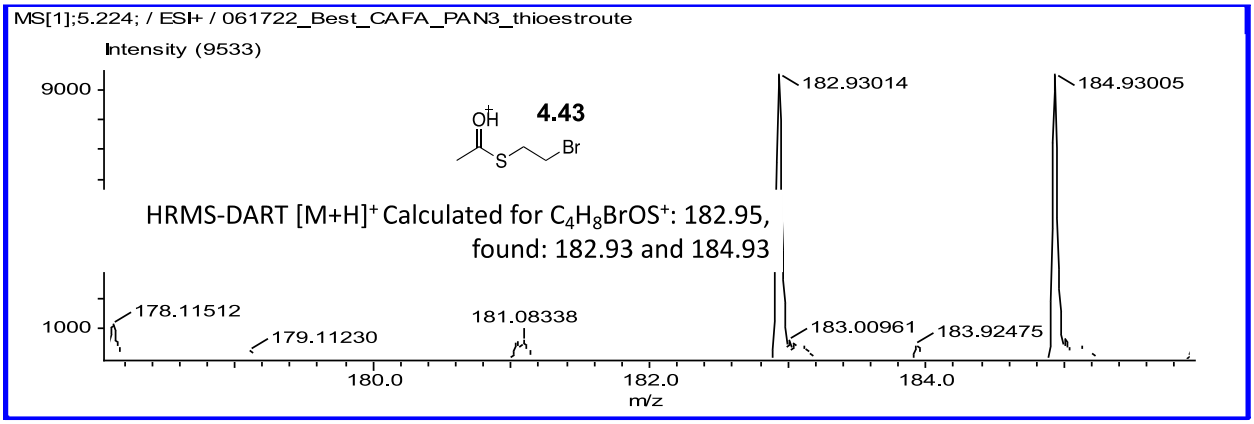

Spectrum A30. HRMS-DART of compound 4.43.

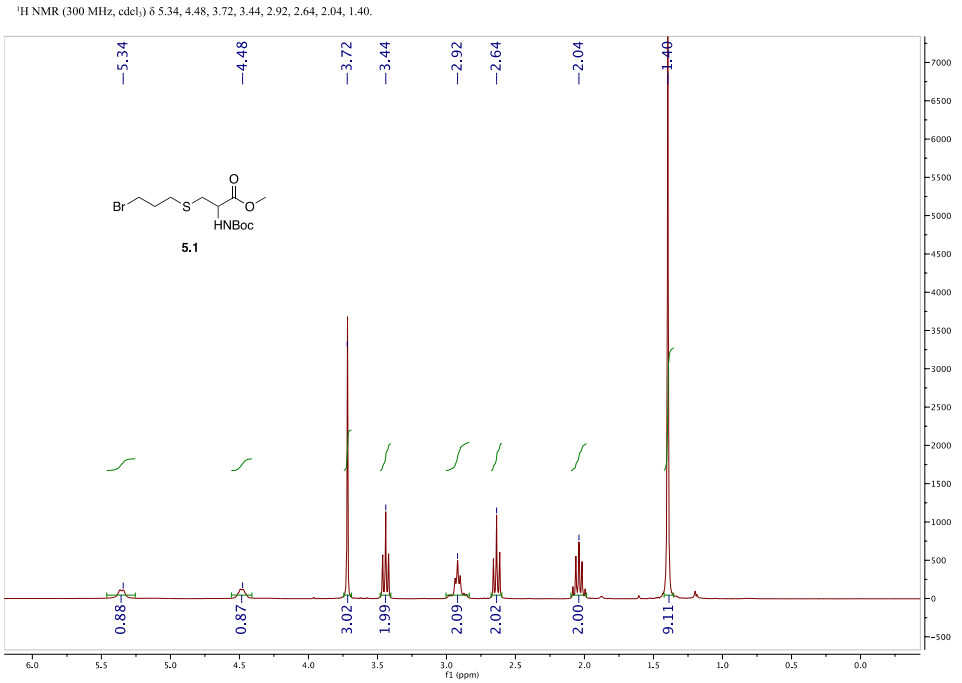

Spectrum A31. ^{1}H NMR of compound 5.1.

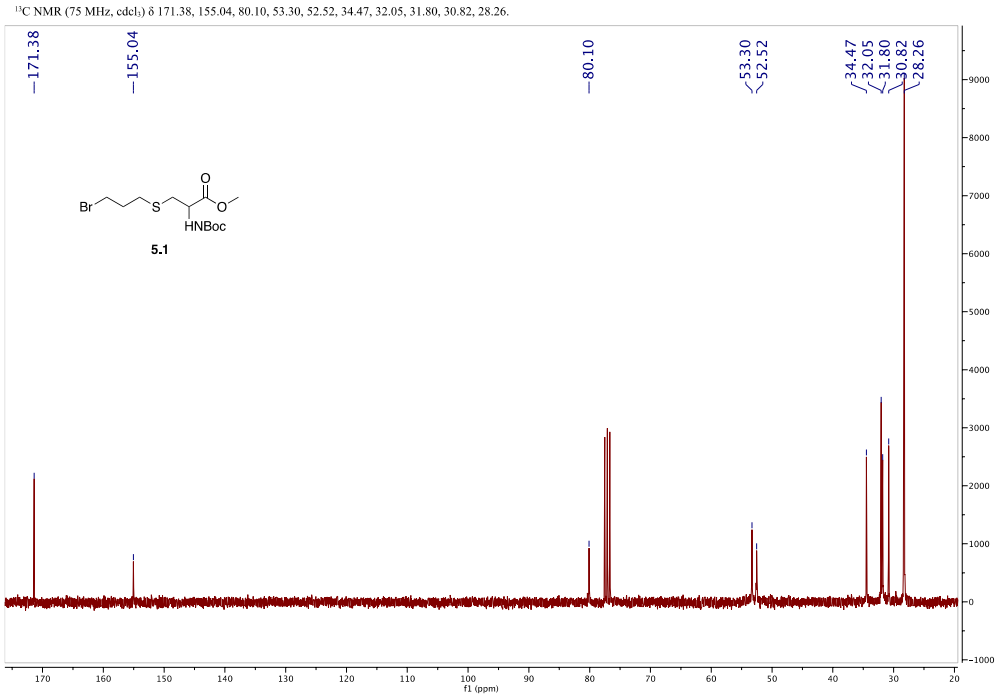

Spectrum A32. ^{13}C NMR of compound 5.1.

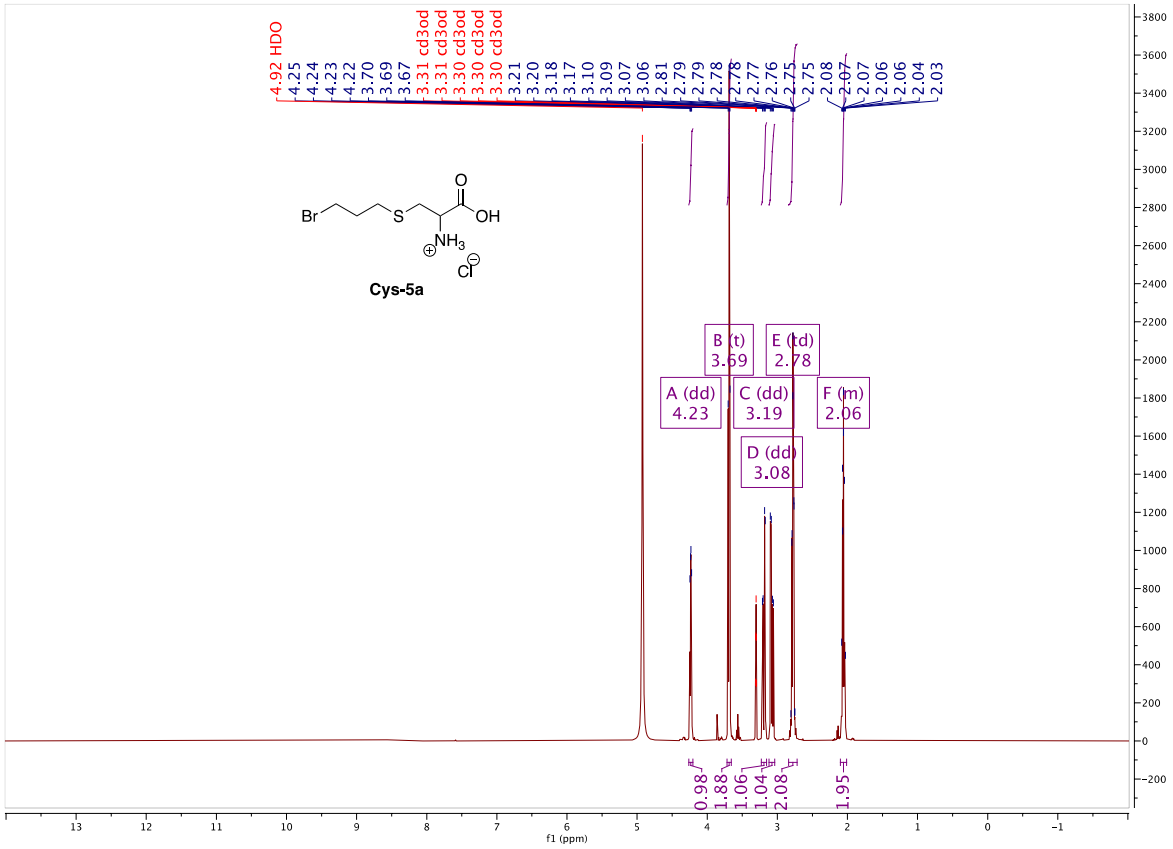

Spectrum A33. ^{1}H NMR of compound Cys-5a.

^{13}C NMR (126 MHz, d_2o) δ 175.35, 53.50, 43.60, 31.87, 31.16, 28.32.

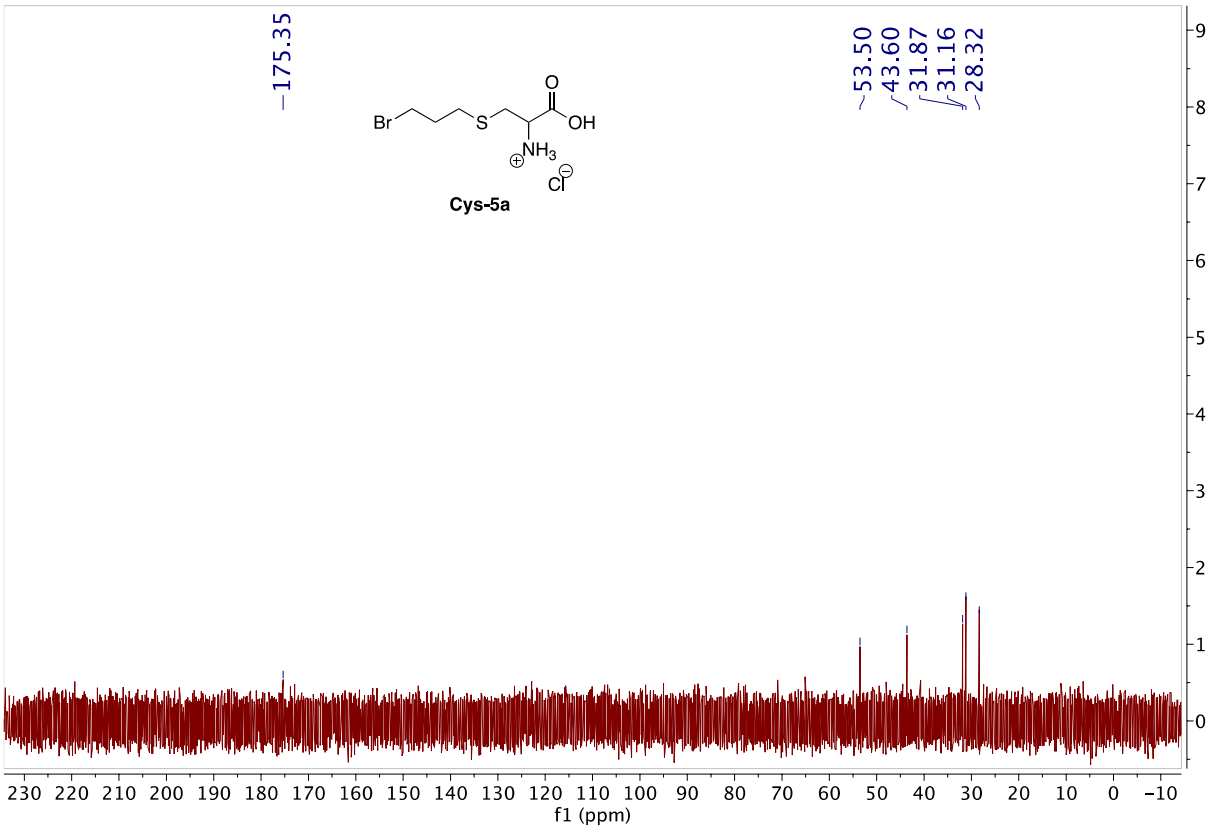

Spectrum A34. ^{13}C NMR of compound Cys-5a.

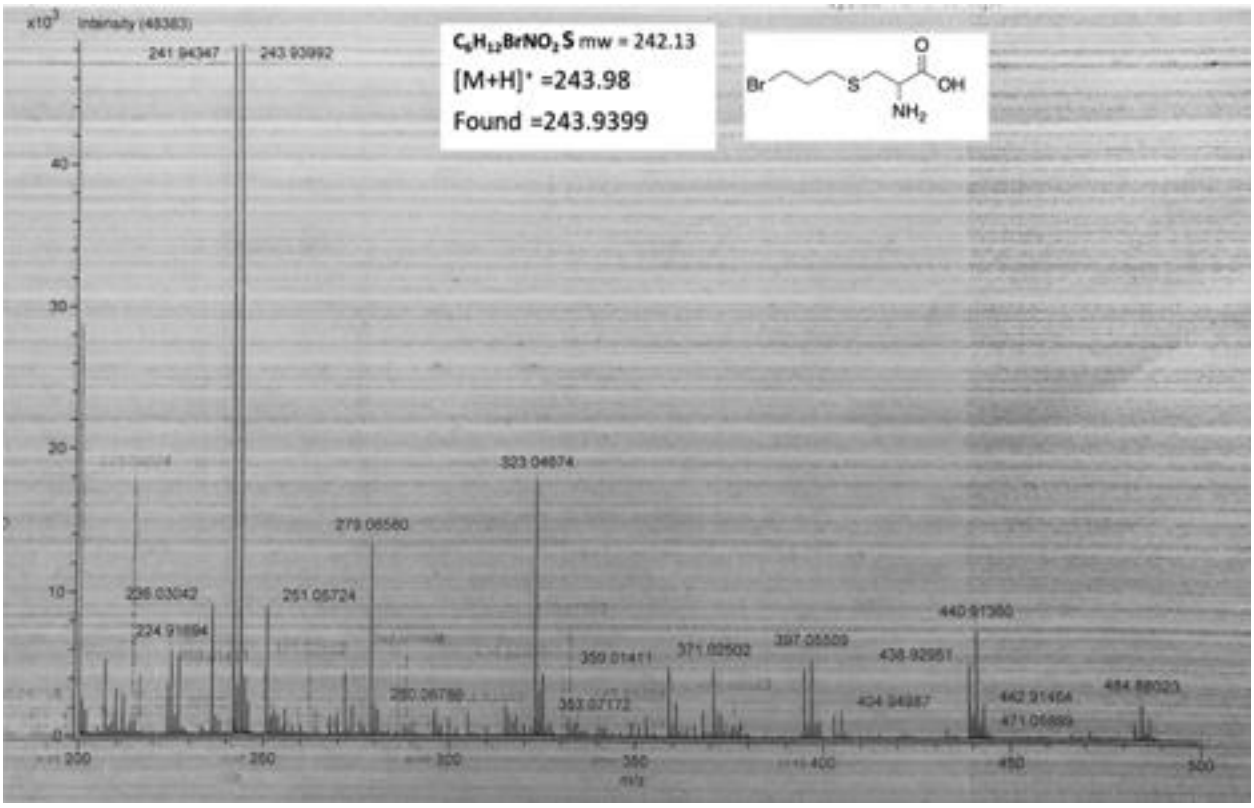

Spectrum A35. HRMS-DART of compound Cys-5a.

^{1}H NMR (500 MHz, cd$_3$od) δ 7.77, 7.44, 4.83, 4.12, 3.55, 3.30, 3.30, 3.30, 2.44, 1.95, 1.28.

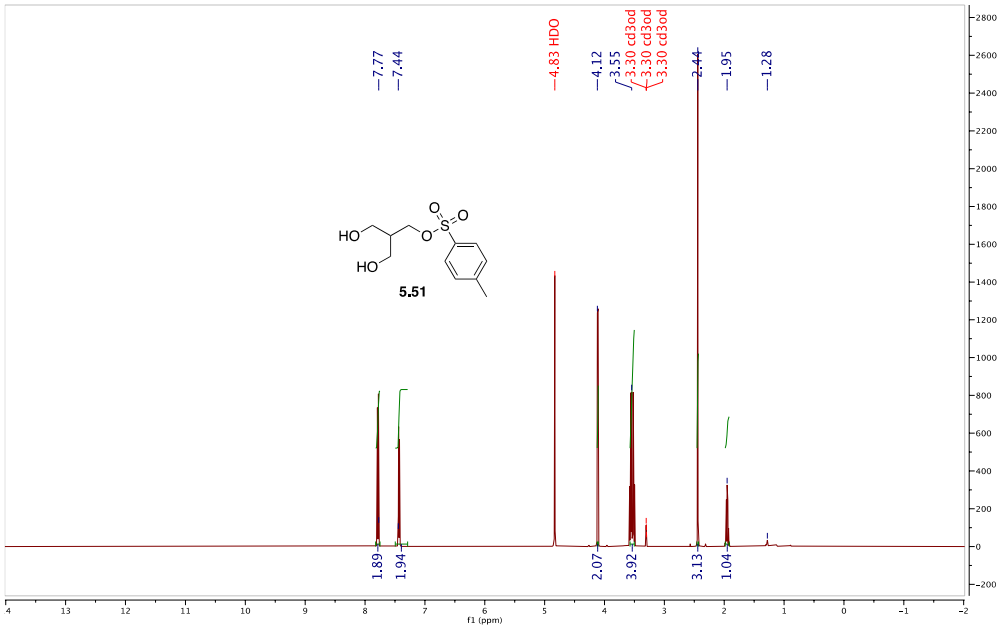

Spectrum A36. ^{1}H NMR of compound 5.51.

^{13}C NMR (126 MHz, cd$_3$od) δ 145.09, 132.87, 129.68, 127.60, 68.47, 58.92, 47.63, 43.44, 20.18.

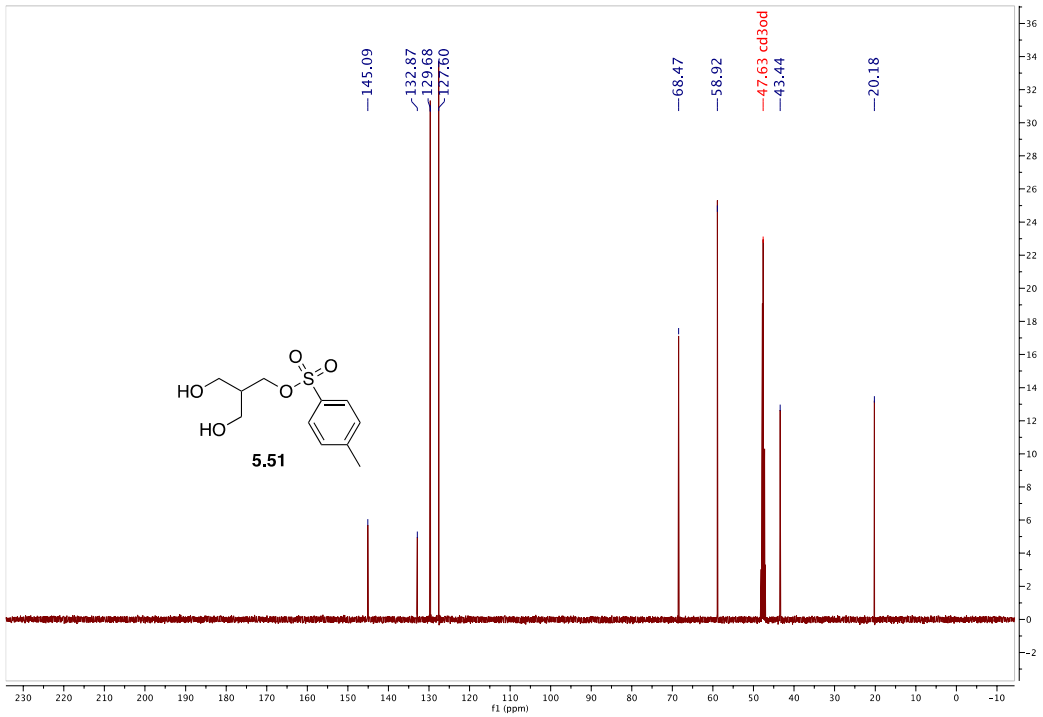

Spectrum A37. ^{13}C NMR of compound 5.51.

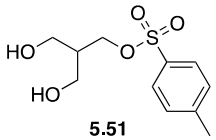

5.51

HRMS-DART: $[M+H]^+$ calculated for $C_{14}H_{20}O_5S$: 301.32094;
Found: 301.07713, 302.07707

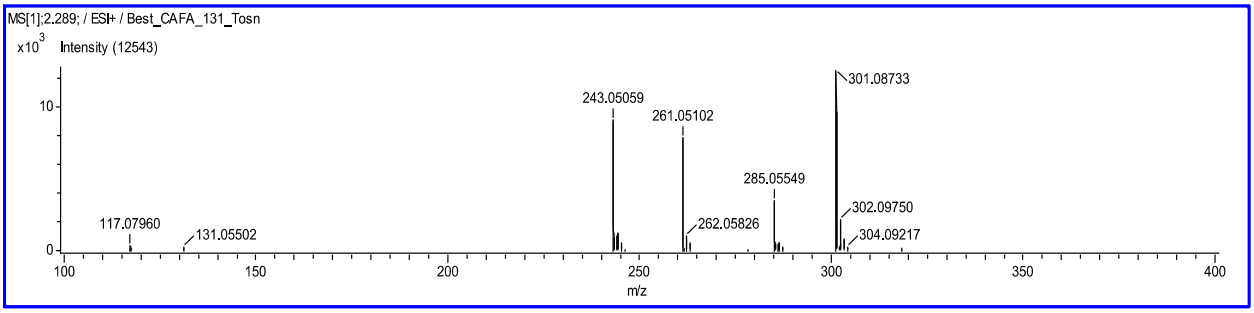

Spectrum A38. HRMS-DART of compound 5.51.

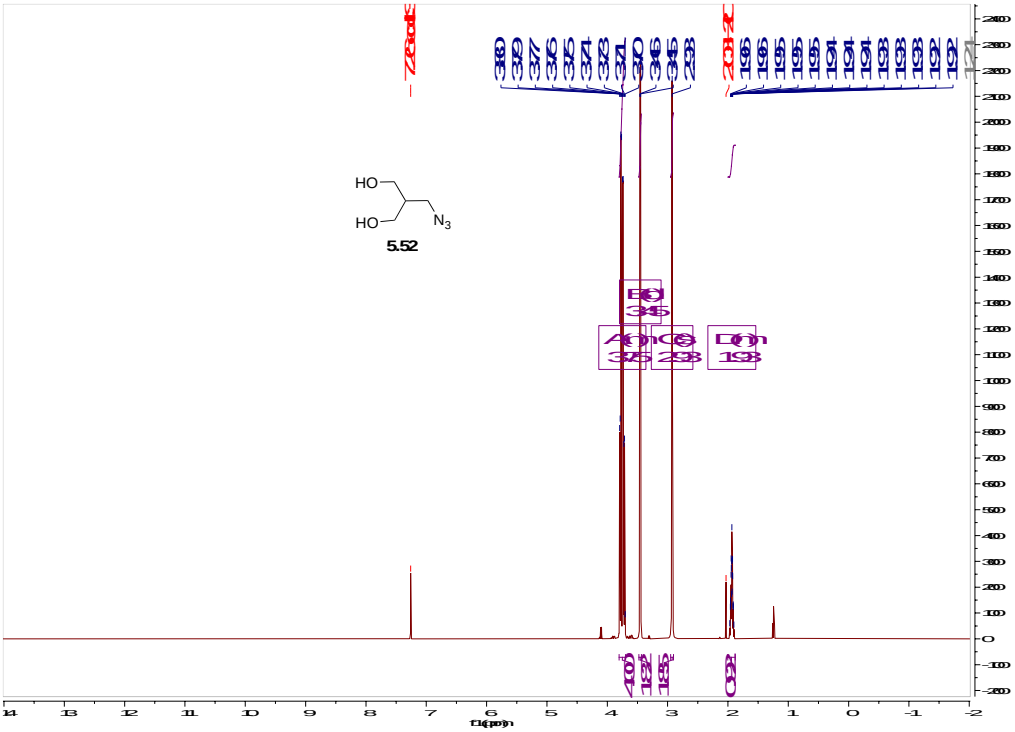

Spectrum A39. ^{1}H NMR of compound 5.52.

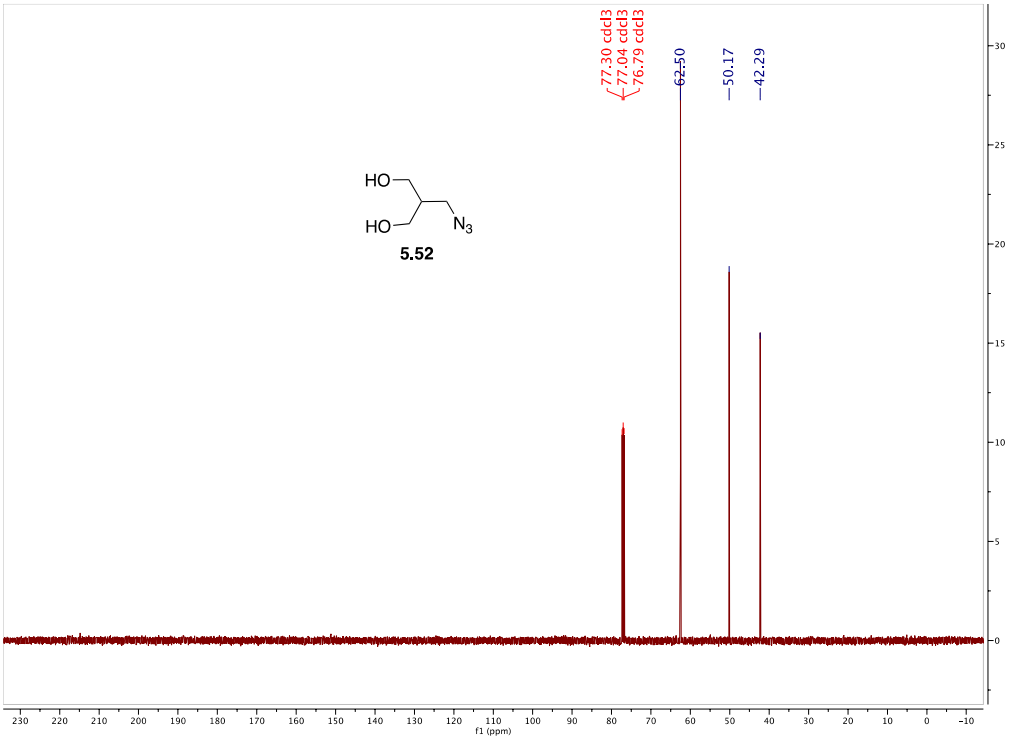

Spectrum A40. ^{13}C NMR of compound 5.52.

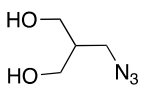

5.52

HRMS-DART: $[M+H]^+$ calculated for $C_4H_9N_3O_2$: 132.1191, found: 133.09192
$[M-N_2+H]^+$ calculated for $C_4H_9N_1O_2$: 104.1057; Found: 104.06893

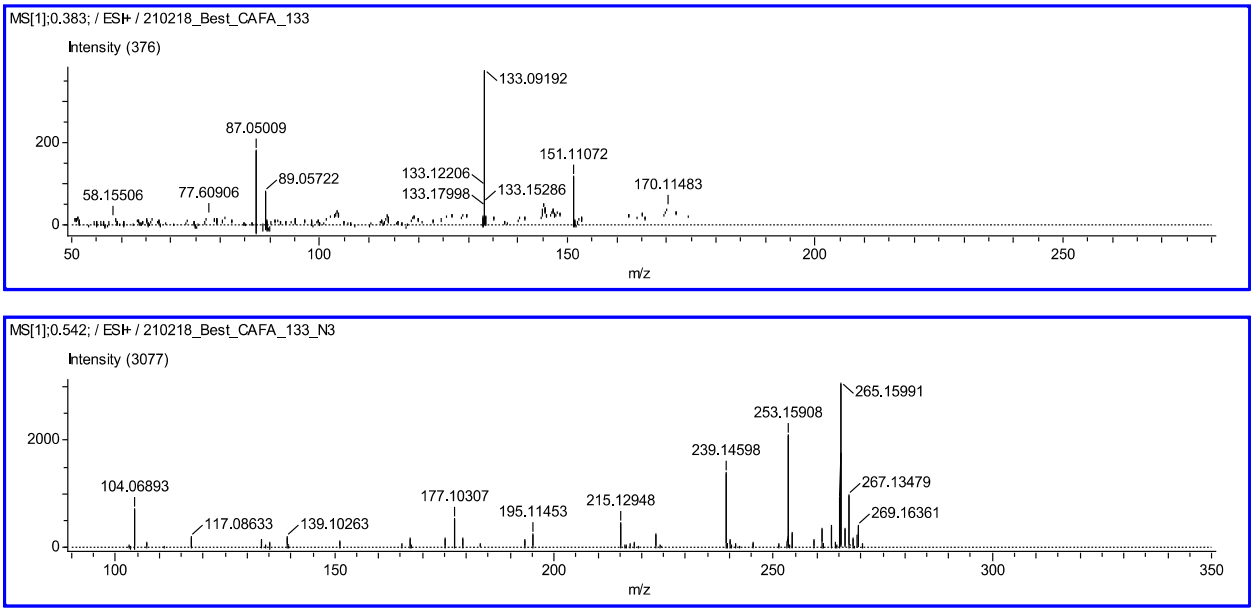

Spectrum A50. HRMS-DART of compound 5.52.

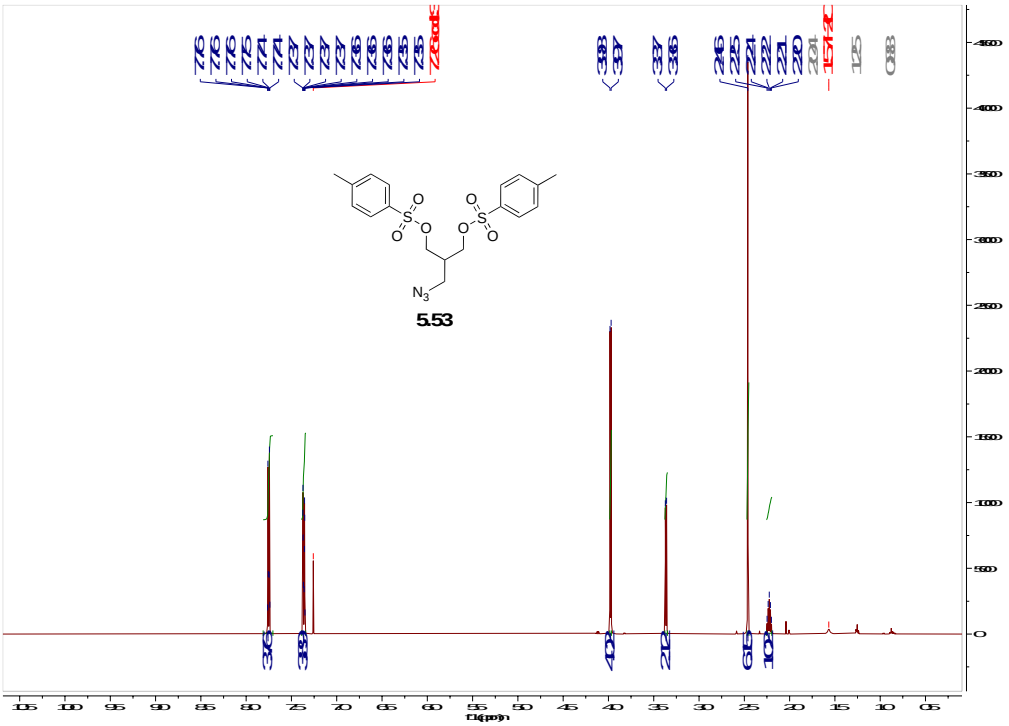

Spectrum A51. ^{1}H NMR of compound 5.53.

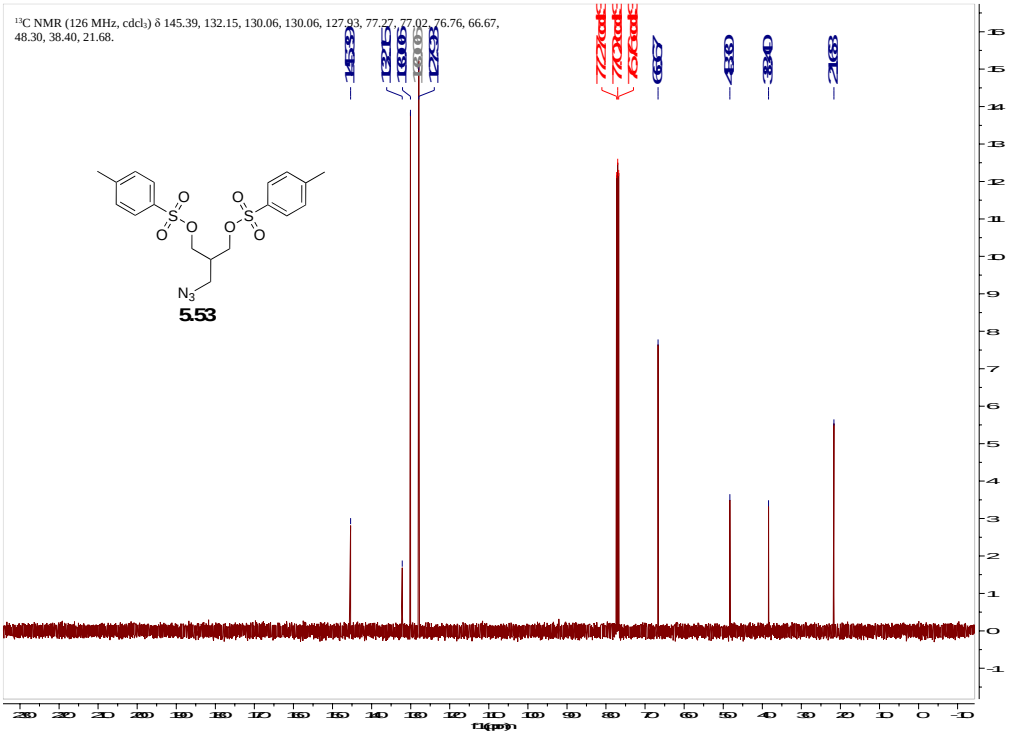

Spectrum A52. ^{13}C NMR of compound 5.53.

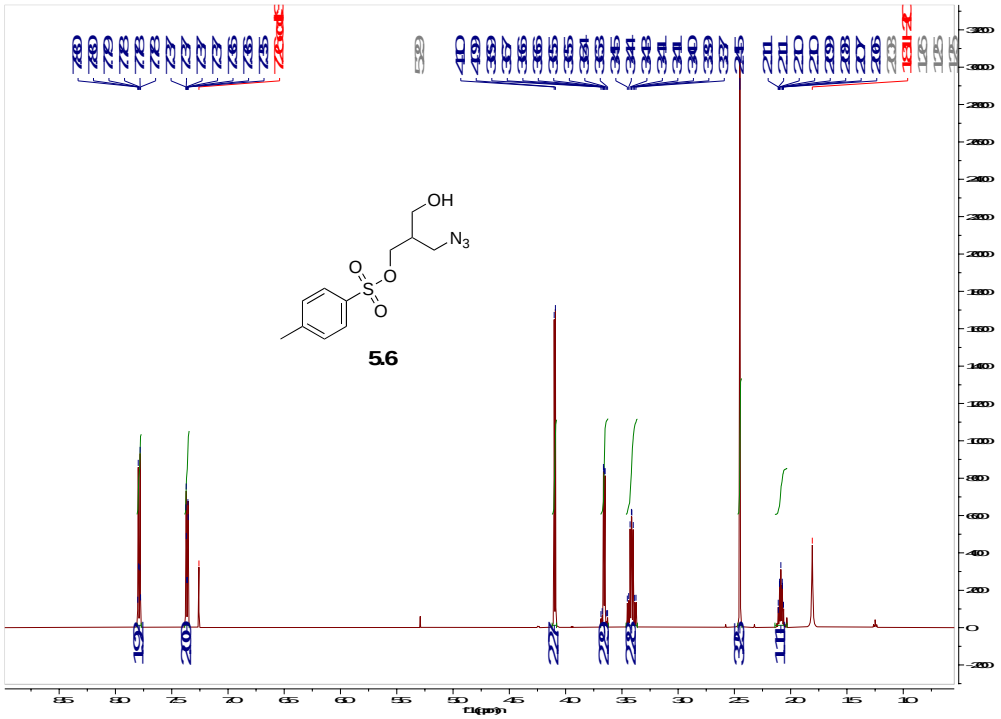

Spectrum A53. ^{1}H NMR of compound 5.6.

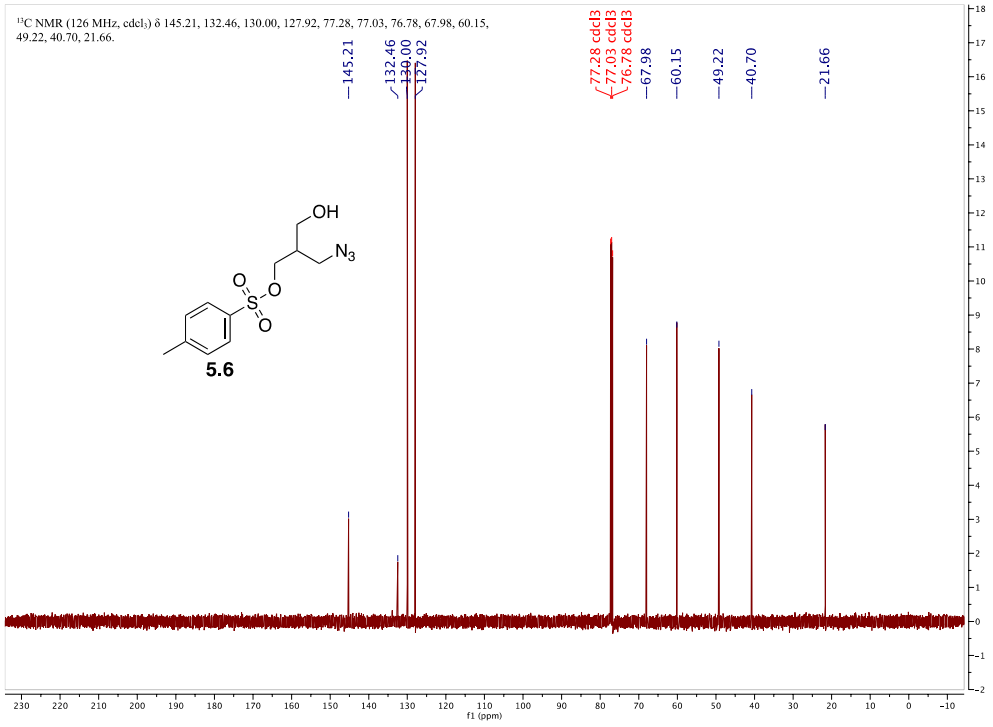

Spectrum A54. ^{13}C NMR of compound 5.6.

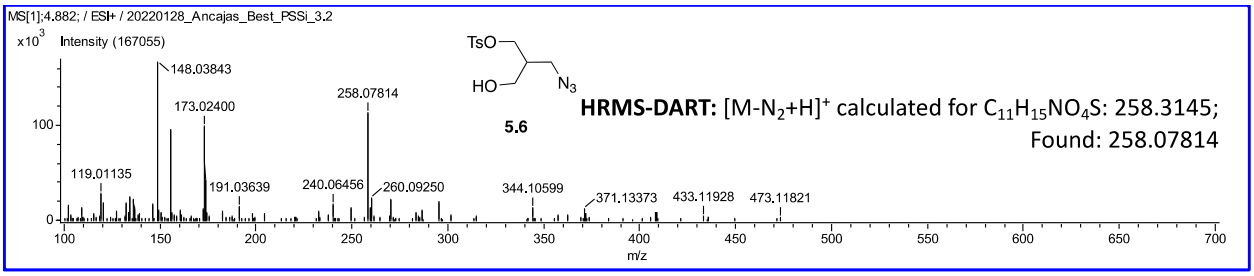

Spectrum A55. HRMS-DART of compound 5.6.

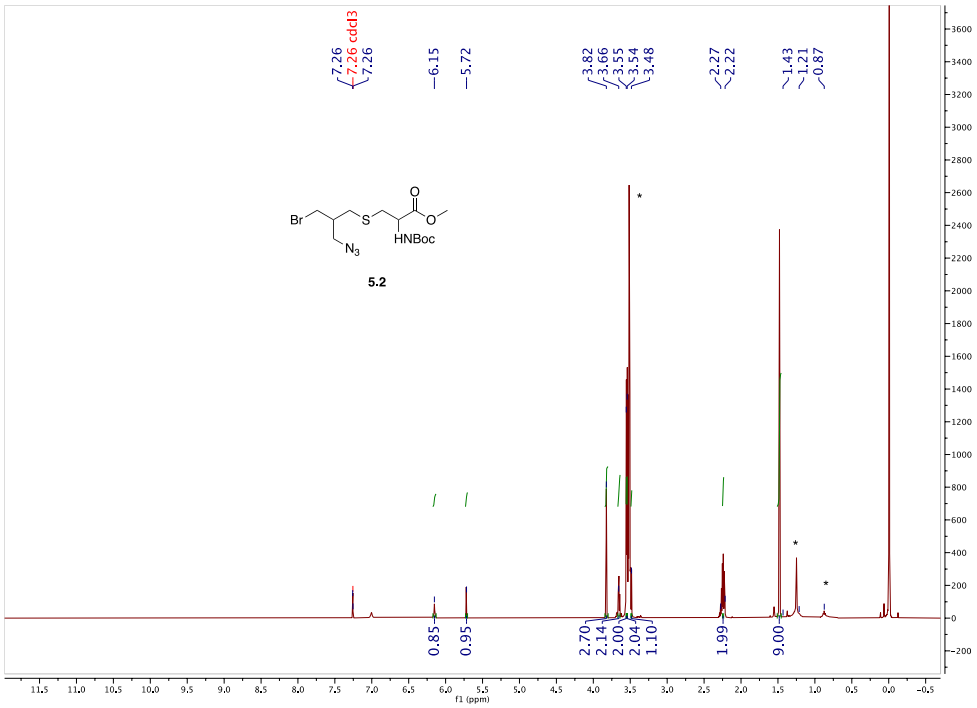

Spectrum A56. ^{1}H NMR of compound 5.2.

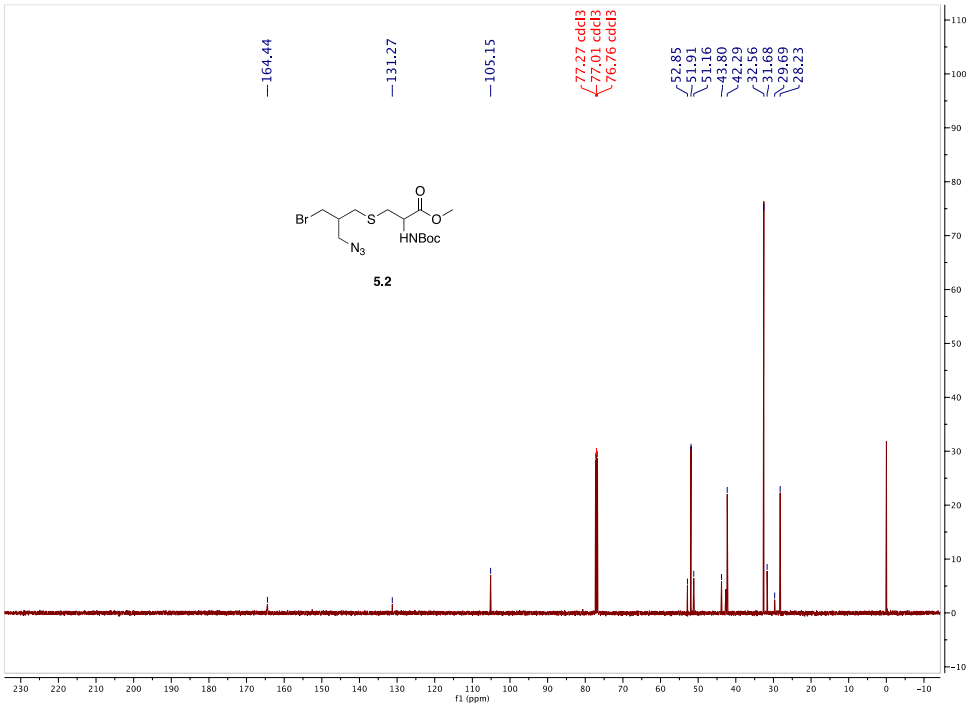

Spectrum A57. ^{13}C NMR of compound 5.2.

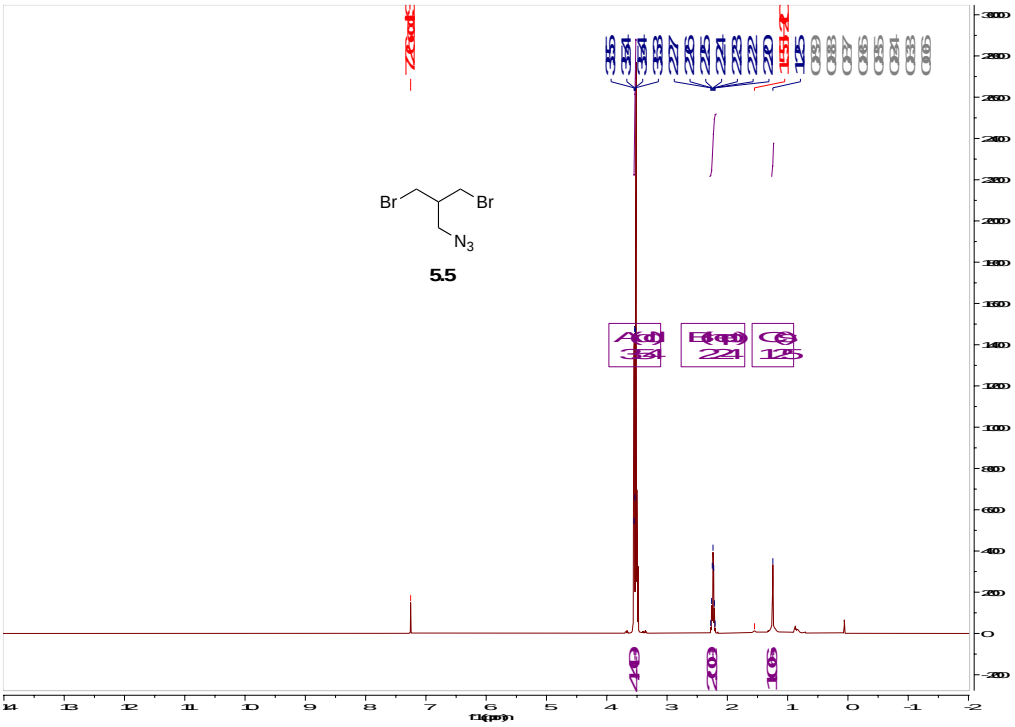

Spectrum A58. ^{1}H NMR of compound 5.5.

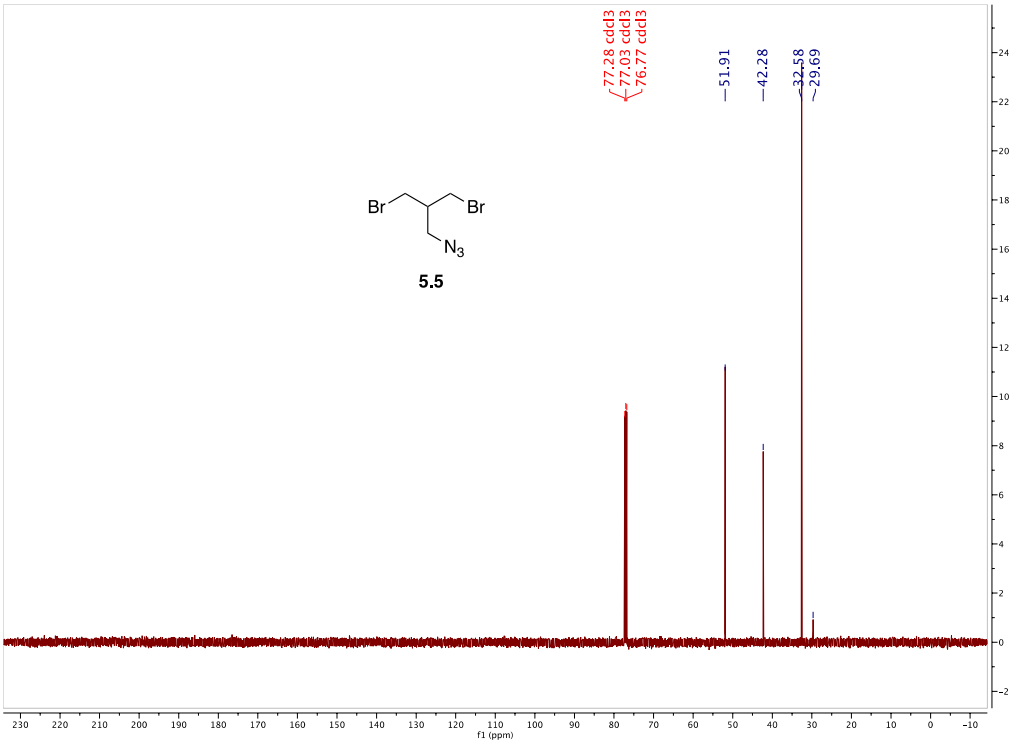

Spectrum A59. ^{13}C NMR of compound 5.5.

Vita

Christelle Anne F. Ancajas was born and raised in Cebu City, Philippines. She attended Bluestone High School in Virginia and graduated in 2014. She developed her interest in research during her time at The Governor's School of Southside VA. She received her Bachelor's Degree in Chemistry (Research Emphasis) from Randolph-Macon College in 2017. During her time at R-MC, she initially participated in undergraduate cell biology research with Dr. James Foster and later explored her interest in physical organic chemistry and synthesis under the supervision of Dr. John Thoburn. In 2018, she entered the Chemistry doctoral program at the University of Tennessee, Knoxville, and joined the lab of Dr. Michael Best to conduct research related to chemical synthesis, lipid biology, and chemical biology.